

IMPROVEMENT OF PUNCHING STRENGTH OF FLAT PLATES BY USING
CARBON FIBER REINFORCED POLYMER (CFRP) DOWELS

A THESIS SUBMITTED TO
THE GRADUATE SCHOOL OF NATURAL AND APPLIED SCIENCES
OF
MIDDLE EAST TECHNICAL UNIVERSITY

BY

HAKAN ERDOĞAN

IN PARTIAL FULFILLMENT OF THE REQUIREMENTS
FOR
THE DEGREE OF DOCTOR OF PHILOSOPHY
IN
CIVIL ENGINEERING

DECEMBER 2010

Approval of the thesis:

**IMPROVEMENT OF PUNCHING STRENGTH OF FLAT PLATES BY
USING CARBON FIBER REINFORCED POLYMER (CFRP) DOWELS**

submitted by **HAKAN ERDOĞAN** in partial fulfillment of the requirements for
the degree of **Doctor of Philosophy in Civil Engineering Department, Middle
East Technical University** by,

Prof. Dr. Canan Özgen _____
Dean, Graduate School of **Natural and Applied Sciences**

Prof. Dr. Güney Özcebe _____
Head of Department, **Civil Engineering**

Prof. Dr. Güney Özcebe _____
Supervisor, **Civil Engineering Dept., METU**

Assoc. Prof. Dr. Barış Binici _____
Co-Supervisor, **Civil Engineering Dept., METU**

Examining Committee Members:

Prof. Dr. Tuğrul Tankut _____
Civil Engineering Dept., METU

Prof. Dr. Güney Özcebe _____
Civil Engineering Dept., METU

Asst. Prof. Dr. Burcu Burak _____
Civil Engineering Dept., METU

Assoc. Prof. Dr. Stathis N. Bousias _____
Civil Engineering Dept., University of Patras

Assoc. Prof. Dr. Şevket Özden _____
Civil Engineering Dept., Kocaeli University

Date: _____

I hereby declare that all information in this document has been obtained and presented in accordance with academic rules and ethical conduct. I also declare that, as required by these rules and conduct, I have fully cited and referenced all material and results that are not original to this work.

Name, Last Name: Hakan Erdoğan

Signature :

ABSTRACT

IMPROVEMENT OF PUNCHING SHEAR STRENGTH OF FLAT PLATES BY USING CARBON FIBER REINFORCED POLYMER (CFRP) DOWELS

Erdoğan, Hakan

Ph.D., Department of Civil Engineering

Supervisor: Prof. Dr. Güney Özcebe

Co-Supervisor: Assoc. Prof. Dr. Barış Binici

December 2010, 202 pages

Due to their practical application, flat-plates have been commonly used slab type in constructions in recent years. According to the investigations that were performed since the beginning of the 20th century, the vicinity of the slab-column connection is found to be susceptible to punching failure that causes serious unrepairable damage leading to the collapse of the structures. The objective of this study is to enhance the punching shear strength of slab-column connections in existing deficient flat plate structures. For this purpose, an economical and easy to install strengthening method was applied to $\frac{3}{4}$ scale flat-slab test specimens. The proposed strengthening scheme employs the use of in house-fabricated Carbon Fiber Reinforced Polymer (CFRP) dowels placed around the column stubs in different numbers and arrangements as vertical shear reinforcement. In addition, the effect of column aspect ratio on strengthening method was also investigated in the scope of this study. Strength increase of at least 30% was obtained for the CFRP retrofitted

specimens compared to the companion reference specimen. Three-dimensional finite element analyses of test specimens were conducted by using the general purpose finite element analyses program. 3-D finite element models are successful in providing reasonable estimates of load-deformation behavior and strains. The experimental punching shear capacities and observed failure modes of the specimens were compared with the estimations of strength and failure modes given by punching shear strength provisions of ACI 318-08, Eurocode-2, BS8110-97 and TS500. Necessary modifications were proposed for the existing provisions of punching shear capacity in order to design CFRP upgrading.

Keywords: Carbon Fiber Reinforced Polymer, punching failure, column aspect ratio, finite element analysis.

ÖZ

DÜZ-DÖŞEMELERİN ZIMBALAMA DAYANIMININ KARBON FİBER TAKVİYELİ POLİMER (CFRP) DÜBELLER KULLANILARAK İYİLEŞTİRİLMESİ

Erdoğan, Hakan

Doktora, İnşaat Mühendisliği Bölümü

Tez Yöneticisi: Prof. Dr. Güney Özcebe

Ortak Tez Yöneticisi: Doç. Dr. Barış Binici

Aralık 2010, 202 sayfa

Pratik uygulanma özelliği nedeniyle düz döşemeler, son yıllarda yapılarda sıkça kullanılan bir döşeme tipidir. 20. yüzyıl başından günümüze kadar yapılan araştırmalar sonucunda, düz döşemelerdeki kolon-döşeme birleşim bölgesinin, yapılarda onarılması güç hasarlara neden olan zımbalama göçmesine oldukça müsait olduğu gözlenmiştir. Yapılacak olan bu proje kapsamında, düz döşemeli yapılardaki kolon-döşeme birleşim bölgesi zımbalama dayanımının, Karbon Fiber Takviyeli Polimer (CFRP) malzeme kullanılarak arttırılması hedeflenmektedir. Önerilen güçlendirme yöntemi, laboratuvarında imal edilen Karbon Fiber Takviyeli Polimer (CFRP) dübellerin düşey kesme donatısı olarak kolon etrafına değişik sayı ve diziliş biçimleriyle uygulanmıştır. İlave olarak, kolon dikdörtgenselliğinin, güçlendirme yöntemi üzerindeki etkileri de bu çalışma kapsamında araştırılmıştır. Güçlendirilen numunelerde, güçlendirilmemiş numunelere oranla en az %30'a

varan dayanım artışı elde edilmiştir. Deney numunelerine ait üç boyutlu sonlu eleman analizleri yapılmıştır. Yapılan bu analizlerde, üç boyutlu modellerin, gerçek yük-deplasman ve gerilme davranışlarını makul bir şekilde tahmin edebildiği gözlenmiştir. Deneylerden elde edilen zımbalama kapasitesi değerleri ve gözlenen göçme tipleri, ACI 318-05, Eurocode-2, BS8110-97 ve TS500 yönetmelikleri tarafından önerilen kapasite ve göçme tipleri ile karşılaştırılmıştır. Bahsedilen yönetmeliklere, uygulanan güçlendirme yöntemini de göz önünde bulunduracak şekilde gerekli değişiklik önerilerinde bulunulmuştur.

Anahtar Kelimeler: Karbon fiber takviyeli polimer, zımbalama göçmesi, kolon boyut oranı, sonlu eleman analizi

To my family...

ACKNOWLEDGEMENTS

I would like to express my deepest gratitude to my supervisor Dr. Güney Özcebe and co-supervisor Dr. Barış Binici for their guidance, constructive criticism, enthusiasm and encouragement throughout this research. It is my honor to have opportunity to work with such talented researchers.

I would also like to extend my appreciation to my committee members Dr. Tuğrul Tankut and Dr. Burcu Burak for sharing their experience and knowledge in the field of experimental research, Dr. Şevket Özden for his continuous optimism and valuable contribution to my personality as a researcher and Dr. Stathis N. Bousias for his attendance.

Furthermore I would like to thank Dr. Amir Mirmiran for his collaboration and support during my stay at Florida International University as a visiting researcher.

A special thanks is extended to the staff of the Middle East Technical University Structure Laboratory for their valuable support during the experimental part of this research.

This study is funded by the METU Scientific Research Projects Coordination Grant No: BAP-08-11-DPT2002K120510 which is gratefully acknowledged.

I also want to thank my friends Beyhan Bayhan and Emre Akın for their colleagueship.

I am grateful to my “brother” Erdem Arıkan and “sister” Gökçe Fışkın Arıkan for their family like approach and being magical pills for my homesickness.

My friends Tolgahan Kozbay and Umut Sami Artuk also deserve appreciation for being such kind people.

My sister “Yeliz” and her husband “Murat” deserve my deepest thanks for their love, support and never ending hospitality. Special thanks also go for my cousin “Arzu” and her husband “Murat”. They were always at my side, when I was getting used to the life in Ankara.

Finally, I would like to dedicate this dissertation to my parents “Fatma & Zafer” for their understanding, patience, never ending support and encouragement. Their existence and love makes me feel extra motivated and strong throughout this study and in my life as well.

TABLE OF CONTENTS

ABSTRACT.....	iv
ÖZ	vi
ACKNOWLEDGEMENTS.....	ix
TABLE OF CONTENTS.....	xi
LIST OF TABLES	xv
LIST OF FIGURES	xvii
CHAPTER	
1. INTRODUCTION.....	1
1.1 GENERAL.....	1
1.2 PARAMETERS INFLUENCING THE PUNCHING SHEAR STRENGTH OF FLAT PLATES.....	4
1.2.1 Concrete Strength.....	4
1.2.2 Slab Dimensions.....	5
1.2.3 Tension and Compression Reinforcement	5
1.2.4 Column Shape and Aspect Ratio.....	6
1.2.5 Existence of Openings in the Vicinity of Slab-Column Connection.....	6
1.3 PREVIOUS STUDIES ON PUNCHING FAILURE.....	7
1.3.1 Previous Studies on Retrofitting and Repair of Flat Plates against Punching Failure.....	8
1.4 BUILDING CODE APPROACHES	18
1.4.1 ACI 318 (2008).....	19
1.4.2 Eurocode-2 (2003).....	21
1.4.3 BS8110 (1997).....	22
1.4.4 TS500 (2000).....	22
1.5 OBJECTIVE AND SCOPE OF THE STUDY	23

2. DESCRIPTION OF THE EXPERIMENTAL PROGRAM	26
2.1 GENERAL	26
2.2 MATERIALS	26
2.2.1 Concrete Mix	26
2.2.2 Steel Reinforcement	27
2.2.3 Carbon Fiber Reinforced Polymer (CFRP)	28
2.3 TEST SPECIMENS AND TEST PROCEDURE	31
2.3.1 Specimen Design	31
2.3.2 Control Specimens	34
2.3.3 Strengthening Method and Strengthened Specimen	36
2.3.4 Design of CFRP Dowels	43
2.3.5 Test Parameters	45
2.3.6 Test Setup	47
2.3.7 Instrumentation	49
2.3.8 Testing Procedure	49
3. TEST RESULTS AND DISCUSSIONS	52
3.1 GENERAL	52
3.2 TEST RESULTS	52
3.2.1 Load- Slab Center Deflection Curves	52
3.2.2 Slab Deflection Profiles	61
3.2.3 Longitudinal Steel Strains	61
3.2.4 Crack Patterns and Failure Modes	85
3.3 DISCUSSION OF TEST RESULTS	101
3.3.1 Strength, Stiffness and Ductility	101
3.3.2 Effect of Test Parameters	108
3.3.4 Post-Punching Behavior	110
3.3.5 Comparison of Test Results with the Proposed Models in the Literature	114
3.3.5.1 Model by Menetrey	114
3.3.5.2 Model by Fernandez and Muttoni	116

3.3.5.3 Comparison of Model Predictions with Experimental Results.....	119
4. FINITE ELEMENT ANALYSES.....	121
4.1 GENERAL.....	121
4.2 MATERIAL MODELS.....	121
4.2.1 Concrete Constitutive Model.....	121
4.2.2 Concrete in Compression.....	122
4.2.3 Concrete in Tension.....	124
4.2.4 Shear Behavior.....	125
4.2.5 Steel Reinforcement and CFRP Model.....	126
4.3 MODELING AND ANALYSIS.....	127
4.3.1 Finite Element Mesh.....	127
4.3.2 Iteration Criteria.....	128
4.4 NUMERICAL ANALYSES RESULTS AND COMPARISONS WITH THE EXPERIMENTAL RESULTS.....	129
4.4.1 Principal Stress.....	131
4.4.2 Load-Deflection Comparison.....	134
4.4.3 Longitudinal Steel Strain.....	139
4.4.4 CFRP Strain.....	146
5. EVALUATION OF PUNCHING SHEAR STRENGTH BY USING CODE PROVISIONS.....	149
5.1 GENERAL.....	149
5.2 EXPERIMENTAL DATABASE.....	149
5.2.1 Evaluation of Test Specimens Experiencing Outside Failure.....	163
5.2.2 Evaluation of Test Specimens Experiencing Inside Failure.....	170
5.2.3 Design Procedure.....	176
6. SUMMARY AND CONCLUSIONS.....	186
6.1 SUMMARY.....	186
6.2 CONCLUSIONS.....	187
6.3 RECOMMENDATIONS FOR FUTURE STUDIES.....	189
REFERENCES.....	190
APPENDIX A. DESIGN EXAMPLE FOR INNER SLAB-COLUMN	

CONNECTIONS STRENGTHENED WITH VERTICALLY APPLIED CFRP LAMINATES	197
CURRICULUM VITAE	201

LIST OF TABLES

TABLES

Table 2.1 Concrete mix details.....	27
Table 2.2 Reinforcing steel bar properties.....	28
Table 2.3 Material properties of CFRP and epoxy.....	29
Table 2.4 Coupon test results.....	30
Table 2.5 Design of amount of CFRP.....	44
Table 2.6 Test specimen details.....	45
Table 3.1 Summary of test results.....	54
Table 3.2 Shear crack angles for test specimens with square column stub.....	88
Table 3.3 Shear crack angles for test specimens with rectangular column stub.....	88
Table 3.4 Ductility and stiffness.....	107
Table 3.5 Comparison of model predictions with experimental results.....	120
Table 4.1 Variation of G_{f0} with maximum aggregate size d_{max}	125
Table 4.2 Comparison of experimental FEA results.....	134
Table 5.1 Experimental database.....	150
Table 5.2 Amount of vertically applied CFRP laminates.....	155
Table 5.3 FRP laminate material properties (manufacturer datasheet).....	156
Table 5.4 Comparison of code provisions.....	164
Table 5.5 Comparison of modified code provisions for outside failure.....	169
Table 5.6 Maximum strain values of specimens with outside failure.....	172
Table 5.7 Maximum strain values of specimens with inside failure.....	173
Table 5.8 Summary of FRP and concrete contribution (adopted from Binici 2003).....	174
Table 5.9 Comparison of experimental and design CFRP strains.....	175
Table 5.10 Calculated and experimental punching strength of test specimens	

(TS500).....	178
Table 5.11 Calculated and experimental punching strength of test specimens	
(BS8110).....	179
Table 5.12 Calculated and experimental punching strength of test specimens	
(ACI 318-05).....	180
Table 5.13 Calculated and experimental punching strength of test specimens	
(Eurocode-2).....	181
Table 5.14 Coefficient values for calculation of (w_{\max} / d).....	184

LIST OF FIGURES

FIGURES

Figure 1.1 Punching failure cases.....	3
Figure 1.2 Critical punching perimeter definitions for ACI 318-05 (2005).....	20
Figure 1.3 Critical punching perimeter definitions for Eurocode-2 (2003).....	21
Figure 1.4 Critical punching perimeter definitions for BS8110 (1997).....	22
Figure 1.5 Critical punching perimeter definitions for TS500 (2000).....	23
Figure 2.1 Uniaxial coupon (C3).....	29
Figure 2.2 Stress strain curves of coupon tests.....	30
Figure 2.3 Prototype building.....	32
Figure 2.4 Moment distribution under gravity loading.....	32
Figure 2.5 Steel reinforcement layouts.....	33
Figure 2.6 Yield-Line collapse mechanism.....	34
Figure 2.7 Unstrengthened test specimens (Reference specimens).....	35
Figure 2.8 Column stub reinforcement detailing of specimens R1 and R1-A.....	35
Figure 2.9 View of formwork with the PVC pipes positioned inside.....	37
Figure 2.10 CFRP dowel locations for O-pattern and C-pattern	38
Figure 2.11 Manufacturing process of CFRP dowels.....	39
Figure 2.12 Installation of CFRP dowels through the holes	39
Figure 2.13 Installation of CFRP patches.....	40
Figure 2.14 Fanning out (anchoring) the dowels.....	40
Figure 2.15 Strengthened specimens with CFRP dowels.....	41
Figure 2.16 Assumed punching perimeters for preliminary design.....	44

Figure 2.17 Test matrix	46
Figure 2.18 Test setup and specimen details	48
Figure 2.19 A view of Specimen R1-A before testing	48
Figure 2.20 Instrumentation of test specimens with square column	50
Figure 2.21 Instrumentation of test specimens with rectangular column	50
Figure 2.22 Data acquisition system	51
Figure 3.1 Load-center deflection curve of R1-A	55
Figure 3.2 Load-center deflection curve of R1	55
Figure 3.3 Load-center deflection curve of R2	56
Figure 3.4 Load-center deflection curve of R3	56
Figure 3.5 Load-center deflection curve of OS13	57
Figure 3.6 Load-center deflection curve of OS14	57
Figure 3.7 Load-center deflection curve of OS15	58
Figure 3.8 Load-center deflection curve of CSWOP	58
Figure 3.9 Load-center deflection curve of CSWP	59
Figure 3.10 Load-center deflection curve of OS25	59
Figure 3.11 Load-center deflection curve of OS25-b	60
Figure 3.12 Load-center deflection curve of OS35-b	60
Figure 3.13 Load deflection profiles of R1-A	62
Figure 3.14 Load deflection profiles of R1	63
Figure 3.15 Load deflection profiles of R2	64
Figure 3.16 Load deflection profiles of R3	65
Figure 3.17 Load deflection profiles of OS13	66
Figure 3.18 Load deflection profiles of OS14	67
Figure 3.19 Load deflection profiles of OS15	68
Figure 3.20 Load deflection profiles of CSWOP	69
Figure 3.21 Load deflection profiles of CSWP	70
Figure 3.22 Load deflection profiles of OS25	71
Figure 3.23 Load deflection profiles of OS25-b	72
Figure 3.24 Load deflection profiles of OS35-b	73
Figure 3.25 Load vs strain relationship at column face (strain gage S1) for specimens with square column stub	75

Figure 3.26 Load vs strain relationship at column face in X-direction (strain gage S5) for specimens with column aspect ratio of 2	76
Figure 3.27 Load vs strain relationship at column face in Y-direction (strain gage S1) for specimens with column aspect ratio of 2	76
Figure 3.28 Load vs strain relationship at column face in X-direction (strain gage S5) for specimens with column aspect ratio of 3	77
Figure 3.29 Load vs strain relationship at column face in Y-direction (strain gage S1) for specimens with column aspect ratio of 3	77
Figure 3.30 Top reinforcement strain profile of R1-A	78
Figure 3.31 Top reinforcement strain profile of R1	78
Figure 3.32 Top reinforcement strain profile of OS13	79
Figure 3.33 Top reinforcement strain profile of OS14	79
Figure 3.34 Top reinforcement strain profile of OS15	80
Figure 3.35 Top reinforcement strain profile of CSWOP	80
Figure 3.36 Top reinforcement strain profile of CSWP	81
Figure 3.37 Top reinforcement strain profile of R2	82
Figure 3.38 Top reinforcement strain profile of R3	83
Figure 3.39 Top reinforcement strain profile of OS25	83
Figure 3.40 Top reinforcement strain profile of OS25-b	84
Figure 3.41 Top reinforcement strain profile of OS35-b	84
Figure 3.42 Cutting schemes	87
Figure 3.43 Failure surfaces of and crack patterns of R1-A	89
Figure 3.44 Failure surfaces of and crack patterns of R1	90
Figure 3.45 Failure surfaces of and crack patterns of OS13	91
Figure 3.46 Failure surfaces of and crack patterns of OS14	92
Figure 3.47 Failure surfaces of and crack patterns of OS15	93
Figure 3.48 Failure surfaces of and crack patterns of CSWP	94
Figure 3.49 Failure surfaces of and crack patterns of CSWOP	95
Figure 3.50 Failure surfaces of and crack patterns of R2	96
Figure 3.51 Failure surfaces of and crack patterns of R3	97
Figure 3.52 Failure surfaces of and crack patterns of OS25	98
Figure 3.53 Failure surfaces of and crack patterns of OS25-b	99

Figure 3.54 Failure surfaces of and crack patterns of OS35-b	100
Figure 3.55 Comparison of specimens R1-A and R1	102
Figure 3.56 Comparison of specimens R1, OS13, OS14 and OS15	102
Figure 3.57 Comparison of specimens R1, CSWOP and CSWP	103
Figure 3.58 Comparison of specimens R2, OS25 and OS25-b	104
Figure 3.59 Comparison of specimens R3 and OS35-b	104
Figure 3.60 Effect of column rectangularity on specimen capacities	105
Figure 3.61 Idealized curve definition	103
Figure 3.62 Comparison of displacement ductility	108
Figure 3.63 C-Pattern perimeter definition	110
Figure 3.64 Post-punching capacities of test specimens	111
Figure 3.65 Comparison post punching capacities of test specimens	111
Figure 3.66 Effect of failure locations and strengthening on post-punching capacity	112
Figure 3.67 Representation of punching strength (from Menetrey 1996)	114
Figure 3.68 Punching failure definition (Muttoni 2008)	117
Figure 3.69 Definition of failure inside the shear reinforced zone (2009)	119
Figure 4.1 Loading and unloading regime (DIANA Manual 2005)	122
Figure 4.2 Model for concrete in compression (DIANA Manual 2005)	123
Figure 4.3 Models for concrete in tension (DIANA Manual 2005)	124
Figure 4.4 Modeling of steel reinforcement and CFRP dowels	126
Figure 4.5 Definition of reinforcement in solid element (DIANA Manual 2005)	127
Figure 4.6 Finite element mesh and boundary conditions	128
Figure 4.7 8-node brick element and integration points (DIANA Manual 2005)	128
Figure 4.8 Quasi-Newton Method (DIANA Manual 2005)	129
Figure 4.9 Test setup and reinforcement details (adopted from Binici 2003)	130
Figure 4.10 Strengthening method details (adopted from Binici 2005)	131
Figure 4.11 Principal stress distribution at column corner	132
Figure 4.12 Maximum principal stress distributions (S1)	132
Figure 4.13 Principal stress profiles along column face	133

Figure 4.14 Load-deflection comparisons of specimens tested by Binici (2003).....	135
Figure 4.15 Load-deflection comparisons of specimens R1 and OS15	136
Figure 4.16 Load-deflection comparisons of specimens R3 and OS35-b.....	137
Figure 4.17 Load-deflection comparisons of specimens R2.....	138
Figure 4.18 Deflection contour map at ultimate load (Specimen R1).....	138
Figure 4.19 Comparisons of deflection profiles for specimen R1.....	139
Figure 4.20 Steel strain comparisons for control specimen (Binici 2003).....	140
Figure 4.21 Steel strain comparisons for strengthened specimen (Binici 2003)	141
Figure 4.22 Steel strain comparisons for specimen R1.....	142
Figure 4.23 Steel strain comparisons for specimen OS15	143
Figure 4.24 Steel strain comparisons for specimen R3.....	144
Figure 4.25 Steel strain comparisons for specimen OS35-b.....	145
Figure 4.26 CFRP strains of strengthened specimen at failure (Binici 2003).....	146
Figure 4.27 CFRP strains of specimen OS15 at different load levels.....	147
Figure 4.28 Effect of amount of CFRP per each dowel.....	148
Figure 5.1 Test specimen details adopted from Sissakis (2002).....	152
Figure 5.2 Test specimen details adopted from Binici (2002).....	153
Figure 5.3 Strengthening patterns and punching perimeter definitions	154
Figure 5.4 Distribution of number of specimens in terms of different variables.....	158
Figure 5.5 Amount of strength increase.....	159
Figure 5.6 Flexural capacity to ultimate strength ratio.....	159
Figure 5.7 Effect of s/d ratio on ultimate capacity	160
Figure 5.8 Relationship between reinforcement ratio (ρ) and w/d.....	162
Figure 5.9 Comparison of code estimations and experimental results for the specimens failed outside the strengthened region.....	165
Figure 5.10 Relationship between ϕ_{ACI} and u_o/d ratio.....	166
Figure 5.11 Relationship between ϕ and w/d ratios.....	167
Figure 5.12 Comparison of modified code estimations and experimental results for the specimens failed outside the strengthened region	168

Figure 5.13 Effect of strengthened pattern on failure mode	170
Figure 5.14 Effect of s / d ratio on failure mode.....	171
Figure 5.15 CFRP contribution model (adopted from Binici 2003).....	173
Figure 5.16 Comparison of modified code estimations and experimental results for specimens strengthened with patterns B and C.....	177
Figure 5.17 Parametric study results for design purposes.....	183

CHAPTER 1

INTRODUCTION

1.1 GENERAL

Flat-plate buildings are commonly preferred structural systems for medium to high-rise residential and parking garage constructions due to their financial and functional advantages. The main advantages of this type of construction are low formwork and workmanship cost, less construction duration, high modularity in floor space partitioning and architectural convenience. The eminent disadvantage of flat-plate systems is the possibility of punching failure, which may lead to progressive collapse of the building. Punching failure can be classified as a shear dominant brittle type of failure. Because of its brittle nature, it becomes almost impossible to inspect typical warnings on the structural components prior to failure. Most common reasons that give grounds for failure are;

- i) Poor detailing and inadequate punching shear capacity design.
- ii) Low concrete strength due to poor construction quality or rapid construction and early loading of structure before the concrete reach its adequate strength.
- iii) Undesired and mispredicted additional loading such as earthquakes, hazardous wind loading, devastating effect of fire, change of building use or extension of building by increasing number of storey.

Some of the examples of the reported cases related to partial or total collapse of buildings that are having deficiencies against punching failure are summarized below (Figure 1.1);

- Harbor Cay Condominium, Cocoa Beach, Florida, USA (1981) : Collapse of the building took place during the construction of the fifth floor. Detailed investigations on the collapse of the building indicated that punching failure provisions were not followed in the design stage. Furthermore, unconscious reduction of slab thickness was detected during the construction process. (Kaminetzky 1991)
- Aselsan, Ankara, Turkey (1981) : Sudden punching failure took place during the concrete casting process of second floor. The main reason for collapse of the building was reported as poor concrete quality and early removal of formwork at first floor. (Ersoy et. al. 1981)
- Baybridge Office Plaza, California, USA (1989) : Improper punching design against earthquake loading caused total collapse of the building after the 1989 Loma Prieta Earthquake. (Mitchell et. al. 1990)
- Bullock Department Store California, USA (1994) : Insufficient design of the building could not resist lateral loading caused by Northridge earthquake. (Mitchell et. al. 1995)
- Sampoong Department Store Seoul, South Korea (1995): 500 people were killed due to progressive collapse of the building. The inspections after the failure indicated that the main reason for the collapse of the building is overloading of the fifth floor of the store owing to change of functionality. (Gardner et. al. 2002)
- Underground Car-Parking Building Gretzenbach, Switzerland (2004) : Fire in a residential car park caused deficiency of a slab-column



Harbor Cay Condominium (1981)



Bullock Department Store (1994)



Car-Parking Gretzenbach (2004)

Figure 1.1 Punching failure cases

connection that finally lead to collapse of the roof of the parking garage and killed 7 firefighter. (Muttoni et al. 2005)

- Jaya Supermarket, Selangor Malaysia (2009) : The 35 year old building suddenly collapsed during the demolition process. The heavy machinery (crawler excavator) was located on top of the building and undesired move during demolishment lead to collapse of the building. This is a good example for better understanding the importance of the punching failure, not only at construction stage but also at demolishing stage.

1.2 PARAMETERES INFLUENCING THE PUNCHING SHEAR STRENGTH OF FLAT PLATES

The well-known parameters that influence the punching shear strength of interior slab-column connections are described and discussed below.

1.2.1 Concrete Strength

In the light of previous investigations, one of the major factors that affect the punching resistance of flat plates was described as concrete tensile strength. Preceding research indicate that, exceeding the principal tensile strength of concrete in the vicinity of slab-column connection initiate concrete cracking. The concrete tensile strength is assumed to be proportional to square root of the concrete compressive strength according to majority of the design codes. On the other hand, some researchers claim that using cubic root of concrete compressive strength instead of square root is more reasonable for slabs with f_c values greater than 28 MPa. Thus, it is obvious from the aforementioned relation between the tensile and compressive strength of concrete that any

increase in concrete compressive strength may lead to increase in punching shear resistance and flexural stiffness of the flat plate structures.

1.2.2 Slab Dimensions

The experimental study conducted by Lovrovich and McLean (1990) regarding to the ratio of slab span length to slab effective depth indicated that any decrease of mentioned ratio below three may lead to significant increase in shear strength. In addition, it was observed from the previous experimental studies (Sherif and Dilger 1996, Birkle and Dilger 2008) that increase in slab thickness causes reduction in nominal shear stress resistance of slab-column connections (size effect) that leads to misprediction of code provisions (CSA A23.3-94 and ACI 318-05) for slab thickness values greater than 300 mm. Furthermore, increase in the ratio of column size to slab effective depth ratio result in decrease of punching shear stress of flat-plate members (Moe 1961, Paramasivam and Tan 1993).

1.2.3 Tension and Compression Reinforcement

Use of tension (top) and compression (bottom) reinforcement is recommended by design codes in construction of flat plate members. There are still conflicts among the researchers about the beneficial effects of amount of reinforcement on punching shear behavior. Owing to the experimental studies in the literature, the increase in amount of tension (top) reinforcement leads to increase in punching shear strength of the slab. However, this increase is limited by a certain value of tension (top) reinforcement ratio (Özden 1998). In addition, as the tension (top) reinforcement ratio increases, stiffness of the slab increases and membrane action behavior has considerable effect on the increase of post punching capacity of the slab whereas the ductility and energy absorption capacity decreases. There is an agreement on the fact that the effect

of compression (bottom) reinforcement on punching shear strength of flat plates is negligible. However, the effect of compression (bottom) reinforcement acting as a safety net on post-punching capacity of flat-plate members is significant. On the other hand, detailing of reinforcement may also affect the behavior of the flat-plates in terms of spacing and the size of reinforcing bars.

1.2.4 Column Shape and Aspect Ratio

Punching shear strength of flat-plates also depends on shape and dimensions of the columns. Punching shear strength of flat plates with circular columns is greater than square columns due to nearly uniform stress distribution around the column whereas square columns may have stress concentration near the corners of the columns. Furthermore, the increase of aspect ratio of columns generally decreases the punching shear strength of slabs, due to the variation of shear stress around the column face.

1.2.5 Existence of Openings in the Vicinity of Slab-Column Connection

There are applications of openings on the slabs for different purposes such as electrical, ventilation, heating, sanitary, air conditioning etc. Existence of openings directly affects the punching behavior of flat-plate structures. The studies conducted on existence of openings in the vicinity of slab-column connections indicated significant reduction in terms of punching shear strength. Closeness of openings to the slab-column connection becomes crucial. Main idea of the formulas, generated for slabs with openings, is to reduce the punching perimeter of the slab with respect to existence of openings and distance to the connection to reflect the actual punching behavior of flat plate systems.

1.3 PREVIOUS STUDIES ON PUNCHING FAILURE

Punching shear failure was first investigated by Talbot in 1913. Talbot concentrated on the behavior of single footings. Later on, some other benchmark studies have been conducted by Graf (1933), Richard (1948), Elstner and Hognestad (1956), Whitney (1957), Moe (1961) and Tankut (1969) for better understanding the mechanism of punching failure and implementation of design provisions.

Various techniques have been proposed (column capitals, drop panels, shear reinforcements) in the last four decades to avoid punching failure by increasing the punching shear capacity of the slab-column connections. One of the most practical methods of enhancing punching shear capacity is the installation of vertical shear reinforcement to prevent brittle shear failure and provide a ductile response. In the earlier attempts, steel re-bars were used as vertical shear reinforcement for the new construction. In this context, the use of stirrup shear reinforcement (Graf 1938, Elstner and Hognestad 1956, Carpenter et al. 1970, Broms 1990, Oliviera et al. 2000), shear studs (Dilger and Ghali 1981, Mokhtar et al 1985, Elgabry and Ghali 1987), shearheads (Moe 1961, Anderson 1963, Corley and Hawkins 1968) were the most common applications. It should be noted that use of steel shear reinforcement in the form of stirrups and shear studs are applicable only at the construction stage to enhance punching shear capacity of existing slab-column connections.

In literature, the number of studies that concentrated on the effect of column rectangularity on punching shear capacity of slab-column connections is rather limited (Forsell and Holmberg 1946, Elstner and Hognestad 1956, Mowrer and Vanderbilt 1967, Hawkins et al. 1971, Kuang and Teng 2001, Al Yousif and Regan 2003, Oliviera et al. 2004, Teng et al. 2004).

1.3.1 Previous Studies on Retrofitting and Repair of Flat Plates against Punching Failure

Since the scope of this study covers the strengthening of flat-plates against punching failure, more detailed information is presented related to previous studies conducted on retrofitting and repair of flat plate structures under this caption.

Martinez et al. (1994) studied the repaired performance of post-tensioned slab-connections subjected to biaxial seismic loading. Different repair techniques such as steel-plate bolt, column capital and epoxy repair were implemented to test specimens. Each method provided certain amount of improvement in strength and stiffness with respect to capacity of unstrengthened specimen. Repair methods were discussed and compared in terms of efficiency and the applicability. According to experimental results, implementation of column capital was found to be the most effective method.

Farhey et al. (1995) studied the rehabilitation of flat-slabs that are loaded up to total failure. Four full scale specimens were subjected to reversed cyclic loading and the moment to shear ratio was kept constant during loading process. Fully damaged specimens were repaired by replacing the deteriorated concrete region around the slab-column connection with steel plates and epoxy mortar. Steel plate dimensions, presence of vertical loading and column dimensions were the investigated parameters in the scope of the study. Moment carrying capacity of the rehabilitated connection was upgraded about 4 times that of the capacity of specimen prior to repair. Accordingly, substantial increase was also detected in ductility, stiffness and strength of the repaired specimens compared to specimens without any repair.

Erki and Heffernan (1995) primarily investigated the external application of FRP sheets on tension face of flat slabs for strengthening purposes. One way and two way slab specimens were retrofitted by using unidirectional glass and

carbon fiber reinforced polymer sheets. Effect of orientation of fibers with respect to internal steel reinforcement was also inspected and discussed in this study. Bonding of FRP sheets yielded considerable amount of enhancement in flexural stiffness and punching shear strength by shifting flexural cracking phase to upper load levels.

Hassanzadeh and Sundqvist (1998) performed a series of tests concentrated on external implementation of different strengthening techniques regarding to punching failure of bridge slabs. Upgrading effects of externally installed steel bars, shotcreted column heads, steel collar around the connection were discussed in the scope of the study. All proposed strengthening methods provided considerable amount of enhancement in punching shear capacity of bridge slabs. In terms of applicability, externally applied steel bars were found to be the easiest method to implement.

Ramos et al. (2000) conducted an experimental research focused on repair of flat-slabs by insertion of shear bolts through the thickness of the slab around the slab-column connection. Specimens were subjected to 70% of the failure load before the application of repair method. Effect of different orientations for the location of shear bolts is examined during the experimental study. At least 51% of enhancement was achieved in failure load compared to failure load capacity of unstrengthened specimen.

Robertson and Johnson (2001) undertook an experimental program that mainly focused on repair and strengthening of flat plates having three different types of shear reinforcement. Half scale test specimens were constructed and reinforced considering the ACI 318-63 code regulations. All specimens were subjected to lateral drift before application of any strengthening. After pre-cracking phase, three specimens were strengthened with only epoxy for crack repairing, epoxy plus bonding of CFRP sheets on tension face and epoxy plus CFRP sheets bonding on both faces of the specimen, respectively. The

specimens were again loaded laterally. The second phase results indicated that the initial stiffness of the uncracked specimen cannot be restored by only application of epoxy whereas combined application of epoxy and CFRP sheets on tension face is adequate for restoring the initial stiffness of uncracked specimen. It was also observed that bonding CFRP sheets on compression face of the slabs had no effect on the performance of the slab-column connection. The ultimate load capacities of the strengthened specimens were increased up to 33% of the precracked specimen. In addition, cost effectiveness of proposed strengthening method was also discussed in this study.

Ebead and Marzouk (2002) studied the effects of repair and strengthening of two-way slabs by using steel plates and shear bolts. Steel plates were attached on both surfaces of the specimens and fastened by the help of shear bolts. Before the application of strengthening scheme, specimens were subjected to pre-damage by loading concentrically up to 50% of ultimate capacity of control specimen. Different configurations of steel plates and shear bolt layout were examined to determine the most effective pattern for upgrading the punching shear capacity. The test results revealed that there should not be used at least eight shear bolts should be used for each specimen and minimum thickness of steel plate should be selected as 6 mm. Presence of steel plates considerably increased the flexural rigidity of the specimen, on the other hand, presence of steel bolts played an important role in upgrading the ductility and energy absorption capacities of the strengthened specimens compared to control specimen.

Sissakis (2002) conducted an experimental program that concentrated on strengthening of slab-column connections by external installation of CFRP strands as vertical shear reinforcement. CFRP strands were passed through the holes (similar to stitching process) around the slab-column connection in order to surround and confine the concrete between two adjacent holes. The parameters under consideration were the concrete strength, reinforcement ratio that directly affects the flexural capacity, different patterns of hole layout, hole

spacing and amount of CFRP used for each hole. It was concluded from the experimental work that some of the hole patterns did not provide enough resistance for shear demand and lead to premature failure of the specimens. On the other hand, it is possible to increase the shear strength up to 80% and ductility by a factor of 7 with appropriate hole pattern. An alternative critical shear perimeter definition was also proposed in the light of these test results.

El-Salakawy et al. (2003) investigated the behavior of the slab-column edge connections strengthened with externally installed steel rods and shear bolts through the holes drilled around the connection. Total of six full scale test specimens simulating portion of a typical floor system with three 3.75 m bays were tested. The specimens were subjected to both vertical and horizontal loads through their column stubs. The main parameters studied in the program were the existence of openings, number of rows of steel rods and shear bolts around the slab-column connection. The test results indicated that application of the strengthening method increased the ultimate load capacity and displacement ductility of the test specimens significantly.

Casadei et al. (2003) conducted tests on behavior of flat-slabs with massive openings in the center of the specimens. Three plies of CFRP sheets were bonded on four sides of the openings on the tension face of the specimens to eliminate the shear crack initiation especially through the corner of the openings. A special anchoring method was applied to CFRP in order to clear away the probability of premature failure of CFRP. Authors observed considerable amount of improvement in both stiffness and ultimate load capacity of the strengthened specimens with respect to unstrengthened specimen.

Binici (2003) proposed a strengthening method to enhance the punching shear resistance of flat-plate type floor systems by using carbon fiber reinforced polymer (CFRP). CFRP sheets were cut into strips having 25 mm width and then were put through the holes located around the slab-column connection of

the test specimens by a knitting process to form externally installed closed stirrups. Effect of two different hole orientation on punching shear capacity of specimens was investigated. The amount of CFRP used for each stirrup was controlled by the number of layers wrapped. Two, three and four layers of CFRP strips were wrapped around respectively to decide the design value for CFRP amount. The concrete strength and reinforcement ratio values were kept constant throughout the study. Test specimens were subjected to two different types of loading named as concentric and eccentric loading. Concerning the test results, the author stated that, ultimate load capacity of the test specimens might be increased up to 51% with respect to the reference specimen by applying the proposed strengthening scheme. The behavior of test specimens subjected to eccentric loading indicated that the CFRP strengthening can lead to considerable increase in displacement ductility level and ductile flexural failure can be obtained. The vertical strain values measured on CFRP stirrup legs proved that the limiting strain value, 0.004, proposed by ACI Committee 440 was found to be a reliable threshold value for design purposes.

Harajli and Soudki (2003) investigated the behavior of slab-column connections strengthened with CFRP sheets. The CFRP sheets were bonded on tension face of the test specimens in two perpendicular directions along the full dimension of the specimens. The parameters under investigation were the thickness of the specimens, reinforcement ratio, width of CFRP sheets and number of CFRP layers. The specimens were loaded concentrically through their column stub. According to the test results, considerable amount of increase in flexural strength of the retrofitted specimens was observed, whereas brittle type of shear failure for the strengthened specimens was observed. Existence of CFRP sheets provided up to 45% increase in punching load carrying capacity. The design equation proposed by Mowrer and Vanderbilt (1967) that took into account the flexural capacity was used to make a comparison with experimental results. The equation predictions were in good conformity with the test results since contribution of CFRP sheets to the ultimate capacity was taken into consideration. On the other hand, ACI318-99

and CSA-A23.3 (1994) code predictions were found to be extremely conservative owing to negligence of CFRP sheets.

Robertson and Johnson (2004) conducted an experimental study on seismic performance of slab-column connections retrofitted with CFRP sheets. Half scale test specimens were strengthened by bonding of CFRP sheet on tension face and subjected to reversed cyclic loading to examine the effectiveness of the CFRP retrofitting. The main parameter under investigation was the amount of CFRP sheets. Experimental results stated that the specimen having relatively shorter CFRP sheets experienced a premature failure away from the column face. Application of CFRP sheets increased the lateral load capacity and the stiffness of the specimens compared the control specimen. On the other hand, significant reduction was observed in ductility and lateral drift ratio. Behavior of slab-column connections strengthened with CFRP headed studs under concentric loading was also investigated in the scope of this study. Existence of CFRP headed studs had no significant effect on vertical load capacity of the connections whereas considerable amount of increase in displacement capacity was detected.

El-Salakawy et al. (2004) also conducted an experimental study examining the behavior of edge slab-column connections strengthened with FRP strips only and strengthened with combination of steel bolts and FRP strips. The existence of openings around the slab-column connection was also taken into consideration throughout this study. Type of FRP (glass or carbon) and number of FRP layers are the other investigated parameters. Test specimens were subjected to a combination of vertical and horizontal loading. The ratio of unbalanced moment to vertical shear force was chosen to be 0.3 and kept constant for all tests. The specimens strengthened with only FRP experienced a shear dominant failure mode, however, the use of steel bolts and FRP together lead to change of failure mode from punching to flexure followed by punching. The ultimate shear force predictions recommended by ACI 318-02 and CSA-A23.3 (1994) found to be conservative with respect to experimental results.

Chen and Li (2005) conducted an experimental research focusing on punching shear strength and failure behavior of reinforced concrete slabs strengthened with glass fiber-reinforced polymer (GFRP) laminates. The main objective of the study was to increase the punching shear capacity of the test specimens by external bonding of GFRP sheets to the tension face of the test specimens. The parameters considered were the concrete strength, reinforcement ratio and the number of GFRP layers bonded on the surface. According to the test results, remarkable increase was observed on the specimens that were strengthened with GFRP compared to companion reference specimens. However, the authors stated that the contribution of GFRP to the flexural strength of test specimens may lead to a change in failure mode from ductile to a more brittle one.

Stark et al. (2005) investigated the seismic performance of slab-column connections that were strengthened with externally applied CFRP stirrups. Half scale test specimens were designed according to ACI 318-63 and ACI 318-02 respectively. The strengthening method was inspired from the experimental study of Binici (2003). Prior to application of reversed cyclic load in horizontal direction, specimens were subjected to 90 kN vertical load that corresponds to 40% of the concentric punching capacity. Application of strengthening technique lead to substantial amount of increase in means of lateral displacement ductility, lateral load capacity and accordingly dissipated energy with respect to reference specimens. Presence of CFRP stirrups did not affect the initial lateral stiffness of the specimens significantly. Stiffness degradation was inhibited for higher values of lateral drift ratio for the strengthened specimens compared to control specimens.

Adetifa and Polak (2005) investigated the behavior of inner slab-column connections strengthened with externally installed shear bolts and subjected to concentric loading. Two, three and four rows of shear bolts were arranged in double rail configuration along four sides of the column for strengthening purposes. In addition, efficiency of the strengthening method was also

examined for the slabs with openings. Implementation of shear bolts provided significant enhancement in shear strength, displacement capacity due to prevention against shear crack propagation. Enlarging the area of strengthened region by increasing the number of shear bolt rows resulted in gradual increase in load carrying capacity up to a certain level that corresponds to flexural capacity. Beyond the flexural strength limit increasing the number of rows of shear bolt mainly enhanced the displacement capacity without having much influence on the load carrying capacity. Presence of openings in the vicinity of the column had a detrimental effect on punching shear strength of the connection.

Sharaf et al. (2006) tested full scale flat-plate specimens to investigate the effects of retrofitting with CFRP strips. The major parameters under investigation were the amount and the orientation of the CFRP strips that were bonded on the tension face of the specimens. Substantial contribution to flexural capacity of test specimens was assured by implementation of externally bonded CFRP strips. In addition, flexural rigidity of strengthened specimens considerably increased. Analytical model developed by Harajli and Soudki (2003) was modified in order to consider the effects of proposed strengthening method by means of amount and spacing of CFRP strips. The analytical model gives more accurate results compared to predictions of design codes (CSA-A23.3 1994, ACI 318-99, BS8110-97).

Harajli et al. (2006) developed a new strengthening method to enhance the performance of slab-column connections by combined implementation of FRP sheets and steel bolts. Since it was known from the previous studies (Ebead and Marzouk 2002, El Salakawy et al. 2003, 2004, Adetife and Polak 2005) that shear bolts are effective in increasing the punching shear capacity whereas bonding FRP sheets on the tension face of the slabs are useful for enhancing the flexural rigidity, the authors decided to improve both punching shear capacity and flexural strength by applying the two methods simultaneously. Effect of steel reinforcement ratio, slab thickness, shear bolt area and

configuration and amount of FRP reinforcement are inspected during the experimental course. Additional increase in shear capacity was obtained by combined implementation of shear bolts and FRP sheets compared to single application of either FRP or shear bolts. The test specimens strengthened with combined method failed in a less ductile manner with respect to retrofitted specimens with shear bolts only. The ACI and CSA code predictions were found to be conservative for the test specimens since the effect of flexural strength on the punching shear capacity was not considered. Therefore, a design approach that takes into account the effects of aforementioned combined strengthening scheme was proposed. The analytical data and experimental observations were found to be very close to each other.

Rochdi et al. (2006) conducted an analytical and experimental study for external implementation of CFRP on tensile surface of two way concrete slabs. The model proposed by Menetrey (1996) was modified and expanded to account for contribution of CFRP component to vertical shear carrying capacity. In addition, finite element models were constructed for better understanding of the state of stress in CFRP material. A series of experiments with varying thickness of CFRP were performed to verify the proposed model. The test results are good indicators for applicability of the proposed model for predicting the punching load capacity of slab-column connections.

Widianto (2006) conducted an experimental study that focused on the seismic response of slab-column connections that were pre-damaged by seismic loading prior to strengthening. Effect of three different rehabilitation methods on the seismic behavior of slab-column connections was discussed. Pre-damaged specimens were repaired with external installation of CFRP stirrup, CFRP sheets anchored on tension side of the specimens and steel column collar respectively. Two different reinforcement ratios used to determine the influence of flexural capacity on the behavior. All three repairing methods found to be efficient for increasing the punching strength and the residual capacity of the specimens. Application of the CFRP stirrups is the most

effective method for upgrading the ductility and energy absorption capacity. On the other hand, well anchored CFRP sheets were found to be useful for increasing the shear strength of lightly reinforced slabs. According to test results, the authors claimed that the effect of seismic pre-damage of 1.25% lateral drift has no significant effect on the shear strength of lightly reinforced slabs.

Michel et al (2007) carried out an experimental and analytical study focused on external bonding of CFRP on flat-plate structures. Equally spaced CFRP strips having identical width were bonded continuously in two orthogonal directions to form a mesh on tension face of the test specimens. Total of four specimens were tested during the experimental program. One of the test specimens was a reference specimen without any strengthening. Another specimen was strengthened by using the aforementioned method with only one layer of CFRP. Third specimen was loaded up to a certain level and pre-cracked before strengthening and then strengthened with one layer of CFRP and the last specimen was strengthened with three layers of CFRP. Test results indicated that the flexural rigidity of the strengthened specimens (including the pre-cracked specimen) tended to increase with respect to reference specimen. Owing to the increase in flexural rigidity the displacement values reduced significantly. On the other hand, ultimate load capacity values increased up to 25% compared to reference specimen. In the analytical part, authors proposed specific modifications on the punching failure criterion method by Menetrey (1996) to account for contribution of CFRP material bonded on the tension surface. The experimental results are predicted by the proposed analytical method with a deviation up to 15%.

Bu and Polak (2009) performed another investigation on application of shear bolts for shear strengthening of interior slab-column connections. Apart from the previous studies (El Salakawy et. al 2003, 2004, Adetife and Polak 2005) focused on shear bolt strengthening technique, the authors tested five specimens under vertical (gravity load) and reversed cyclic horizontal (seismic

load) loading. Existence of shear bolts in the vicinity of slab-column connection significantly increased the peak lateral load capacity, drift ratio, amount of dissipated energy. Furthermore, the failure mode of the connection was converted from brittle shear failure to ductile flexural failure by application of shear bolts.

1.4 BUILDING CODE APPROACHES

The punching load carrying capacity provisions of four different building codes (ACI 318 2008, Eurocode-2 2003, BS8110-97 1997, TS500 2000) for interior slab-column connections with and without shear reinforcement are presented in this section. The general expression for calculating the capacity of flat plates without any shear reinforcement consists of product of nominal shear stress, critical perimeter and effective depth for all four codes (Equation 1.1). However each code shows variety on definition of punching perimeter and nominal shear stress. The design load capacity, V_d , of flat plates without any shear reinforcement is generally defined as follows;

$$V_d = v u d \quad (1.1)$$

where v is the nominal shear stress of slab-column connection, u is the punching perimeter defined for slabs without shear reinforcement, and d is the effective depth of the slab.

Two different capacities were defined for slabs with shear reinforcement depending on the failure modes whether inside or outside the shear reinforced region. The punching shear capacity can be decided as the smallest of the capacity inside, (V_i) and outside (V_o) the shear reinforced zone. The capacity outside the shear reinforced region V_o is evaluated by the help of Equation 1.1. The definition of the punching perimeter u , however, changes depending on the

shear reinforcement arrangement. The capacity inside the shear reinforced region is generally calculated by the following equation for all the codes.

$$V_i = V_c + V_s \quad (1.2)$$

where V_c and V_s are the concrete and shear reinforcement contributions to the punching capacity of the slab respectively. Each code has different definitions for V_c and V_s .

1.4.1 ACI 318 (2008)

ACI 318-08 defines the nominal shear stress (v) as the minimum of the three expressions given in Equation 1.3. Those three equations consider the effects of the column rectangularity, location of the connection and the loading area to effective thickness ratio on the nominal shear stress. Critical punching perimeter was assumed be located $d/2$ away from the column face as shown in Figure 1.2 and expressed in Equation 1.4.

$$v = \text{minimum of} \begin{cases} 0.33\sqrt{f'_c} \\ 0.083\sqrt{f'_c} \left(2 + \frac{4}{\beta_c} \right) \\ 0.083\sqrt{f'_c} \left(2 + \frac{\alpha d}{u} \right) \end{cases} \quad (\text{SI units}) \quad (1.3)$$

$$u = 2(c_1 + c_2 + 2d) \quad (1.4)$$

where f'_c is the concrete compressive strength, β_c is the column aspect ratio, α is the coefficient depending on the location of the connection ($\alpha = 20$ for corner columns; 30 for edge columns; 40 for interior columns), u is the punching perimeter defined in Equation 1.4 and Figure 1.2, c_l is the long side

length of the column, c_2 is the short side length of the column d is the effective depth of slab.

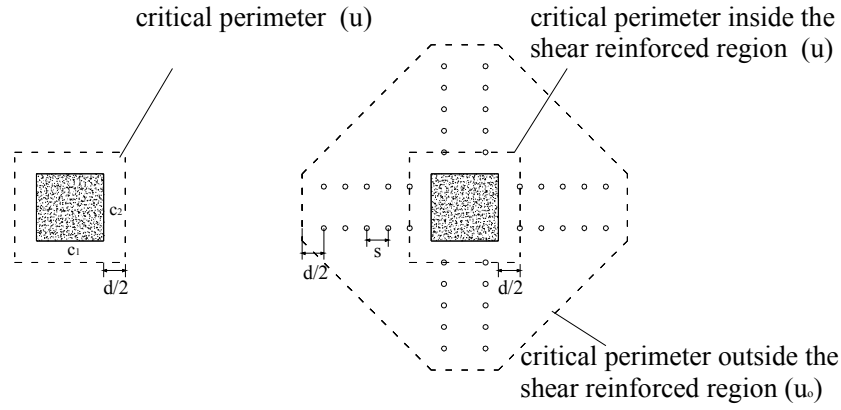


Figure 1.2 Critical punching perimeter definitions for ACI 318-08

The vertical load carrying capacity outside the shear reinforced region V_o for the flat plate members with shear reinforcement can also be calculated by the help of Equation 1.3 and 1.4 by using the critical perimeter definition (u_o) given in Figure 1.2. On the other hand, the capacity inside the shear reinforced region (V_i) can be expressed as;

$$V_i = 0.167\sqrt{f_c}ud + A_{sv}f_{yv}\frac{d}{s} \quad (\text{SI units}) \quad (1.5)$$

where f_c is the compressive strength of the concrete, u is the punching perimeter defined for slab-column connections without any shear strengthening, d is the effective depth, A_{sv} is the total area of the shear reinforcement in one perimeter, f_{yv} is the yield strength of shear reinforcement and s is the spacing of vertical shear reinforcement.

1.4.2 Eurocode-2 (2003)

The nominal shear stress definition in Eurocode-2 take into account the effect of reinforcement ratio and size effect by given expression below;

$$v = 0.18 \left(1 + (200/d)^{1/2} \right) (100 \rho f_c)^{1/3} \quad (1.6)$$

$$u = 2(c_1 + c_2 + 2\pi d) \quad (1.7)$$

where ρ is the reinforcement ratio, u is the critical punching perimeter located $2d$ away from column face defined in Equation 1.7 and given in Figure 1.3, f_c , c_1 , c_2 and d were previously defined in Equations 1.3 and 1.4.

The punching capacity inside the shear reinforced zone is defined as follows in Eurocode-2 ;

$$V_i = 0.75V_d + 1.5A_{sv}f_{yv} \frac{d}{s} \quad (1.8)$$

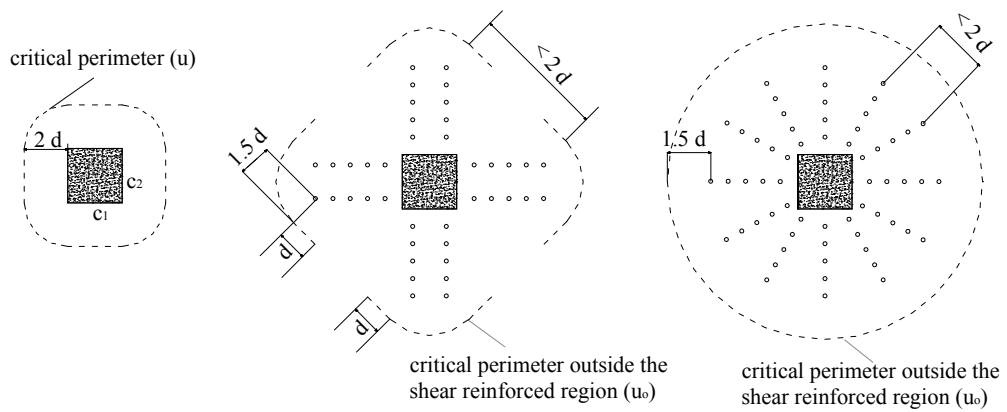


Figure 1.3 Critical punching perimeter definitions for Eurocode-2 (2003)

1.4.3 BS 8110 (1997)

Apart from ACI318-08 and similar to Eurocode-2, nominal shear stress was expressed with cubic root of concrete compressive stress instead of square root and reinforcement and size effect parameters are also considered as given below;

$$v = 0.29(100\rho f_c)^{1/3}(400/d)^{1/4} \quad (1.9)$$

$$u = 2(c_1 + c_2 + 6d) \quad (1.10)$$

$$V_i = V_d + \sum A_{sv} f_{yv} \quad (1.11)$$

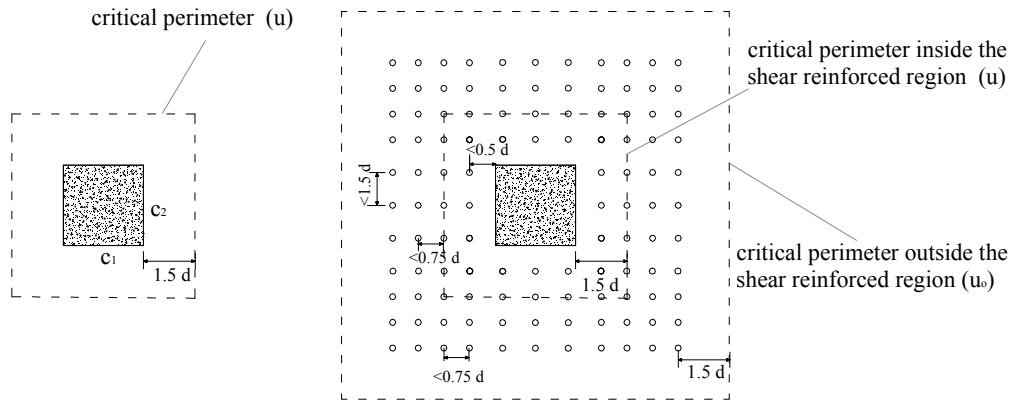


Figure 1.4 Critical punching perimeter definitions for BS8110 (1997)

1.4.4 TS 500 (2000)

Turkish building code (TS500) uses almost similar concept as ACI 318-08 for description of ultimate load carrying capacity against punching failure by neglecting the effects of reinforcement ratio and size effect. In addition, the

location of critical punching perimeter is defined $d/2$ away from the column surface as shown in Figure 1.5. The effect of column rectangularity on punching strength was accounted by reducing the punching perimeter as shown in Figure 1.5. Contrary to other three codes, no specific regulations were offered for flat- plate structures with shear reinforcement in TS500.

$$v = 0.35\sqrt{f_c} \quad (1.9)$$

$$u = 2(c_1 + c_2 + 2d) \quad (1.10)$$

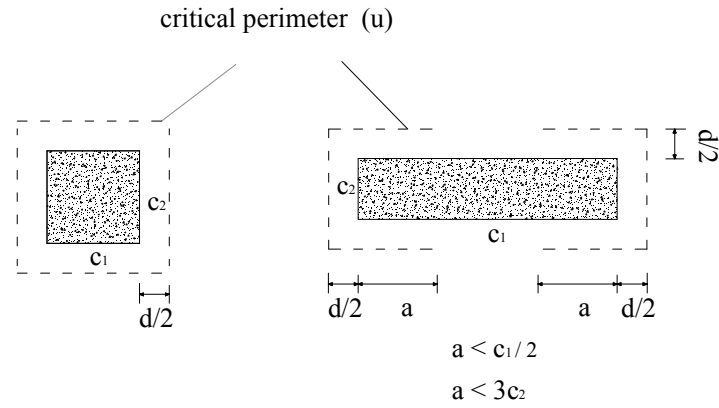


Figure 1.5 Critical punching perimeter definitions for TS-500 (2000)

1.5 OBJECTIVE AND SCOPE OF THE STUDY

The literature review reveals that there are mainly two approaches in the research community to enhance punching shear strength. First one is the use of FRPs bonded on the tension side to increase punching shear strength perhaps in an indirect way (Erki and Heffernan 1995, Tan 1996, Chen and Li 2000, Wang and Tan 2001, Casadei et al. 2003, Harajli and Soudki 2003, Robertson and Johnson 2001, 2004, Rochdi 2004, Chen and Li 2005, Sharaf et al 2006, Michel et al. 2006). Second approach is the installation of vertical

reinforcement either made of FRPs or bolts (Martinez et al 1994, Ramos et al. 2000, Ebead and Marzouk 2002, Sissakis 2002, Binici 2003, El-Salakawy et al. 2003, 2004, Stark et al 2005, Adetifa and Polak 2005, Harajli et al 2006, Widiyanto 2009). Among these two alternatives, second one is more viable as it is a direct approach in holding the inclined cracked region intact.

Based on these arguments, this thesis evolves around approach with the aim of proposing a more practical and economical FRP retrofit method. It is believed that the proposed method would require the use of lower amount of fiber reinforced polymer and speed up the retrofit intervention without sacrificing from obtainable strength increase. In this way more economical retrofit design can be performed for slab-column connections. In addition to experimental program, a series of 3-D nonlinear finite element analyses were performed for the test specimens used in this study and those reported in the literature for better understanding the punching failure mechanism and estimate the behavior of test specimens to predict the ultimate load carrying capacity and effectiveness of the strengthening scheme.

In experimental part of this study, isolated portion of the interior slab-column connections were tested under concentric loading. Behavior of edge and corner slab-column connections and existence of openings in the vicinity of the slab connection are outside of the scope of this study. The dimension of the test specimens and amount of longitudinal steel were kept constant throughout the experimental session whereas column dimensions exhibit variety owing to purpose of parametric study. The investigated parameters can be categorized into four main groups named as CFRP dowel pattern (the localization of CFPP dowels around the slab-column connection), the amount of CFRP dowel (in means of number of CFRP dowels), column aspect ratio and finally the application and detailing of strengthening scheme. The experimental results were evaluated in terms of ultimate punching load, post-punching capacity, slab center deflection capacity, longitudinal steel strain, crack propagation and shear crack inclination.

Finally, the experimental and numerical simulation results regarding to punching shear capacities and observed failure modes of the specimens were compared with the estimations of strength and failure modes given by punching shear strength provisions of four different concrete design codes (ACI 318 2008, Eurocode-2 2003, BS8110 1997, TS500 2000) and applicability of the FRP design strain limit given by ACI440 is examined.

CHAPTER 2

DESCRIPTION OF THE EXPERIMENTAL PROGRAM

2.1 GENERAL

The experimental program mainly focused on the effects of the proposed strengthening method on punching failure of inner slab-connections. The dimensions of the test specimens are kept constant excluding the column dimensions for some of the specimens. The effect of varying column aspect ratio on punching shear strength is one of the main parameters investigated during the experimental work. Total of 12 specimens having identical reinforcement arrangements were tested under monotonically applied concentric loading. The control specimens were designed such a way to ensure shear failure in order to examine the effectiveness of the retrofitting. A new installation method was also proposed for FRPs and its effectiveness was investigated.

2.2 MATERIALS

2.2.1 Concrete Mix

The target compressive strength for concrete was designed to be 30 MPa. Three different aggregate size bands were used in the concrete mix named as fine (0-3 mm), intermediate (3-7 mm) and coarse aggregate (7-15 mm)

respectively. Standard Portland Cement (PC-32.5) was chosen as the binder for concrete mix. Workability of the concrete during casting was increased by addition of superplasticizer. The concrete mix was prepared in a mixer with a capacity of 500 kg. Four sets of 500 kg concrete mix were composed together to finalize casting process of each slab. Total of 12 standard cylinder samples having dimensions of 150 mm diameter and 300 mm height were cast (three samples for each set of concrete mix) to determine test day strength of specimens. Concrete mix design details and percentages of components are tabulated in Table 2.1

Table 2.1 Concrete mix details

Component	Weight (kg)	Percentage (%)
Fine aggregate (0-3 mm)	152.5	30.5
Intermediate aggregate (3-7mm)	137.5	27.5
Coarse aggregate (7-15 mm)	77.5	15.5
Cement	91.5	18.3
Water	40	8
Superplasticizer	1	0.2
Total	500	100

2.2.2 Steel Reinforcement

Three different sizes of steel reinforcing bars having diameters of 10 mm, 12 mm and 16 mm respectively were used during construction of test specimens. In order to determine the characteristics of reinforcing steel bars, randomly chosen six samples having length of 40 cm for each type of reinforcing bars were tested in uniaxial testing machine at Materials Laboratory (METU). The results regarding to average material properties of steel reinforcing bars are presented in Table 2.2.

Table 2.2 Reinforcing steel bar properties

Steel bar diameter (mm)	Elasticity Modulus (MPa)	Yield stress (MPa)	Yield stain	Ultimate tensile stress (MPa)	Ultimate tensile strain
10	195000	430	0.0022	624	0.21
12	195000	426	0.0022	661	0.19
16	195000	448	0.0023	692	0.21

2.2.3 Carbon Fiber Reinforced Polymer (CFRP)

High strength unidirectional CFRP sheet is employed as the strengthening material throughout the experimental program. For the impregnation process, the two-component structural epoxy resin, part A and B, are mixed using manufacturer specified weight ratios (0.25:0.75). Afterwards epoxy mix is wiped on both faces of CFRP sheets prior to installation of the CFRP composite. The material properties of CFRP and epoxy resin reported by the manufacturer are summarized in Table 2.3. Since material properties of CFRP sheets impregnated with epoxy may be different than that of the composite, four uniaxial coupon tests were performed. CFRP sheets were cut into strips having dimensions of 25 mm x 250 mm x 0.165 mm and then impregnated with epoxy resin. After the curing process, the thickness of hardened CFRP + epoxy composite coupons was measured. This thickness of the coupon specimens was 0.8 mm. Coupons were placed in the uniaxial testing machine as shown in Figure 2.1. Longitudinal strains were measured during testing by a strain gauge attached at the center of coupons. Experimental stress-strain curves obtained from coupon tests are illustrated by the graph in Figure 2.2. The material properties of composite (CFRP + epoxy) obtained from uniaxial tests are summarized in Table 2.4. It should be noted that, specimens C1 and C4 failed close to clamp point due to stress concentration and specimen C2 did

not experience any rupture due to slip at clamp points. On the other hand, specimen C3 failed in an ideal manner that the rupture occurring just in the middle of the specimens as shown in Figure 2.1. Therefore, it is recommended to consider the results of specimen C3.

Table 2.3 Material properties of CFRP and epoxy

Component	Elasticity Modulus (MPa)	Ultimate Tensile Stress (MPa)	Ultimate Tensile Strain
CFRP	230000	3450	0.015
Epoxy	3000	50	0.025

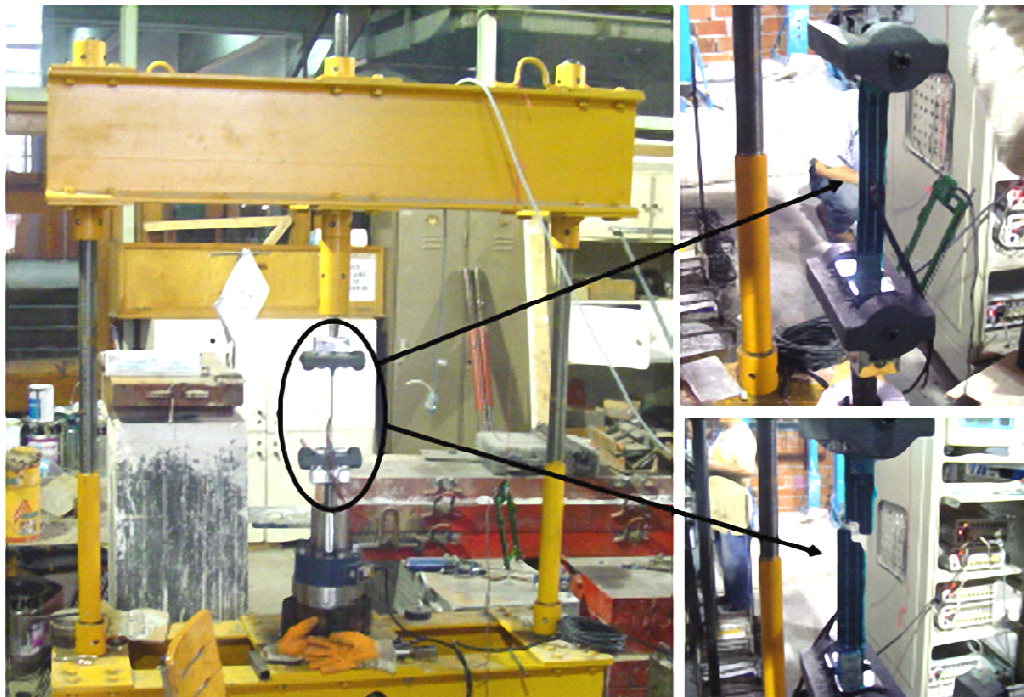


Figure 2.1 Uniaxial coupon test (C3)

Table 2.4 Coupon test results

Coupon Specimen	Ultimate Load (kN)	Ultimate Strain	Ultimate Stress (MPa)	Elasticity Modulus (MPa)	Thickness
C1	1211	0.0083	606	72800	0.8
C2	934	0.006	467	75500	0.8
C3	1274	0.0088	637	72400	0.8
C4	1237	0.0084	618	74000	0.8

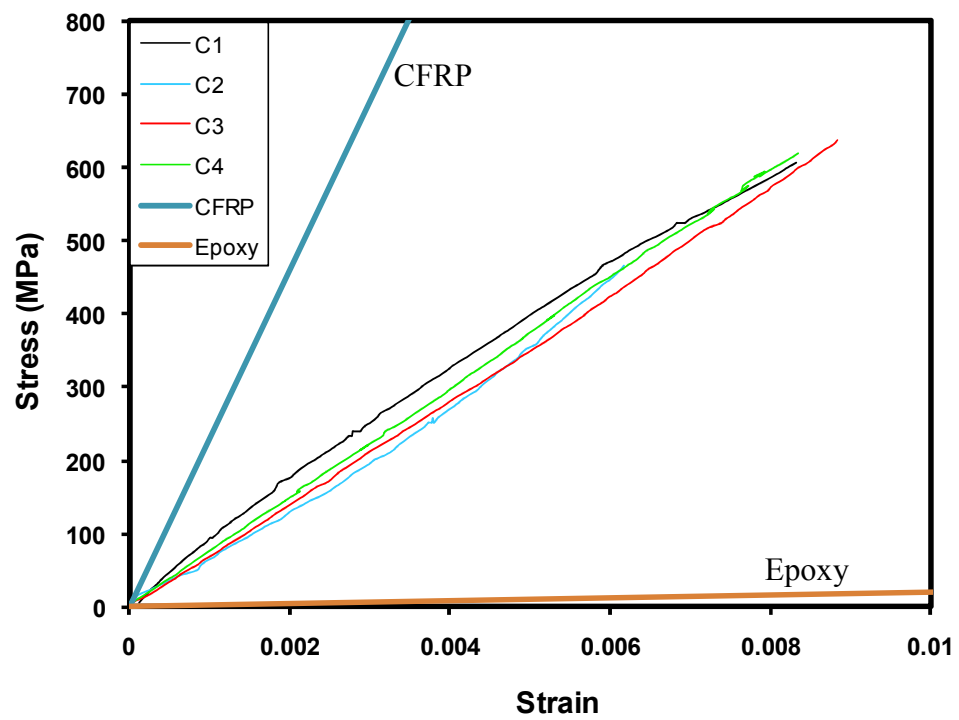


Figure 2.2 Stress-strain curves of coupon tests

2.3 TEST SPECIMENS AND TEST PROCEDURE

The test setup and test specimen details were inspired from a study performed by Niksarlıoğlu (1998) at METU Structural Laboratory.

2.3.1 Specimen Design

A prototype flat plate floor system supported on columns was designed under uniform gravity loads to decide on the specimen dimensions (Figure 2.3). The flat plate floor has 5 bays in both directions with a span of 6 m. The linear elastic analysis results showed that for a typical interior slab-column connection, the dimensions of the area bounded by lines of contraflexure has dimensions of about 0.4 times the bay width (Figure 2.4). Upon scaling the dimensions of this region by 3/4, test specimen having dimensions of 2000 x 2000 x 150 mm, bounded by lines of zero bending moment were obtained. Such dimensions for test specimens were commonly employed in the literature (Elstner and Hognestad 1956, Dilger and Ghali 1981, Mokhtar et al 1985, Elgabry and Ghali 1987, Broms 1990, Sissakis 2002, Binici 2003). The reinforcement ratio (ρ) of the test specimen was intentionally selected to be relatively high compared to code provisions in order to assure punching failure for the specimens without any retrofitting.

Steel reinforcement layout is identical for all test specimens. Top reinforcement of the test specimens consisted of 16 mm bars at 120 mm equal spacing in the two orthogonal directions of specimens with 20 mm clear cover which corresponds to 1.4% of reinforcement ratio. Half of top reinforcement (0.7%) is provided as bottom reinforcement consisting of 12 mm bars at 150 mm equal spacing in the two orthogonal directions of specimens with 25 mm clear cover (Figure 2.5).

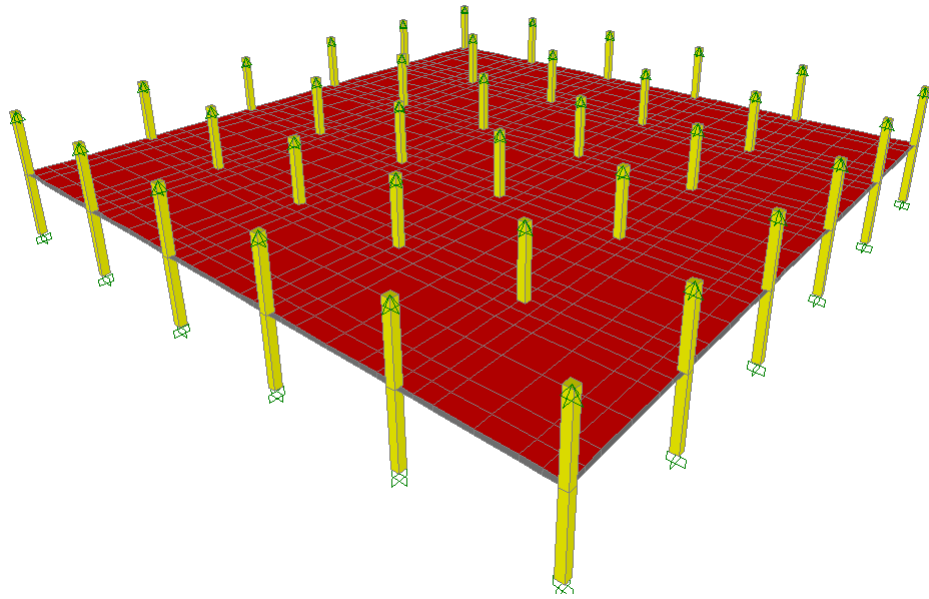


Figure 2.3 Prototype building

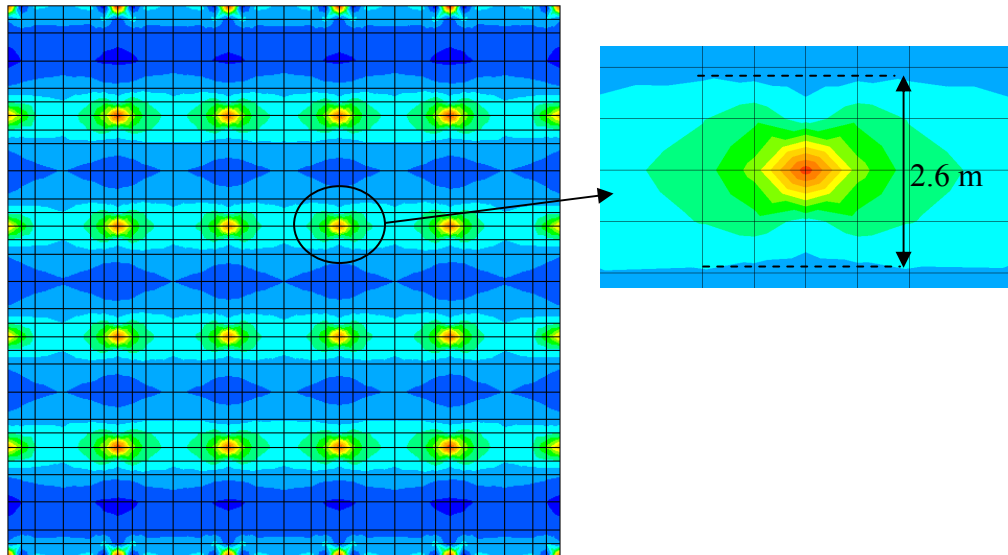


Figure 2.4 Moment distribution under gravity loading

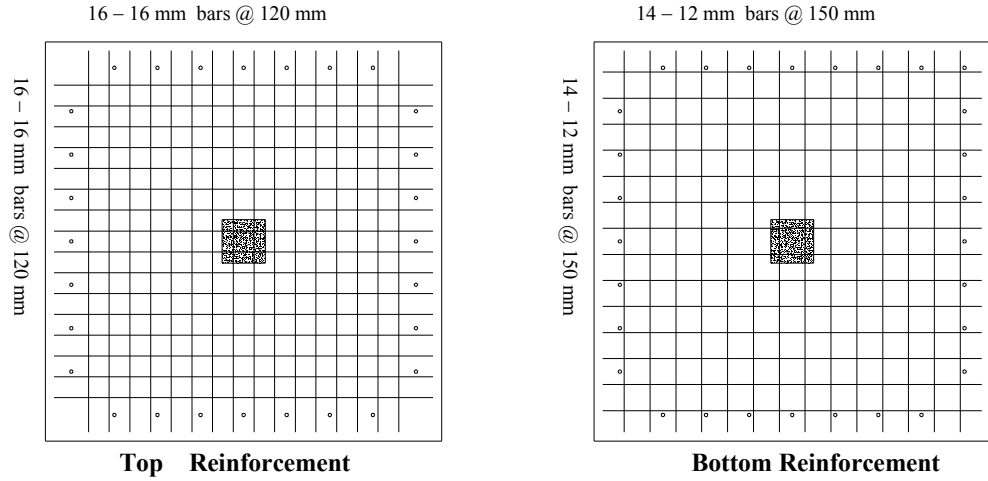


Figure 2.5 Steel reinforcement layouts

The flexural capacity of test specimens, V_{flex} , was calculated by adopting the yield line theory (Elstner and Hognestad 1956) for the collapse mechanism shown in Figure 2.6. This mechanism accounts for the uplift movement of the corners and also shape of supporting column. In order to determine V_{flex} values for each specimen, work method was utilized simply by equating the potential energy caused by vertical load (V_{flex}) to the dissipated energy by yield lines of proposed collapse mechanism. The minimum value of V_{flex} was determined as the proposed flexural capacity of test specimens such that x and y values result in the minimum potential energy (the distances between the column corner and axis of rotation on two orthogonal directions) in governing Equation 2.1.

Potential Energy = Dissipated Energy :

$$V_{flex} = 2m(L - 2y)\left(\frac{2}{L - c_1}\right) + 2m(L - 2x)\left(\frac{2}{L - c_2}\right) + 4m\left(\sqrt{x^2 + y^2}\right)n \quad (2.1)$$

where m is the moment capacity of the slab per unit width, L is the span length of the square slab, c_1 is the short side length of the supporting column, c_2 is the long side length of the supporting column, n is the bisecting line length.

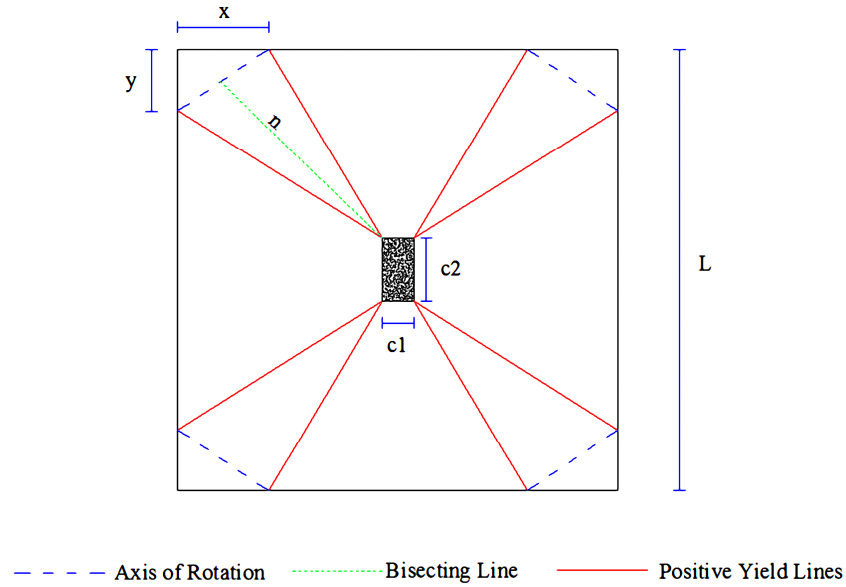


Figure 2.6 Yield-Line collapse mechanism

Total of 12 specimens were tested to investigate the punching shear failure behavior of flat slab structures. Test specimens can be classified into two main groups depending on whether they were strengthened with CFRP material or not.

2.3.2 Control Specimens

First group consisted of four control specimens without any strengthening application (Figure 2.7). One of the control specimens, R1-A, was the only specimen cast with a single column stub extending downwards from the compression face of the slab to simulate the flat plate of a top story. The longitudinal reinforcement of the column stub for this specimen was bent 90° and anchored into the slab (Figure 2.8). The second control specimen R1 was cast with two column stubs extending from both faces of the slab in order to mimic the behavior of intermediate floors in a flat plate structure. The column stubs of specimens R1-A and R1 had 250 mm by 250 mm square cross-sections. The clear height of column stubs was 300 mm. Other two control

specimens R2 and R3 had rectangular column stubs with column aspect ratios of 2 and 3 respectively. The column section dimensions of specimens R2 and R3 were designed to be 167 x 333 mm and 125 x 375 mm in order to have constant column perimeter value of 1000 mm that is also equal to column perimeter of specimen R1 having square column stub (Figure 2.7).

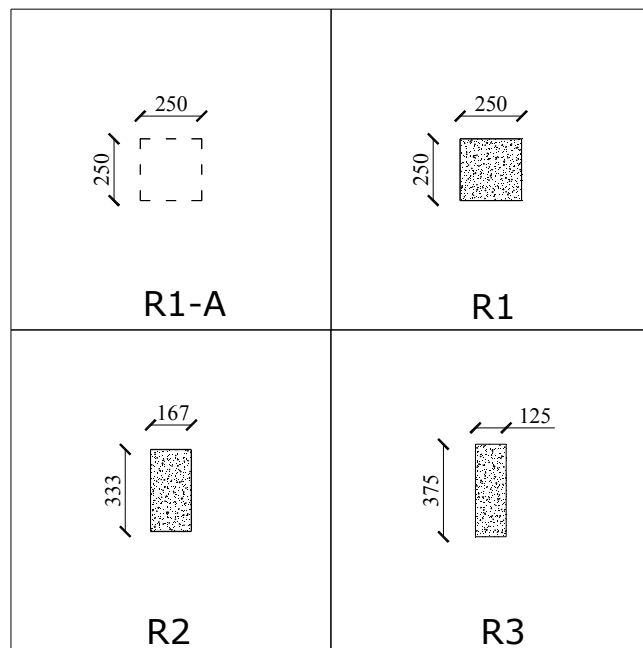


Figure 2.7 Unstrengthened test specimens (Reference specimens)

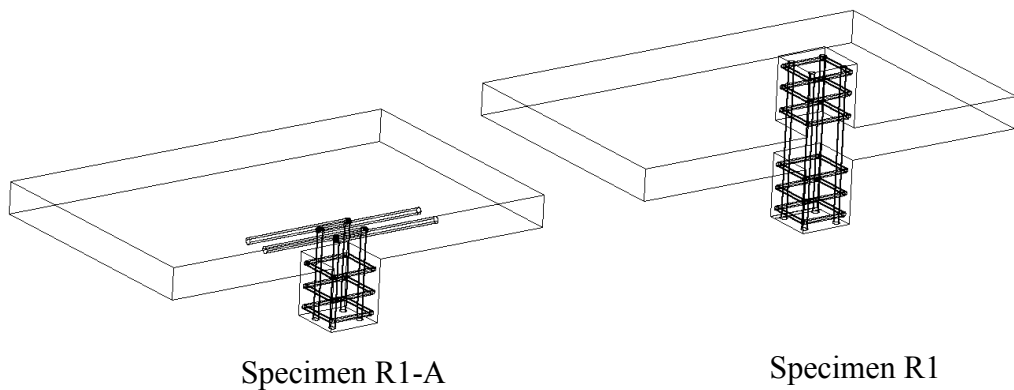


Figure 2.8 Column stub reinforcement detailing of specimens R1-A and R1

2.3.3 Strengthening Method and Strengthened Specimens

The main idea of proposed strengthening method was to apply in-house CFRP dowels as vertical shear reinforcement through the slab depth to provide resistance in the vertical direction after the initiation of the inclined punching shear crack.

Two different techniques were used to create the dowel-holes for CFRP dowel installation. In the first approach, PVC pipes having outer diameter of 14 mm and height of 150 mm were placed around the column stub before casting and were removed after casting prior to CFRP dowel installation. Afterwards, edges of the holes were blunted to avoid premature rupture of CFRP dowels at sharp locations. These steps simulate in fact the drilling and smoothening of the holes in an actual flat plate for strengthening purposes. In laboratory conditions, creating hole reservations by using PVC pipes were found much more practical. The drilling technique was only used in one of the specimens to have an opportunity to make comparison between the two methods. While drilling was performed; extreme care was taken in order not to damage longitudinal reinforcing steel and cover concrete in the vicinity of the dowel-hole locations. After completing the drilling operation, the sharp edges of the holes were blunted similarly. By comparing the two approaches it was confirmed that use of PVC pipes to simulate drilling of holes is an acceptable method for testing purposes as long as longitudinal reinforcement is not damaged during the drilling operation. The positioned PVC pipes in formwork were represented in Figure 2.9

A similar method of creating holes with PVC pipes before casting for test specimens was also used in previous studies (Sissakis 2002, Binici 2003). In those studies it was noted that creating hole reservations with PVC pipes was found to be convenient for specimen preparation purposes and had no influence on the behavior of specimens due to this difference.

Two different strengthening patterns regarding to location of CFRP dowel holes was studied (Figure 2.10). The first pattern was similar to traditional applications of stirrups and shear studs used as shear reinforcement for flat slabs. CFRP dowels were arranged in double rail configuration along four sides of the column stub as shown in Figure 2.10. This pattern was simply named as “O-pattern” since the dowels are located orthogonal to four sides of the column stub. The spacing of vertical CFRP dowels was 60 mm, which was nearly equal to half of the effective depth of the slab to ensure that dowels are effective for a crack having an inclination angle of 45 degrees.

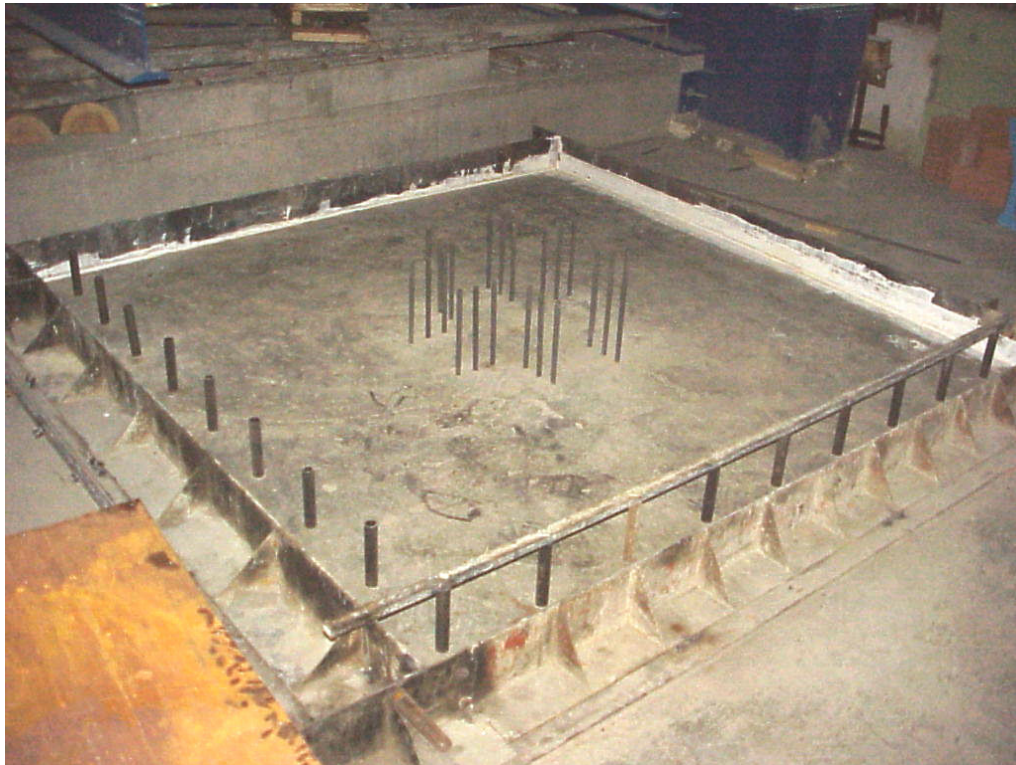


Figure 2.9 View of formwork with the PVC pipes positioned inside

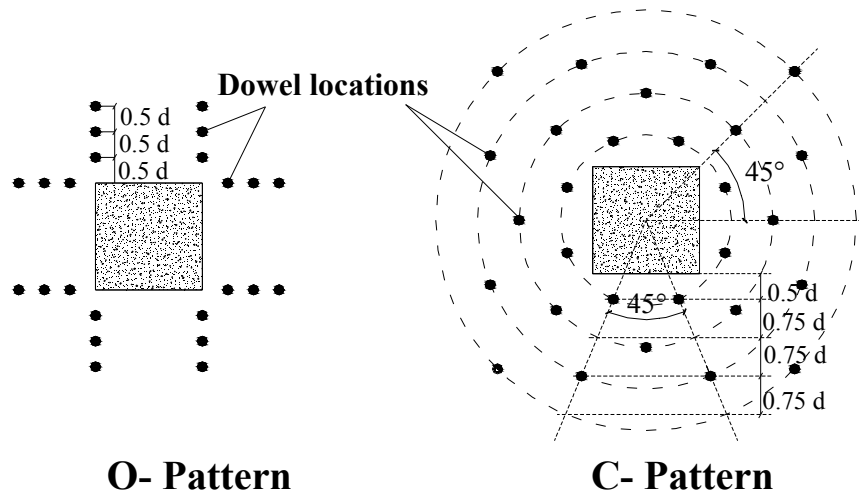


Figure 2.10 CFRP dowel locations for O-pattern and C-pattern

In the second pattern, it was decided to use CFRP dowels in a circular pattern formed by four concentric circles. The radial spacing of CFRP dowels for specimens had a circular dowel arrangement as presented in Figure 2.10. This pattern was simply named as “C- pattern”. The spacing between the CFRP dowels follow the recommendations of ACI 318-08, Eurocode-2 and BS8110-97. For Eurocode-2, it is required to use a reduced perimeter at the critical region outside the shear reinforced zone when the lateral spacing of shear reinforcement legs exceed two times the effective depth of the slab.

After preparation of CFRP dowel holes, CFRP sheets were cut to rectangular pieces in order to manufacture CFRP dowels. After impregnating with epoxy resin, CFRP sheets were rolled around 6 mm diameter steel reinforcing bars with carbon fibers oriented along the bar as shown in Figure 2.11. Steel bars were non-structural and merely used to provide a cost effective stiff material with a smooth wrapping surface while embedding CFRP dowels through the holes. Those steel bars were removed after installing the CFRP dowels. Figure 2.12 illustrates the CFRP dowel installation process.

Additional CFRP patches were passed through the CFRP dowel ends and bonded on the compression and tension faces of the slab before fanning-out the free-ends of the CFRP dowels in order to provide a better anchorage of the dowels and a smooth stress transfer between the dowels and the slab (Figure 2.13).

After bonding CFRP patches on the slab surfaces, ends of each dowel were fanned out and bonded over the CFRP patch surfaces by epoxy as shown in Figure 2.14.

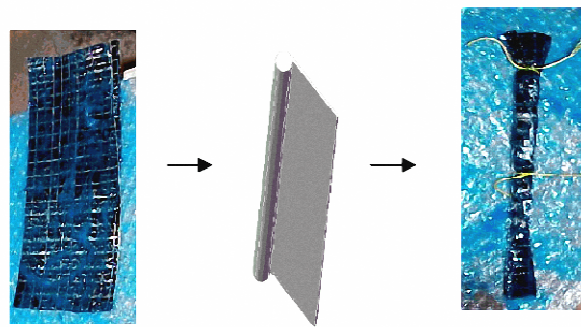


Figure 2.11 Manufacturing process of CFRP dowels

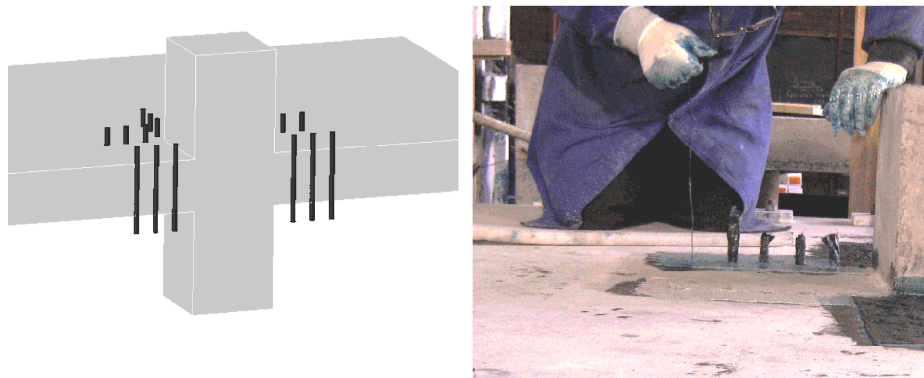


Figure 2.12 Installation of CFRP dowels through the holes

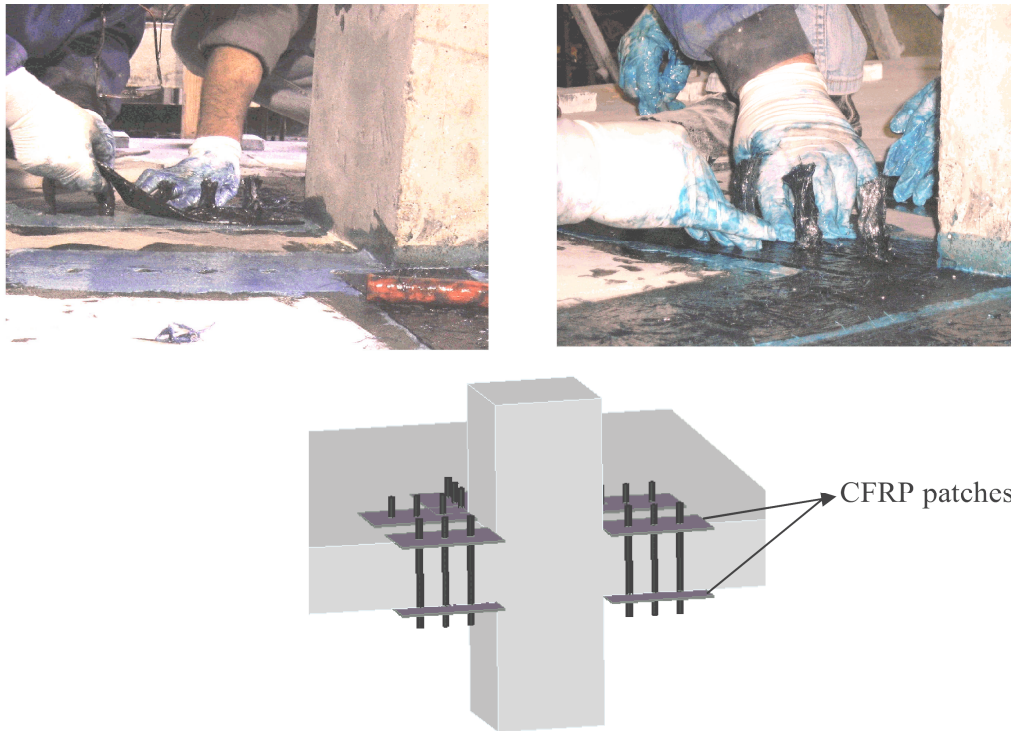


Figure 2.13 Installation of CFRP patches

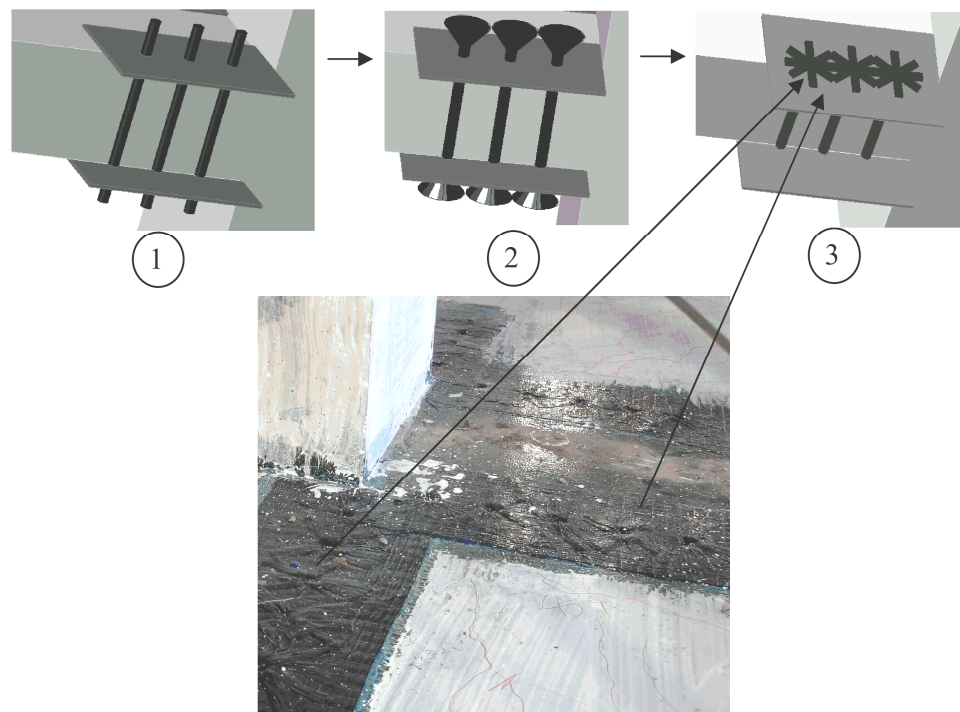


Figure 2.14 Fanning out (anchoring) the dowel ends

Total of eight specimens were strengthened by application of proposed strengthening method above (Figure 2.15). Strengthened specimens can be classified into 3 subgroups regarding to strengthening pattern and column stub rectangularity, such as;

- i) specimens having square column stub strengthened with O-pattern
- ii) specimens having rectangular column stub strengthened with O-pattern
- iii) specimens having square column stub strengthened with C-pattern

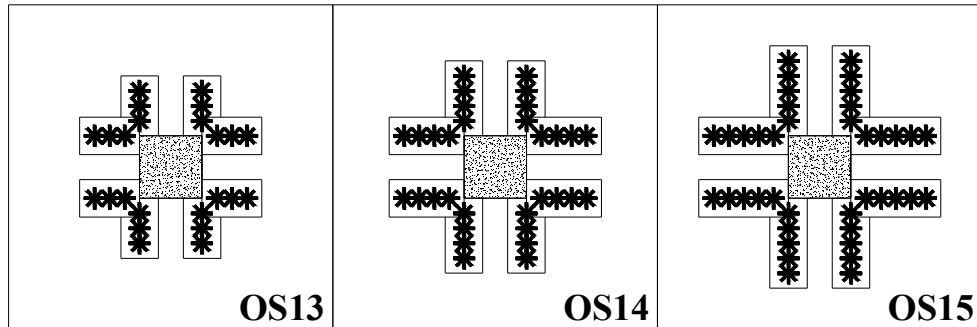
First group consist of three specimens with square column stubs and strengthened with three, four and five rows of CFRP dowels arranged in double rail configurations (O-Pattern) along four sides of the column stubs. Those specimens were named as OS13, OS14, OS15, respectively regarding to number of rows. (Figure 2.15a)

The arrangement used in specimen OS15 with five rows of CFRP dowels also applied to three specimens having rectangular column stubs in order to determine the effectiveness of proposed strengthening scheme on slabs supported with rectangular columns. Specimens OS25 and OS25-b had column aspect ratio of 2 that is similar to control specimen R2. The only difference between the specimens OS25 and OS25-b was the amount of CFRP used for each dowel. The strengthened specimen, OS35-b with column aspect ratio of 3 was also strengthened with the same amount of CFRP used in specimen OS25-b Figure 2.15b)

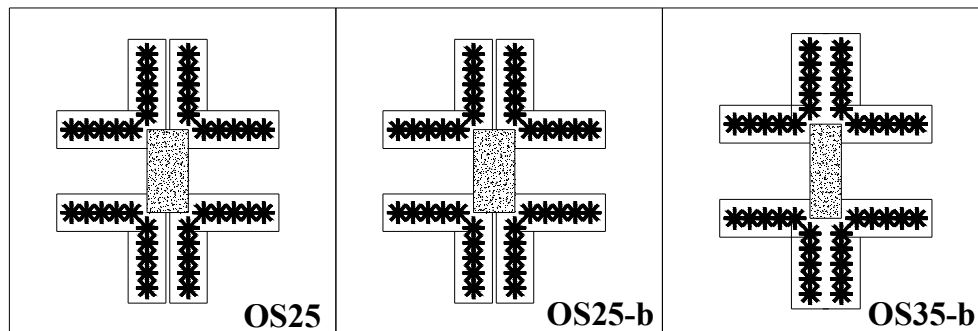
Two specimens named as CSWOP and CSWP having square column stub were strengthened with circular strengthening pattern (C-pattern). There were two main differences between those two specimens. One of them was the presence of the CFRP patches bonded to surfaces of the slab for specimen CSWP. In this way, it was aimed to investigate the effect of additional surface FRP patches in anchoring vertical CFRP dowels. The other difference is the construction

method of the CFRP dowel holes. The drilling technique was used for creating the dowel holes in specimen CSWOP.

a) specimens having square column stub strengthened with O-pattern



b) specimens having rectangular column stub strengthened with O-pattern



c) specimens having square column stub strengthened with C-pattern

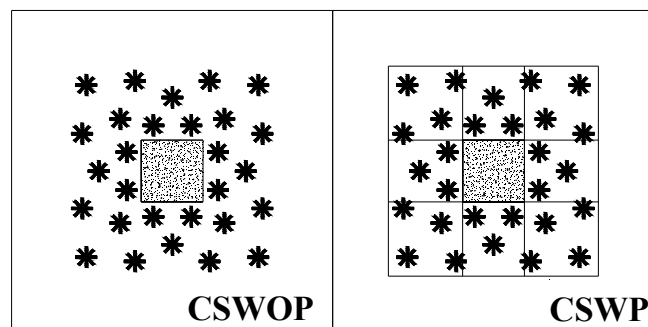


Figure 2.15 Strengthened specimens with CFRP dowels

2.3.4 Design of CFRP dowels

The design provisions of three different codes (ACI 318-08, Eurocode-2 and BS8110-97) presented in Section 1.4 were used to determine the punching shear capacity by assuming the failure outside the shear reinforced region with the critical punching perimeters given in Figure 2.16. The outside capacities V_o were then used to compute the required amount of CFRP for each specimens by using Equation 2.2.

$$V_o = V_i = (V_c + nA_{CFRP}f_{CFRP}) \quad (2.2)$$

where V_i is the capacity inside the shear reinforced region, V_c is the concrete contribution, n is the number of CFRP dowels in a perimeter, A_{CFRP} is the area of CFRP per dowel (the thickness of the composite material is measured to be 0.8 mm in the coupon tests), f_{FRP} is the tensile strength of the composite material (CFRP + Epoxy) equal to 637 MPa according to the coupon tests performed in METU Structural Laboratory (Section 2.2.3).

The required CFRP width for each specimen is presented in Table 2.5. The results indicated that the amount of CFRP required by ACI318-08 is more than Eurocode-2 and BS8110-97. This difference may be explained by the concrete contribution, since ACI 318-08 has the lowest concrete contribution among three codes.

The width of CFRP sheets used for each is selected to be 120 mm for all the strengthened specimens. However, it was decided to increase the amount of CFRP used for each dowel by 50% in specimen OS25-b and OS35-b after evaluating the test results and failure mode of the specimen OS25. The height of the CFRP sheets used for manufacturing the dowel is taken as 250 mm. The two 50 mm long ends of each dowel were fanned out and bonded over the CFRP patches. This distance found to be sufficient to overlap the fans (this

overlapping process was also employed by Widiyanto 2006) of dowels in two consecutive perimeters.

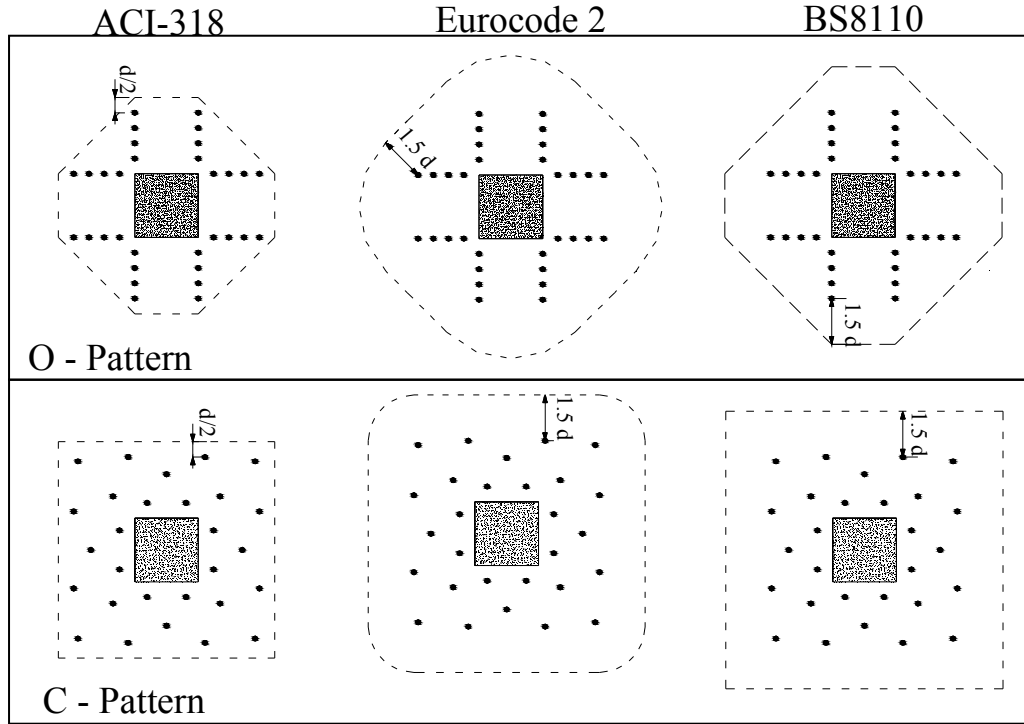


Figure 2.16 Assumed punching perimeters for preliminary design

Table 2.5 Design of amount of CFRP

Specimen	Number of holes per perimeter	Code Predictions , V_o (kN)			Required CFRP width (mm)			Applied CFRP width per hole (mm)
		ACI-318	EC2	BS8110	ACI-318	EC2	BS8110	
OS13	8	479	531	467	81	57	24	120
OS14	8	514	587	523	89	70	37	120
OS15	8	549	644	576	98	84	50	120
CSWOP	8	586	671	686	107	91	77	120
CSWP	8	586	671	686	107	91	77	120
OS25	8	549	643	576	98	84	50	120
OS25-b	8	549	643	576	98	84	50	180
OS35-b	8	521	643	576	91	84	50	180

2.3.5 Test Parameters

All test specimen details are presented in Table 2.6 considering the test variables. To summarize, parameters studied during the experimental session can be categorized into four main groups according to variation and combination of all test specimens presented in Table 2.6 and Figure 2.17;

- i) CFRP dowel pattern (O-pattern, C-pattern)
- ii) Number of CFRP dowels around the column stub
- iii) Column Rectangularity
- iv) Detailing

Table 2.6 Test specimen details

Specimen	Column aspect ratio	CFRP pattern	Column stub	# of CFRP dowels	# of CFRP perimeters	Amount of CFRP per hole (dry) (mm ²)
R1-A	1	_____	One face	_____	_____	_____
R1	1	_____	Both faces	_____	_____	_____
R2	2	_____	Both faces	_____	_____	_____
R3	3	_____	Both faces	_____	_____	_____
OS13	1	O	Both faces	24	3	19.8
OS14	1	O	Both faces	32	4	19.8
OS15	1	O	Both faces	40	5	19.8
OS25	2	O	Both faces	40	5	19.8
OS25-b	2	O	Both faces	40	5	29.7
OS35-b	3	O	Both faces	40	5	29.7
CSWOP	1	C	Both faces	28	4	19.8
CSWP	1	C	Both faces	28	4	19.8

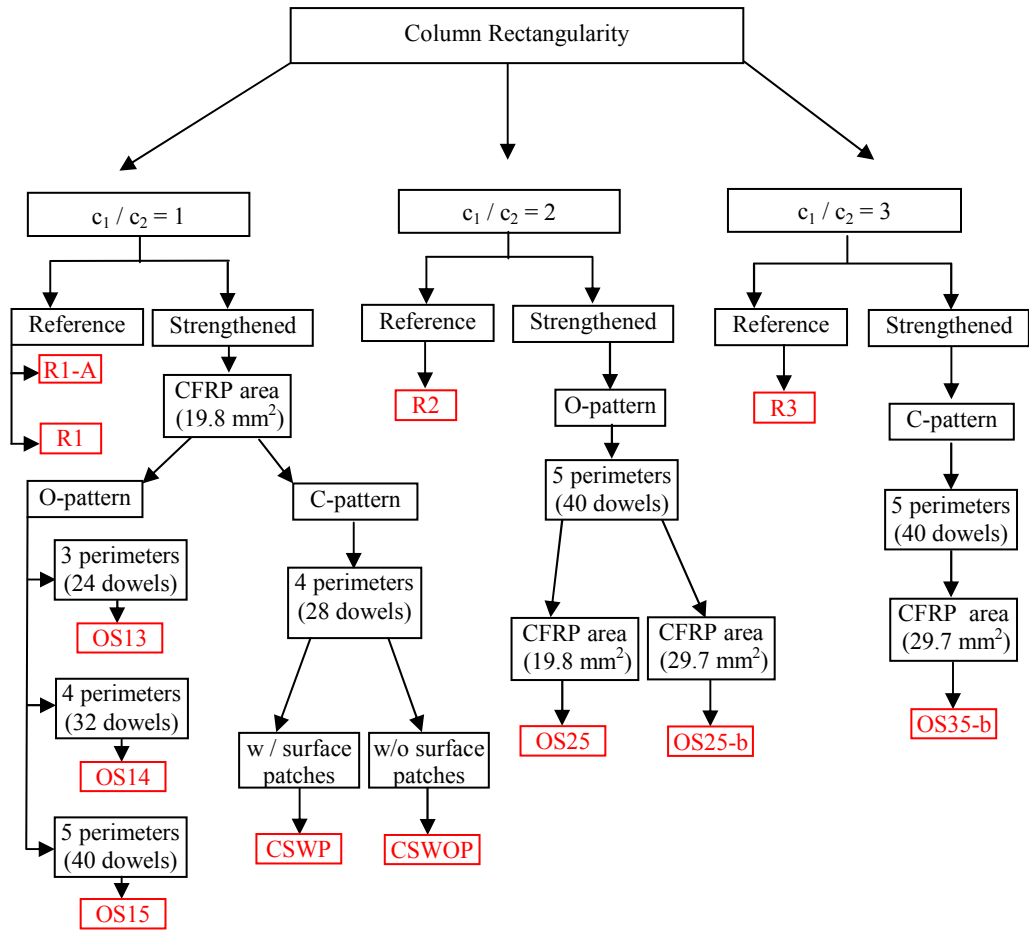


Figure 2.17 Test matrix

Two different CFRP dowel arrangements, named as O pattern and C patterns (as explained in Section 2.3.3), were investigated to determine the most efficient pattern in terms of load carrying capacity and failure mode.

Effect of number of CFRP dowels used around the column stub was one of the main parameter investigated. Specimens OS13, OS14, OS15 had CFRP dowels arranged in O pattern with total number of dowels 24, 32 and 40 respectively. Specimen CSWP can also be added to this group with 28 CFRP dowel arranged in C-pattern with different spacing compared to O-pattern specimens.

Total of seven specimens (R1, R2, R3, OS15, OS25, OS25-b and OS35-b) were constructed to study effect of column aspect ratio on punching failure

behavior of strengthened flat-slabs. All specimens had constant column perimeter value of 1000 mm with varying rectangularity (column aspect ratios equal to 1, 2 and 3).

Three different detailing applications that may possibly affect the punching behavior of both control and strengthened specimens were also studied. Two control specimens R1-A and R1 were tested to discuss existence of column stub on only one face of the slab (simulating a slab-column connection on the roof floor of a building) and both faces of the column (simulating a slab-column connection simulating an intermediate floor of a building). Effect of CFRP dowel holes construction method either by drilling after casting concrete or fixing PVC pipes in the formwork before casting was also investigated. For this purpose the holes in specimen CSWOP was created by drilling process. The holes in all the other strengthened specimens were created by using PVC pipes before casting. Another issue discussed about detailing is presence and absence of bonded CFRP patches on both faces of the test specimens. For this purposes two strengthened specimens CSWP and CSWOP were strengthened with and without application of CFRP patches on the specimens.

2.3.6 Test Setup

All test specimens were simply supported on all four sides with corners free to deflect (Figure 2.18). High strength 18 mm diameter threaded rods (tie rods) were used to connect the specimens to four channel section (C300) steel beams along four sides of specimens, which were connected to laboratory strong floor with high strength threaded rods (Figure 2.18). Each side of the specimens had seven support locations with 250 mm spacing. 20 mm thick steel plates were connected to the support points to prevent concrete crushing due to stress concentration around the supports. Monotonically increasing vertical load was applied by using a hydraulic jack (capacity of 1000 kN) to the column stub reacting against the laboratory strong floor (Figure 2.19). A spherical ball

bearing was used to ensure that no moment is transferred at the load application point. A rigid steel plate that perfectly fits to the column stub was used between the spherical ball and test specimen in order to transfer the load uniformly to the test specimen.

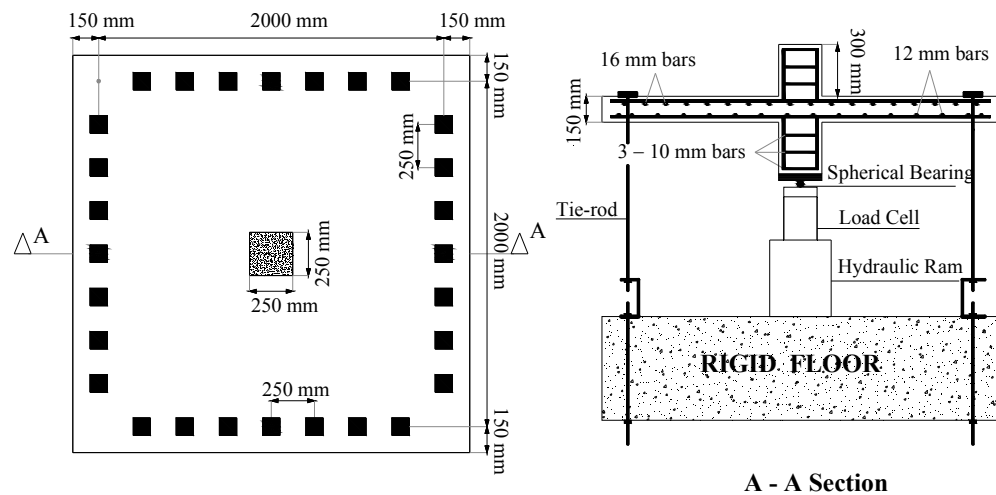


Figure 2.18 Test setup and specimen details

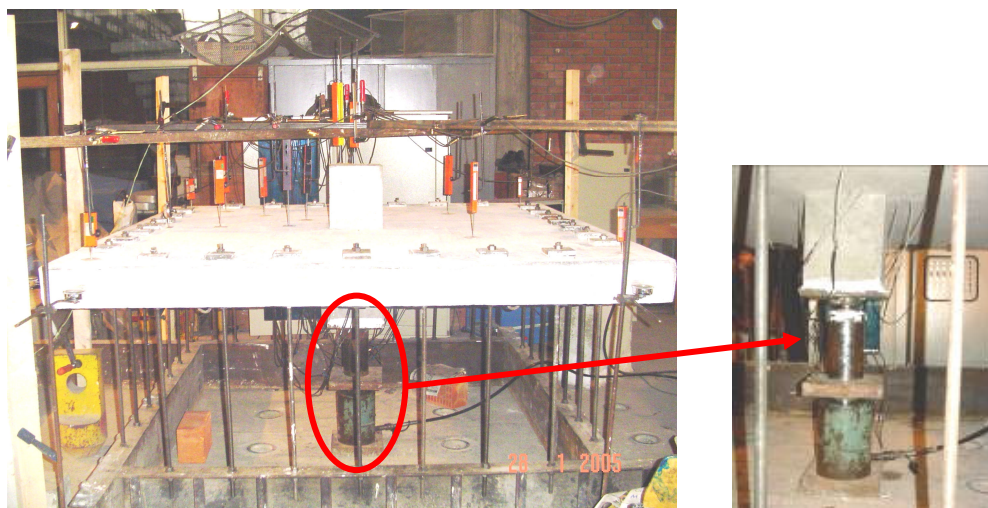


Figure 2.19 A view of Specimen R1 before testing

2.3.7 Instrumentation

Different types of instruments were used to measure the applied load, displacement and top reinforcement strain values during the tests. A load cell with a capacity of 1700 kN was connected to the hydraulic jack in order to obtain load readings (Figure 2.19). Linear Variable Differential Transducers (LVDT) having 50 mm and 100 mm strokes, dial gages having 50 mm, 30 mm and 20 mm strokes were employed to measure vertical displacement readings of test specimens. The displacement sensors were placed on the specimens in order to gather data for orthogonal and diagonal displacement profiles along the span length as shown in Figures 2.20 and 2.21. Two different layout was used for positioning the displacement transducers regarding to shape of column stub (square and rectangular) as shown in Figures 2.20 and 2.21. Strain gages were attached to top reinforcement to capture strain history of reinforcing rebars. The positions of strain gages are shown in Figures 2.20 and 2.21. It was also attempted to attach strain gages to CFRP dowels in order to read vertical strain values however, no reliable readings were obtained due to unsuccessful mounting process.

All the sensors were connected to a 64 channel analog to digital converter as shown in Figure 2.22. The converted data was visualized by the help of data acquisition system.

2.3.8 Testing Procedure

All the test sensors were double checked to assure that they were properly working and all initial readings were reset to zero prior to testing. Extreme care was taken during the application of the load to avoid side effects of loading rate. Duration of each test was approximately 1 hour. The loading was paused at each 50 kN increment to monitor, mark and take photographs of the crack propagations on the test specimens. The loading process was carried on for a

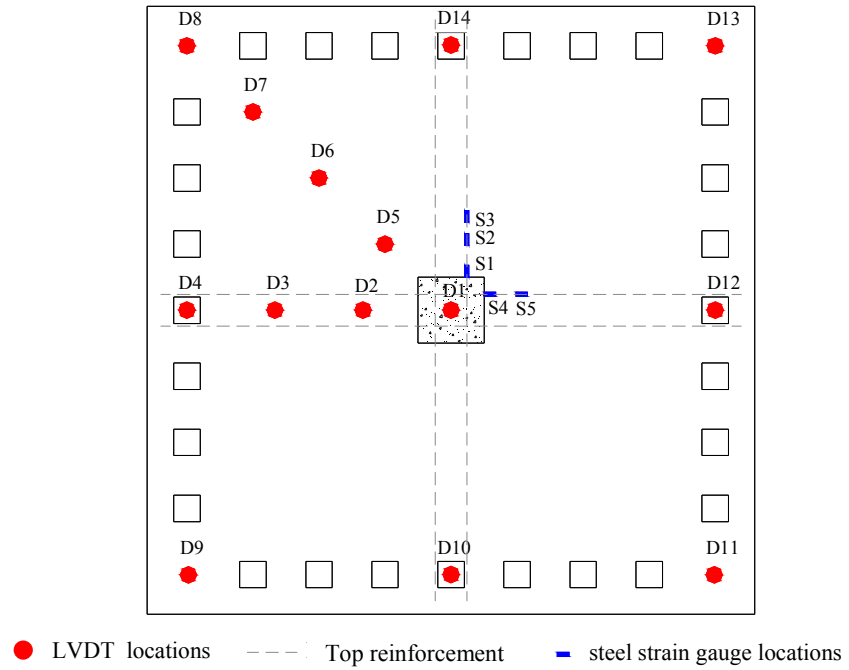


Figure 2.20 Instrumentation of test specimens with square column

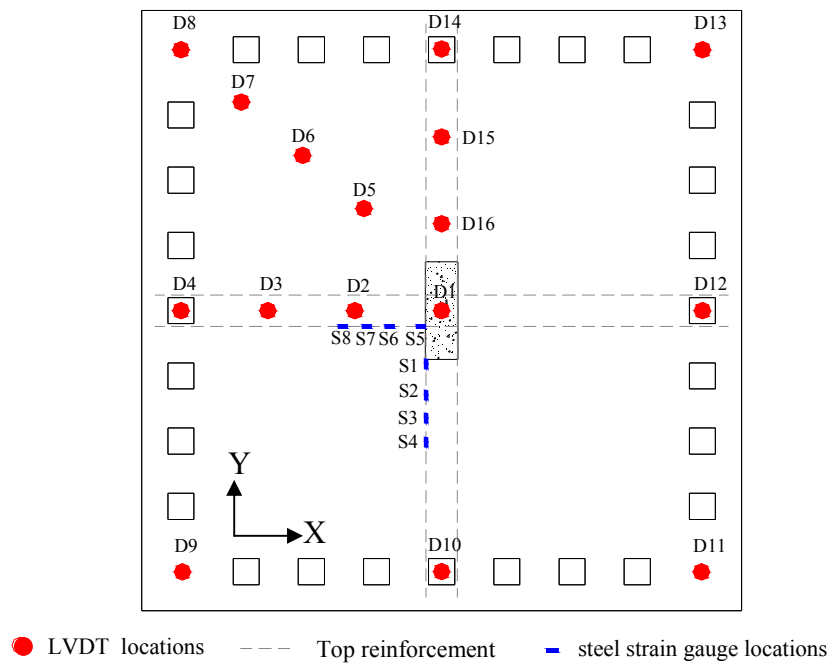


Figure 2.21 Instrumentation of test specimens with rectangular column

while after experiencing the punching failure in order to capture the post punching capacity of each specimen. The test data was recorded to a newly generated test database for each specimen after finalization of testing procedure.



Figure 2.22 Data acquisition system

CHAPTER 3

TEST RESULTS AND DISCUSSION

3.1 GENERAL

This chapter consists of two main sections. In test results section, experimental data (load, displacement and strain sensors) and visual observations (crack propagation and failure modes) are presented. In the discussion section, the informative database obtained from test results section was organized to compare, discuss and lay out the effects of test parameters on the behavior of test specimens.

3.2 TEST RESULTS

3.2.1 Load- Slab Center Deflection Curves

One of the most important outputs of any experimental study conducted in structural engineering is the load-deflection response. Numerous valuable information can be derived from those curves such as load carrying capacity, stiffness change and ductility of any test specimen. For this purpose, a displacement transducer was positioned in the center of the test specimen to measure the vertical displacement at the proximity of the slab- column connection. In order to obtain the relative center deflection of the slab-column connections, the average value obtained from the LVDTs located at the support points was subtracted from the values measured by the displacement sensor

positioned in the center of the test specimen. The locations of LVDTs' are presented in Figure 2.20 and Figure 2.21.

Load-deflection curves are also supported with the informative data such as first cracking point and first yielding point of each specimen as determined by inspection of the load-deflection curves and strain gages on longitudinal reinforcement, respectively.

A series of analyses were performed to study the effect of bonded CFRP patches on the flexural strength of slab sections having unit widths. The results of these analyses have shown that the contribution of the bonded CFRP patches in the flexural capacity of the specimens was only 8 percent when sufficient anchorage length was ensured. Since the anchorage length of the patches was not sufficient to develop this action, the contribution of the CFRP patches to the flexural capacity of the strengthened specimens can be neglected as it was stated in the previous studies in literature (Sissakis 2002, Binici 2003).

The flexural capacity results for each specimen found to be identical and equal to 582 kN which indicates that the column rectangularity does not have any effect on the flexural capacity of test specimens used in this particular study. The first cracking points are identified as the points where load-deflection curve deviated from initial stiffness slope (that is obtained by using finite element analysis which will be discussed in detail in Chapter 4). The load level at which first yielding was measured in the top reinforcement was labeled as the first yielding point. Test results are summarized in Table 3.1. The plots of applied vertical load versus center deflection of each test specimen are presented in Figure 3.1 to Figure 3.12. In those figures, the elastic stiffness, first crack and first yield values are clearly indicated.

Table 3.1 Summary of test results

Specimen	f_c (MPa)	V_u (kN)	Δ_u (mm)	V_{cr} (kN)	Δ_{cr} (mm)	V_y (kN)	Δ_y (mm)	V_{pp} (kN)	$\frac{V_u}{V_{flex}}$	Failure Location
R1-A	35	457	12.9	79	0.57	341	7.74	166	0.79	_____
R1	32	500	17.5	68	0.52	347	9.28	175	0.86	_____
R2	29	423	14.4	57	0.5	297	8.07	162	0.73	_____
R3	30	414	13.8	71	0.5	328	8.69	159	0.79	_____
OS13	33	601	35.5	98	0.78	357	9.38	283	1.03	Outside
OS14	26	571	35.9	64	0.79	317	9.99	370	0.98	Outside
OS15	31	656	49.1	115	0.93	325	8.17	405	1.13	Outside
OS25	33	649	35.6	94	0.78	380	9.02	246	1.12	Inside
OS25-b	30	571	33.1	72	0.60	305	8.17	280	0.98	Inside
OS35-b	30	564	27.8	73	0.47	356	9.37	412	0.97	Outside
CSWOP	31	594	34.2	58	0.57	337	9.00	271	1.02	Inside
CSWP	30	592	31.8	98	0.78	316	7.43	230	1.01	Inside

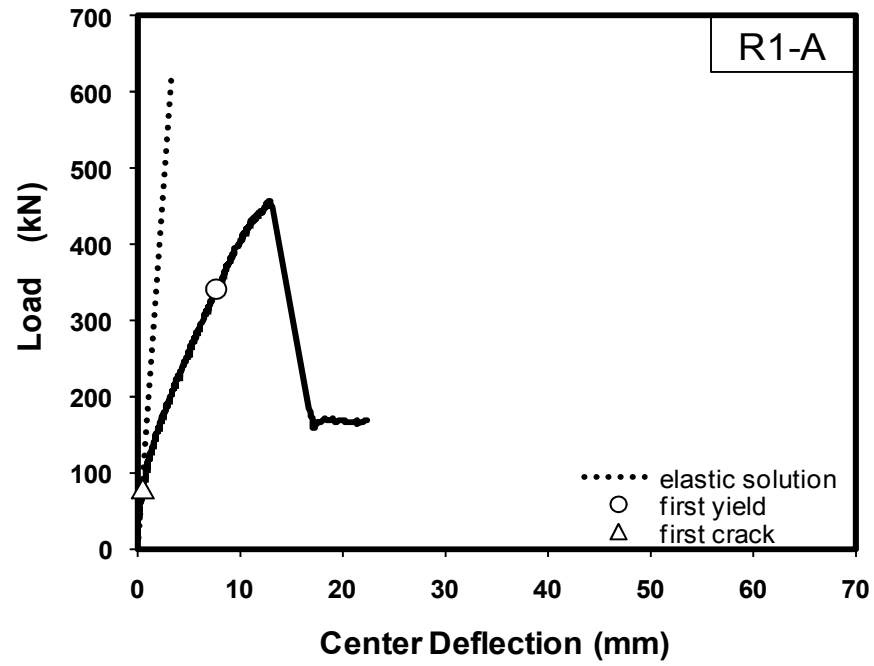


Figure 3.1 Load-center deflection curve of R1-A

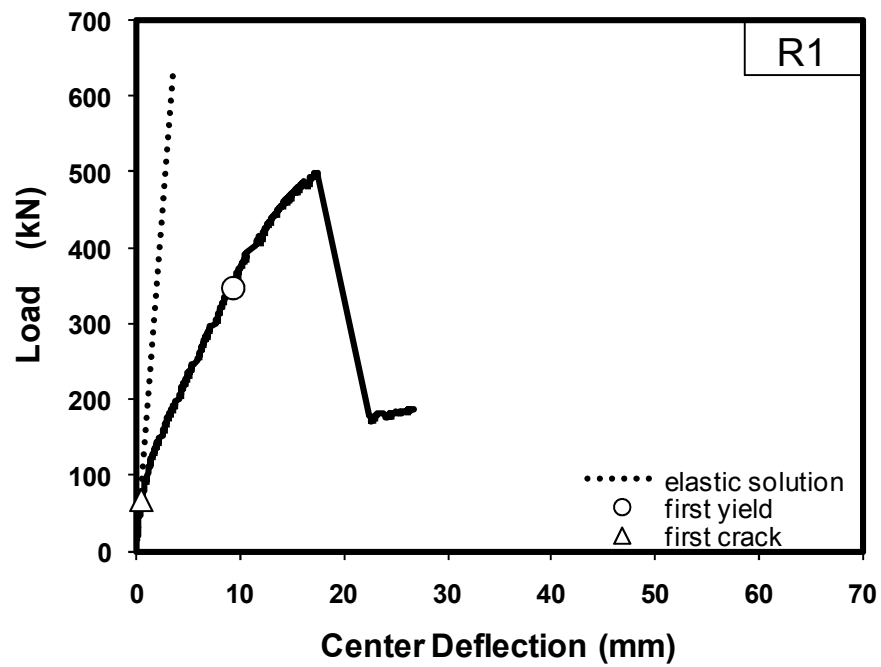


Figure 3.2 Load-center deflection curves of R1

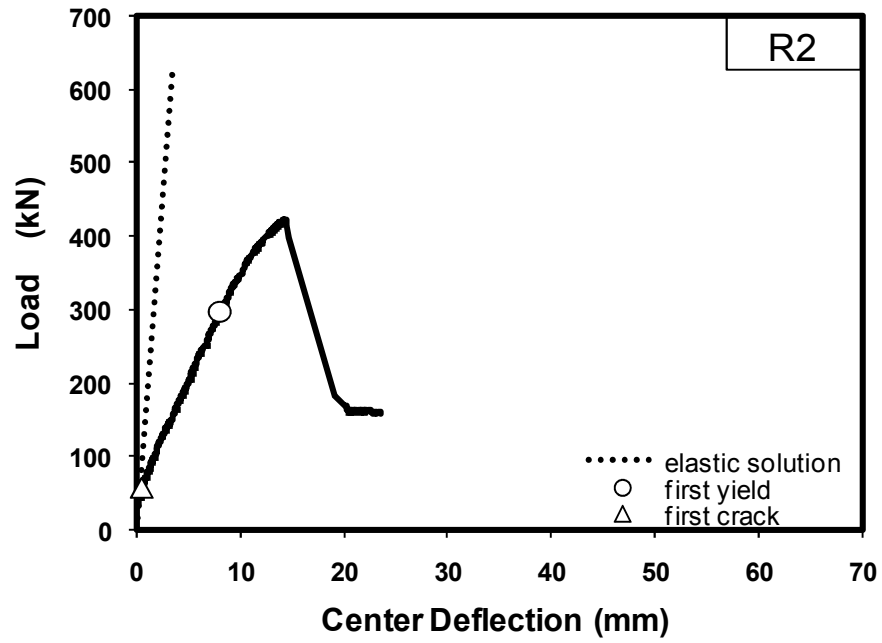


Figure 3.3 Load-center deflection curves of R2

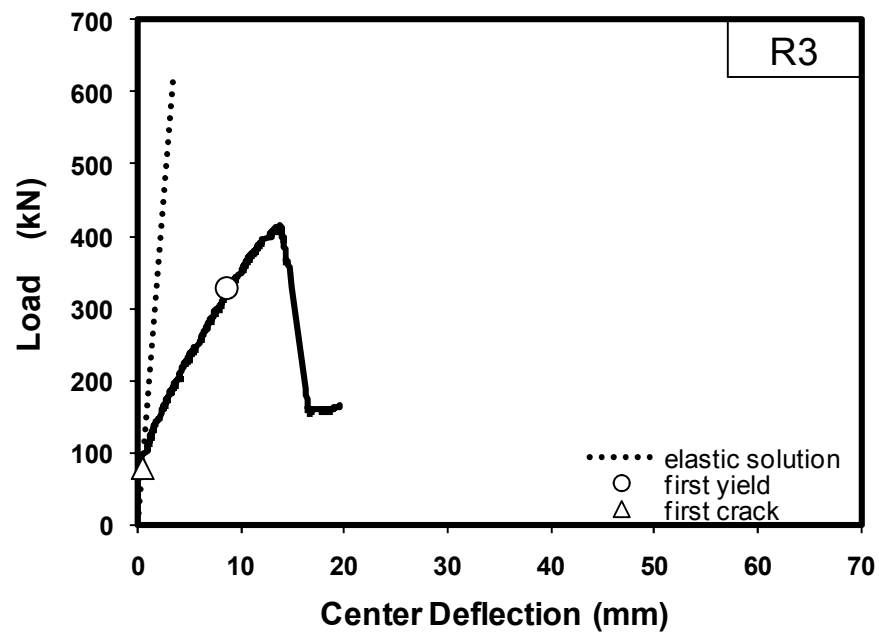


Figure 3.4 Load-center deflection curves of R3

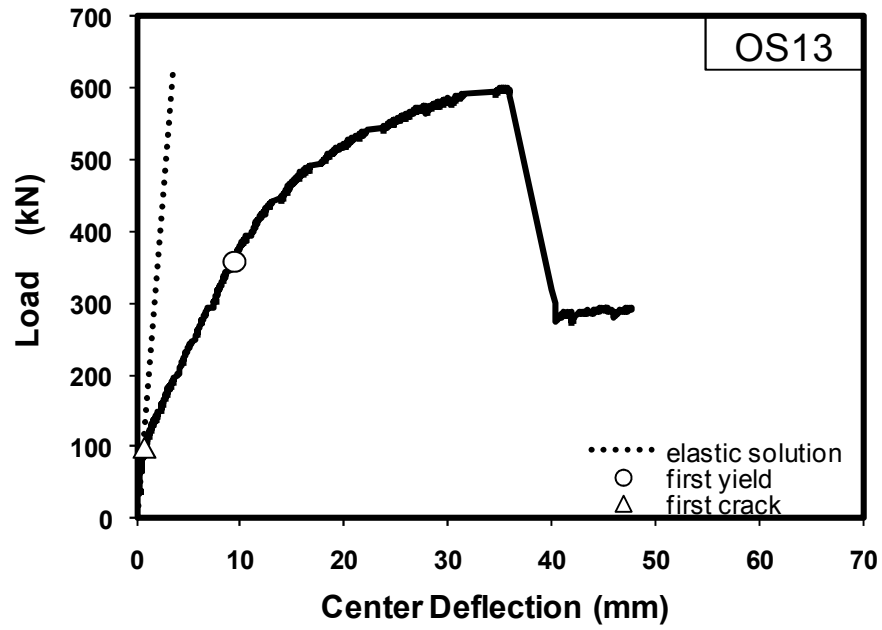


Figure 3.5 Load-center deflection curves of OS13

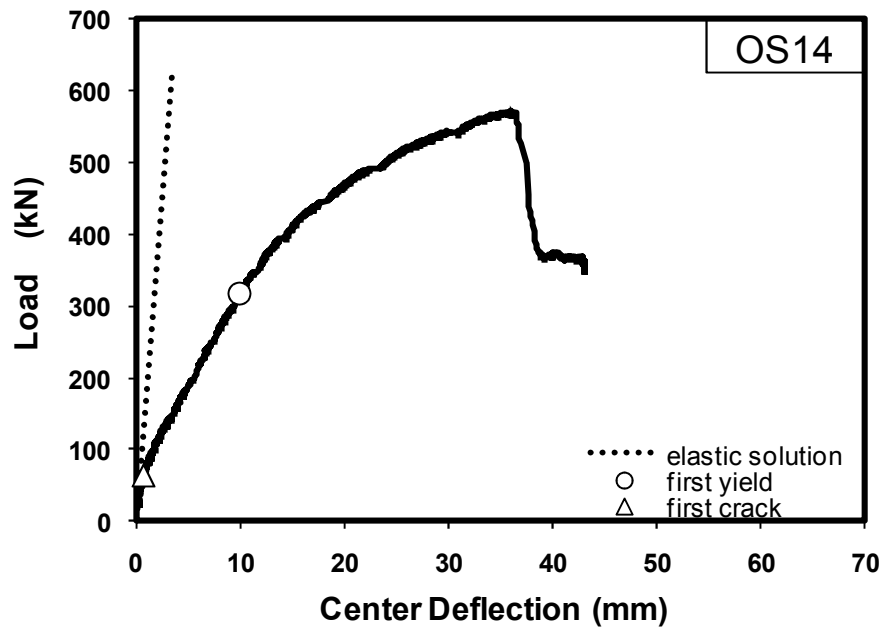


Figure 3.6 Load-center deflection curves of OS14

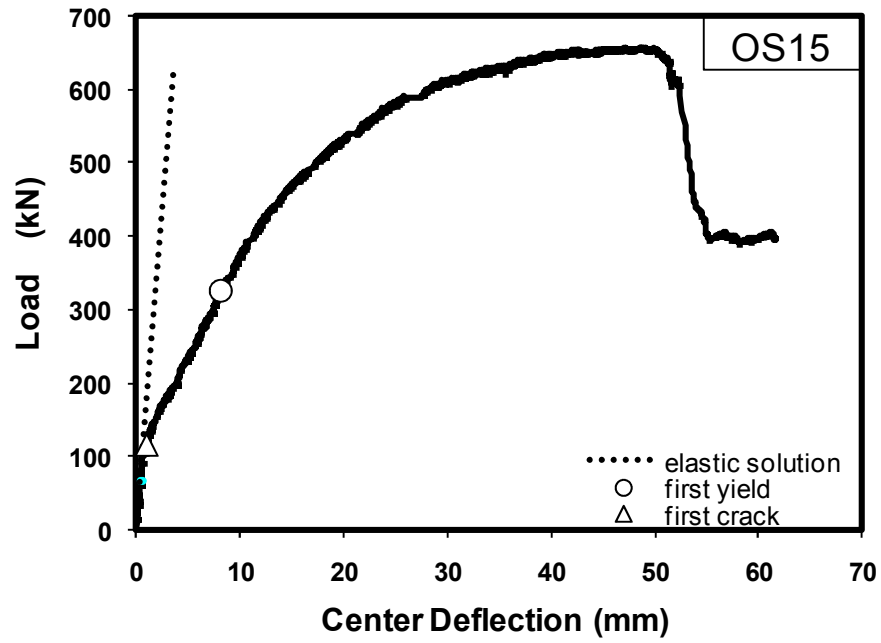


Figure 3.7 Load-center deflection curves of OS15

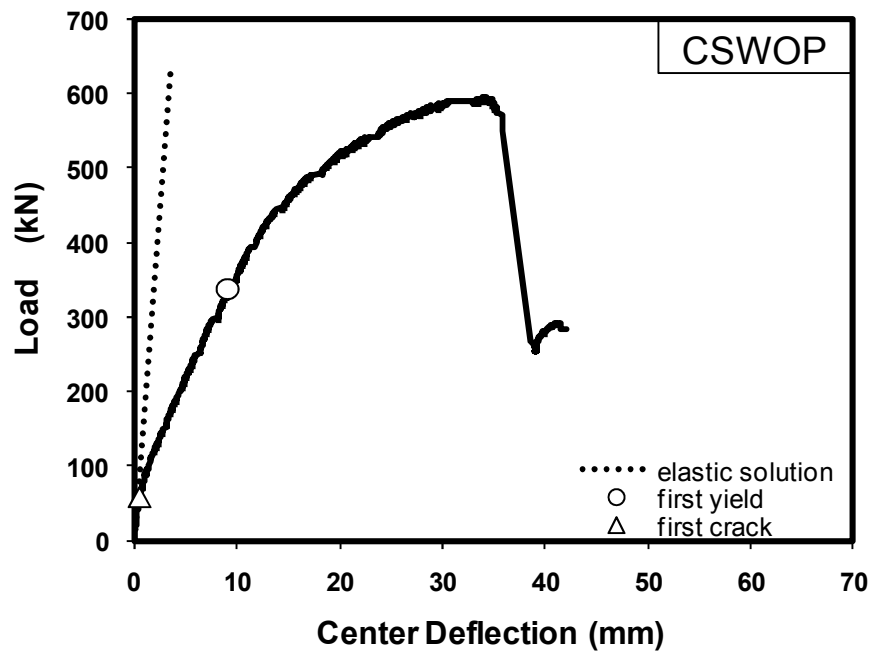


Figure 3.8 Load-center deflection curves of CSWOP

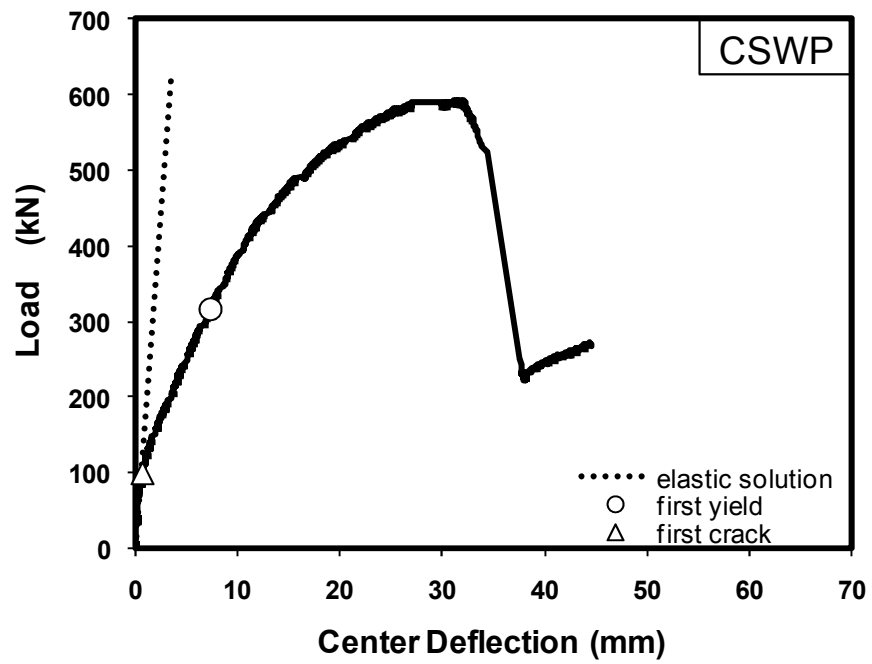


Figure 3.9 Load-center deflection curves of CSWP

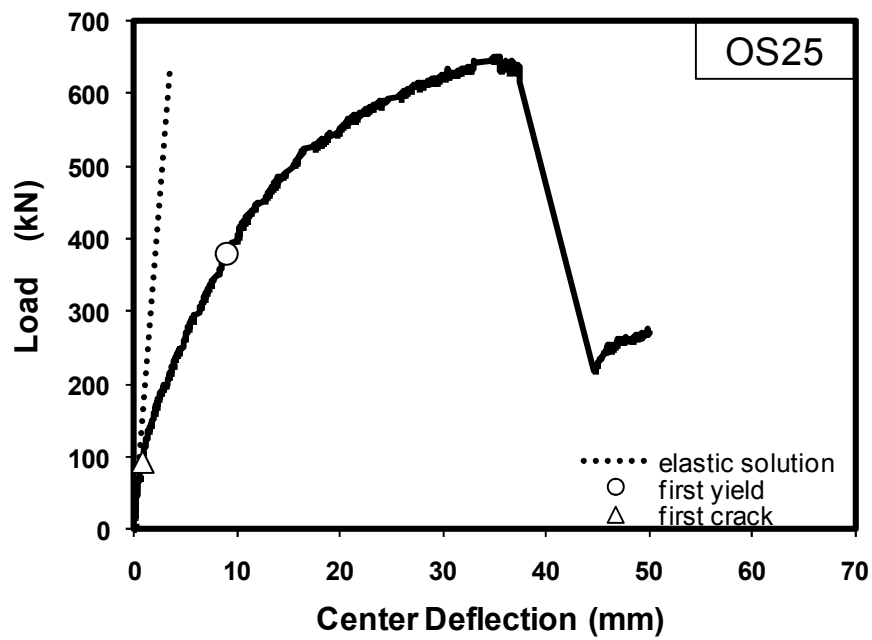


Figure 3.10 Load-center deflection curves of OS25

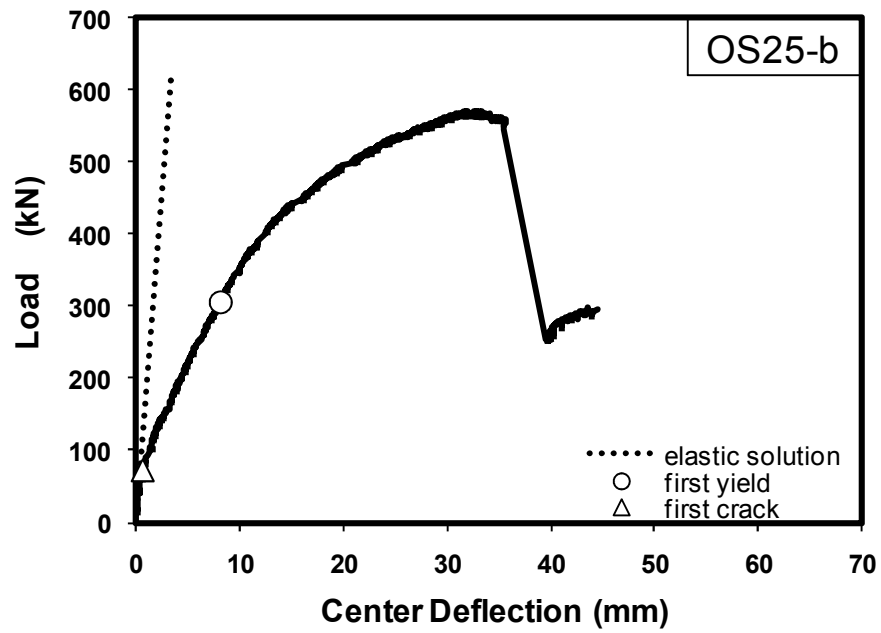


Figure 3.11 Load-center deflection curves of OS25-b

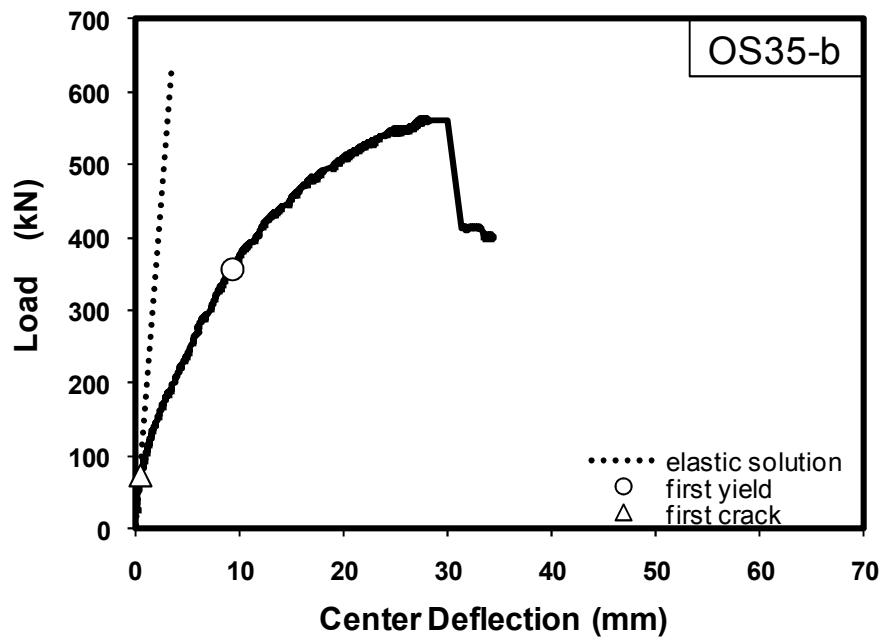


Figure 3.12 Load-center deflection curves of OS35-b

3.2.2 Slab Deflection Profiles

Vertical deflection profiles of all specimens in orthogonal and diagonal directions were measured with LVDTs positioned as shown in Figures 2.20 and 2.21. The plots of deflection profiles are presented in Figures 3.13 to 3.24 for different load levels. Since the span length in X and Y direction differs for specimens with rectangular column stub, orthogonal deflection profiles for both directions (X and Y) are presented in the same figure. The downward movement of the corners can be easily observed by the help of diagonal deflection profiles of each specimen.

3.2.3 Longitudinal Steel Strains

The locations of steel strain gages are illustrated in Figures 2.20 and 2.21 for specimens with square and rectangular column respectively. Steel strain gages were located at column face, d away from column face and $1.75 d$ away from column face respectively for all specimens with both square and rectangular column stub. However, additional strain gages at location of $2.5 d$ away from column face were attached to specimens with rectangular column stub (R2, R3, OS25, OS25-b and OS35-b). The results also show that strain values higher than 5000 microstrain are not reliable because of possible debonding of the strain gages.

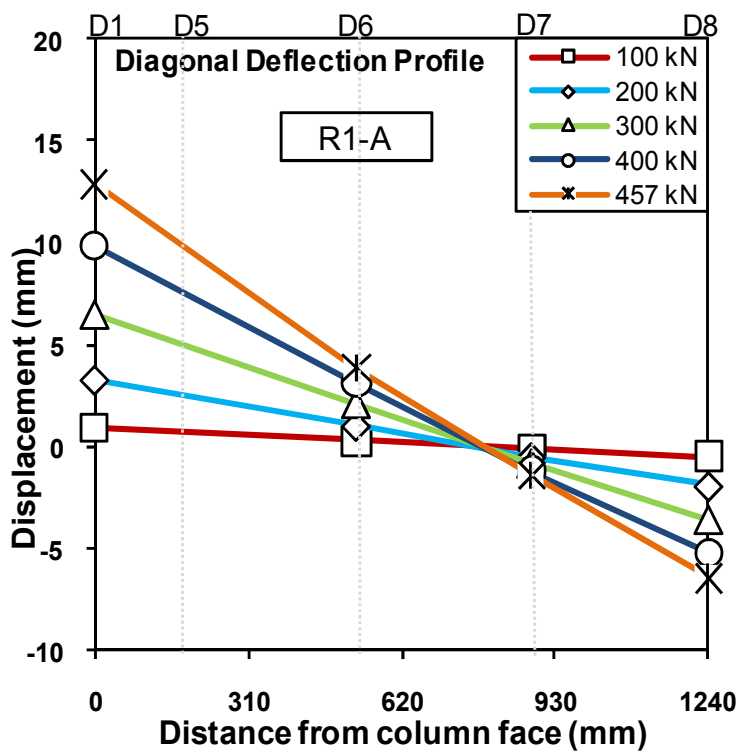
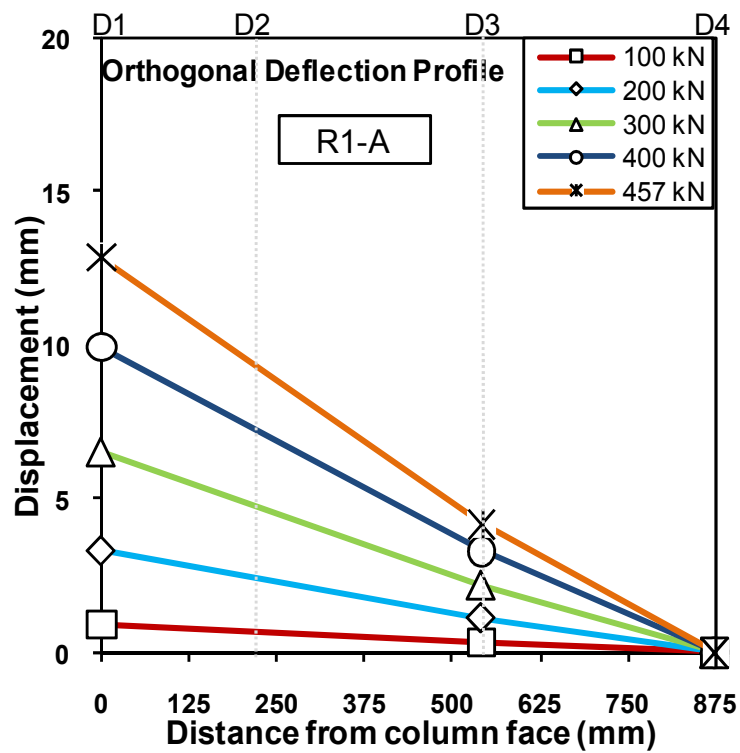


Figure 3.13 Load deflection profiles of R1-A

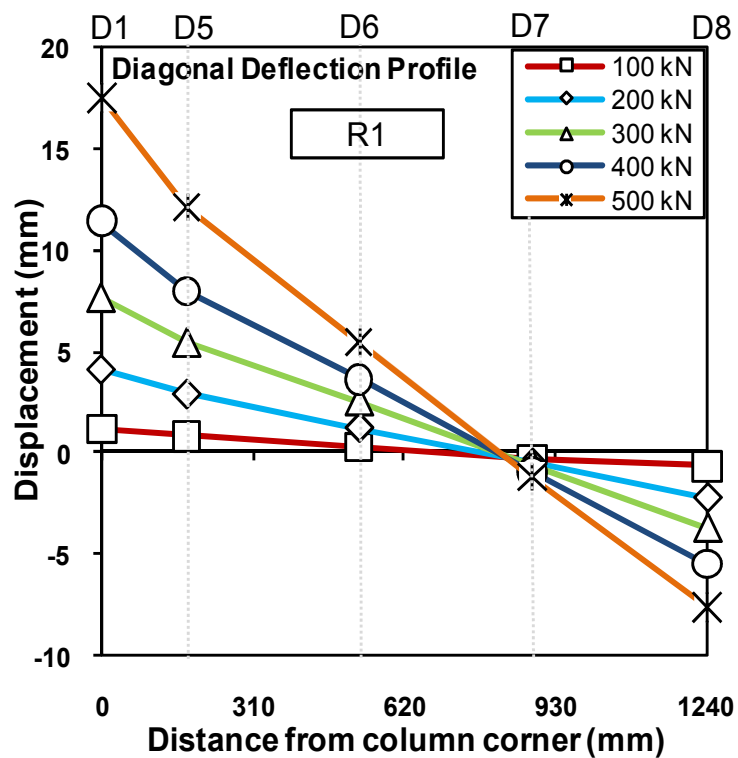
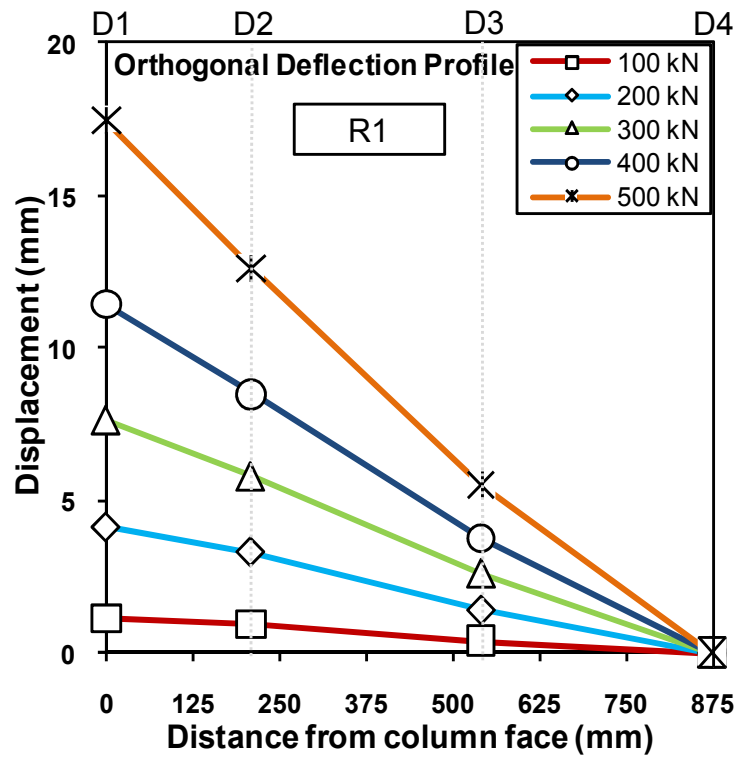


Figure 3.14 Load deflection profiles of R1

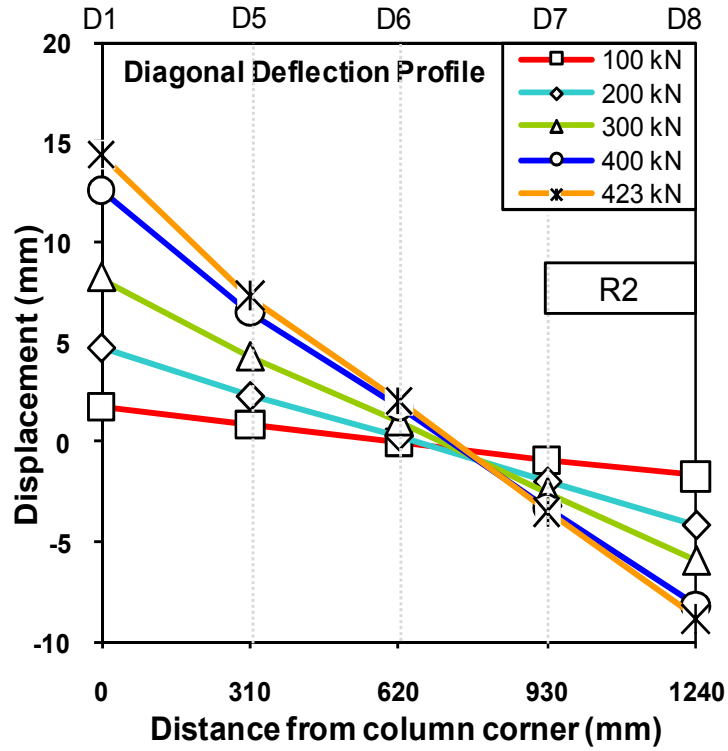
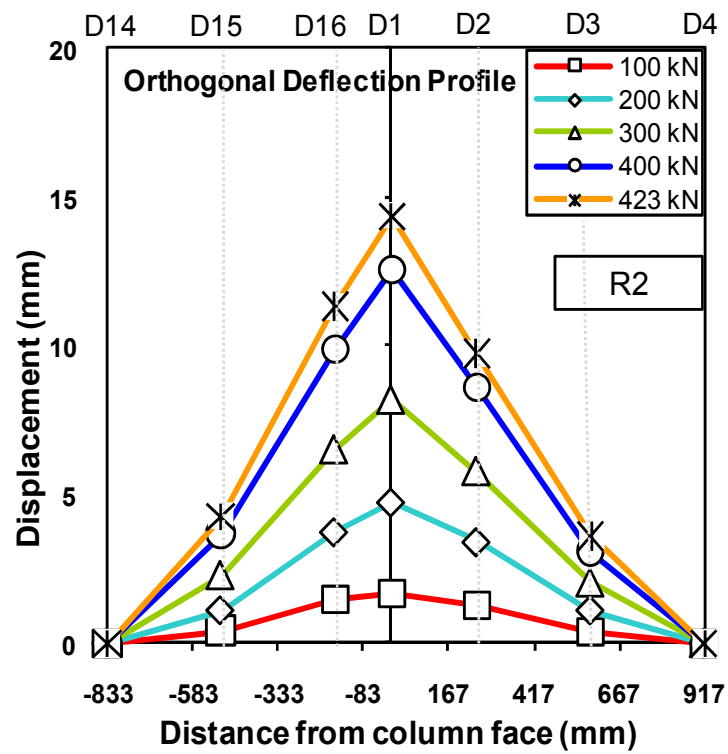


Figure 3.15 Load deflection profiles of R2

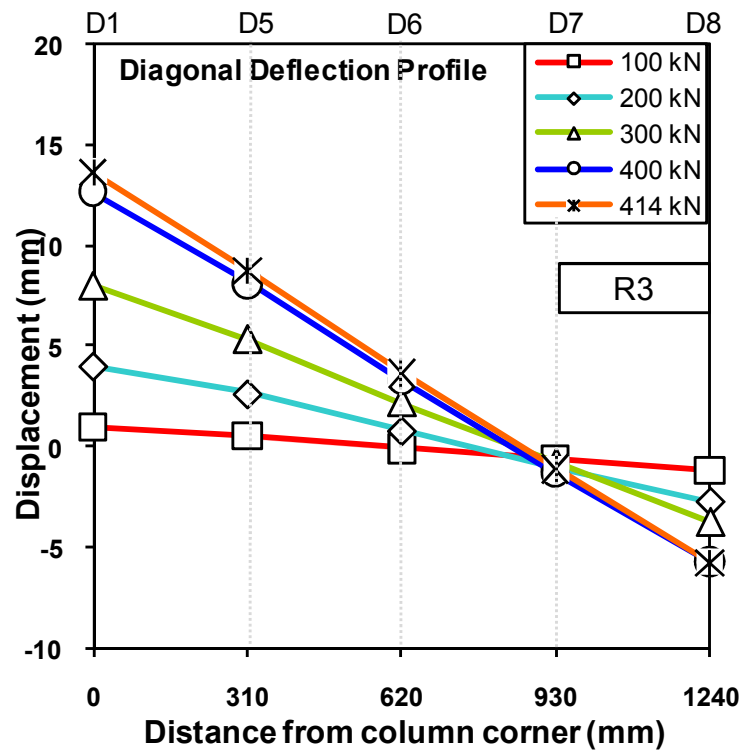
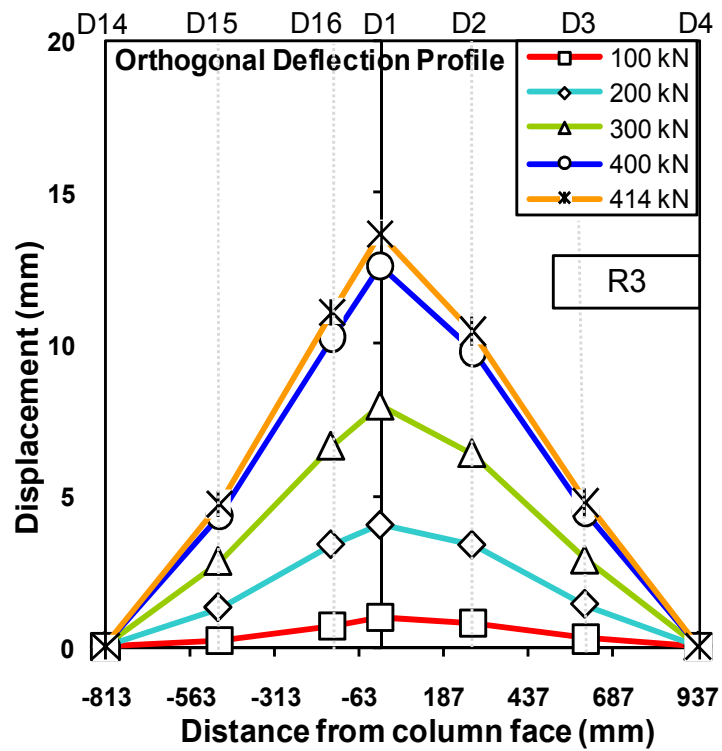


Figure 3.16 Load deflection profiles of R3

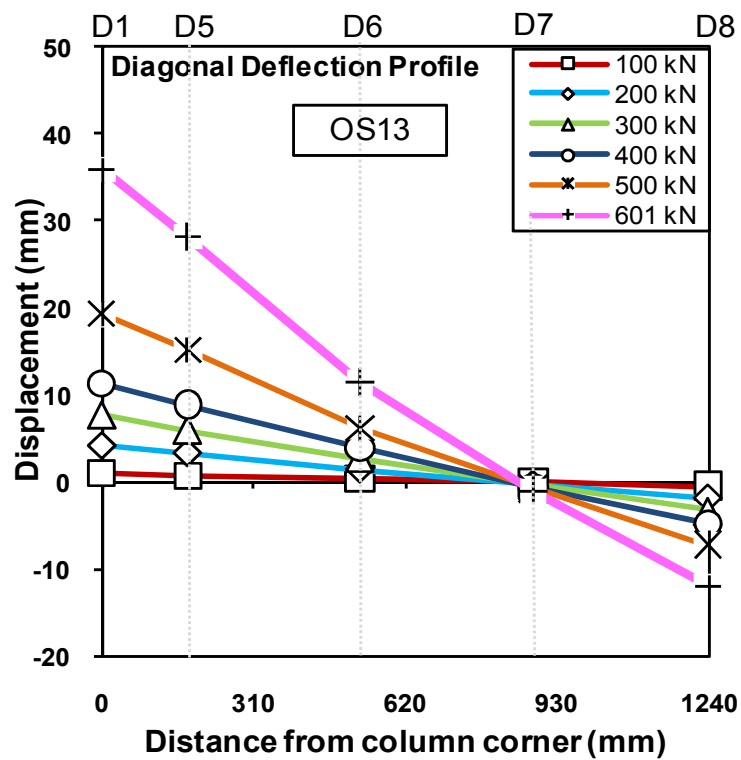
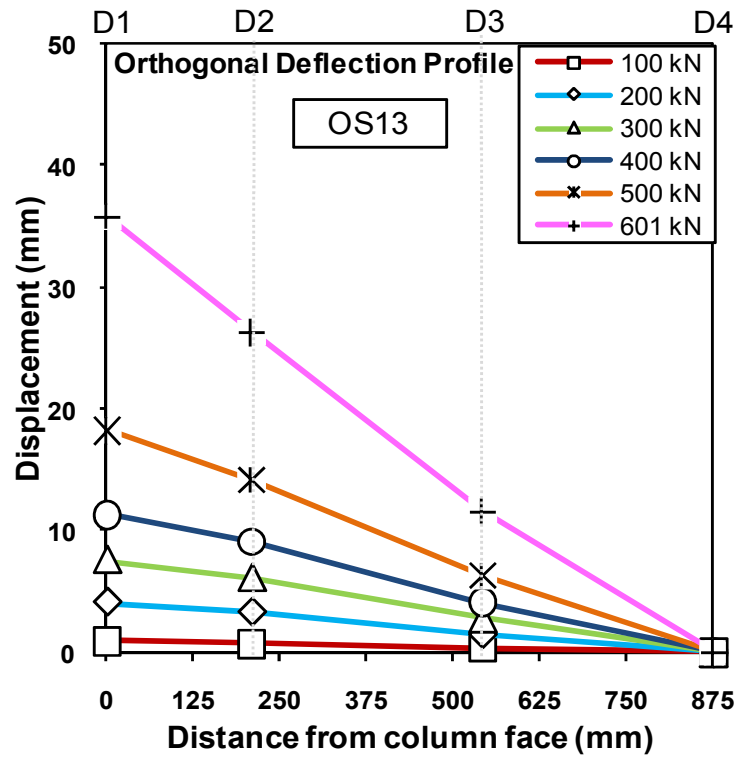


Figure 3.17 Load deflection profiles of OS13

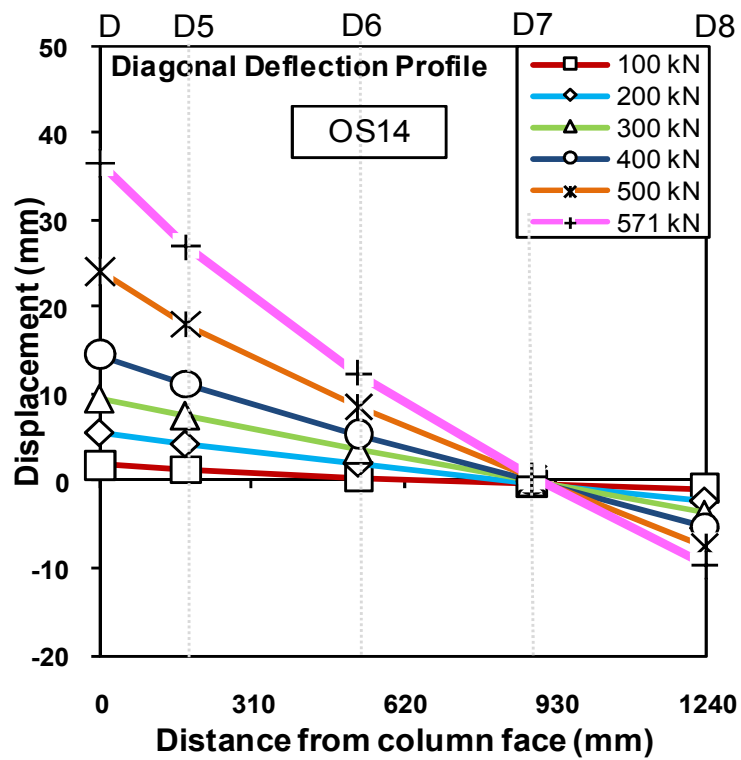
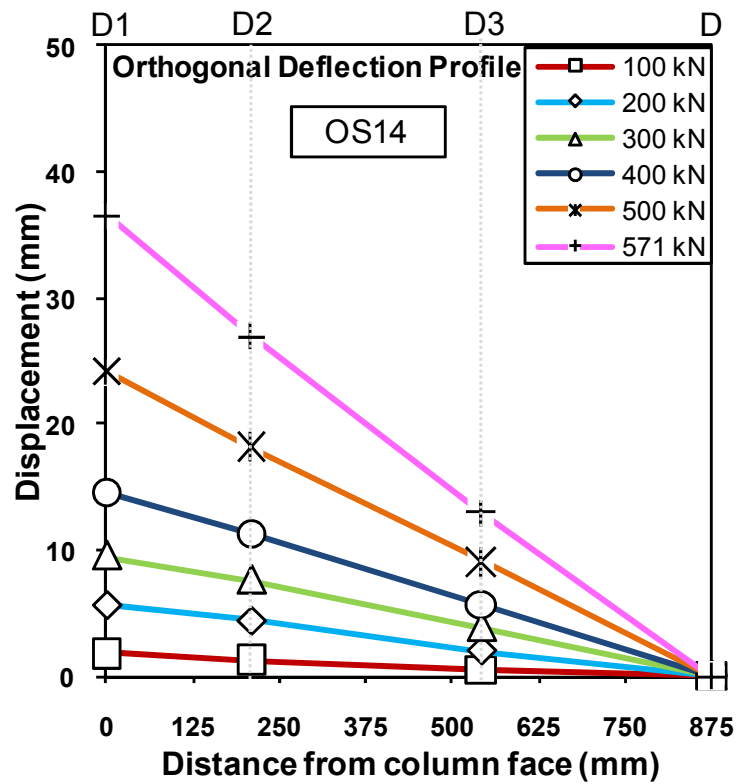


Figure 3.18 Load deflection profiles of OS14

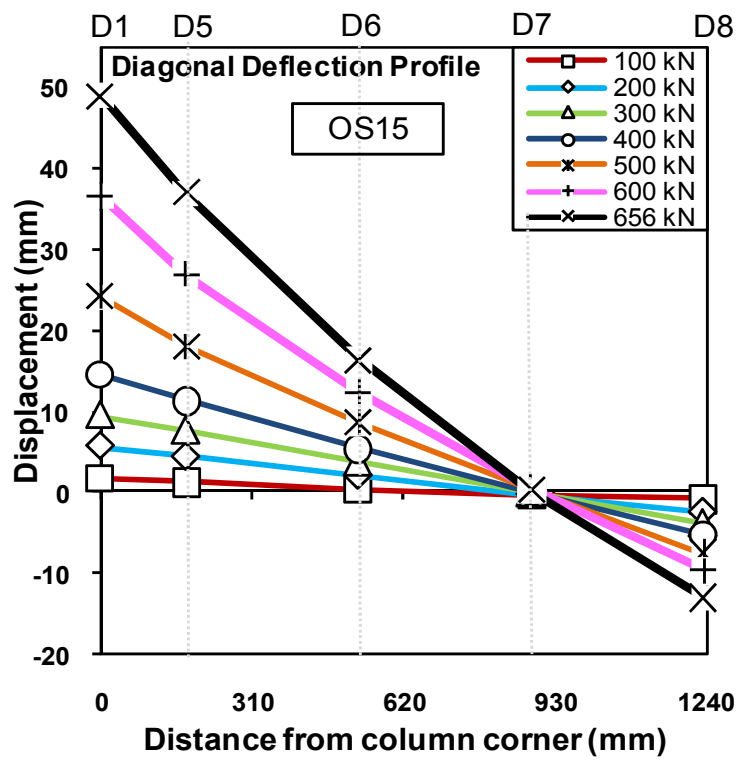
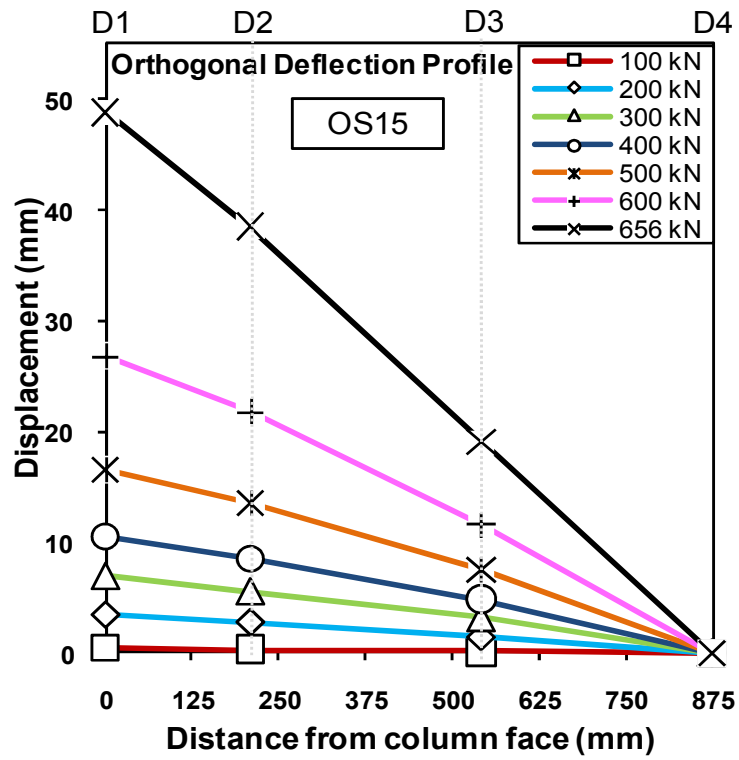


Figure 3.19 Load deflection profiles of OS15

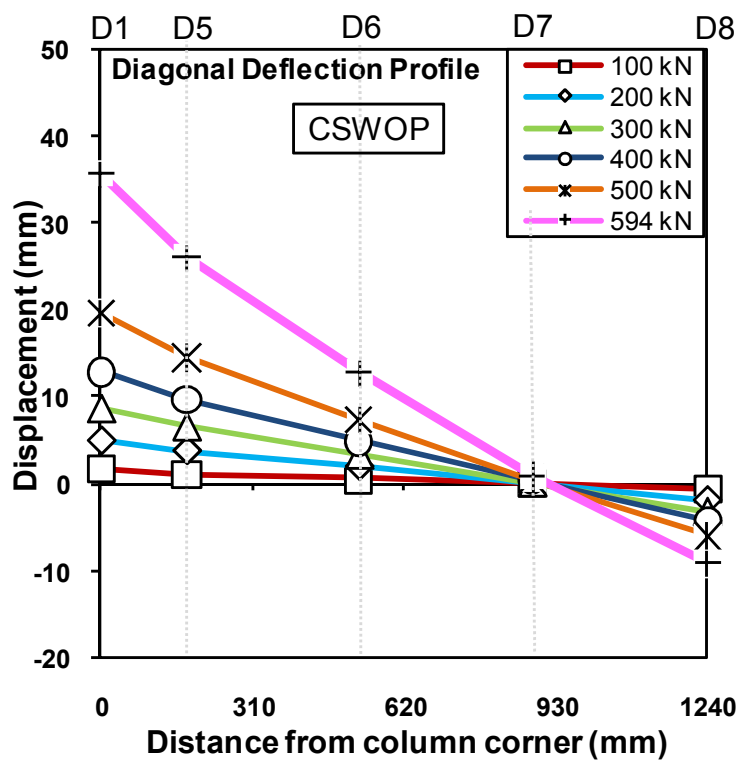
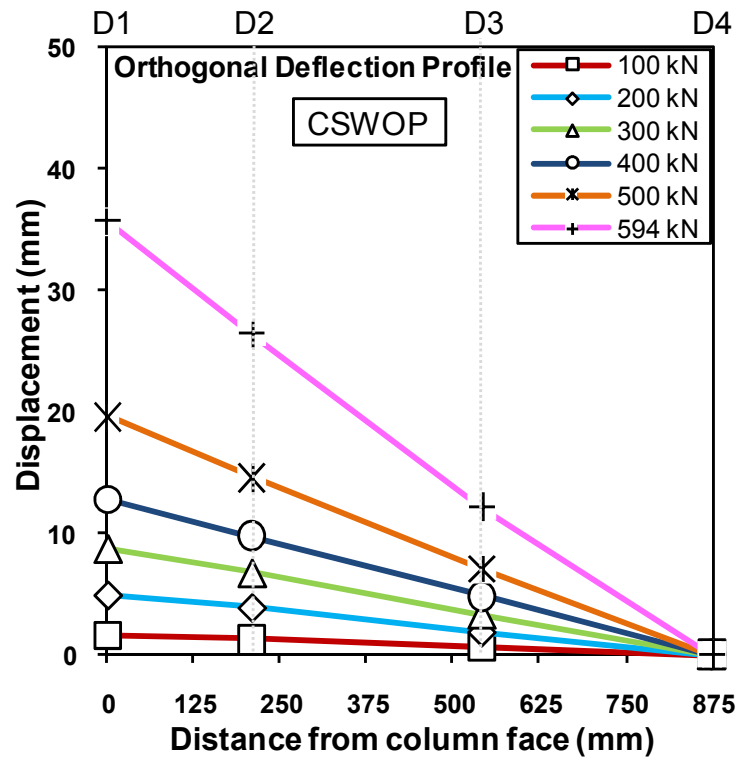


Figure 3.20 Load deflection profiles of CSWOP

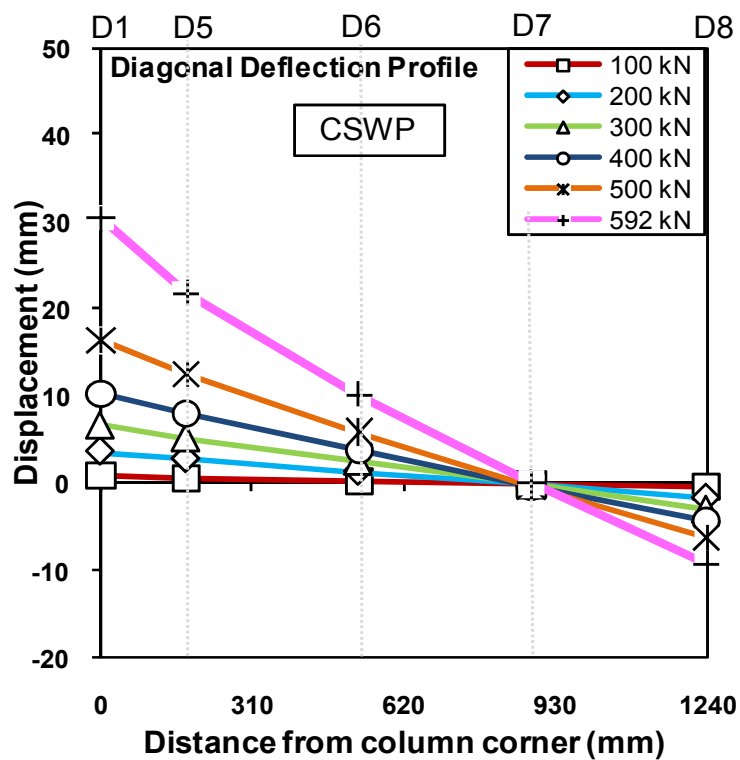
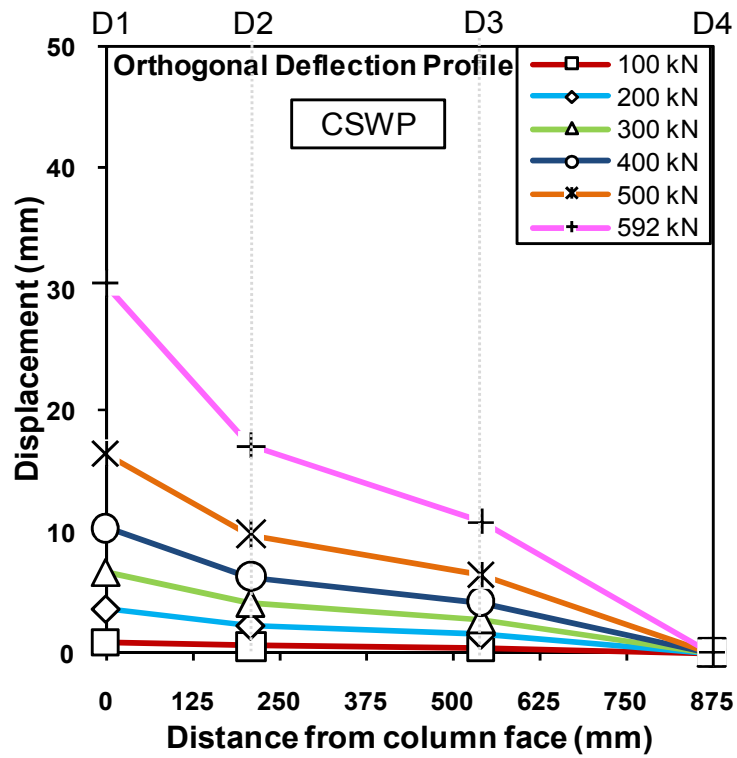


Figure 3.21 Load deflection profiles of CSWP

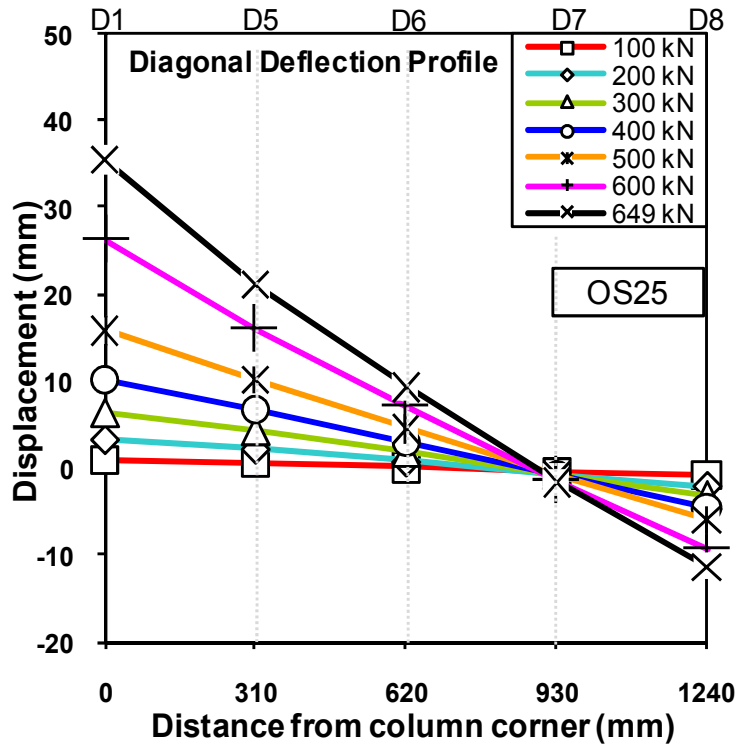
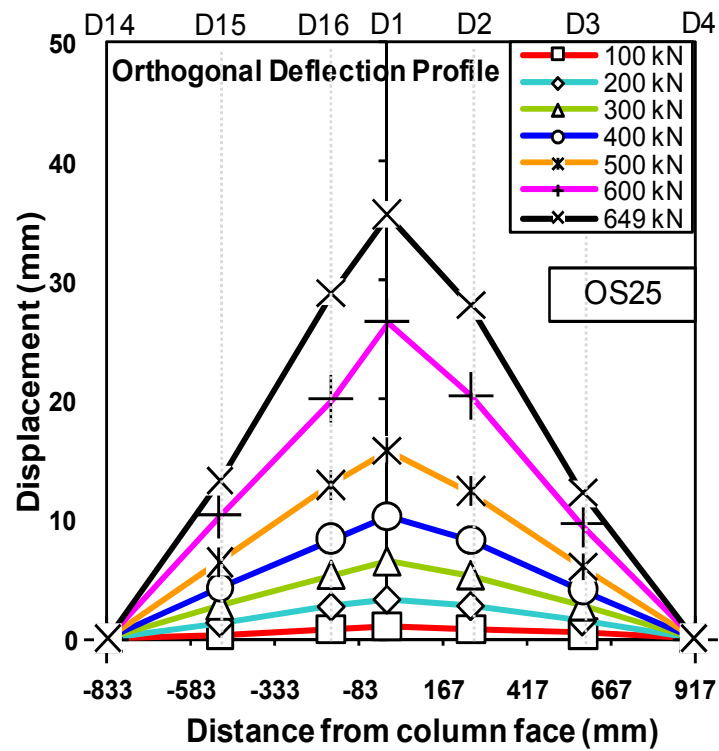


Figure 3.22 Load deflection profiles of OS25

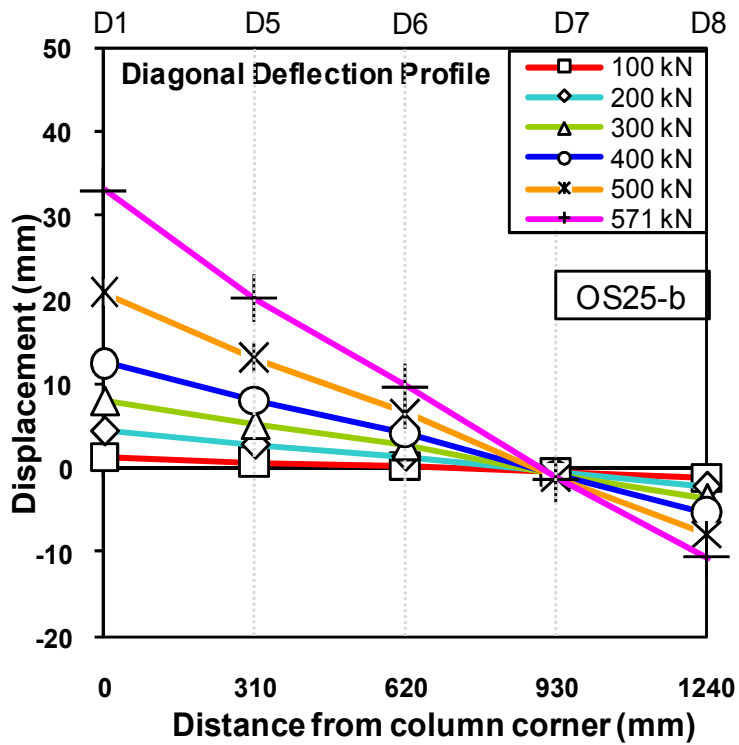
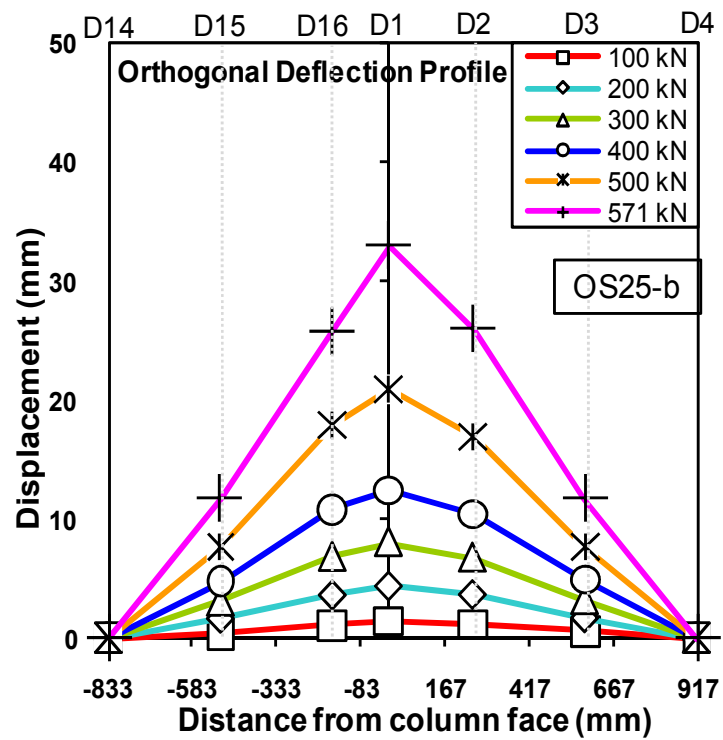


Figure 3.23 Load deflection profiles of OS25-b

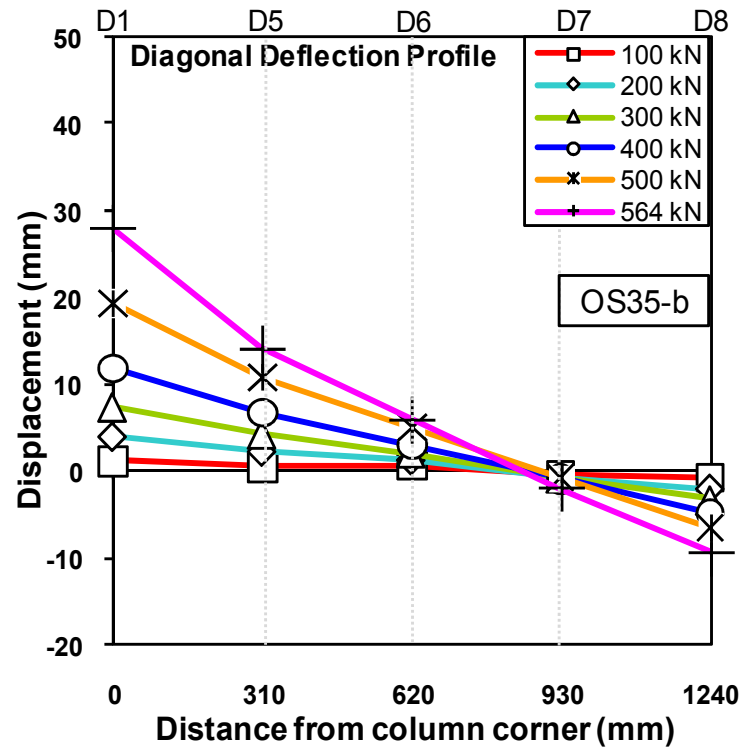
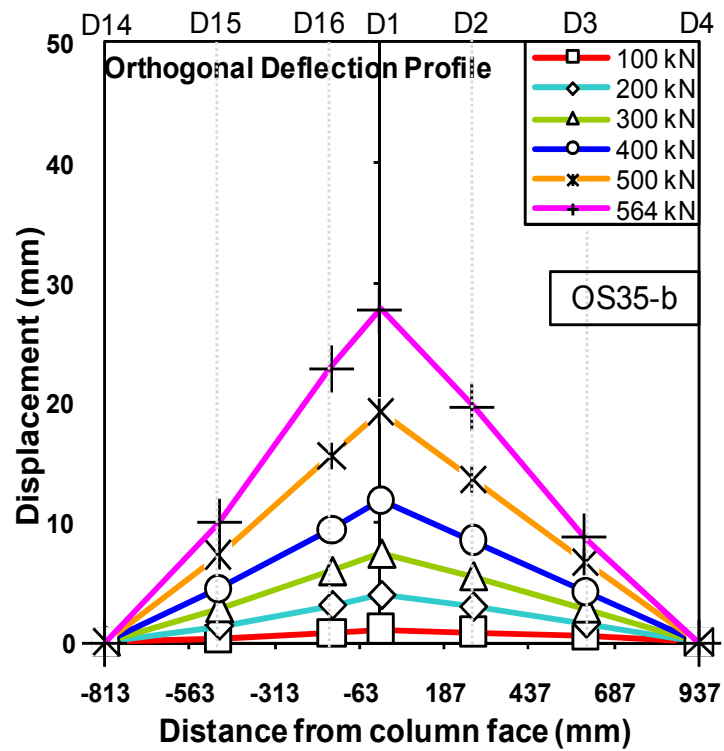


Figure 3.24 Load deflection profiles of OS35-b

Load vs. steel strain relationship measured by strain gage S1 at column face for the specimens with square column stub is illustrated in Figure 3.25. The yield strain value for longitudinal reinforcement is also indicated with the black line. It is apparent from the figure that the initial yielding of the reinforcing steel was observed at a load level of 320 kN to 350 kN for the specimens with square column stub.

Figures 3.26 to 3.29 represent the load vs. longitudinal steel strain curves at column face for specimens with rectangular column stub. The strain distribution along two orthogonal directions X and Y are plotted separately since the span lengths are not identical. It was clearly observed from the graphics that initial yielding took place on the longer side of the column stub (along X axis) at a load range of 300 to 370 kN. On the other hand, first yielding on shorter face of the column stub (along Y axis) was detected at a load range of 420-460 kN for specimens R2, OS25, OS25-b and OS35-b. Specimen R2 has failed just after the yielding took place on shorter face (along Y axis of specimen R3, since the specimen failed at 413 kN.

Top reinforcement strain values measured from strain gages S1 (d away from column face) and S3 (1.75 d away from column face) at load levels corresponding to $\frac{1}{4}$, $\frac{1}{2}$, $\frac{3}{4}$, 1 times ultimate load for specimens with square column stub are illustrated in Figures 3.30 to 3.36.

The strain measurements at ultimate load level obtained by S2 and S3 were below the yield strain value for the control specimens (R1-A and R1) as shown in Figures 3.30 and 3.31. This indicates that yielding zone was bounded somewhere between the column face and location of strain gage S2 (located d mm away from column face) for control specimens with square column stub. It was observed from Figure 3.32 that yielding took place somewhere between strain gages S2 and S3 at failure load level for strengthened specimen OS13. For specimens OS14, CSWP and CSWOP, strain values measured by gage S3 at failure were slightly above the yielding strain which means yielding zone has

almost spread through $1.75 d$ away from column stub (Figures 3.33, 3.35 and 3.36). On the other hand, specimen OS15, experienced extensive yielding beyond the location of strain gage S3 up until the ultimate load level as shown in Figure 3.34.

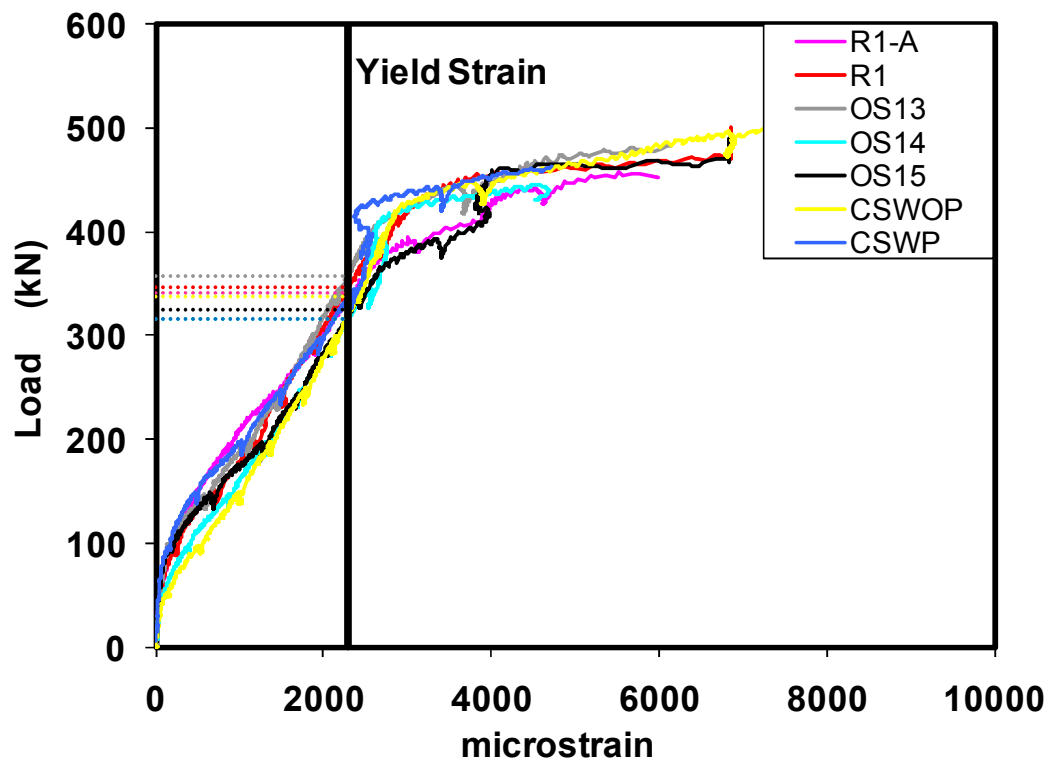


Figure 3.25 Load vs. strain relationship at column face (strain gage S1) for specimens with square column stub

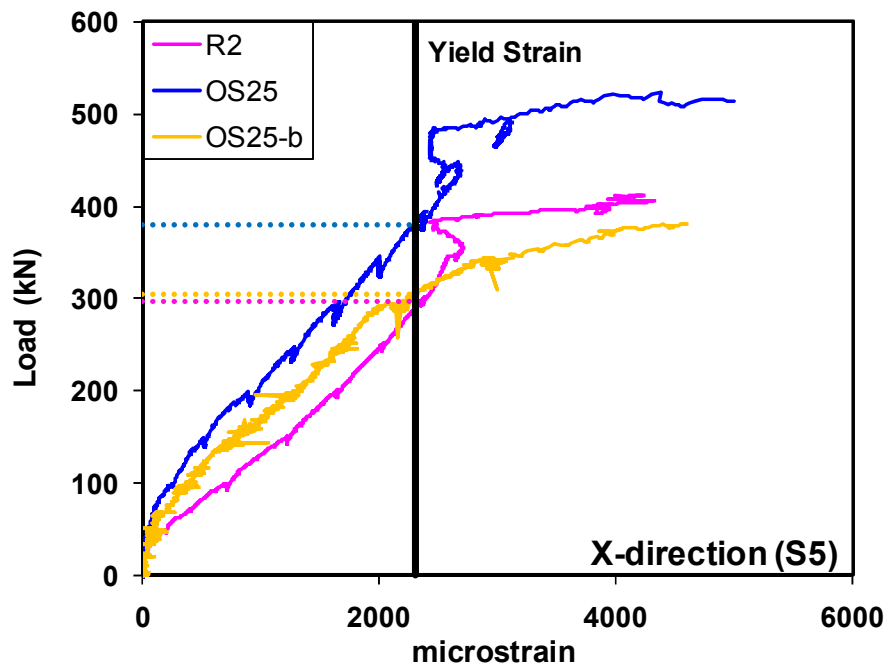


Figure 3.26 Load vs. strain relationship at column face in X-direction (strain gage S5) for specimens with column aspect ratio of 2.

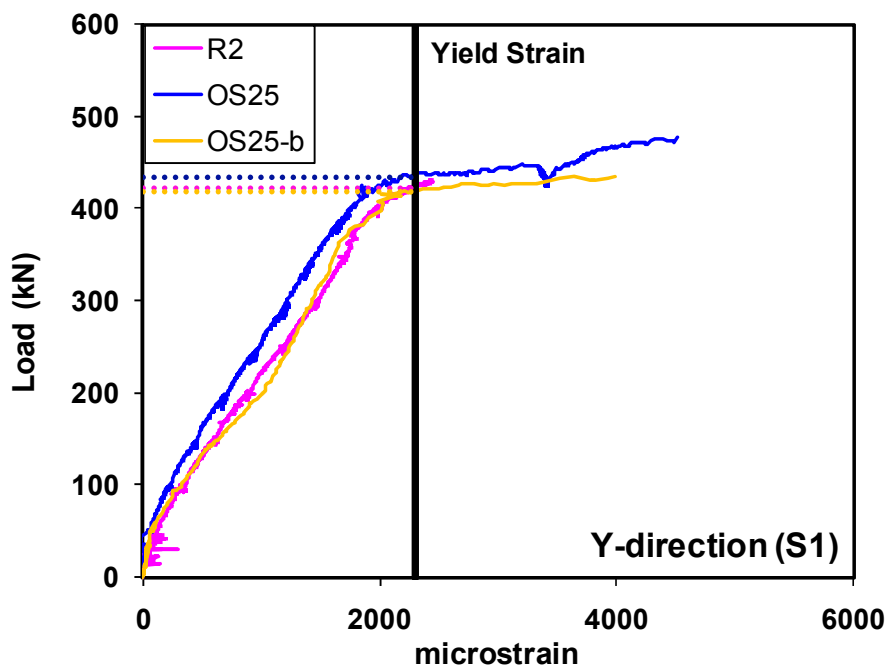


Figure 3.27 Load vs. strain relationship at column face in Y-direction (strain gages S1) for specimens with column aspect ratio of 2.

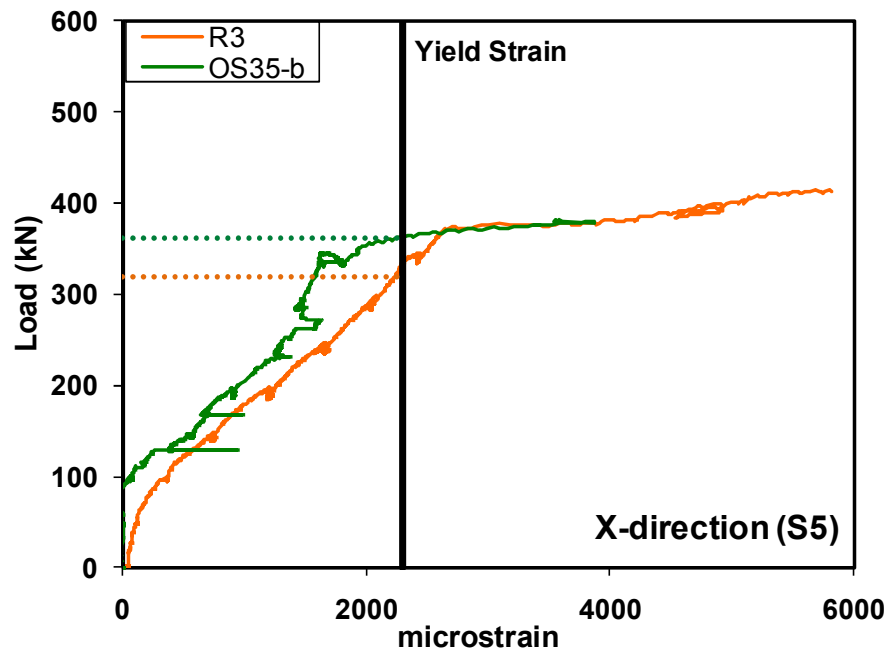


Figure 3.28 Load vs. strain relationship at column face in X-direction (strain gage S5) for specimens with column aspect ratio of 3.

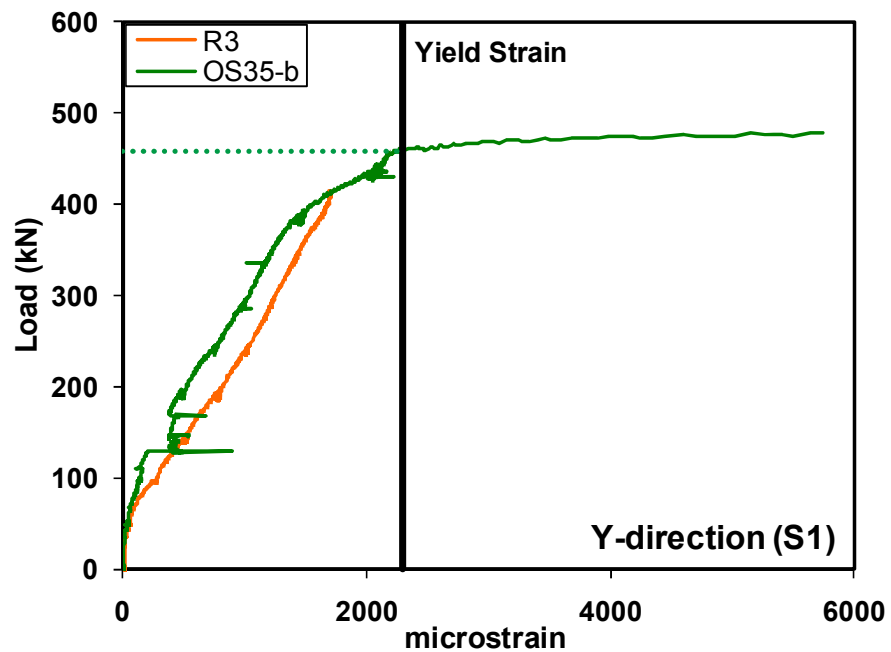


Figure 3.29 Load vs. strain relationship at column face in Y-direction (strain gages S1) for specimens with column aspect ratio of 3.

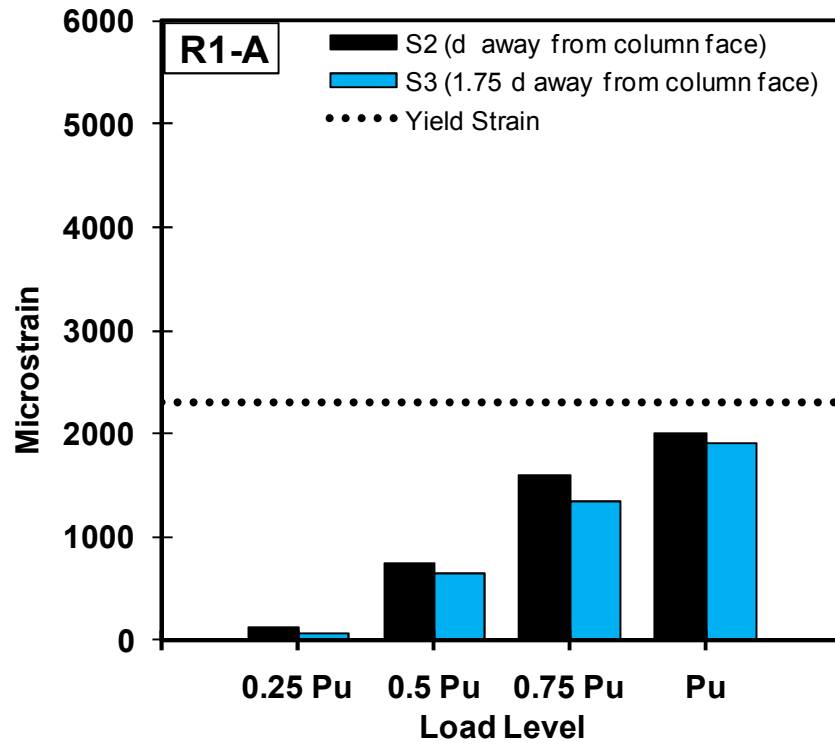


Figure 3.30 Top reinforcement strain profile of R1-A

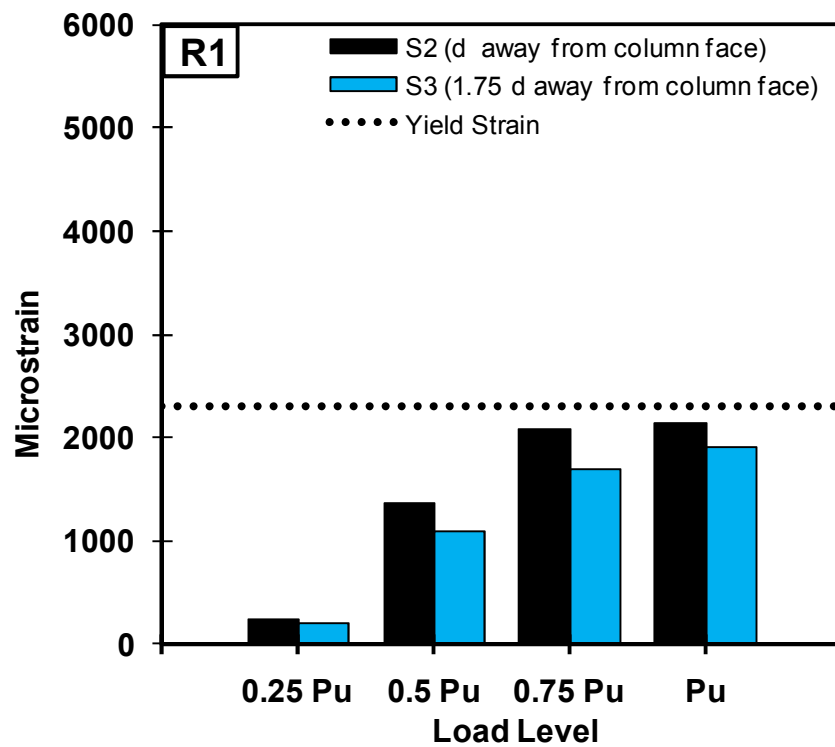


Figure 3.31 Top reinforcement strain profile of R1

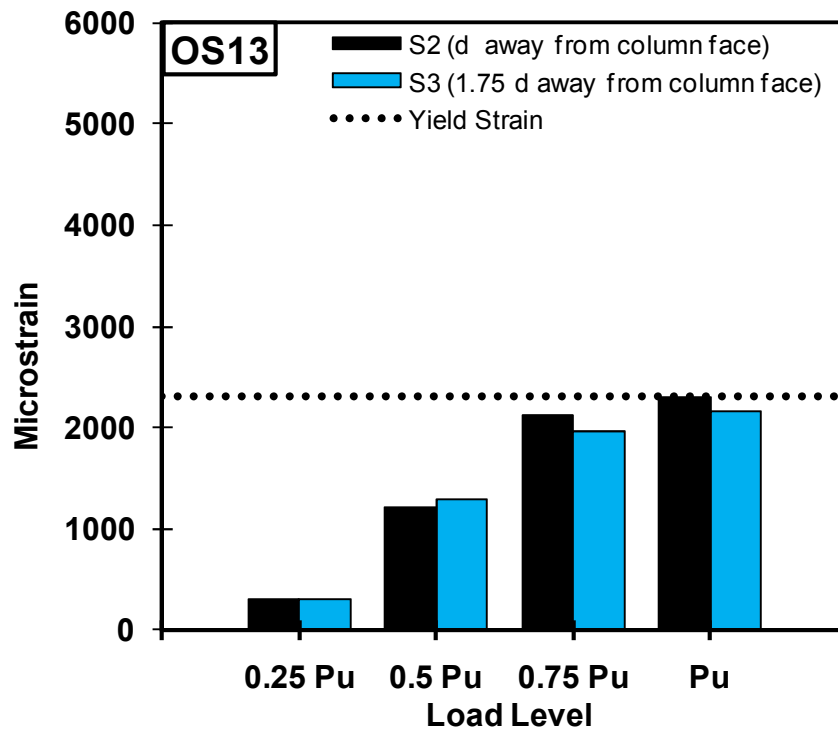


Figure 3.32 Top reinforcement strain profile of OS13

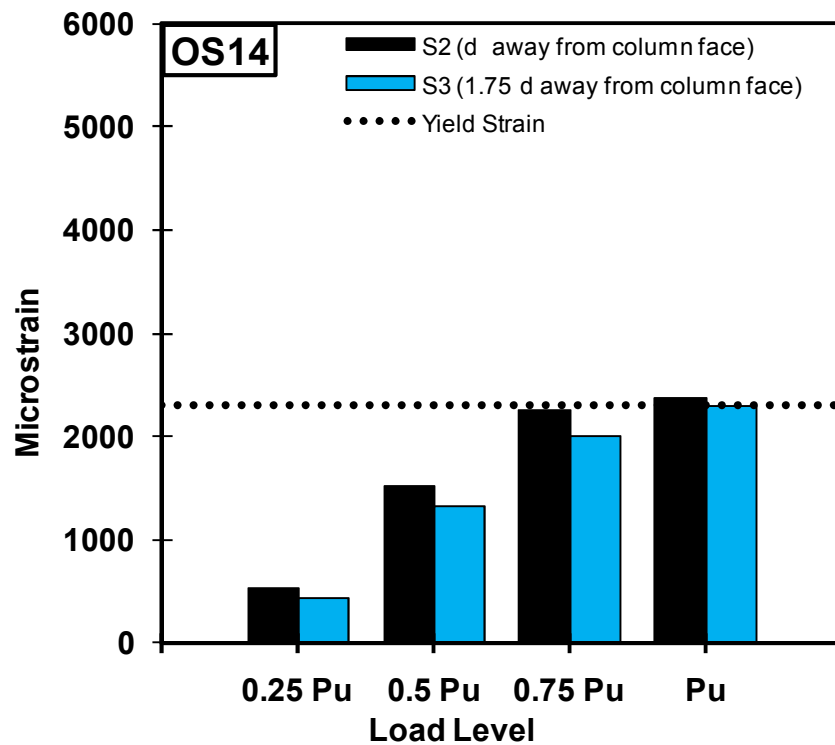


Figure 3.33 Top reinforcement strain profile of OS14

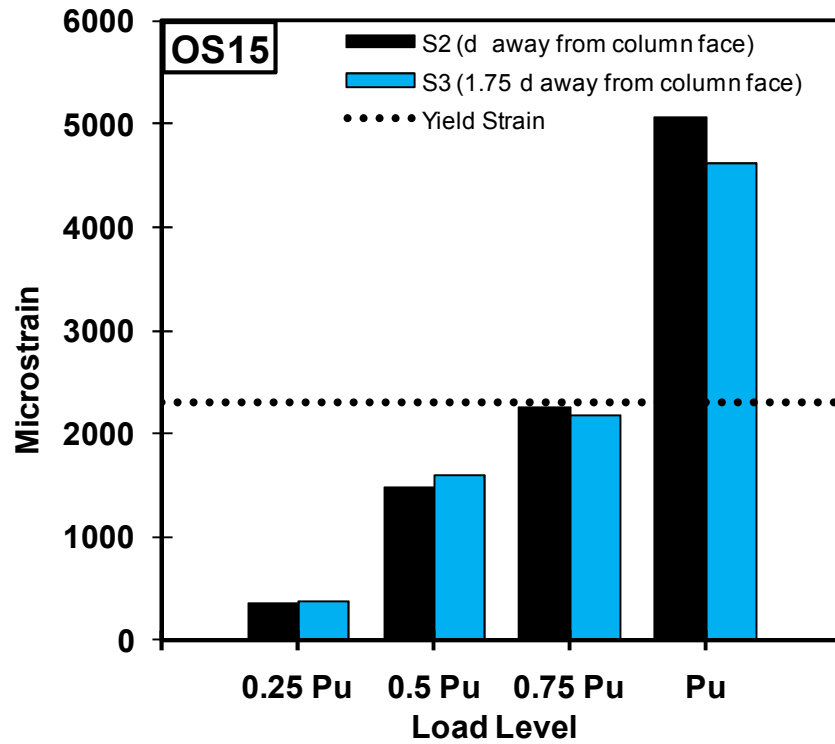


Figure 3.34 Top reinforcement strain profile of OS15

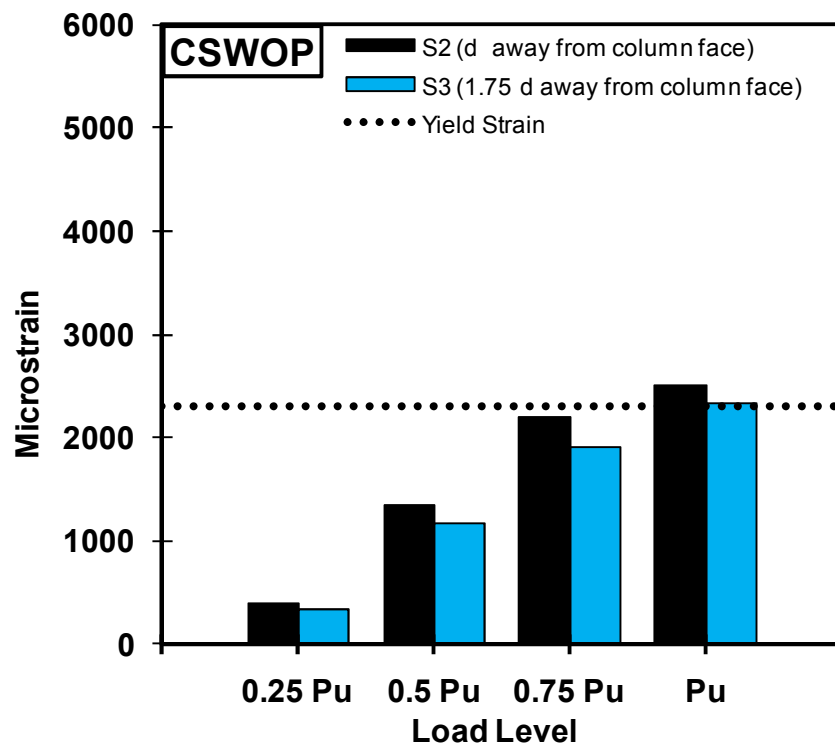


Figure 3.35 Top reinforcement strain profile of CSWOP

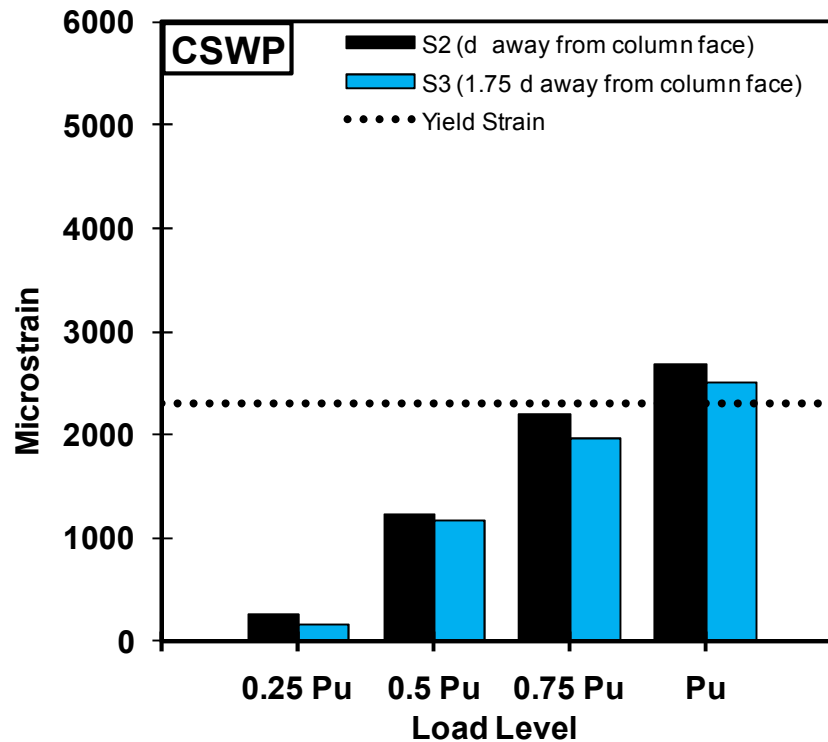


Figure 3.36 Top reinforcement strain profile of CSWP

Strain gages labeled as S2, S3 and S4 were attached to measure reinforcing steel strain along Y axis and strain gages S6, S7 and S8 were attached to measure strain values along X axis for specimens with rectangular column stub (Figure 2.21). The variations of steel strains are illustrated for load levels of $\frac{1}{4}$, $\frac{1}{2}$, $\frac{3}{4}$, and 1 times ultimate load (Figures 3.37 to 3.41).

No yielding was detected on any of the strain gages in any direction for control specimen R2 as shown in Figure 3.37. Yielding was just detected by strain gage S6 along X axis at location d away from longer face of column stub for control specimen R3 (Figure 3.38). Yield zone spread through 1.75 d away from longer face of column stub for specimen OS25 (Figure 3.39). No data was gathered from strain gage S8 (located 2.5 d away from column face) since it did not function during test. In Y direction, yielding has just taken place at d away from column face and did not spread through 1.75d away for specimen

OS25 at failure. Strain history for specimen OS25-b was almost similar to specimen OS25, yielding has been detected at d away from column face in X direction (S7 and S8 has been out of order during test) and in Y direction, the strain value measured at d away from column face at failure was barely above the yield strain (Figure 3.40). Yielding was just observed at strain gages located at d away from column face (S5 and S2) along X and Y directions respectively for specimen OS35-b. In X direction, yielding spread through almost $1.75 d$ away from column face on the other hand, in Y direction yielding zone was bounded at d away from column face (Figure 3.41).

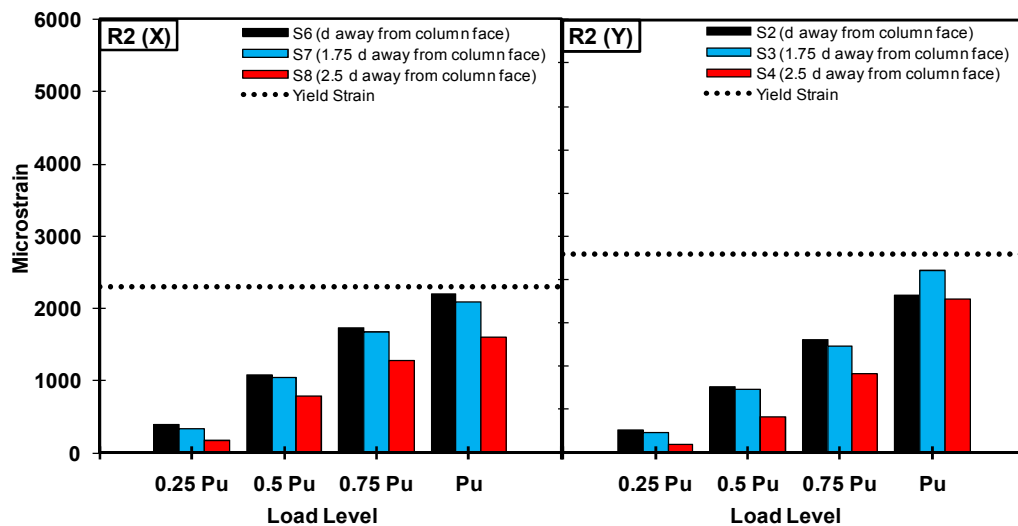


Figure 3.37 Top reinforcement strain profile of R2

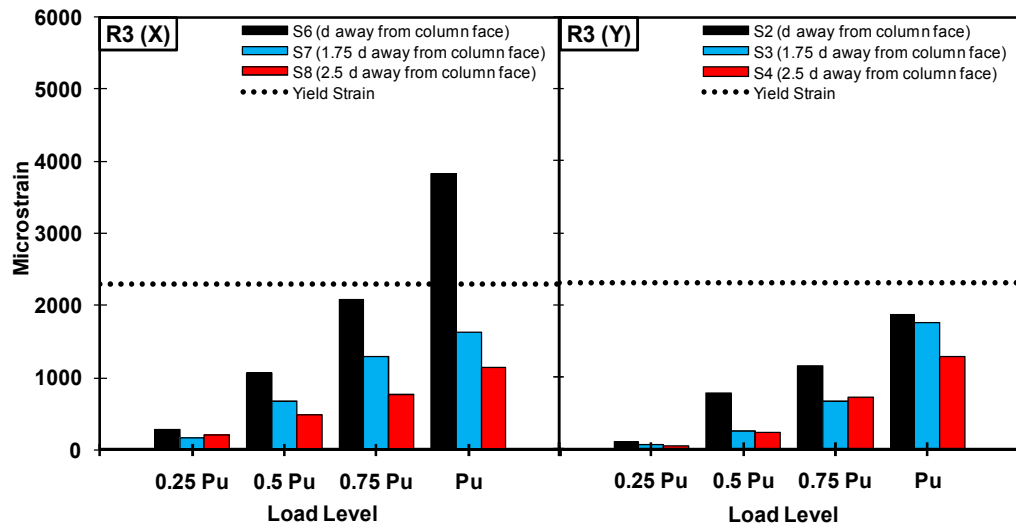


Figure 3.38 Top reinforcement strain profile of R3

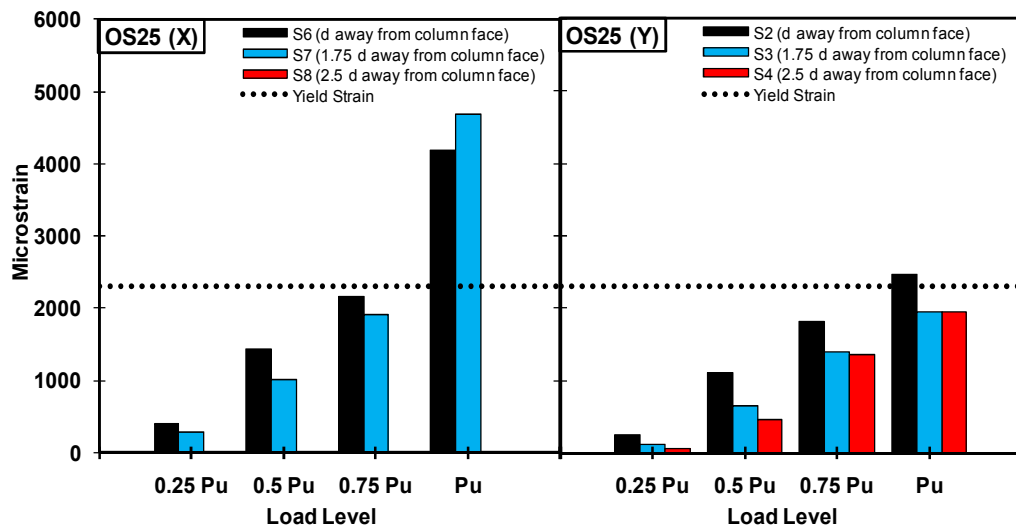


Figure 3.39 Top reinforcement strain profile of OS25

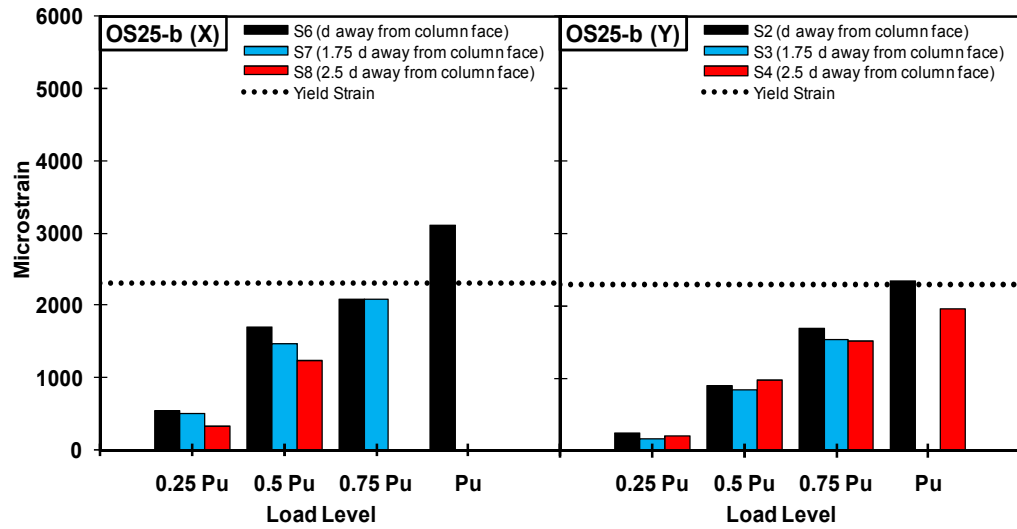


Figure 3.40 Top reinforcement strain profile of OS25-b

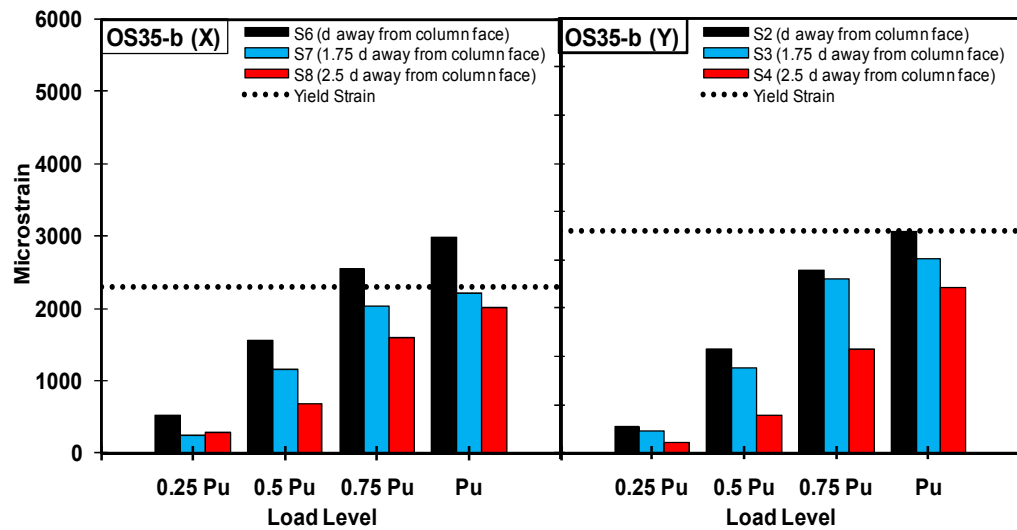


Figure 3.41 Top reinforcement strain profile of OS35-b

3.2.4 Crack Patterns and Failure Modes

Crack propagations on tension face of all specimens were marked during testing. After completion of testing process, photographs of compression and tension face of the specimens were taken and then specimens OS14, OS15, CSWOP and CSWP were cut into two pieces through their punching cones. One quarter of specimens with rectangular column stubs (R2, R3, OS25, OS25-b and OS35-b) were sliced to investigate the inclination of the shear crack in two orthogonal directions (Figure 3.42). The shear crack inclination angles are tabulated in Tables 3.2 and 3.3. The damage picture illustrations are presented in Figures 3.43 to 3.54 for all test specimens.

First flexural cracks occurred on the tension face of the slabs between the load values of 58-116 kN for all specimens (Table 3.1). The corresponding displacement values for the first cracking stage, Δ_{cr} , were detected to be between 0.47 to 0.93 mm (Table 3.1). The radial flexural cracks propagated from the column stub face through slab corners as the load was monotonically increased up to the ultimate load level for control specimens (R1-A, R1, R2 and R3). Those radial cracks were initiated from the CFRP patch boundaries for strengthened specimens (OS13, OS14, OS15, CSWP, OS25, OS25-b and OS35-b). For specimen CSWOP, the radial cracks were propagated from the column corner through the slab edge following the CFRP patch-free path around the CFRP dowel locations.

The first tangential cracks occurred around the column stub at the load range of 350-400 kN for all the test specimens. At this load level, crunching noises were detected for the specimens with CFRP patches (OS13, OS14, OS15, CSWP, OS25, OS25-b and OS35-b) which are due to stretching of CFRP patches with increasing deflection.

Delamination of CFRP patches observed for specimens OS13, OS14, OS15, CSWP, OS25, OS25-b and OS35-b at load level of about 500 kN. The radial and tangential crack excessively widened at this point.

The failure modes of all specimens were punching shear failure in a sudden manner with audible sound. However, considering the excessive yielding of top reinforcement, the failure mode of strengthened specimens can be described as flexural punching. Therefore, the displacement capacities of strengthened specimens considerably increased with respect to companion reference specimens. The locations of the punching cones (either inside or outside the shear reinforced region) of strengthened specimens are presented in Table 3.1. The inclined shear failure cracks for two control specimens R2 and R3 are shown in Figures 3.50b and 3.51a. The average inclination angle values for shear crack in two orthogonal directions were measured to be about 25° for specimens R2 and R3. The punching shear crack initiated outside the shear reinforced region for the strengthened specimens OS13, OS14, OS15 and OS35-b. The average of the observed inclined shear crack angles for specimen OS14 was 31° . This value was consistent with the inclination angle values of the test specimens of Binici (2003). On the other hand, a steeper average crack inclination (38°) was observed in specimen OS15. This difference may be attributed to the reduced distance between supporting boundary and crack tip on the compression side of the specimen due to the use of more perimeters for CFRP dowels. No damage was observed on the CFRP dowels after failure of specimens OS14, OS15 and OS35-b (Figures 3.46b, 3.47c and 3.54a). Punching shear cracks were observed inside the shear reinforced zone for the specimens CSWP and CSWOP with average shear crack inclinations of 36° and 45° respectively. It should be noted that these specimens were strengthened by using C-pattern. The two specimens OS25 and OS25-b had rectangular column stub with aspect ratio of 2 also experienced punching inside the shear reinforced region. Increasing the amount of CFRP material used for each dowel did not have any effect on failure mode of those two specimens.

CFRP dowels (especially the ones located in the first and the second rows) of the specimens (CSWOP, CSWP, OS25 and OS25-b) that failed inside the shear reinforced zone ruptured in a similar manner close to dowel ends where stress concentration took place.

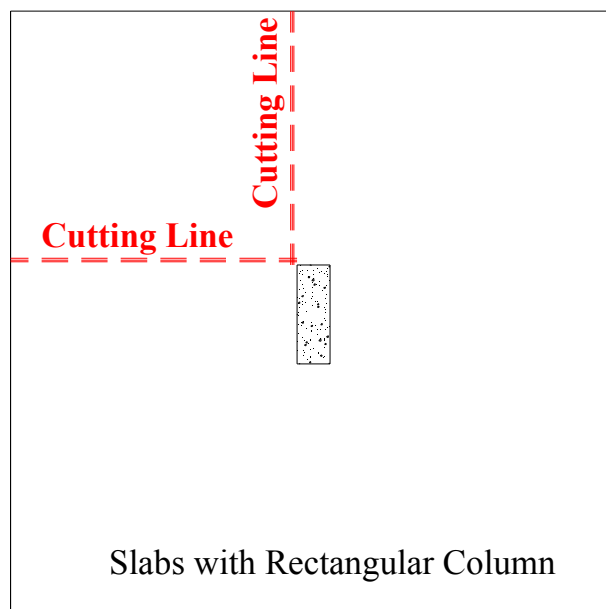
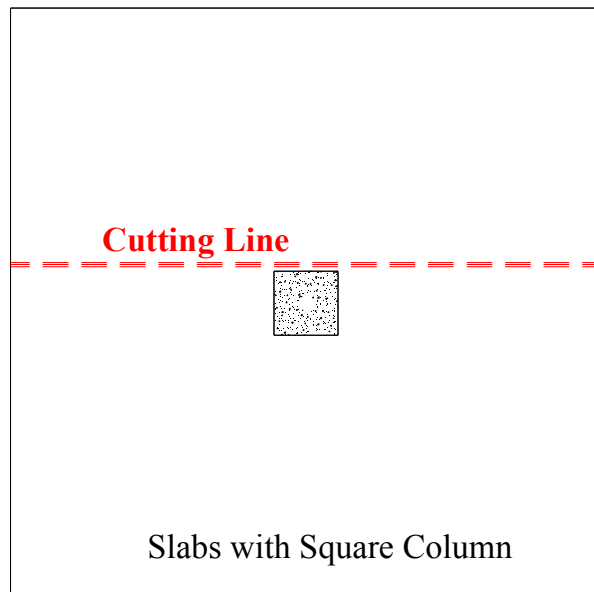


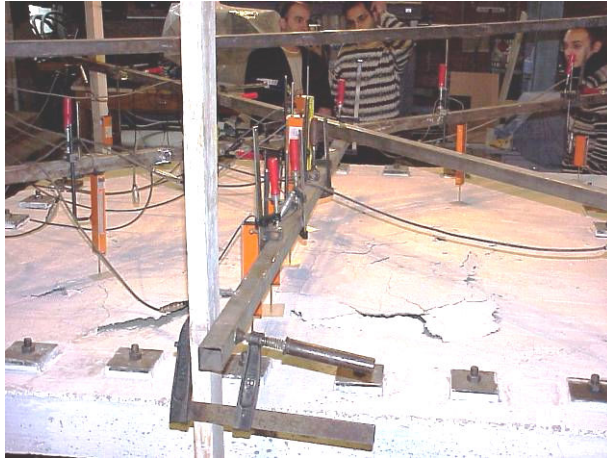
Figure 3.42 Cutting schemes

Table 3.2 Shear crack angles for test specimens with square column stub

Specimen	LEFT	RIGHT	Average	Failure Location
OS14	33°	28°	30°	Outside
OS15	36°	40°	38°	Outside
CWOSP	38°	33°	36°	Inside
CWSP	44°	45°	45°	Inside

Table 3.3 Shear crack angles for test specimens with rectangular column stub

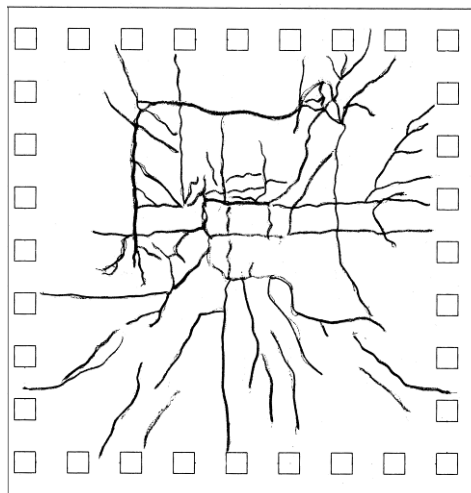
Specimen	X direction	Y direction	Average	Failure Location
R2	26°	25°	26°	-----
R3	24°	23°	24°	-----
OS25	38°	42°	40°	Inside
OS25-b	32°	36°	34°	Inside
OS35-b	33°	30°	32°	Outside



a) Top view



b) Bottom view



c) Tension face cracking sketch

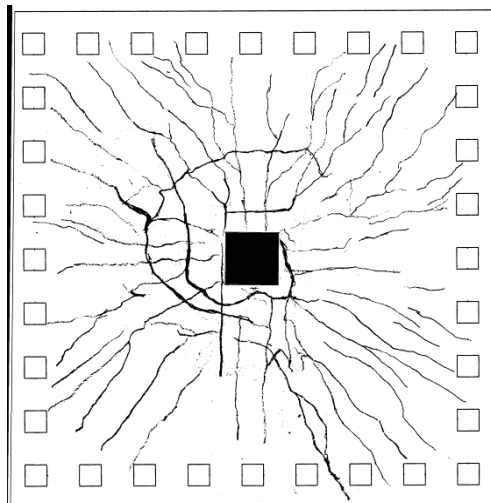
Figure 3.43 Failure surfaces and crack patterns of specimen R1-A



a) Top view



b) Bottom view



c) Tension face cracking sketch

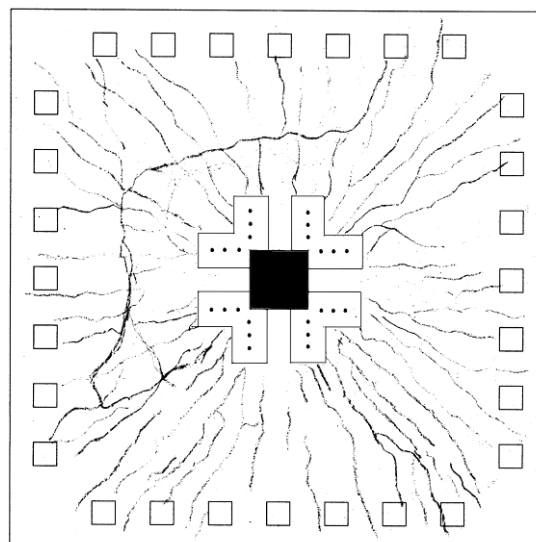
Figure 3.44 Failure surfaces and crack patterns of specimen R1



a) Top view



b) Bottom view



c) Tension face cracking sketch

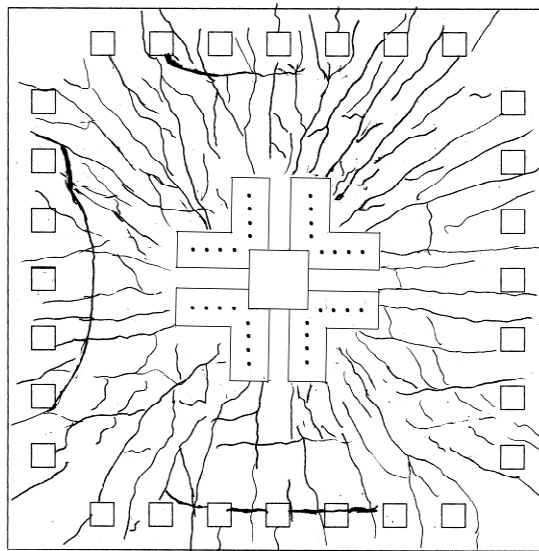
Figure 3.45 Failure surfaces and crack patterns of specimen OS13



a) Bottom view

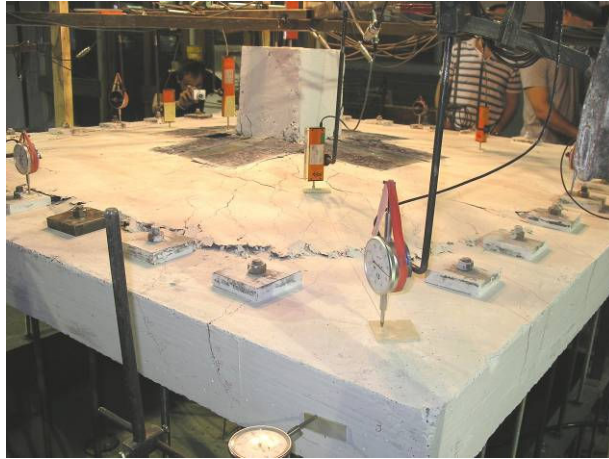


b) Inclined shear crack



c) Tension face cracking sketch

Figure 3.46 Failure surfaces and crack patterns of specimen OS14



a) Top view



b) Bottom view

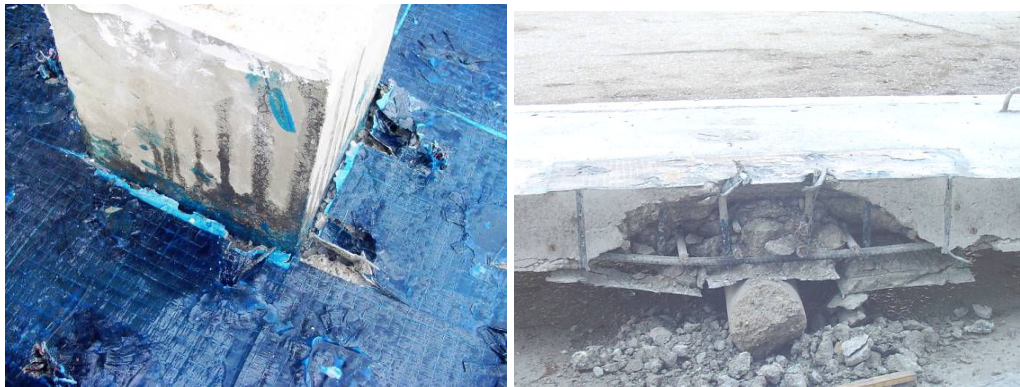


c) Inclined shear crack

Figure 3.47 Failure surfaces and crack patterns of specimen OS15



a) Top view



b) Rupture of CFRP dowels

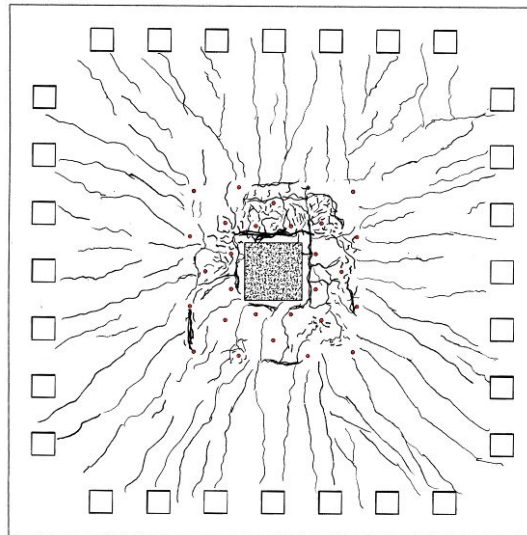


c) Inclined shear crack

Figure 3.48 Failure surfaces and crack patterns of specimen CSWP



a) Bottom view



b) Tension face cracking sketch



c) Inclined shear crack

Figure 3.49 Failure Surfaces and Crack patterns of Specimen CSWOP



a) Top view



b) Inclined shear crack

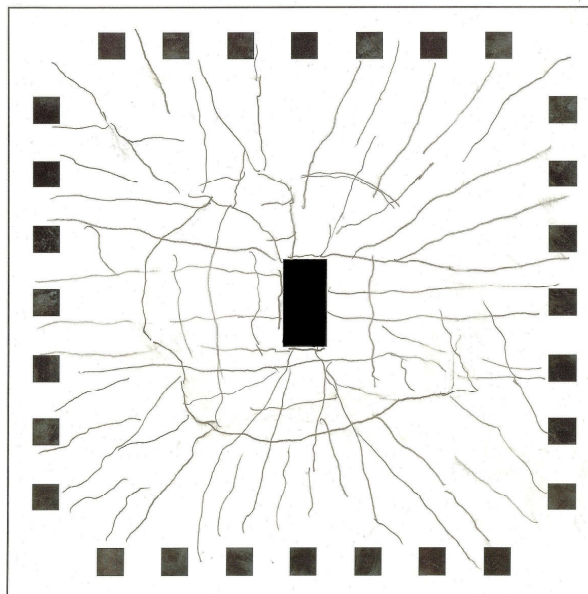
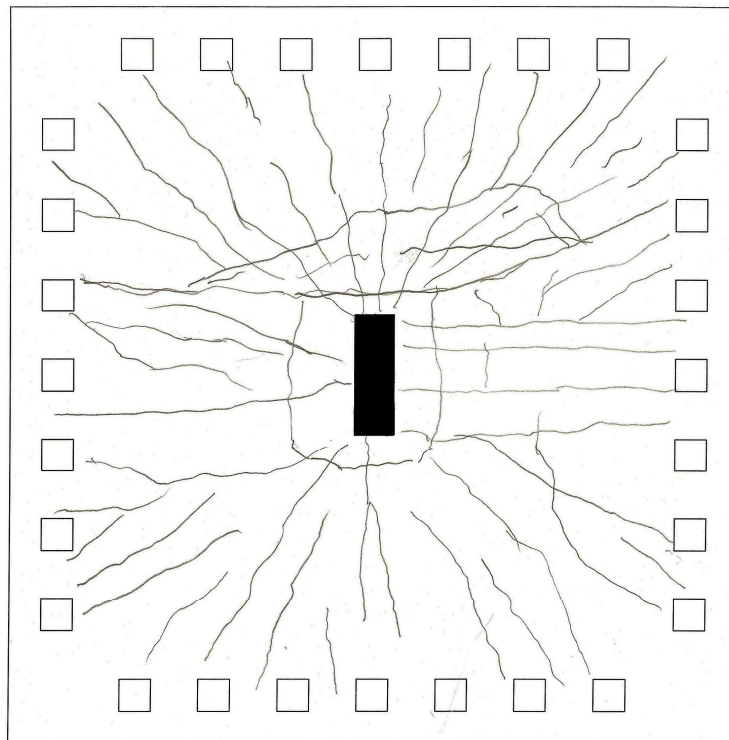


Figure 3.50 Failure surfaces and crack patterns of specimen R2



a) Inclined shear crack



b) Tension face cracking sketch

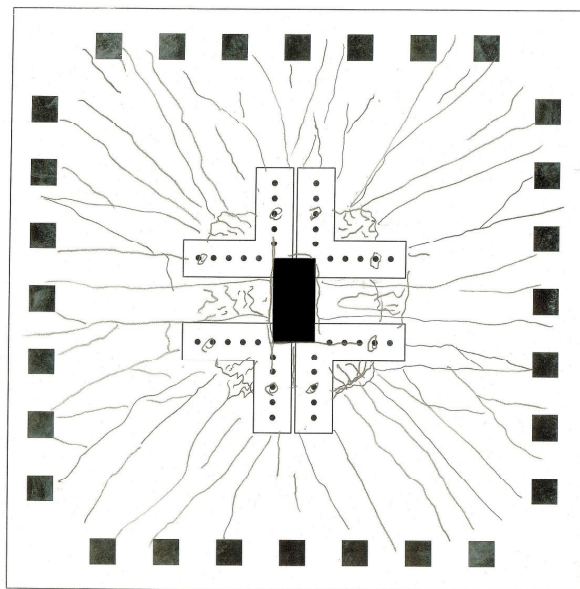
Figure 3.51 Failure surfaces and crack patterns of specimen R3



a) Top view



b) Inclined shear crack



c) Tension face cracking sketch

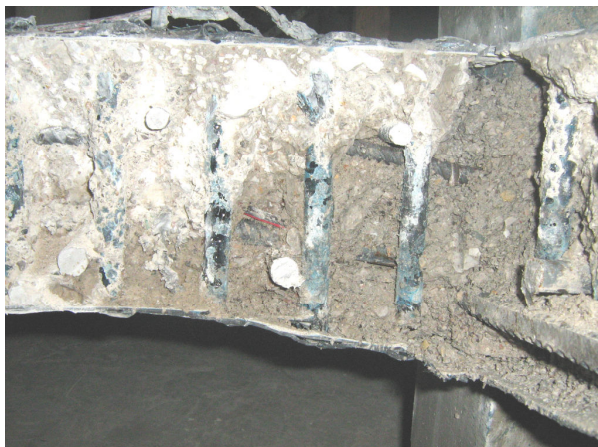
Figure 3.52 Failure surfaces and crack patterns of specimen OS25



a) Top view



b) Inclined shear crack



c) Rupture of CFRP dowels

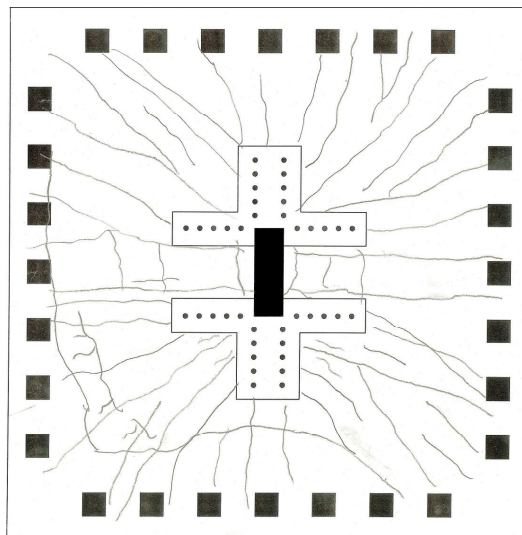
Figure 3.53 Failure surfaces and crack patterns of specimen OS25-b



a) Bottom view



b) Inclined shear crack



c) Tension face cracking sketch

Figure 3.54 Failure surfaces and crack patterns of specimen OS35-b

3.3 DISCUSSION OF TEST RESULTS

3.3.1 Strength, Stiffness and Ductility

Load-center deflection curves of two control specimens R1-A and R1 having one and two column stubs respectively are presented in Figure 3.55. Both specimens had a similar load-deflection response, however the ultimate load capacity (V_u) of specimen R1 was 9% greater compared to specimen R1-A. The increase in displacement value at ultimate load level (Δ_u), in specimen R1 was almost 35% relative to specimen R1-A. Specimen R1-A reached 79% of its flexural capacity whereas this ratio was equal to 86% for specimen R1.

Load-center deflection curves of specimens R1, OS13, OS14 and OS15 are illustrated in Figure 3.56 to present the effect of increasing number of CFRP dowel perimeters organized in O-pattern. The ultimate load and failure deflection values were gradually enhanced by increasing the number of perimeters from 3 to 5. However, due to lower concrete strength, the ultimate capacity of specimen OS14 is observed to be less than that of specimens OS13. Specimen OS15, with highest number of CFRP dowels, experienced the maximum strength enhancement (31.2%), deformability of punching shear failure 181% of the control specimen and post punching resistance 131% of the control specimen. The theoretical flexural capacity was exceeded by specimens OS13 and OS15. Criswell (1974) stated that this exceedence may be attributed to contribution of membrane action and strain hardening and may provide up to 25% increase over the capacity calculated by yield line analysis.

In Figure 3.57, load-center deflection plots of specimens CSWP and CSWOP are presented together with the response of control specimen R1. The curves of both specimens CSWP and CSWOP are almost identical indicating that additional surface patches bonded on both faces does not have significant effect on response of specimens. Both specimens reached their theoretical flexural capacities just before punching shear failure.

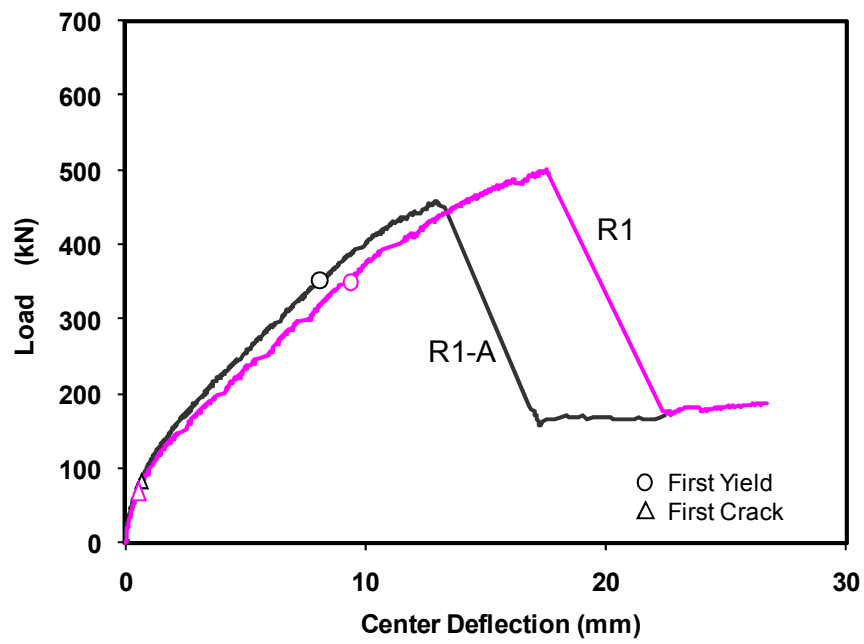


Figure 3.55 Comparison of specimens R1-A and R1

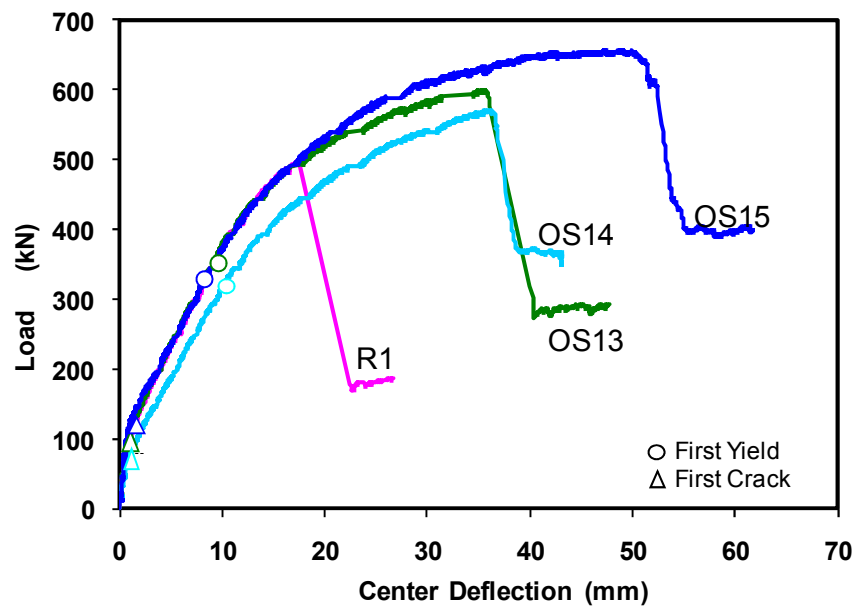


Figure 3.56 Comparison of specimens R1, OS13, OS14 and OS15

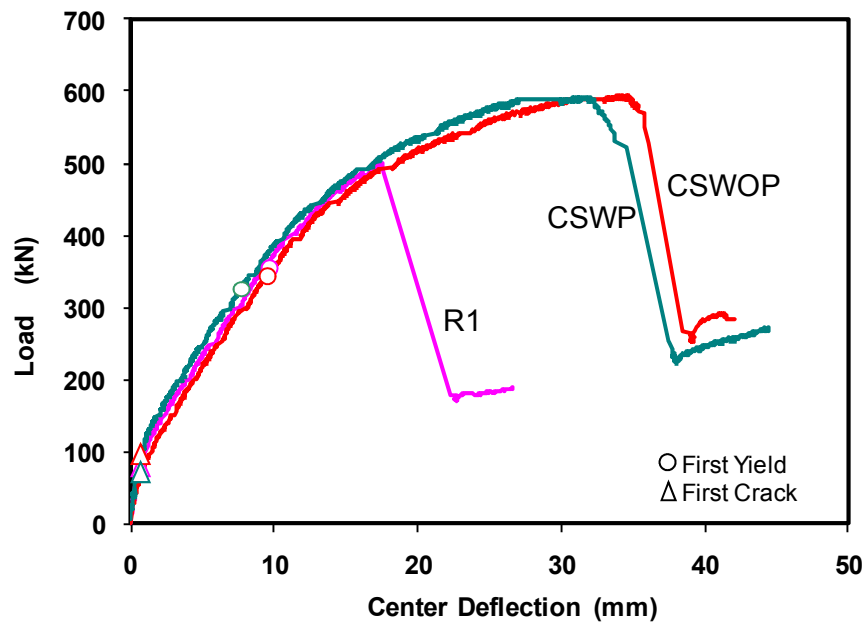


Figure 3.57 Comparison of specimens R1, CSWOP and CSWP

The amount of vertical load carrying capacity increase by application of strengthening method to specimens having column aspect ratio of 2 (OS25 and OS25-b) is 53% and 35% respectively compared to companion control specimen R2 (Figure 3.58). On the other hand, 36% increase was obtained in terms of ultimate punching load for the specimen OS35-b with respect to reference specimen R3 (Figure 3.59). The test results of specimens OS25 and OS25-b reveal that increasing the amount of CFRP may have detrimental effect on punching shear capacity and can not shift the failure cone outside the shear reinforced region. It is believed that highly reinforced dowels create an artificial weakness in the surrounding concrete.

Punching load carrying capacities of specimens R1, R2 and R3 indicated that increasing rectangularity of supporting columns in flat plate systems had a detrimental effect on punching strength. The decrease in strength of specimens R2 and R3 are 15% and 17% compared to ultimate load of specimen R1 (Figure 3.60).

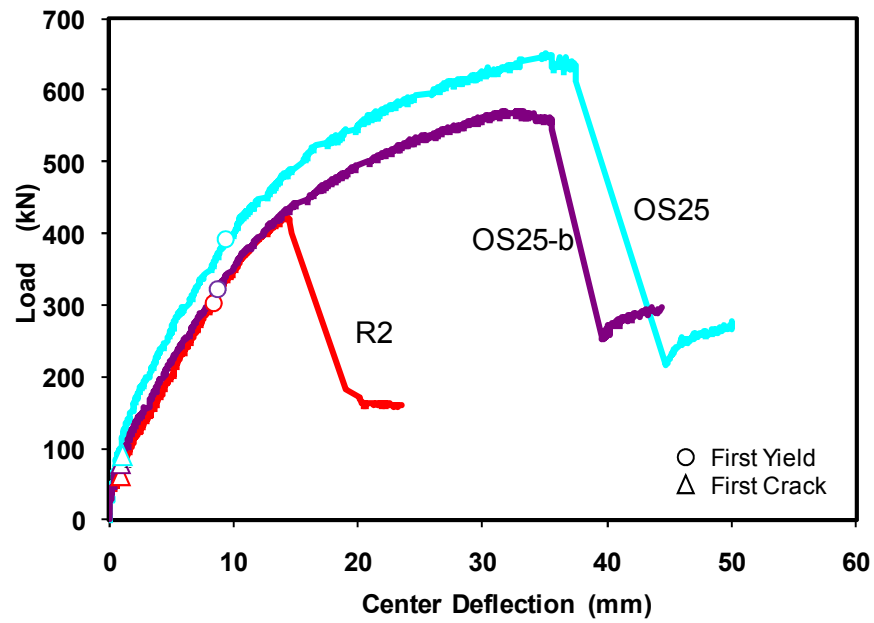


Figure 3.58 Comparison of specimens R2, OS25 and OS25-b

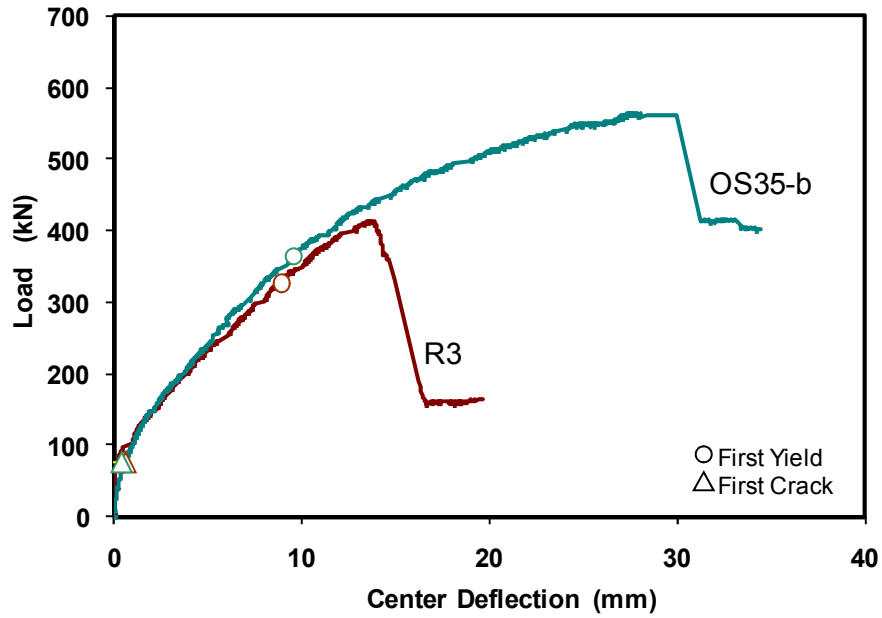


Figure 3.59 Comparison of specimens R3 and OS35-b

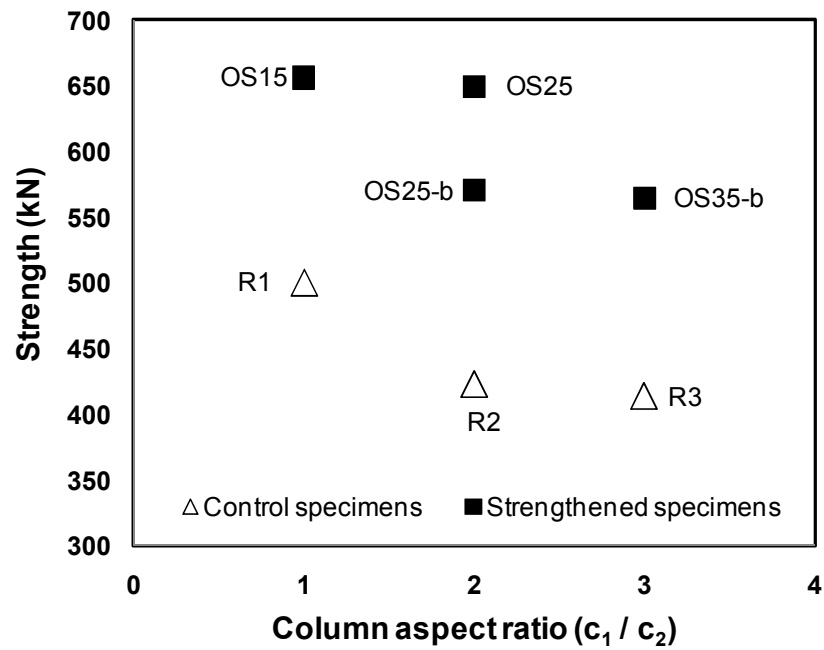


Figure 3.60 Effect of column rectangularity on specimen capacities

On the other hand, Figure 3.60 explicitly implies that at least 30% of strength increase was guaranteed by application of proposed strengthening method to the specimens with varying column aspect ratio from 1 to 3.

The load-center deflection curves of all specimens tested in this study can be idealized with a trilinear curve by the help of load-deflection curves shown in Figure 3.61. Three different stiffness slopes were named as elastic stiffness (K_1), post cracking stiffness (K_2) and post yielding stiffness (K_3) respectively. Two of those stiffness slopes (K_1 and K_2) can be obtained from experimental data. The initial slope (K_1) of the trilinear curve was determined by the help of cracking load and deflection data of the test specimens given in Table 3.1

Load and center deflection values for first cracking point of idealized curve selected to be 79 kN and 0.65 mm respectively that were equal to average values of test results (Table 3.4). The slope of the post cracking portion (K_2) up to first yielding ranged between 27 to 37 kN/mm for all the specimens as stated in Table 3.4

The slope of the post cracking portion of the idealized curve was assumed to be equal to average value of 31.8 kN/mm and was retained up to 495 kN (that is equal to 85% of flexural capacity) instead of 334 kN that is equal to average yielding load value. Since, it is obvious from the Figure 3.61 that post cracking stiffness governs beyond the average yielding point till 85% of flexural capacity is reached for this particular study. Up to this point it was possible to estimate an empirical bilinear path for load-center deflection curves of test specimens used in this study regardless from experimental results, since, elastic stiffness, first cracking sectional moment and corresponding deflection and flexural capacity values can be calculated theoretically to construct the initial and post-cracking stiffnesses (K_1 and K_2).

On the other hand, post yielding stiffness (K_3) was estimated by using the ultimate load capacity and failure deflection of specimen OS15. The slope of the third portion found to be 7.98kN/mm which was equal to 4.6 % of initial slope (K_1).

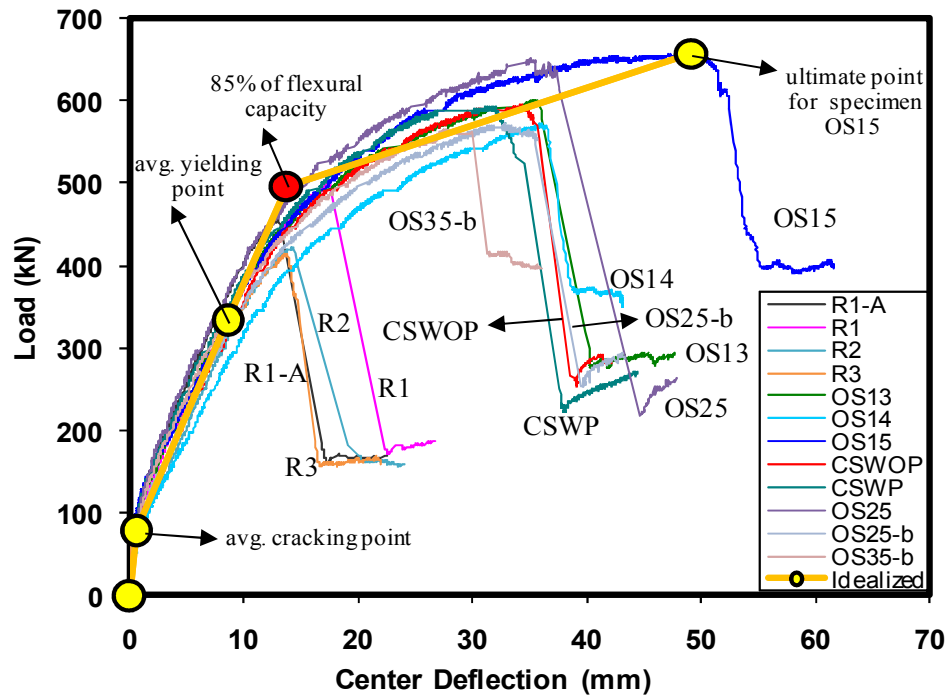


Figure 3.61 Idealized curve definition

In general, displacement ductility factor is simply defined as the ratio of displacement value at ultimate load level to deflection value at first yield as shown in Equation 3.1. The calculated μ values for all test specimens were summarized in Table 3.4. A similar trend was also observed in strengthened specimens with varying column aspect ratio. In addition, displacement ductility values for strengthened specimens OS15, OS25, OS25-b and OS35-b significantly increased compared to reference specimens R1, R2 and R3 respectively. Figure 3.62 shows the ductility enhancement as the theoretical flexural capacity is reached.

$$\mu = \frac{\Delta_u}{\Delta_y} \quad (3.1)$$

Table 3.4 Ductility and stiffness

Specimen	μ	K_1	K_2	K_2 / K_1
R1-A	1.67	138.6	36.69	0.26
R1	1.89	130.8	31.84	0.24
R2	1.78	114	31.70	0.28
R3	1.59	142	31.37	0.22
OS13	3.78	125.6	30.15	0.24
OS14	3.59	81	27.50	0.34
OS15	6.00	123.6	29.00	0.23
OS25	3.95	120.5	34.70	0.29
OS25-b	4.05	120	30.77	0.26
OS35-b	2.96	155	31.79	0.21
CSWOP	3.80	102	33.09	0.32
CSWP	4.30	125.6	32.78	0.26

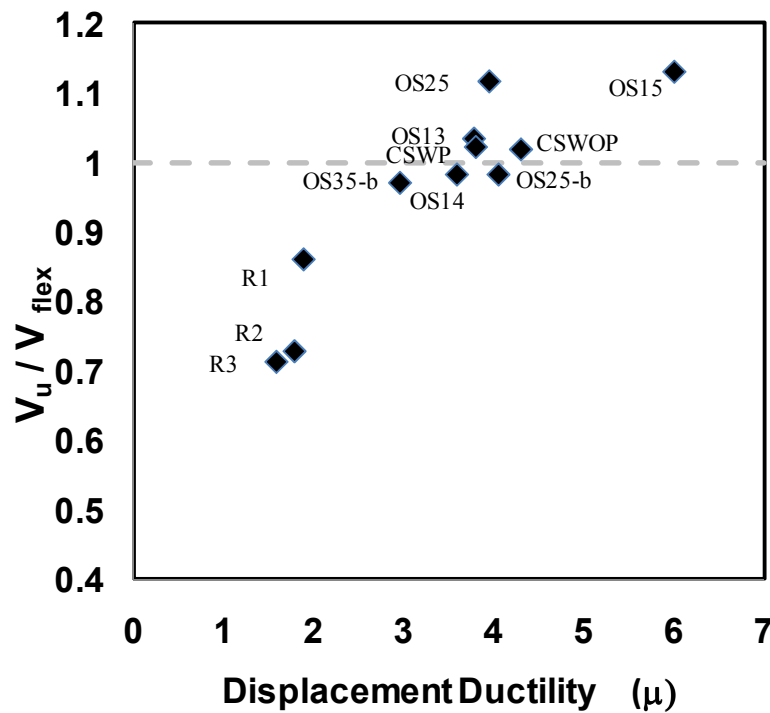


Figure 3.62 Comparison of displacement ductility

3.3.3 Effect of Test Parameters

Column Stub

The presence of column stub on the tension side for control specimen R1 significantly affected the ultimate load and corresponding failure displacement values of the specimen compared to R1-A. This difference can be attributed to the additional restraint provided by the stub located on the tension face of the slab, which delays cracking right above the connection region.

In the light of these results, assuming that the specimen R1-A represents the slab-column connection of the top floor of flat-plate structures and R1 simulates the slab-column connection located in intermediate floors of flat-plate structures, it can be concluded that the slab-column connections on the roof of the flat-plate structures are relatively more susceptible to punching under vertical loading with respect to intermediate floor slab-column connections.

Strengthening Pattern

Punching shear failure occurred outside the strengthened region for specimens OS13, OS14 and OS15 with square column stub. The punching failure perimeter of those specimens were enhanced owing to the increase in number of CFRP dowels and number of CFRP perimeters accordingly that eventually leads to augmentation of load carrying capacity. Specimens CSWP and CSWOP experienced punching shear failure inside the shear reinforced region. In these tests, there were apparently a weak interface developing between perimeters marked as I and III in Figure 3.63. This may be due to the fact that the spacing between the perimeters II and III was $0.75d$ and the number of dowels falling on these two perimeters was only four. The number of dowels on perimeter I, however, was eight and the punching shear crack was observed to initiate from perimeter I.

The two main differences among the specimens CSWP and CSWOP were the existence of CFRP sheet patches bonded between the slab and the fans of the CFRP dowels and the construction method of CFRP holes. The use of the CFRP surface sheets to provide better anchorage for the dowels and changing construction method of CFRP holes did not make any significant change in the response of mentioned specimens. The failure loads, displacement values at failure and post-punching failure load values of both specimens were almost identical. The only benefit of the surface patches, if to mention one, was to increase the first cracking load value of the specimens OS13, OS14, OS15 and CSWP with respect to specimen CSWOP by contributing to the tensile strength of the concrete.

The load center deflection plots indicated that the response of strengthened specimens OS13, OS14, CSWOP and CSWP were almost identical, although the strengthening patterns and the failure mechanisms were different. The major drawbacks of the C-pattern used for specimens CSWP and CSWOP are the insufficient amount of the CFRP dowels and the excessive spacing between

CFRP dowel perimeters leading to undesired punching failure inside the shear reinforced region.

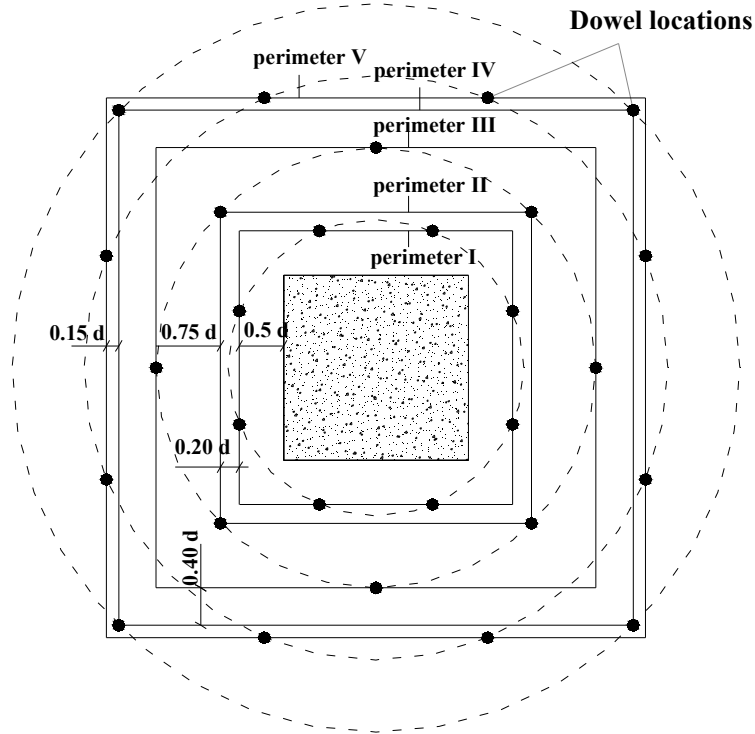


Figure 3.63 C-Pattern perimeter distribution

3.3.4 Post-Punching Behavior

Application of proposed CFRP strengthening method led to significant increase in post-punching capacity (V_{pp}) of all the strengthened specimens. However, test results indicated that failure mode of test specimens has a deterministic effect on residual capacity of strengthened specimens after failure. On the other hand, varying column aspect ratio has no significant effect on post-punching behavior of both control and strengthened specimens for this particular study. The post punching capacity of all test specimens are presented in Figure 3.64. The residual capacity values of control specimens with different column aspect ratios varied between 159 kN and 175 kN (Figure 3.65a). Considering the specimens OS13 and OS14, the post punching capacity had tendency to

increase up to 80% of control specimen R1. This rising trend can be explained by the increase in the amount of top and bottom reinforcement owing to the extension of failure cone that contributes to the shear resistance by means of dowel action passing through the column stub. The failure mode and residual capacity of specimen OS15 was almost identical to OS14 (Figure 3.65b). This indicates that the post-punching capacity can be upgraded by enlarging the strengthened region (provided that the failure outside the shear reinforced zone is ensured) around the slab-column up to a limited extent. In addition, the residual capacities of strengthened specimens OS15 and OS35-b are almost identical (Figure 3.65c). Since the location of punching failure cone is outside the shear reinforced zone for both specimens, it is obvious that column aspect ratio has no significant effect on post-punching capacity for the specimens having identical column perimeter. The residual capacities after failure for four strengthened specimens (CSWOP, CSWP, OS25 and OS25-b) that failed inside the strengthened region are presented in Figure 3.65d separately.

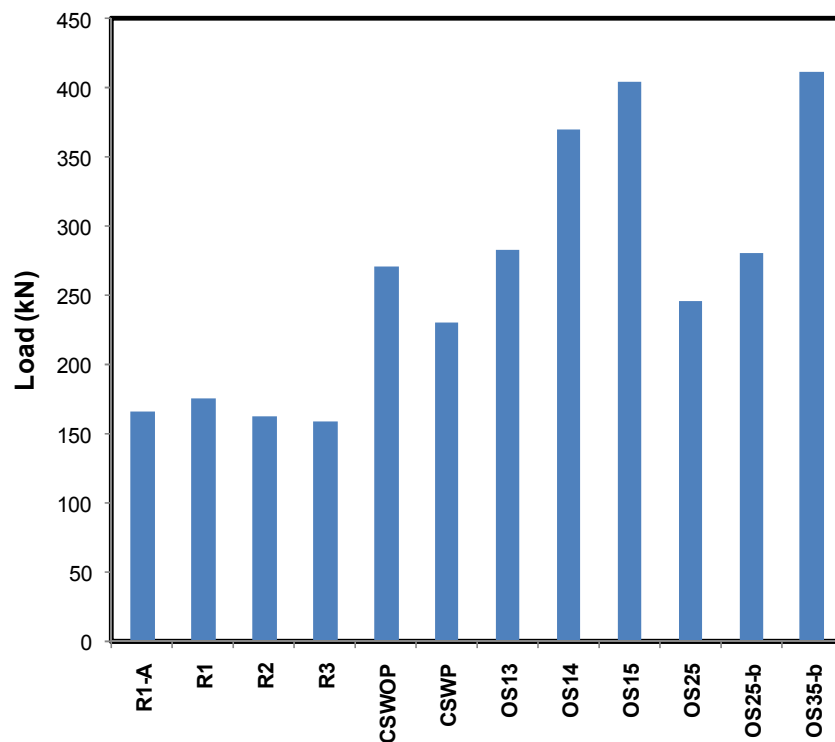


Figure 3.64 Post-punching capacities of test specimens

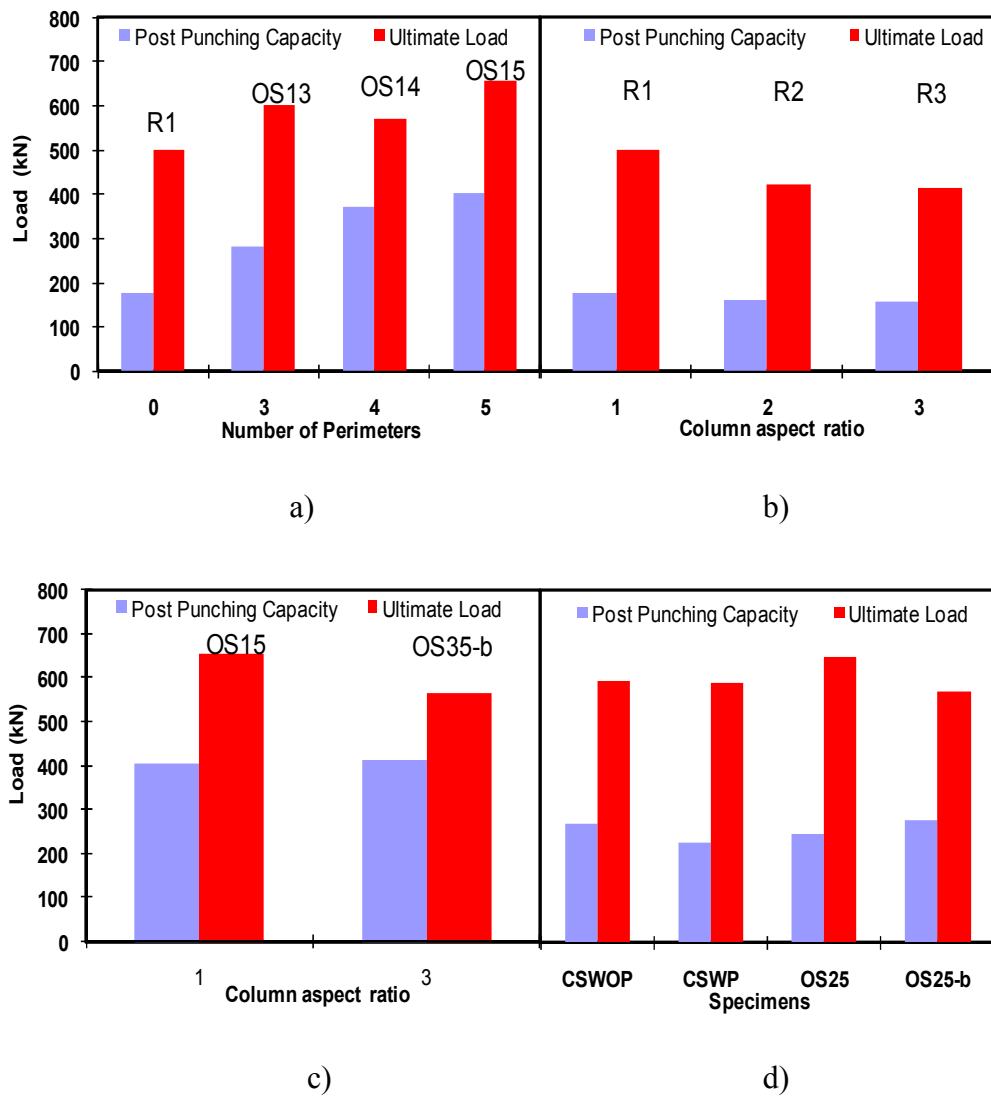


Figure 3.65 Comparison of post-punching capacities of test specimens

In order to represent the variation in the residual load capacity, it may be possible to categorize all the test specimens into three groups regarding the failure mode and existence of strengthening.

First group consist of reference specimens (R1-A, R1, R2, R3), second group consist of strengthened specimens displaying failure inside the shear reinforced region (CSWOP, CSWP, OS25, OS25-b), finally the third group consists of strengthened specimens that display failure outside the shear reinforced region

(OS13, OS14, OS15, OS35-b) (Figure 3.66). It is apparent from Figure 3.66 that the application of shear strengthening has an augmenting effect on post punching capacity. In addition, ensuring punching failure outside the shear reinforced region has an additional enhancement in post punching capacity compared to post punching capacity results of test specimens that were failed inside the shear reinforced region.

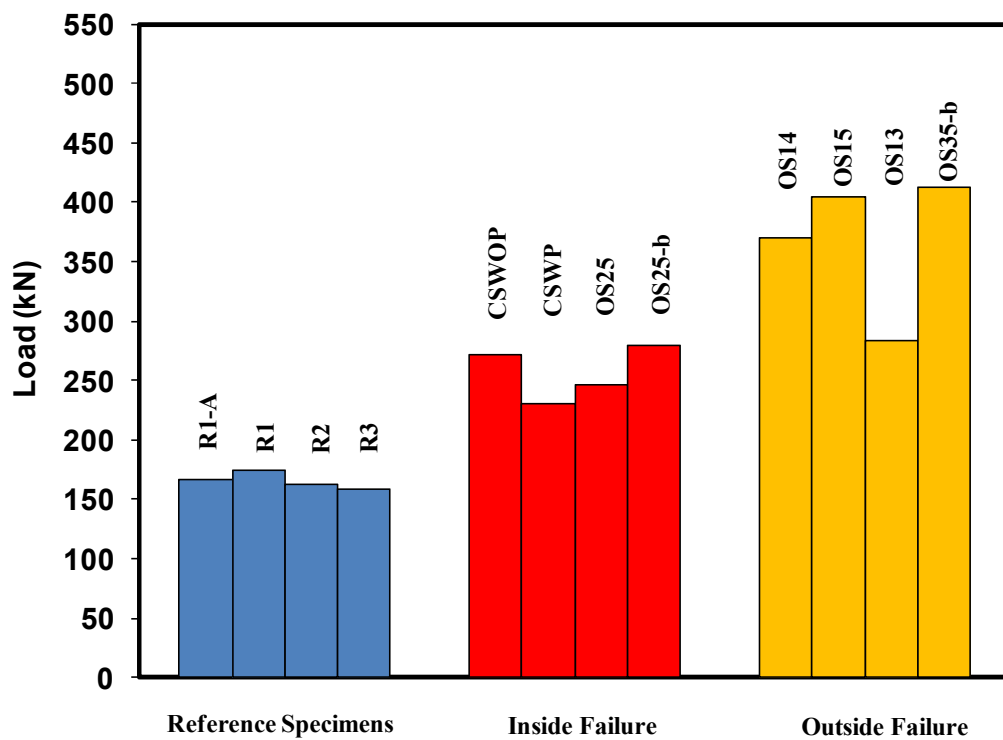


Figure 3.66 Effect of failure location and strengthening on post-punching capacity

3.3.5 Comparison of Test Results with the Proposed Models in the Literature

3.3.5.1 Model by Menetrey (1996)

Menetrey (1996) proposed a mechanical model to compute the punching shear capacity of slab-column connections with and without shear reinforcement. The model mainly considers the integration of tensile stress of concrete and reinforcement through the punching crack (Figure 3.67). The total punching shear resistance consists of four components as shown in Equation 3.3.

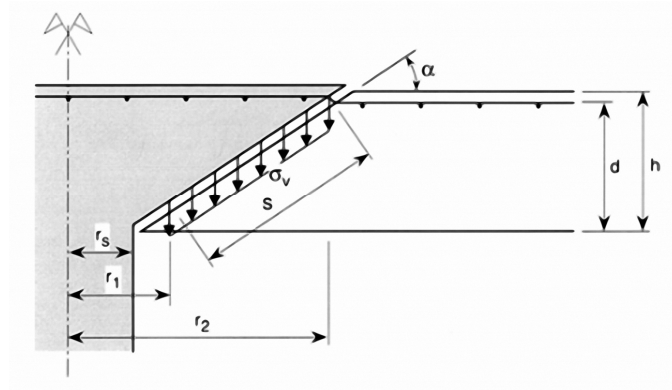


Figure 3.67 Representation of punching strength (from Menetrey 1996)

$$F_{pun} = F_{ct} + F_{dow} + F_{sw} \quad (3.3)$$

where F_{ct} is the vertical component of the concrete tensile force, F_{dow} is the resistance provided by the dowel action, F_{sw} is the vertical force component of the studs, stirrups or bent-up bars.

Concrete resistance is computed by integration of the vertical tensile stress σ_v in the borderline of punching crack. However, the effect of aggregate interlock is neglected. The model assumes a truncated shape for the punching surface restricted between two radii r_1 and r_2 as illustrated in Figure 3.67 and expressed in Equations 3.3 and 3.4.

$$r_1 = r_s + \frac{1}{10} \frac{d}{\tan \alpha} \quad (3.3)$$

$$r_2 = r_s + \frac{d}{\tan \alpha} \quad (3.4)$$

$$s = \sqrt{((r_2 - r_1)^2 + (0.9d)^2)} \quad (3.5)$$

where r_s is the radius of the column, α is the inclination of shear crack, d is the effective depth and s is the inclined length.

The contribution of the concrete tensile force, F_{ct} , on punching capacity by assuming a constant stress distribution is expressed by Equation 3.6. Three parameters ξ , μ , and η were involved in the Equation 3.6 in order to consider the effects of amount of reinforcement, slab thickness and shear crack inclination radius respectively (Equations 3.7 to 3.9).

$$F_{ct} = \pi(r_1 + r_2)s\sigma_v = \pi(r_1 + r_2)s f_t^{2/3} \xi \eta \mu \quad (3.6)$$

$$\xi = \begin{cases} -0.1\rho^2 + 0.46\rho + 0.35 & 0 < \rho < 2\% \\ 0.87 & \rho \geq 2\% \end{cases} \quad (3.7)$$

$$\mu = 1.6(1 + d/d_a)^{-1/2} \quad (3.8)$$

$$\eta = \begin{cases} 0.1(r_s/h)^2 + 0.5(r_s/h) + 1.25 & 0 < r_s/h < 2.5 \\ 0.625 & r_s/h \geq 2.5 \end{cases} \quad (3.9)$$

where f_t is the concrete tensile strength, ρ is the reinforcement ratio, d_a is the maximum aggregate size, h is the slab thickness.

The CEB-FIP model code expression for dowel effect is adopted to compute the punching shear capacity of flat slabs as given in Equation 3.10.

$$F_{dow} = \frac{1}{2} \sum^{bars} \phi_s^2 \sqrt{f_c f_t (1 - \zeta^2)} \sin \alpha \quad (3.10)$$

$$\zeta = \sigma_s / f_s \quad , \quad \sigma_s = \frac{V_{pun} / \tan \alpha}{\sum^{bars} A_s} \quad (3.11)$$

where ϕ_s is the diameter of reinforcing bar, f_c is the concrete compressive strength, f_s is the steel yield strength, σ is the axial tensile stress in the reinforcing bars that is obtained by projection of the force in the compressive strut and A_s is the reinforcement area.

The dowel action contribution, V_{dow} , is calculated iteratively, since the tensile stress in the reinforcing bar is dependent on the punching load V_{pun} .

The vertical shear reinforcement contribution is computed by summation of the each active stirrup as expressed in Equation 3.12.

$$F_{sp} = \frac{1}{2} \sum^{stirrups} A_{sw} f_s \sin(\beta_s) \quad (3.12)$$

where A_{sw} is the cross section of one stirrup, β_s is the inclination of the stirrups with the plane of the slab.

3.3.5.2 Model by Fernandez and Muttoni (2009)

A different physical model was proposed by Fernandez and Muttoni to predict the punching shear strength of shear reinforced flat-slabs. The model was based on a critical shear crack theory (Muttoni 2008) that takes into account the

relation between the critical shear crack width at failure and the rotation (ψ) of the flat-slabs (Figure 3.68).

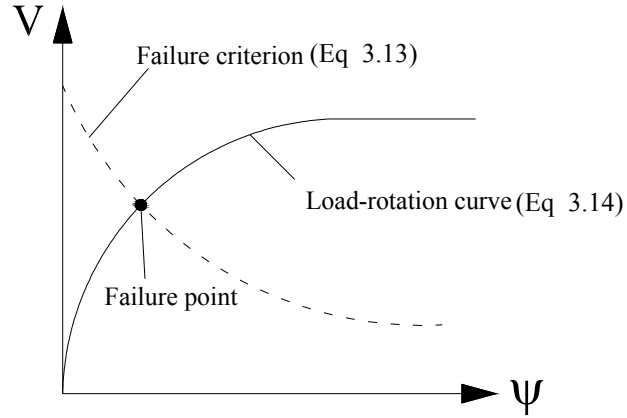


Figure 3.68 Punching failure definition (Muttoni 2008)

In the light of numerical analysis, Muttoni (2008) proposed the punching failure point as the intersection of load - rotation curve (Equation 3.13) with the failure criterion curve (Equation 3.14) for slabs without shear reinforcement (Figure 3.68). The punching strength is computed by iterative solution of two Equations 3.13 and 3.14.

$$V_{pun} = \frac{2}{3} \frac{bd\sqrt{f_c}}{1 + 20 \frac{\psi d}{d_{g0} + d_g}} \quad (3.13)$$

$$\psi = 1.5 \frac{r_s}{d} \frac{f_y}{E_s} \left(\frac{V}{V_{flex}} \right)^{\frac{3}{2}} \quad (3.14)$$

where d is the effective slab depth, b is the critical punching perimeter located $d/2$ away from the column face, f_c is the compressive strength of the concrete,

ψ is the maximal rotation of the slab, d_{g0} is the reference aggregate size set to 16 mm, d_g is the maximum aggregate size, r_s is the distance from the edge of the column to the line of contraflexure of bending moments (can be taken as 0.22L where L is the span length of the flat slab), f_y is the yield strength of reinforcement, E_s is the elasticity modulus of steel and V_{flex} is the flexural capacity of the flat-slab.

Fernandez and Muttoni then modified the critical shear crack theory on the purpose of predicting the punching capacity of flat slabs with shear reinforcement. Two main failure modes, inside and outside the shear reinforced region were considered in order to determine the punching capacity of shear reinforced flat slabs.

The punching capacity outside the shear reinforced region can be computed by iterative solution of Equations 3.13 and 3.14 by replacing the critical punching perimeter b value with the suitable critical punching perimeter (b_{out}) outside the shear reinforced zone.

The punching capacity inside the shear reinforced region (V_i) can be computed by summation of concrete (V_c) and shear reinforcement (V_s) resistances (Equation 3.14). The concrete contribution (V_c) can be calculated by Equation 3.13 whereas the shear reinforcement contribution (V_s) can be computed by the Equation 3.15. It should be noted that an identical rotation value should be determined by iterative solution of Equations 3.13 and 3.14 as indicated in Figure 3.69.

$$V_i = V_c + V_s \quad (3.14)$$

$$V_s = \frac{E_s \psi}{6} A_{sw} \leq f_{ywd} A_{sw} \quad (3.15)$$

where A_{sw} is the amount of shear reinforcement within a perimeter at d away from column face and f_{ywd} is the yield strength of the shear reinforcement.

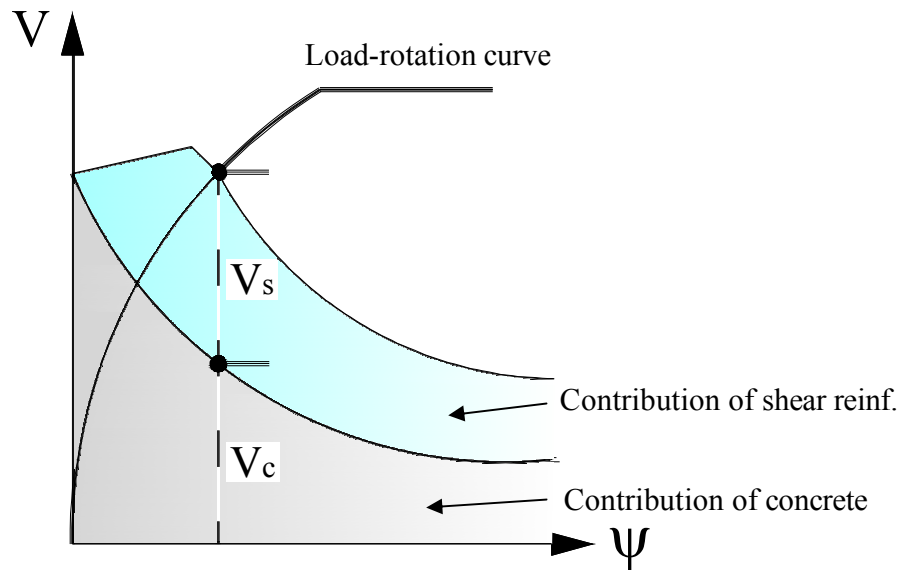


Figure 3.69 Definition of failure inside the shear reinforced zone (Muttoni 2009)

3.3.5.3 Comparison of Model Prediction with Experimental Results

The comparison of predicted capacities calculated by two aforementioned models and the experimental capacities are given in Table 3.5. The average value for the ratios of predicted capacities by Menetrey (1996) to experimental capacities were calculated as 0.93 with a standard deviation of 0.07. Computed capacities of all specimens were conservative excluding the two control specimens with rectangular column stub (R2, R3). This unconservative prediction may be due to ignorance of column rectangularity. In addition, the punching failure locations were not estimated correctly for all specimens by Menetrey (1996).

The ratio of predicted to experimental capacity was varied between 0.81 and 1.09 with a mean of 0.95 by use of the model proposed by Fernandez and Muttoni (2009). This model is successful in estimating the failure location of all test specimens excluding the specimens OS25 and OS25-b. However, this model also does not take into account the effect of column aspect ratio which

leads to overestimation of load carrying capacities of specimens OS25-b and OS35-b.

Table 3.5 Comparison of model predictions with experimental results

Specimen	Experimental		Menetrey					Muttoni				
	V_{exp}	Failure Location	V_i	V_o	V_u	$\frac{V_u}{V_{exp}}$	Failure Location	V_i	V_o	V_u	$\frac{V_u}{V_{exp}}$	Failure Location
R1	500	-----	492		492	0.98	-----	406		406	0.81	-----
R2	423	-----	449		449	1.06	-----	393		393	0.93	-----
R3	414	-----	443		443	1.07	-----	398		398	0.96	-----
OS13	601	Outside	742	523	523	0.87	Outside	772	551	551	0.92	Outside
OS14	571	Outside	788	495	495	0.87	Outside	682	556	556	0.97	Outside
OS15	656	Outside	937	576	576	0.88	Outside	746	627	627	0.96	Outside
CSWOP	594	Inside	791	536	536	0.90	Outside	534	668	534	0.90	Inside
CSWP	592	Inside	783	528	528	0.89	Outside	528	661	528	0.89	Inside
OS25	649	Inside	811	562	562	0.87	Outside	772	637	637	0.98	Outside
OS25-b	571	Inside	972	537	537	0.94	Outside	886	621	621	1.09	Outside
OS35-b	564	Outside	962	530	530	0.94	Outside	886	621	621	1.09	Outside
					Mean	0.93			Mean	0.95		
					Std.dv	0.07			Std.dv	0.08		

CHAPTER 4

FINITE ELEMENT ANALYSES

4.1 GENERAL

In order to verify the experimental test results presented in Chapter 3 and for a better-understanding of the behavior of flat-slab specimens, three-dimensional finite element models of test specimens were generated. DIANA (2005) general purpose finite element program was employed for the nonlinear finite element analysis to simulate the behavior of reinforced concrete slab specimens. In addition to specimens of this study, two other flat-plate specimens (Control-1 and strengthened specimen - A8) tested by Binici (2003) were also modeled in same manner to verify the applicability and reliability of proposed finite element method on the specimens having different dimensions, reinforcement ratio and different strengthening methods. The analytical results were compared with the experimental results. Moreover, a parametric study was performed to investigate the relation between the ultimate failure load and ultimate CFRP strain for different amounts of CFRP used for each dowel.

4.2 MATERIAL MODELS

4.2.1 Concrete Constitutive Model

Total strain crack concept is fundamentally based on the Modified Compression Field Theory proposed by Vecchio and Collins (1993). This theory was then modified to three-dimensional version by Selby and Vecchio

(1993). In total strain crack concept, loading and unloading is defined with secant stiffness (Figure 4.1).

DIANA offers two sub-models named as rotating and fixed crack models respectively (Selby and Vecchio 1993), regarding to orientation of coordinate system during cracking. Preliminary analyses results indicated that fixed crack modeling provided better estimations for load-deformation response in terms of computational stability and representing the post cracking stiffness of the test specimens, so that total strain fixed crack model was adopted for all the analysis throughout the analytical part.

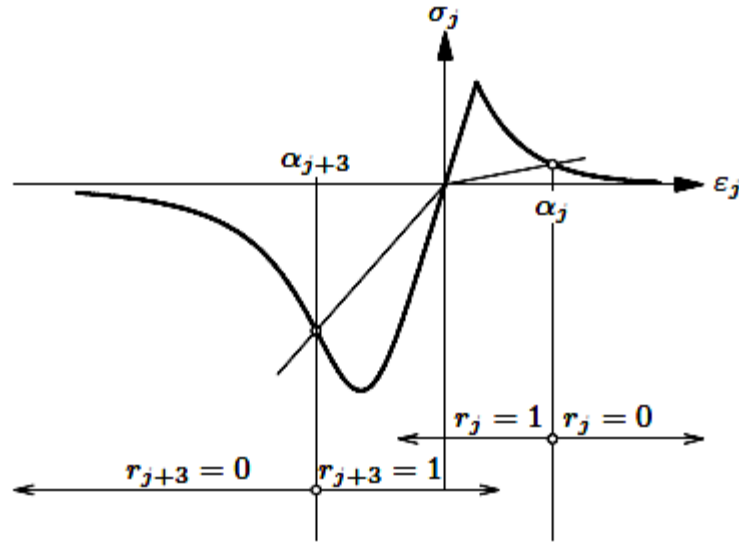


Figure 4.1 Loading-unloading regime (DIANA Manual 2005)

4.2.2 Concrete in Compression

DIANA presents seven different predefined curves for modeling the compression behavior of concrete as shown in Figure 4.2. Depending on the simplicity and applicability of the analysis it was possible to assign relatively simpler curves such as elastic (Figure 4.2a), idealized (Figure 4.2b) and linear (Figure 4.2d) for compression behavior of concrete by just implying the

concrete strength value and hardening stiffness values. For more complicated and advanced models DIANA offers more detailed compression curves such as Thorenfeldt et al. (1987) (Figure 4.2c), multilinear (Figure 4.2e), saturation hardening (Figure 4.2f) and parabolic curves (Figure 4.2g) that enable more realistic approach for softening region of the compressive stress-strain relationship.

Compressive behavior of concrete was accounted by parabolic curve for all the performed analyses in this study. The formulation of parabolic curve was mainly based on fracture energy, proposed by Feenstra (1993). Two main variables that should be input to the program were concrete compressive strength (f_c) and compressive fracture energy (G_c). G_c was assumed to be 100 times greater than the Mode-I fracture energy (G_f) as recommended in CEB-FIP Model Code (1990).

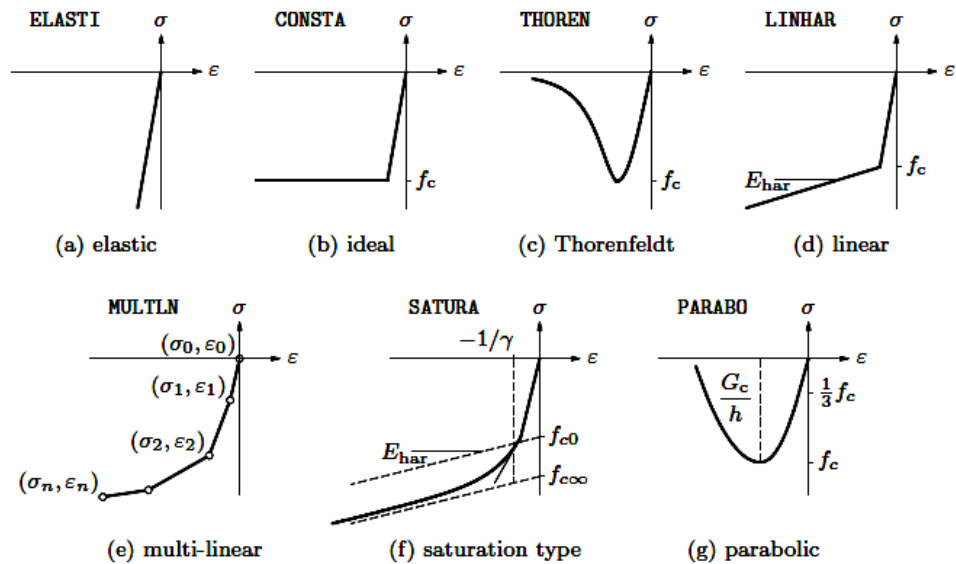


Figure 4.2 Models for concrete in compression (DIANA Manual 2005)

4.2.3 Concrete in Tension

Similar to definition of compressive behavior, DIANA enables seven different curves for simulating the behavior of concrete in tension. Three of those based on basic assumptions such as elastic idealized and brittle behavior with non-realistic softening branch as shown in Figure 4.3. The other four curves (linear, multi-linear, exponential, and Hordijk 1992) consider the tension softening regime beyond the tensile strength limit.

Tensile behavior of concrete was taken into account by the stress-strain relationship proposed by Hordijk (1992) for all analyses performed in this study. The curve is directly dependent to fracture energy as it is previously described in compression behavior. Two main variables that should be input to the program were concrete tensile strength (f_t) and Mode-I fracture energy (G_f). Lateral confinement and cracking effects are also taken into consideration during analysis using the model proposed by Selby and Vecchio (1993).

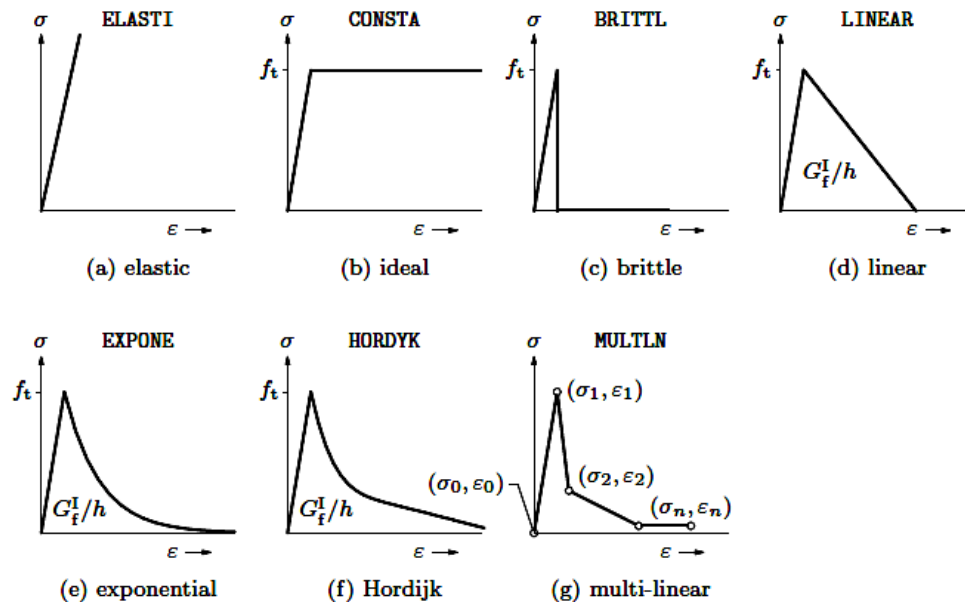


Figure 4.3 Models for concrete in tension (DIANA Manual 2005)

Mode-I fracture energy value (G_f) was calculated by the given formulations in Equations 4.1 and 4.2 according to European CEB-FIP Model Code (1990). In Equation 4.2, G_{f0} value was a parameter varying with maximum aggregate size as presented in Table 4.1.

$$f_{cm} = f_{ck} + 8MPa \quad (4.1)$$

$$G_f = G_{f0} \left(\frac{f_{cm}}{10} \right)^{0.7} \quad (4.2)$$

Table 4.1 Variation of G_{f0} with maximum aggregate size d_{max}

d_{max} (mm)	G_{f0} (J/m ²)
8	25
16	30
32	58

4.2.4 Shear Behavior

Shear stiffness tends to decrease due to cracking of concrete. DIANA offers a shear retention concept for total strain fixed crack models to reflect the behavior of concrete due to the reduction in shear stiffness. Elastic shear stiffness (G) was multiplied by a factor called shear retention factor (β) to obtain the cracked shear stiffness (G_{cr}). β value can be defined either as function of shear strain or as a constant value. Constant shear retention factors varying from 0 to 0.3 were used in the previous studies (Hu and Schnobrich, 1990, Megally 1998, Megally and Ghali 2000, Binici 2003). In this study, a shear retention value of 0.2 was employed. Further parametric studies showed

that shear retention values between 0.1 and 0.3 have negligible effect on simulating the overall behavior.

4.2.5 Steel Reinforcement and CFRP Model

Both steel reinforcement and CFRP dowels were modeled such a way that there assumed to be perfect bond between concrete and reinforcement (Steel and CFRP). In other words, bond-slip behavior between reinforcement (CFRP and steel) and concrete was neglected in all analyses. Bilinear elasto-plastic stress-strain curve based on Von-Mises yield criterion was used for reinforcing steel bars. Strain hardening effect was neglected and not taken into accounting for modeling since higher strain values were not reached during testing. CFRP material was assumed to be linear elastic in order to determine the limiting strain value for failure. Numerical integration process of reinforcing steel bars was performed by 2 x 2 Gauss integration scheme. Embedded reinforcement bars were also used for modeling the CFRP dowels (Figure 4.4). Equivalent cross sectional area of CFRP dowels were assigned to embedded bar reinforcement elements (Figure 4.5).

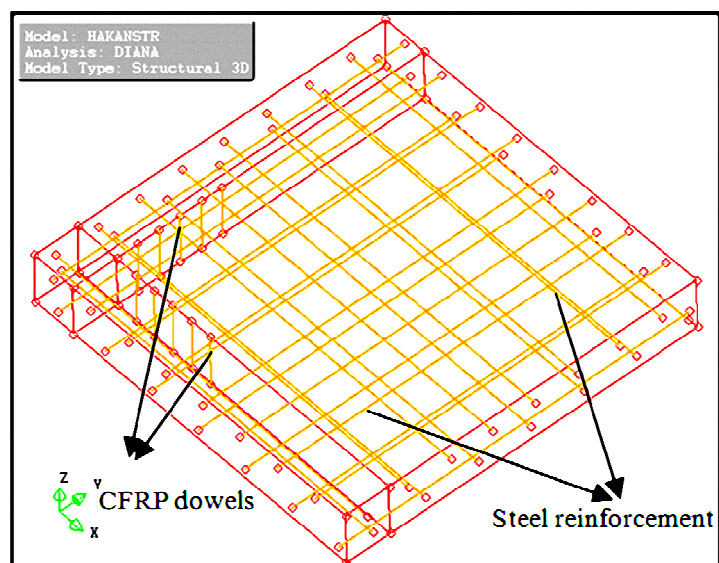


Figure 4.4 Modeling of steel reinforcement and CFRP dowels

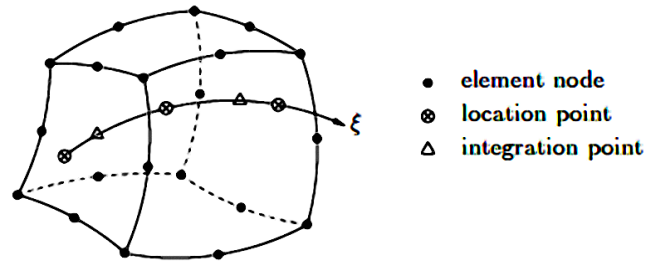


Figure 4.5 Definition of reinforcement in solid element (DIANA Manual 2005)

4.3 MODELLING AND ANALYSIS

4.3.1 Finite Element Mesh

Only one-quarter of the specimens were modeled on account of symmetrical boundary conditions and geometry. Regions labeled as symmetry boundary conditions 1 and 2 in Figure 4.6 were constrained in the x and y direction respectively. The simply supported edges, on the other hand, were assigned constraints in the z direction only to reflect the presence of supporting rods in the test setup. Eight-node isoparametric solid brick elements based on linear interpolation and 2 x 2 x 2 Gauss integration scheme were used to generate the finite element mesh (Figure 4.7). The number of elements used for each model was different due to variation of slab and column dimensions. However, the thicknesses of all models were divided into four segments in the light of previous studies (Megally 1998, Binici 2003) considering the accuracy of the analysis and time consumption.

Displacement controlled loading was applied to each specimen with an increment of 0.01 mm based on Quasi-Newton method. For this purpose, a master node was defined at the corner of the slabs on the compression face where the column stub located. The other nodes at the location of column stub were coupled and constrained to master node in vertical direction to provide the application of same incremental deflection through the column stub.

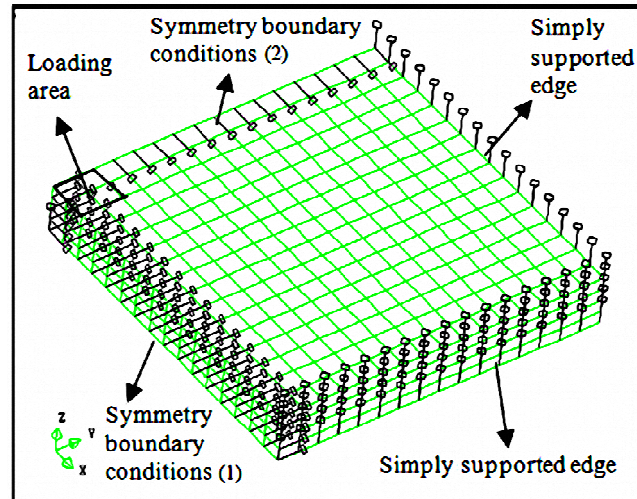


Figure 4.6 Finite element mesh and boundary conditions

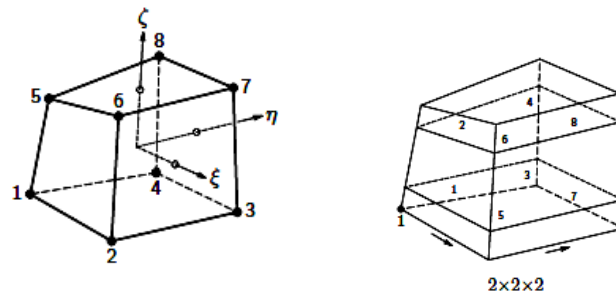


Figure 4.7 8-node brick element and integration points (DIANA Manual 2005)

4.3.2 Iteration Criteria

Quasi-Newton method is also known as variable metric method mainly based on the Regular Newton-Raphson Method. However, Quasi-Newton method uses the known positions at the equilibrium path (previous solution vectors and out of balance vectors) for determination of the stiffness matrix instead of constructing totally new stiffness matrix at every iteration step (Figure 4.8). Three different algorithms were implemented in DIANA called as Broyden, Broyden-Fletcher-Goldfarb-Shanno and Crisfield methods. The tolerance of 0.1% was selected for convergence criteria of both displacement and unbalanced force for termination of iteration steps.

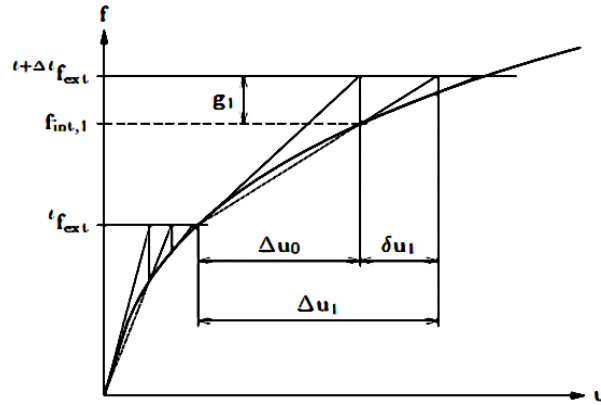


Figure 4.8 Quasi-Newton Method (DIANA Manual 2005)

4.4 NUMERICAL ANALYSES RESULTS AND COMPARISONS WITH THE EXPERIMENTAL RESULTS

Finite element analyses results regarding the total of seven test specimens including two specimens in the literature tested by Binici (2003) are presented and compared with the experimental results in terms of displacement, longitudinal steel strain, principal stresses and CFRP strain in order to verify the accuracy of proposed finite element models.

The control specimen (without any strengthening) tested by Binici (2003) had square span length of 1981 mm and thickness of 152 mm. The square loading plate representing the column had a side length of 304 mm. The tensile reinforcement ratio was selected to be 1.76%. The test specimen and setup details are shown in Figure 4.9. The specimen A8 was strengthened by the application of CFRP strips as closed form stirrups through the holes around the loading plate. The spacing of holes selected to be 58 mm (equal to half of effective depth). Total of 8 perimeters were arranged around the slab-column connection. Application details of strengthening scheme are given in Figure 4.10.

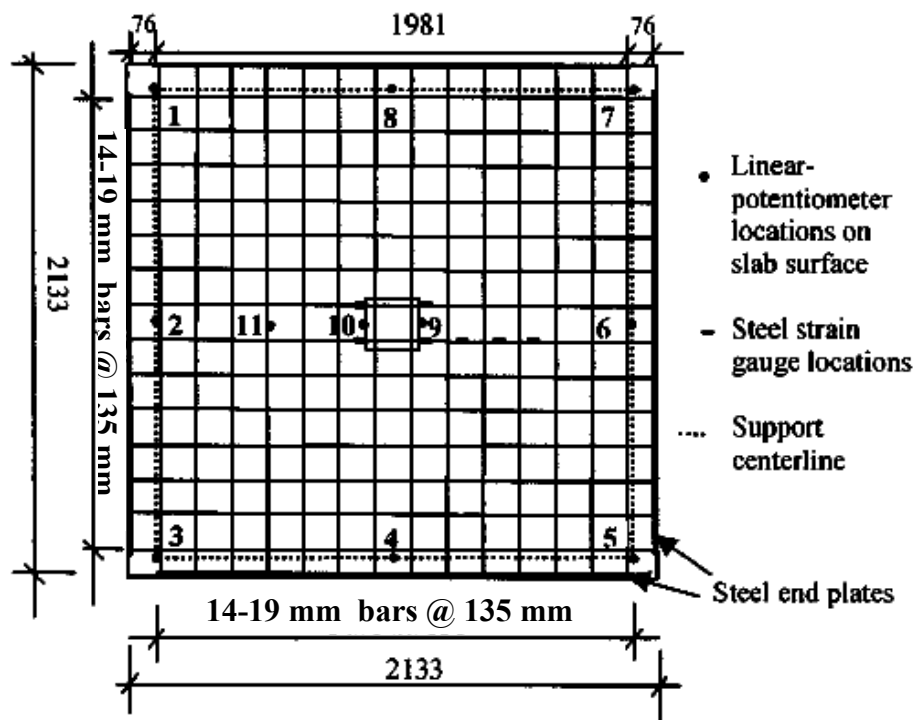
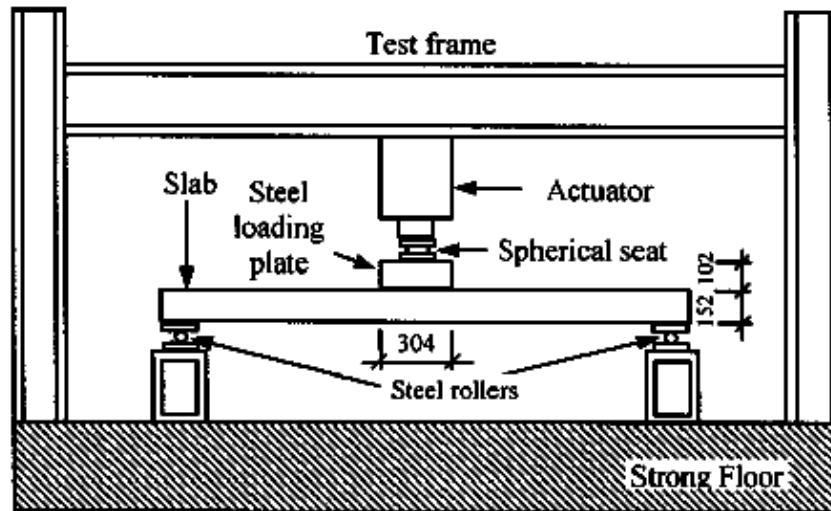


Figure 4.9 Test setup and reinforcement details (adopted from Binici 2003)

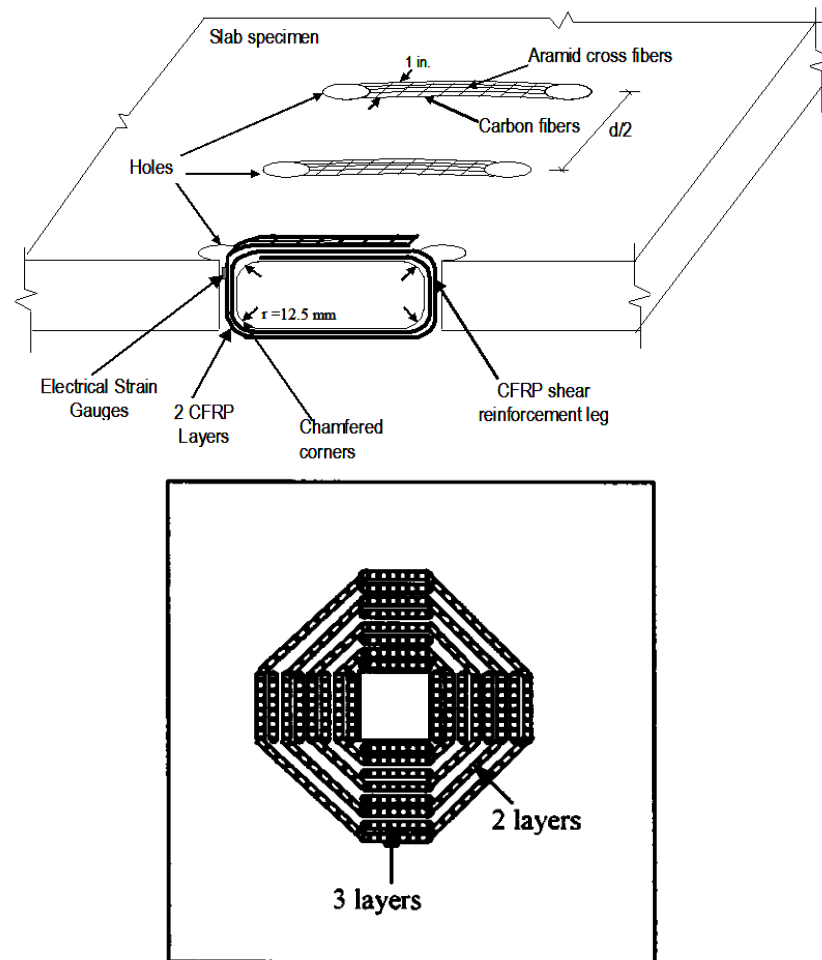


Figure 4.10 Strengthening method details (Binici 2003)

4.4.1 Principal Stress

The variation of three principal stress values (S_1 , S_2 and S_3) with the applied displacement at the corner of column compression face (where the loading is applied) for specimens without any strengthening (R1, R2, R3 and control specimen of Binici (2003) are given in Figure 4.11. The analysis results for the applied load and maximum principal stress values (S_1) at the corner of loading plate for three reference specimens (R1, R3 and control specimen of Binici (2003) indicated that the point where maximum principal stress value (S_1) changed its sign (i.e. from compression to tension) was observed to be a good indicator for punching failure (Figure 4.12).

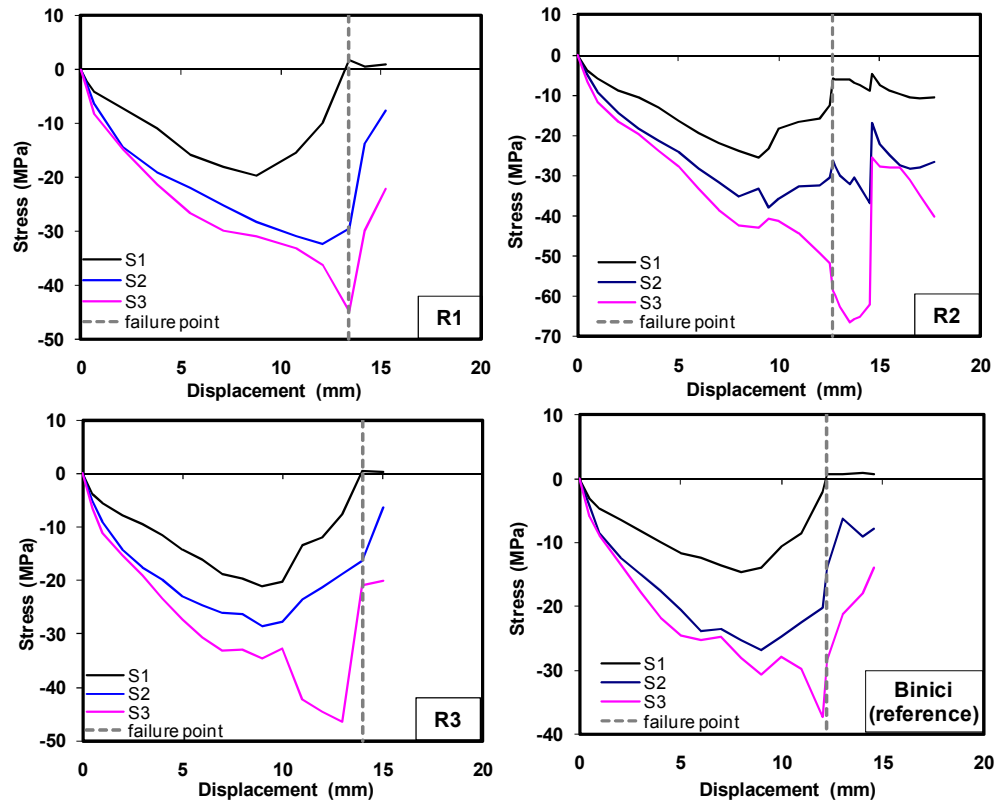


Figure 4.11 Principal stress distributions at column corner

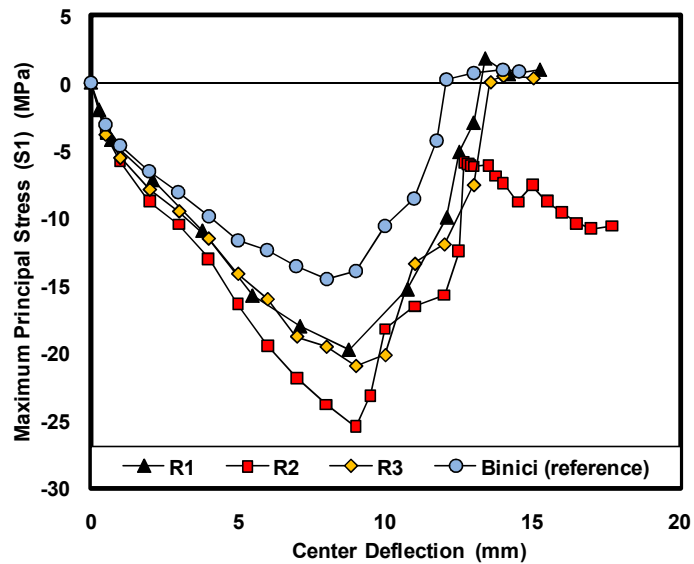


Figure 4.12 Maximum principal stress distributions (S1)

In other words, when the triaxiality of the state of stress was lost at the corner of the loading area where the inclined crack penetrated into compression zone. On the other hand, maximum principal stress (S1) distribution of specimen R2 did not change its sign throughout the loading, however, the point where the maximum stress value was reached during loading is assumed to be the failure point (Figure 4.12). The principal stress profile along the column face line of the control specimen R1 is presented in Figure 4.13 for different load levels.

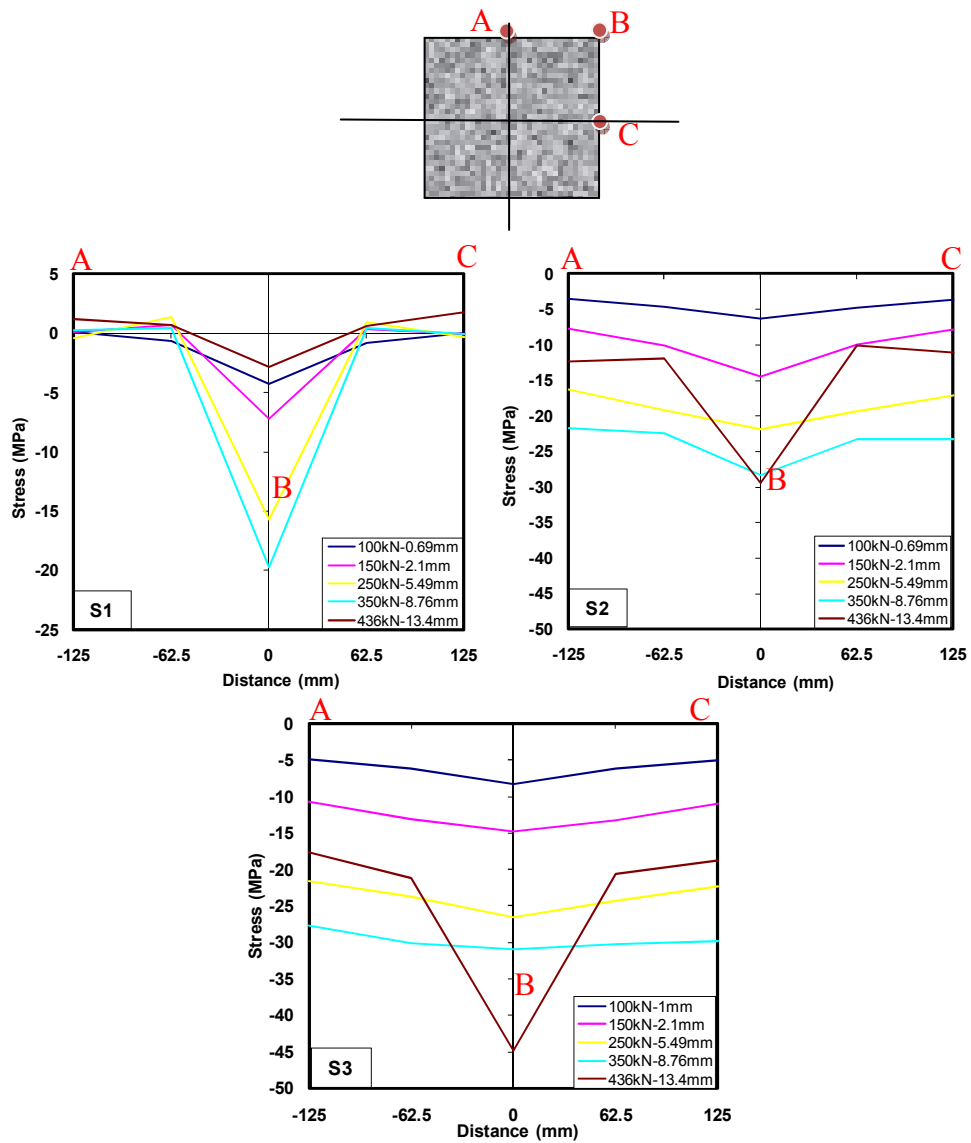


Figure 4.13 Principal stress profiles along column face

4.4.2 Load – Deflection Comparison

The comparison of load - center deflection curves obtained from finite element analysis and experimental results are presented in Figures 4.14 to 4.17. Finite element analyses results regarding the ultimate load and deflection at failure point are tabulated in Table 4.2. The ratio of the analytical ultimate load predictions (V_{ua}) to experiment load carrying capacity (V_u) of seven test specimens varied between 0.87 to 1.07 with a mean of 0.97 and standard deviation of 0.04. In addition, the ratio of maximum slab center deflection is in the range of 0.77 to 1.47.

The validity of the finite element model is also ensured by comparing the orthogonal and diagonal deflection profiles of the control specimen R1 at different load levels. The contour plot of vertical deflection is presented in Figure 4.18. Furthermore, it is apparent from the Figure 4.19 that neglecting the downward movement of corners by modeling the specimens as simply supported on four sides has no significant effect on the deflection behavior of the slab in the critical punching failure region.

Table 4.2 Comparison of experimental and FEA results

Specimen	Ultimate FEA Load, V_{ua} (kN)	Deflection at V_{ua} , Δ_{ua} (mm)	V_u (kN)	Δ_u (mm)	V_{ua} / V_u	Δ_{ua} / Δ_u
Binici (reference)	468	12.2	491	11.3	0.95	1.08
R1	437	13.4	500	17.5	0.87	0.77
R2	421	12.7	423	14.4	1.00	0.88
R3	412	13.6	414	13.8	1.00	0.99
Binici (strengthened)	712	18.4	744	20.7	0.96	0.89
OS15	622	57.6	656	49.1	0.95	1.17
OS35-b	604	40.8	564	27.8	1.07	1.47
Mean :					0.97	1.04
Std. dev. :					0.06	0.22

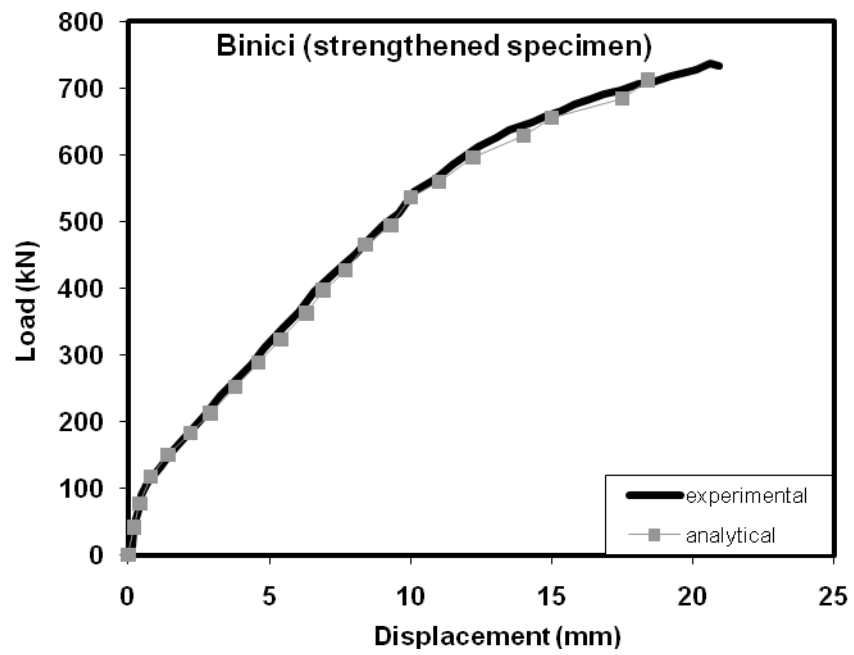
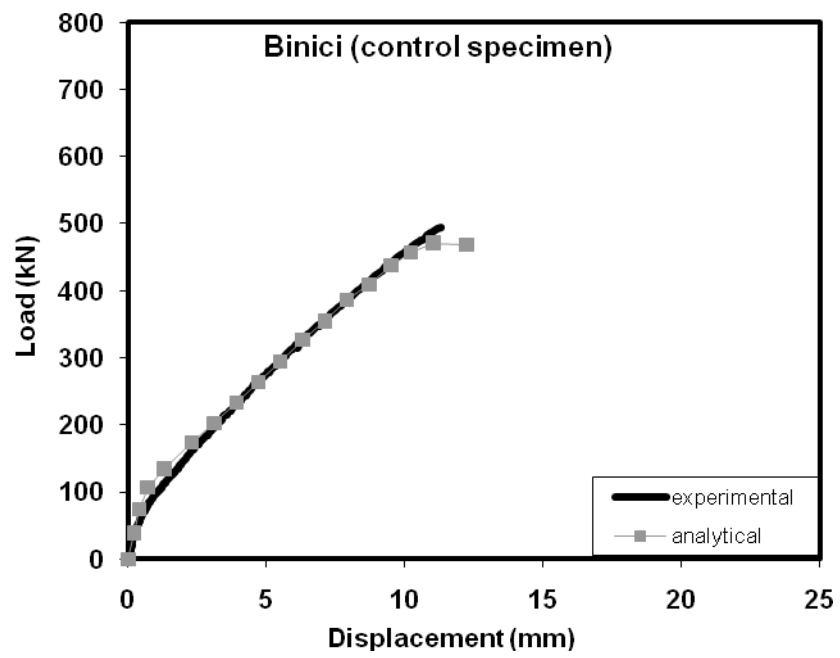


Figure 4.14 Load- deflection comparisons of specimens tested by Binici (2003)

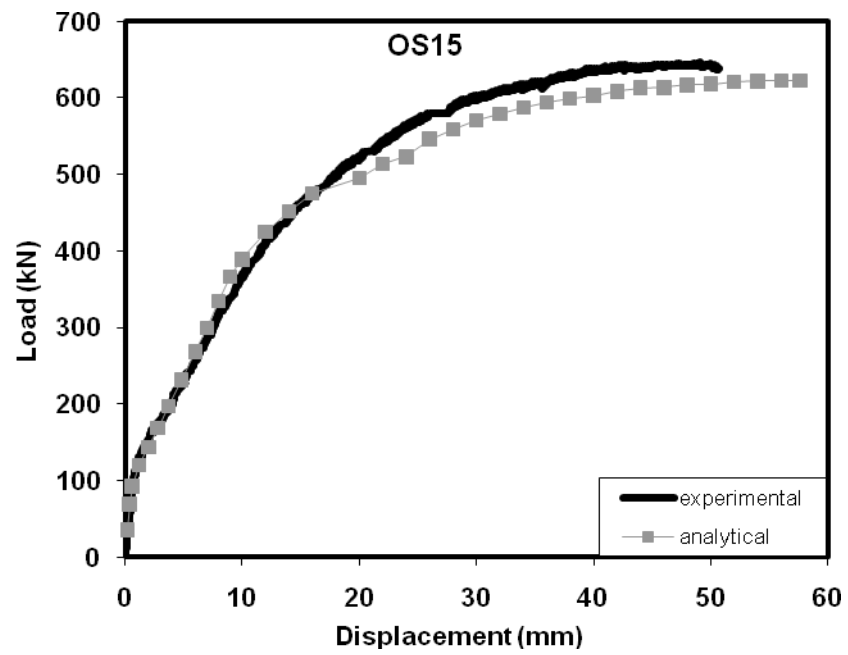
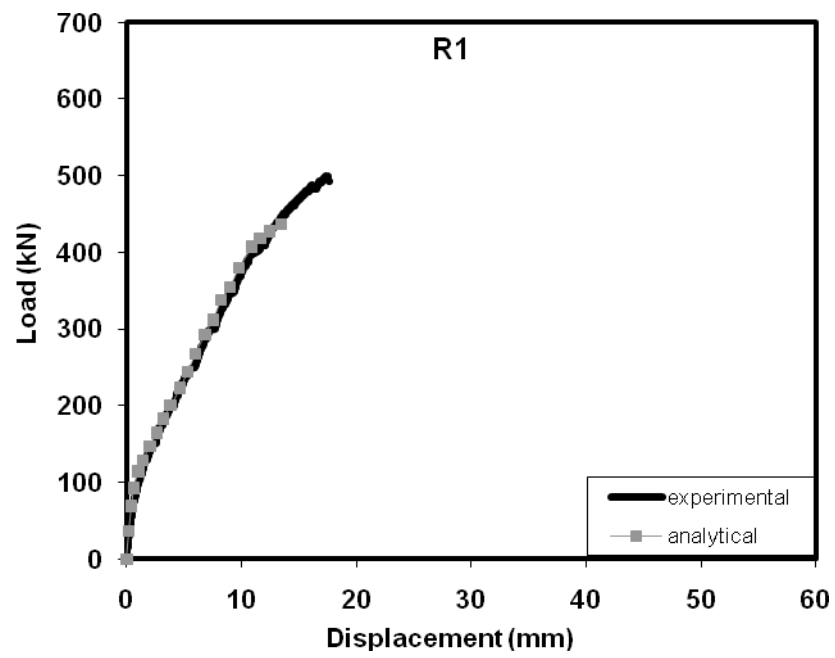


Figure 4.15 Load- deflection comparisons of specimens R1 and OS15

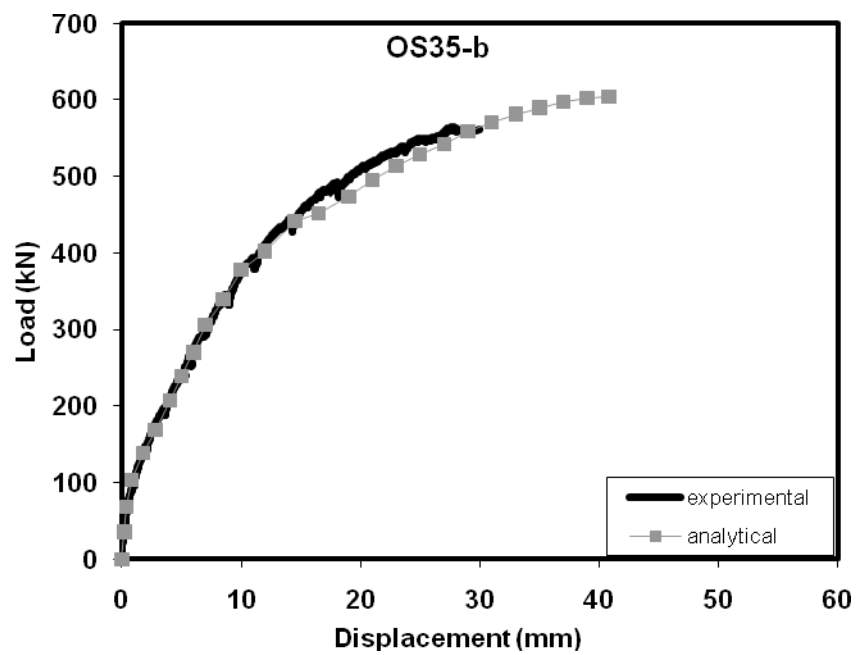
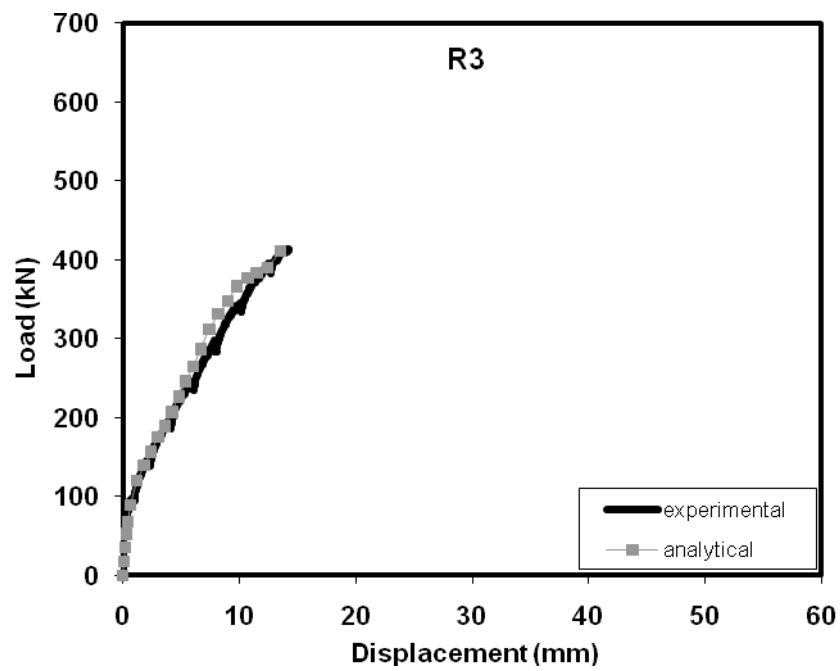


Figure 4.16 Load- deflection comparisons of specimens R3 and OS35-b

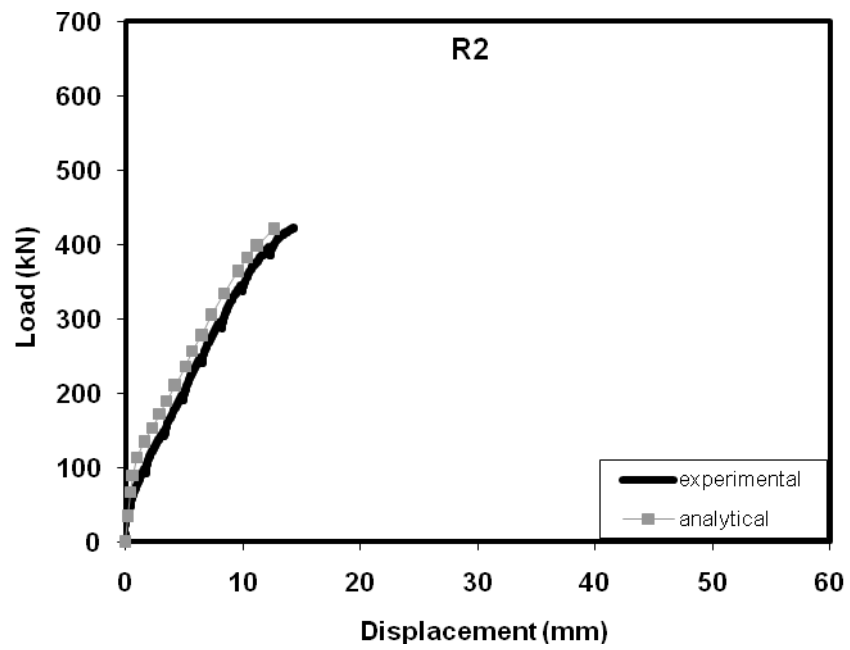


Figure 4.17 Load- deflection comparisons of specimens R2

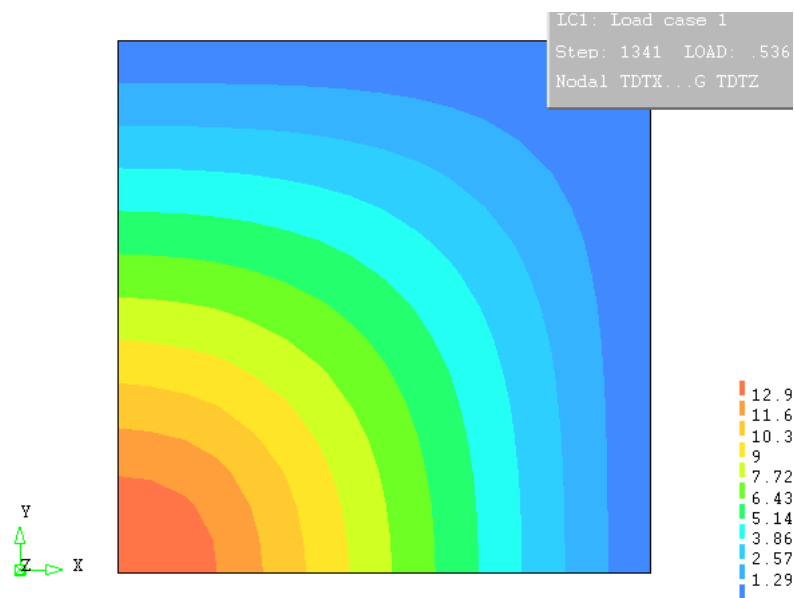


Figure 4.18 Deflection contour map at ultimate load (specimen R1)

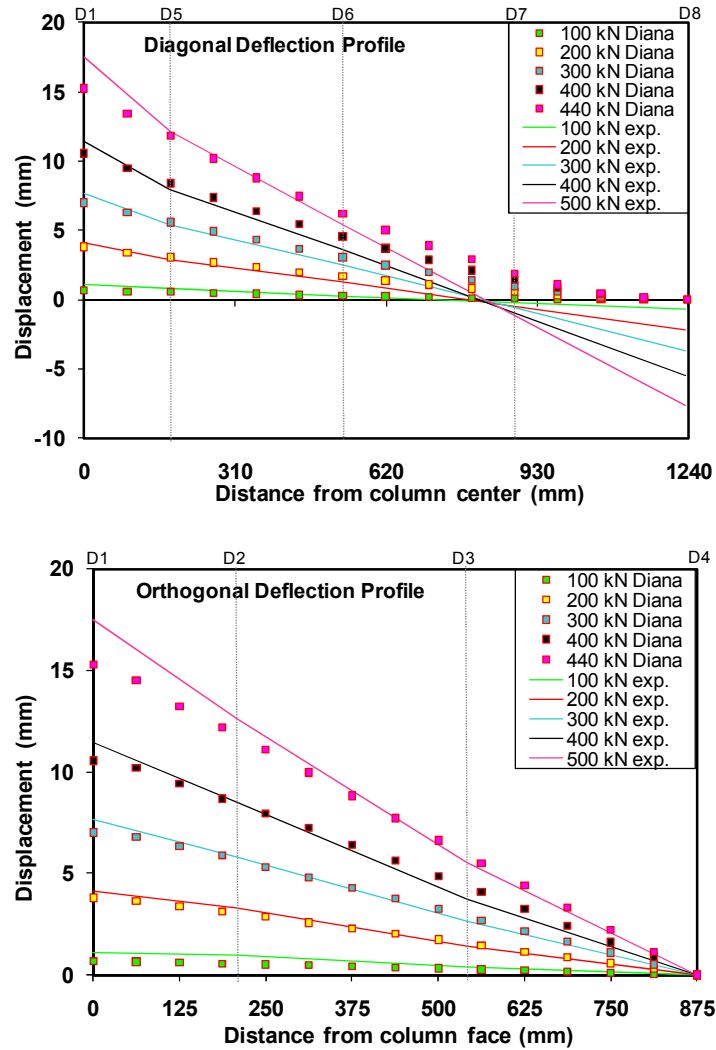


Figure 4.19 Comparison of deflection profiles for specimen R1

4.4.3 Longitudinal Steel Strain

In order to ensure reliability of computer model, computed steel strain values were also compared with the experimental steel strain measurements. The strain measurements obtained from longitudinal steel bar strain gages located at various distances away from column face are plotted against FEA results in Figures 4.20 to 4.25 for seven different specimens. It is apparent from the figures that, the analytical model estimations are in reasonable conformity with the experimental results.

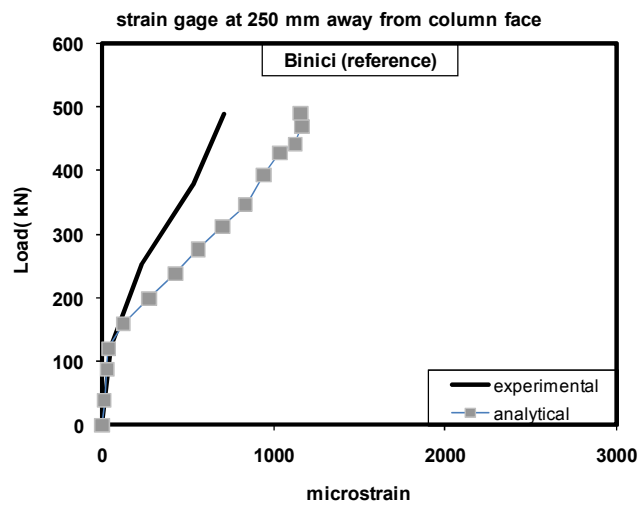
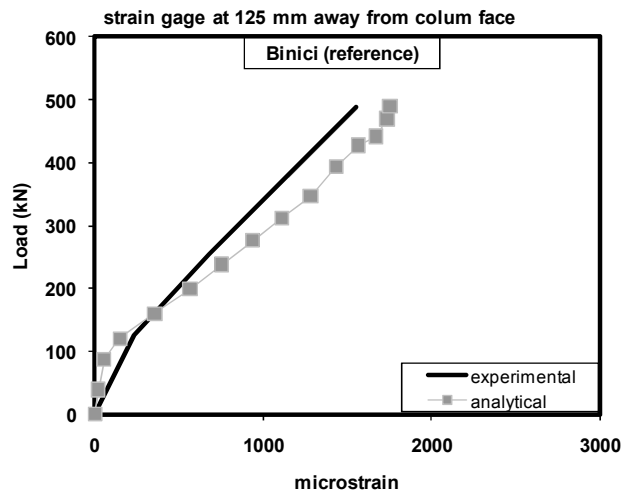
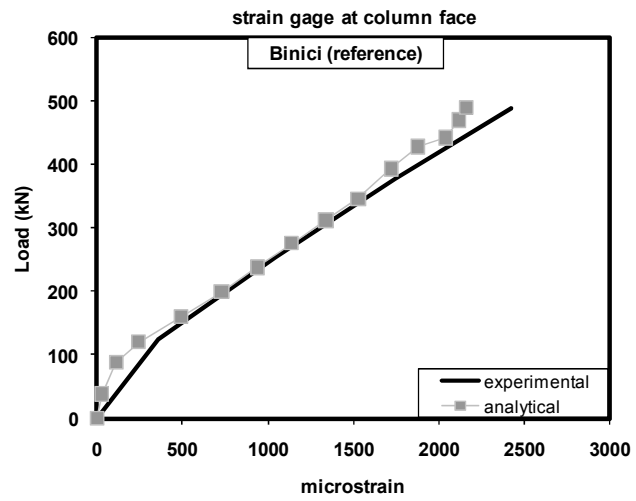


Figure 4.20 Steel strain comparisons for control specimen (Binici 2003)

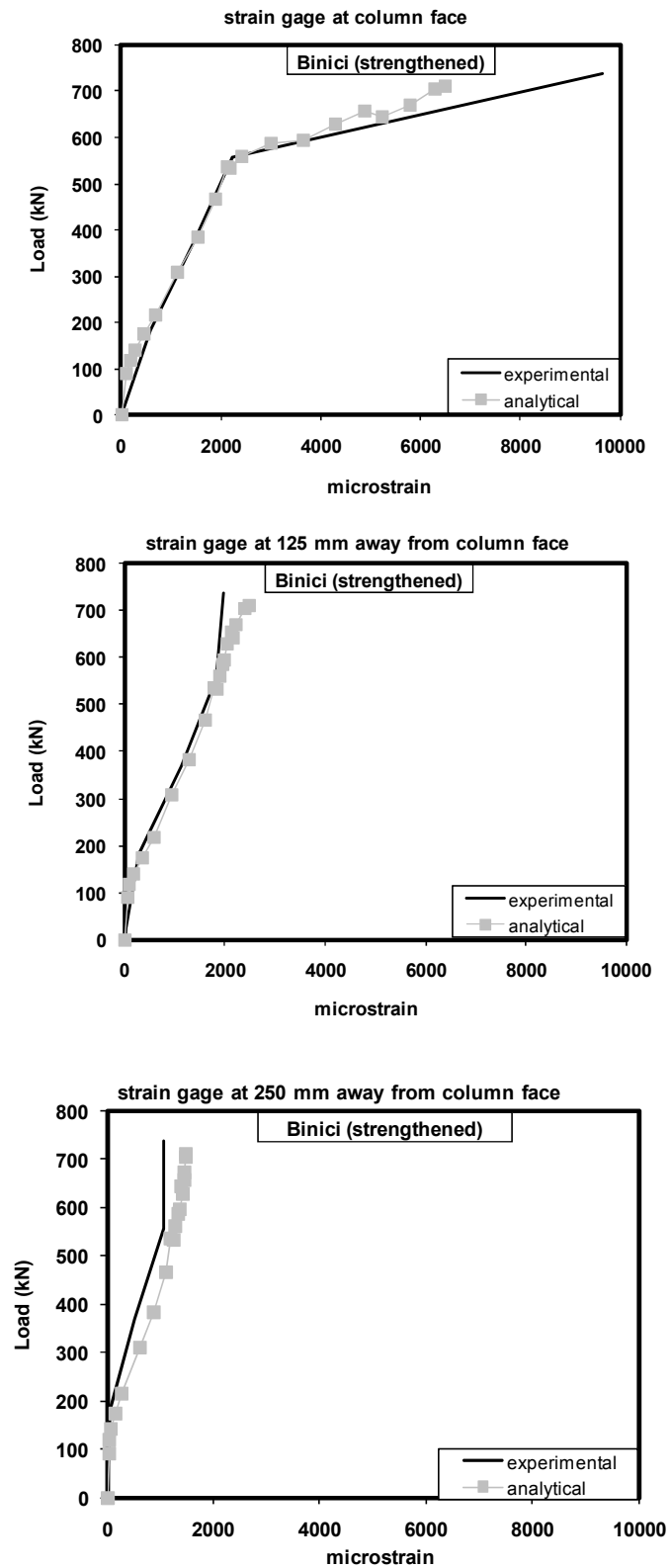


Figure 4.21 Steel strain comparisons for strengthened specimen (Binici 2003)

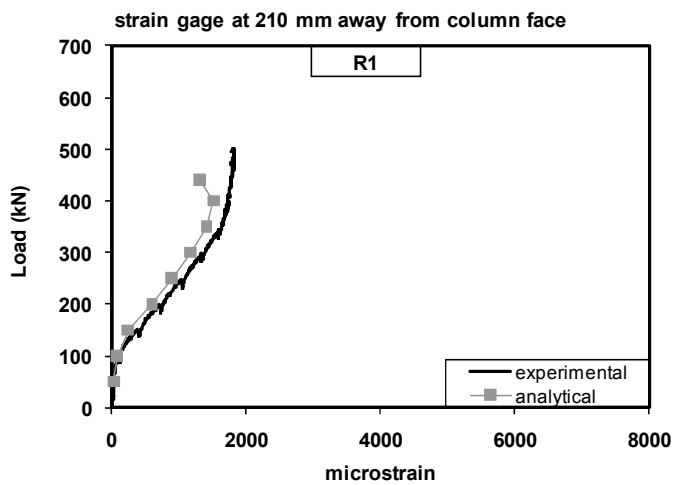
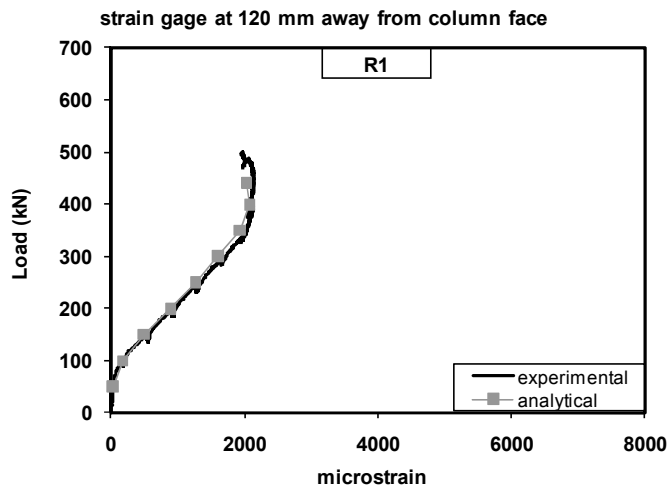
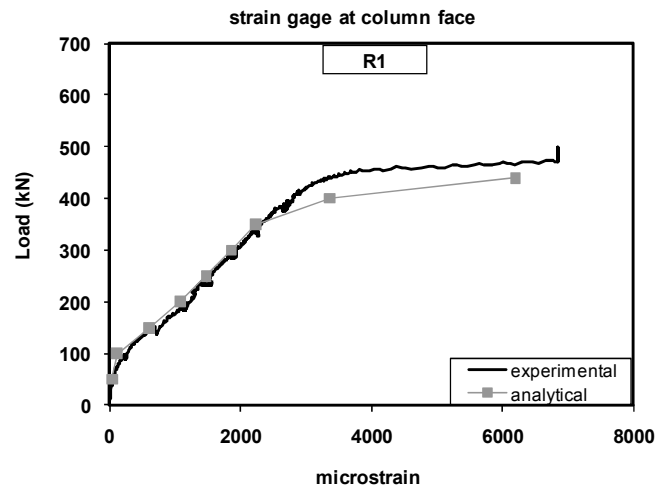


Figure 4.22 Steel strain comparisons for specimen R1

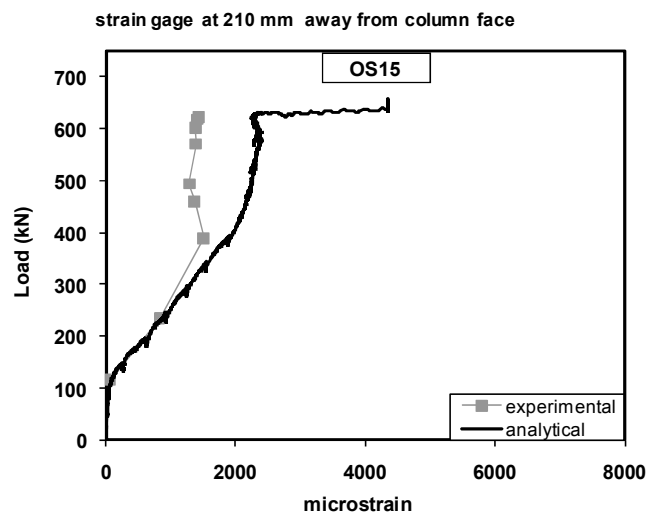
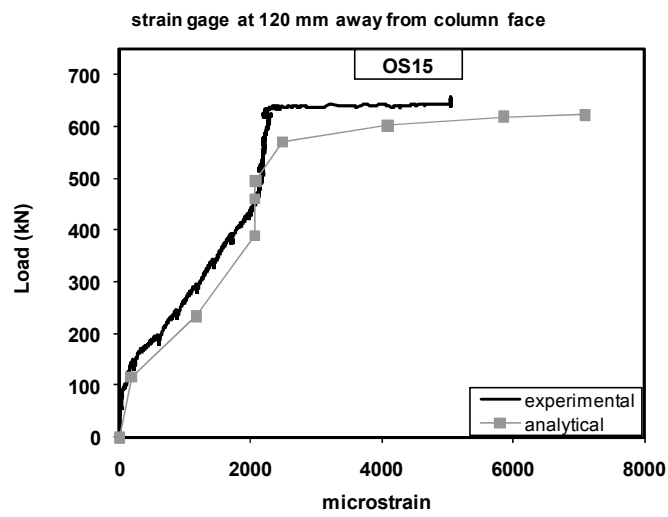
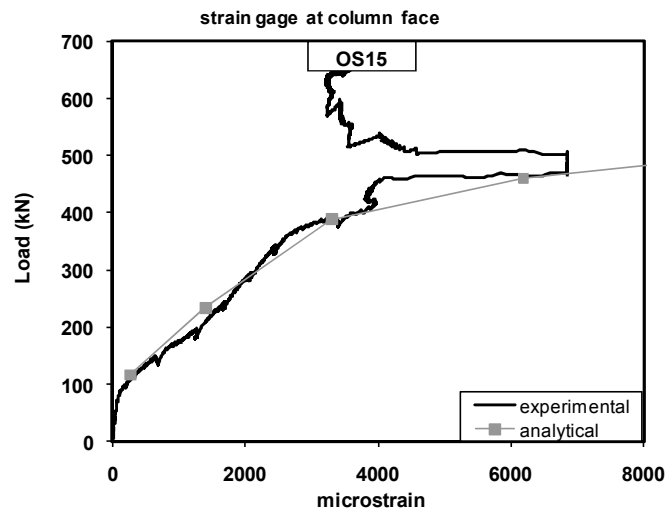


Figure 4.23 Steel strain comparisons for specimen OS15

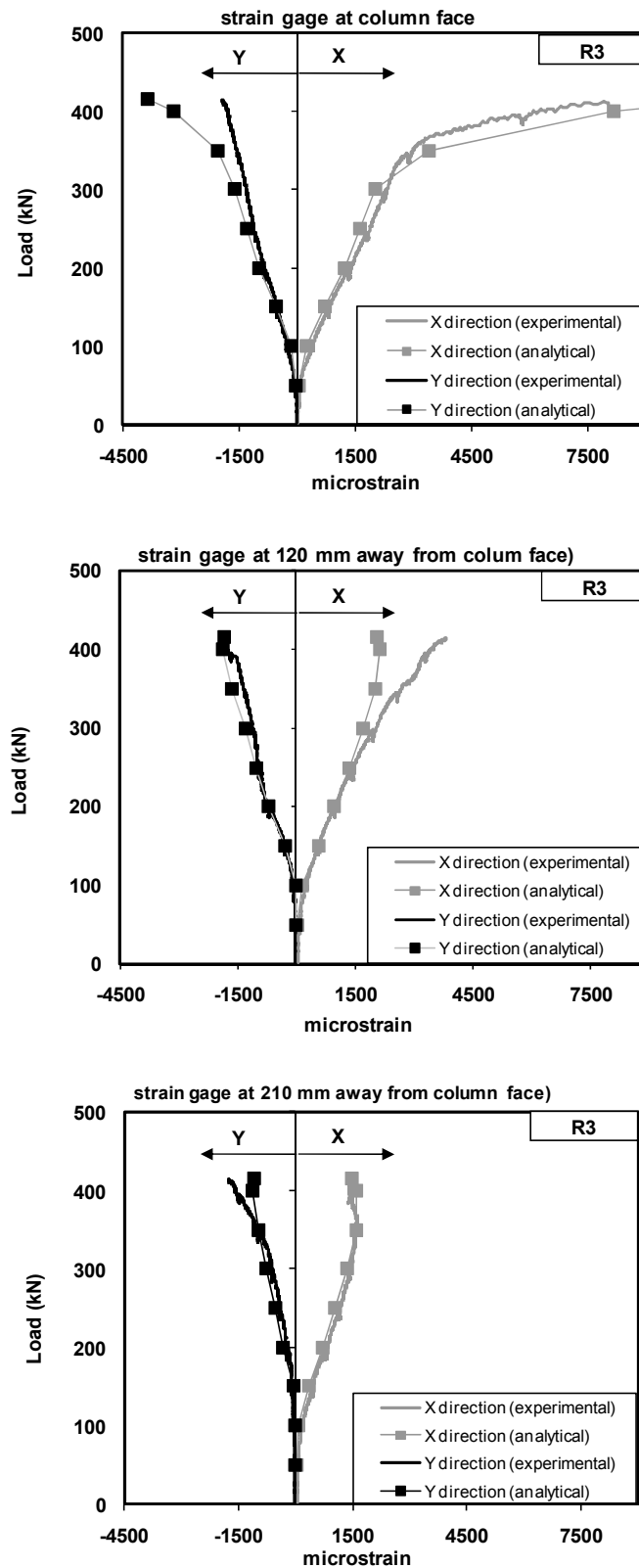


Figure 4.24 Steel strain comparisons for specimen R3

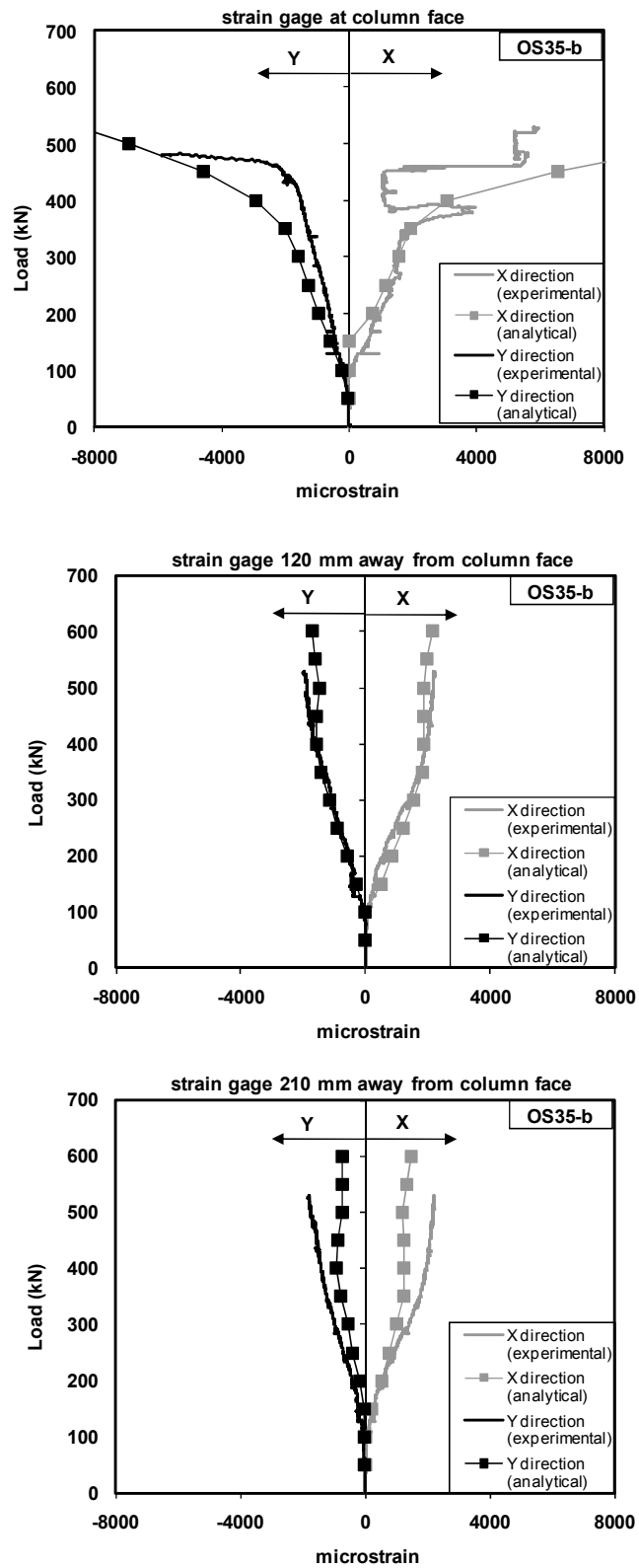


Figure 4.25 Steel strain comparisons for specimen OS35-b

4.4.4 CFRP strain

Since, no data regarding to CFRP dowels strains was obtained during experimental part of the present study, it was not possible to compare the validity of the finite element model for the calculated CFRP strain. However, CFRP strain results obtained by Binici (2003) were compared with the results of finite element analysis as presented in Figure 4.26. The strain distribution on each perimeter of CFRP dowels for specimen OS15 obtained from finite element analysis are illustrated in Figure 4.27 for load levels of $0.2V_{ua}$, $0.4V_{ua}$, $0.6V_{ua}$, $0.8V_{ua}$ and V_{ua} respectively. A trend of decrease in CFRP strain values is observed with increasing distance from the column face as shown in the analytical and experimental results in Figures 4.26 and 4.27. In addition, both Figures 4.26 and 4.27 indicates a sudden drop in CFRP strain values in the distance range of 60 mm to 150 mm away from the column face.

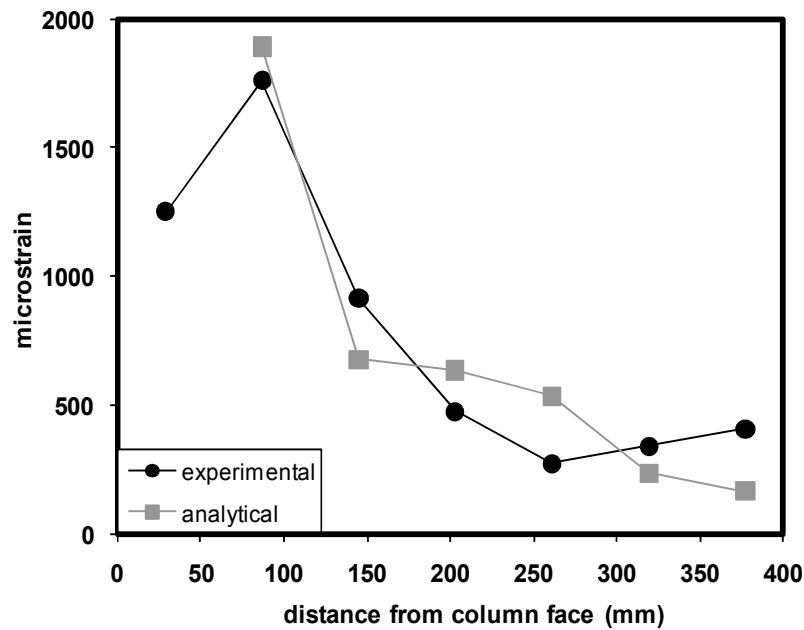


Figure 4.26 CFRP strains of strengthened specimen at failure (Binici 2003)

Since the results are in good agreement, a parametric study was performed to investigate the relation between the ultimate failure load and ultimate CFRP strain for different amounts of CFRP used for each dowel for present study. The amount of CFRP used in each dowel for specimen OS15 was reduced to 1/2, 1/4 and 1/8, respectively. The results of parametric study show that the ultimate load capacity had a tendency to decrease with decreasing amount of CFRP. CFRP strain – load curves presented in Figure 4.28 indicates that the limiting strain value of 0.004, which was also recommended by Binici (2003) and design guidelines (ACI Committee 440, 2002) seems to be consistent and reliable limit in estimating the CFRP contribution for the considered strengthening method.

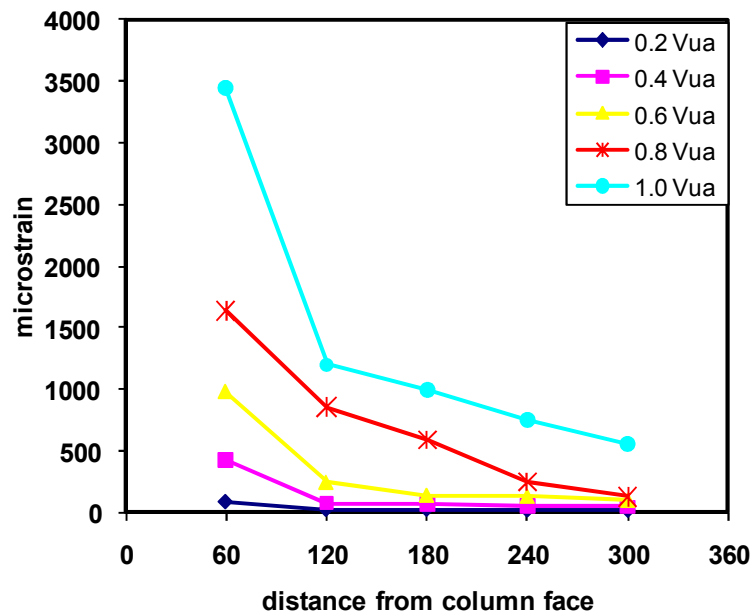


Figure 4.27 CFRP strains of specimen OS15 at different load levels

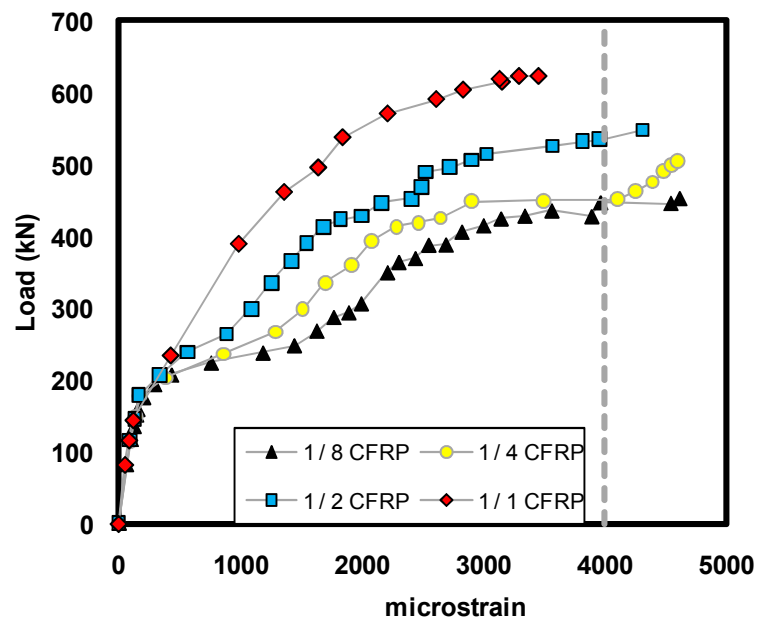


Figure 4.28 Effect of amount of CFRP per each dowel

CHAPTER 5

EVALUATION OF PUNCHING SHEAR STRENGTH BY USING CODE PROVISIONS

5.1 GENERAL

A database including two previous studies in the literature (Sissakis 2002, Binici 2003) that were concentrated on slab-column connections retrofitted by using CFRP material as vertical shear reinforcement is presented in this chapter in order to determine the design limits for externally applied vertical CFRP shear strengthening schemes against punching failure. In addition, comparison of four different code provisions (BS8110-97, ACI 318-05, Eurocode-2 and TS500) for the test specimens in the given database is also discussed in this chapter. Necessary modifications were proposed for the existing provisions of punching shear capacity in order to design CFRP upgrading.

5.2 EXPERIMENTAL DATABASE

The database consists of square test specimens representing the interior slab-column connection with an identical thickness of 150 mm. Specimen details and experimental test results of totally 49 test specimens are summarized in Table 5.1.

Twenty eight of those specimens were tested by Sissakis (2002). Sissakis mainly focused on the effects of concrete strength, reinforcement ratio,

Table 5.1 Experimental database

	Specimen	a	d	c ₁	c ₂	f _c	f _y	s/d	ρ	V _{flex}	V _u	$\frac{V_u}{V_{flex}}$	Failure Location
Sissakis	RS1-149	1350	120	200	200	42.6	428	-----	1.49	643	575	0.89	-----
	A4-149	1350	120	200	200	42.6	428	0.5	1.49	643	632	0.98	Outside
	RS2-149	1350	120	200	200	36.1	428	-----	1.49	631	439	0.70	-----
	A3-149	1350	120	200	200	36.1	428	0.75	1.49	631	591	0.94	Outside
	B3-149	1350	120	200	200	36.1	428	0.75	1.49	631	659	1.04	Inside
	B4-149	1350	120	200	200	36.1	428	0.5	1.49	631	638	1.01	Outside
	C3-149	1350	120	200	200	36.1	428	0.75	1.49	631	612	0.97	Inside
	C4-149	1350	120	200	200	36.1	428	0.5	1.49	631	673	1.07	Outside
	D3-149	1350	120	200	200	36.1	428	0.75	1.49	631	550	0.87	Inside
	D4-149	1350	120	200	200	36.1	428	0.5	1.49	631	605	0.96	Inside
	RS3-223	1350	120	200	200	34.5	480	-----	2.23	966	476	0.49	-----
	A3-223	1350	120	200	200	34.5	480	0.5	2.23	966	591	0.61	Inside
	A5-223	1350	120	200	200	34.5	480	0.5	2.23	966	671	0.69	Outside
	B3-223	1350	120	200	200	34.5	480	0.5	2.23	966	744	0.77	Outside
	B5-223	1350	120	200	200	34.5	480	0.5	2.23	966	791	0.82	Outside
	C3-223	1350	120	200	200	34.5	480	0.5	2.23	966	775	0.80	Outside
	C5-223	1350	120	200	200	34.5	480	0.5	2.23	966	858	0.89	Inside
	D3-223	1350	120	200	200	34.5	480	0.5	2.23	966	616	0.64	Inside
	D5-223	1350	120	200	200	34.5	480	0.5	2.23	966	617	0.64	Inside
	RS4-223	1350	120	200	200	26.6	480	-----	2.23	902	479	-----	-----
	A4-223	1350	120	200	200	26.6	480	0.5	2.23	902	595	0.66	Outside
	A6-223	1350	120	200	200	26.6	480	0.5	2.23	902	631	0.70	Inside
	B4-223	1350	120	200	200	26.6	480	0.5	2.23	902	701	0.78	Outside
	B6-223	1350	120	200	200	26.6	480	0.5	2.23	902	791	0.88	Outside
	C4-223	1350	120	200	200	26.6	480	0.5	2.23	902	781	0.87	Outside
	C6-223	1350	120	200	200	26.6	480	0.5	2.23	902	872	0.97	Outside
	D4-223	1350	120	200	200	26.6	480	0.5	2.23	902	634	0.70	Inside
	D6-223	1350	120	200	200	26.6	480	0.5	2.23	902	639	0.71	Inside
Binici	RB-176	1981	114	304	304	28.3	448	-----	1.76	730	494	0.68	-----
	B4-176-1	1981	114	304	304	28.3	448	0.5	1.76	730	595	0.82	I / O
	B4-176-2	1981	114	304	304	28.3	448	0.5	1.76	730	668	0.92	Outside
	B4-176-3	1981	114	304	304	28.3	448	0.5	1.76	730	618	0.85	Inside
	B4-176-4	1981	114	304	304	28.3	448	0.5	1.76	730	600	0.82	Inside
	B6-176	1981	114	304	304	28.3	448	0.5	1.76	730	721	0.99	Outside
	B8-176	1981	114	304	304	28.3	448	0.5	1.76	730	744	1.02	Outside
	C4-176	1981	114	304	304	28.3	448	0.5	1.76	730	756	1.04	Outside
	C6-176	1981	114	304	304	28.3	448	0.5	1.76	730	752	1.03	Outside
	C8-176	1981	114	304	304	28.3	448	0.5	1.76	730	778	1.07	Outside
Erdoğan	RE1-140	2000	114	250	250	32	448	-----	1.4	582	500	0.86	-----
	RE2-140	2000	114	167	333	29	448	-----	1.4	582	423	0.73	-----
	RE3-140	2000	114	125	375	30	448	-----	1.4	582	414	0.71	-----
	B3-140	2000	114	250	250	33	448	0.5	1.4	582	601	1.03	Outside
	B4-140	2000	114	250	250	26	448	0.5	1.4	582	571	0.98	Outside
	B5-140-1	2000	114	250	250	31	448	0.5	1.4	582	656	1.13	Outside
	E4-140-1	2000	114	250	250	31	448	0.75	1.4	582	594	1.02	Inside
	E4-140-2	2000	114	250	250	30	448	0.75	1.4	582	592	1.02	Inside
	B5-140-2	2000	114	167	333	33	448	0.5	1.4	582	649	1.12	Inside
	B5-140-3	2000	114	167	333	30	448	0.5	1.4	582	571	0.98	Inside
	B5-140-4	2000	114	167	333	30	448	0.5	1.4	582	564	0.97	Outside

the spacing of shear reinforcement and vertically applied CFRP reinforcement arrangement in the vicinity of the connection. Four different concrete strength values ranging from 26.6 MPa to 42.6 MPa were selected by Sissakis (2002). Effect of two different reinforcement ratios ($\rho=1.49$ and 2.23%) with an effective depth of 120 mm was investigated. The vertical loading was applied by a 200 mm square steel loading plate representing the column. CFRP laminates were passed through the holes in the vicinity of the slab-column connection in such way to form hoops surrounding the concrete as shown in Figure 5.1. The holes around the connection were arranged in four different types named as A, B, C and D respectively (Figure 5.1). The spacing between the CFRP perimeters was selected to be $0.5d$ and $0.75d$.

Binici (2003) also performed an experimental study focused on application of CFRP laminates through the holes around the slab-column connection in the form of closed stirrups (Figure 5.2). The reinforcement ratio, concrete strength and effective depth values were kept constant for all the test specimens and were equal to 1.76% , 28.3 MPa and 114 respectively. The side length of the square loading plate was selected to be 304 mm. Two different shear reinforcement patterns (B and C) were defined by Binici as shown in Figure 5.2. The original specimen names were modified in order to provide a common basis of comparison among different studies. The specimens starting with letter “R” representing the control (reference) specimens without any strengthening, in naming the control specimens, second letter represents the capital letter of the researchers name, i.e. “S” for Sissakis, “B” for Binici and “E” for Erdogan. A number was used at the end of specimen ID for the studies having more than one control specimens. The strengthened specimens were labeled with respect to strengthening pattern and reinforcement ratio. The first letter denotes the strengthening pattern (i.e. A, B, C, D or E) (Figure 5.3) and the number denotes the reinforcement ratio respectively.

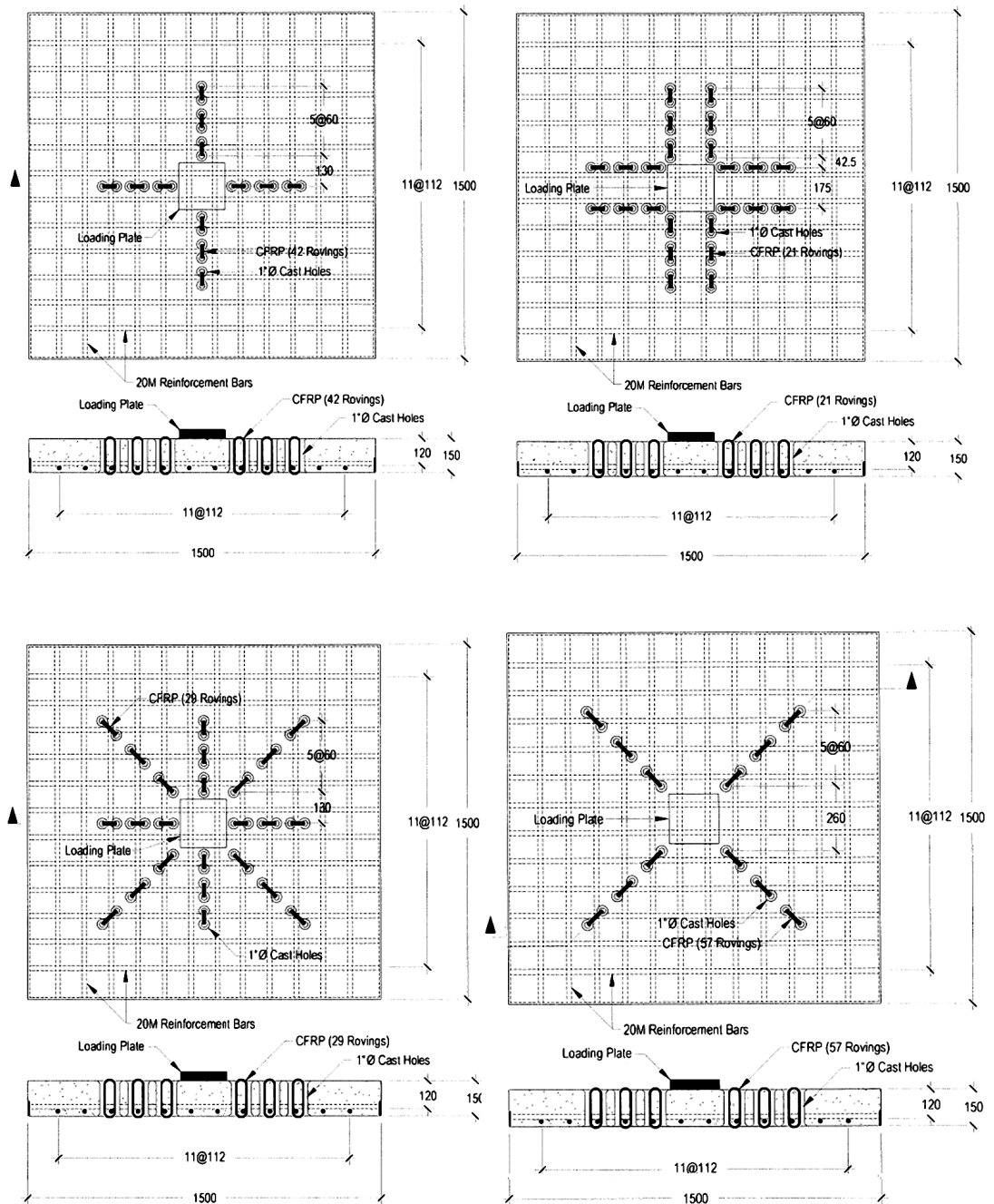


Figure 5.1 Test specimen details adopted from Sissakis (2002)

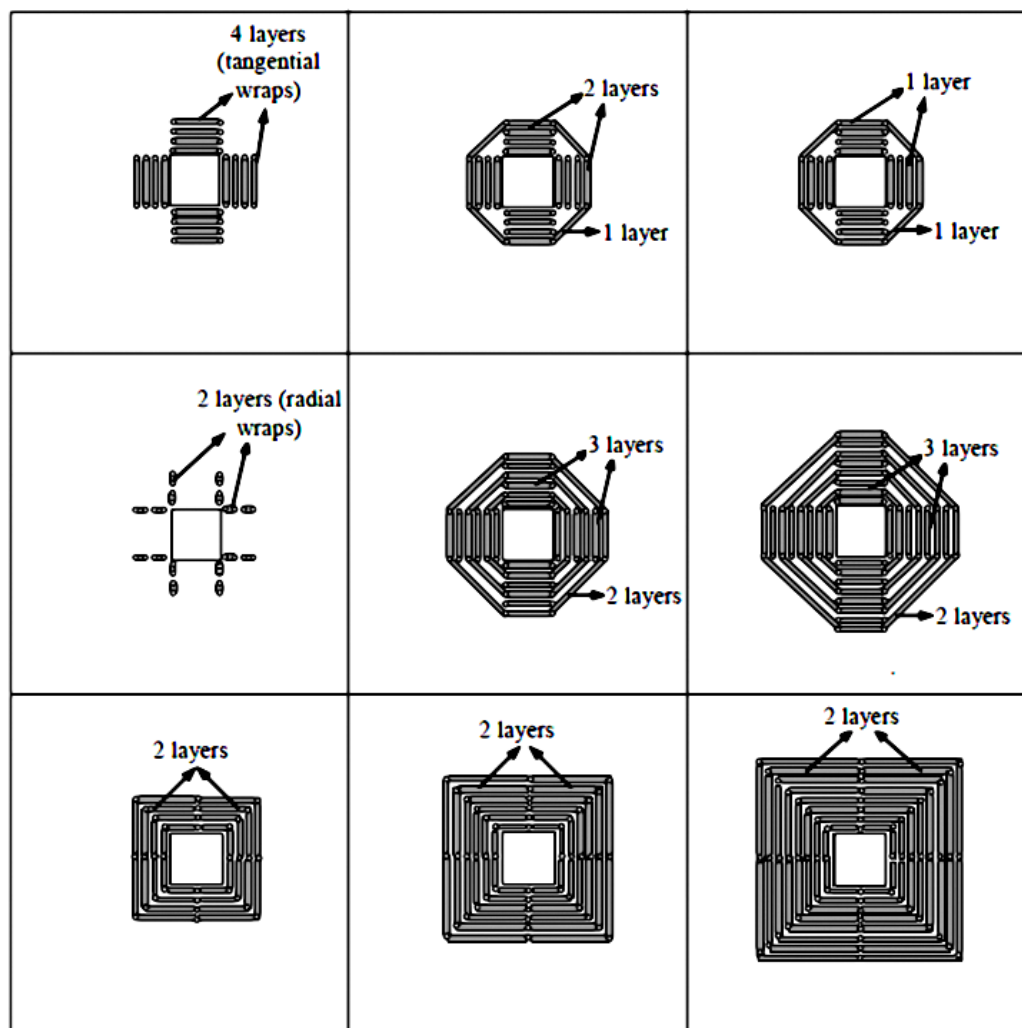
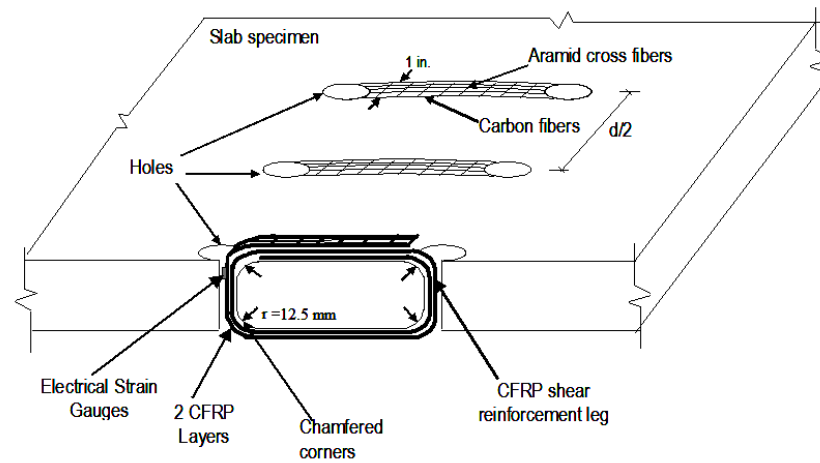


Figure 5.2 Test specimen details adopted from Binici (2003)

Eurocode-2

BS8110-97

ACI 318-05 & TS500

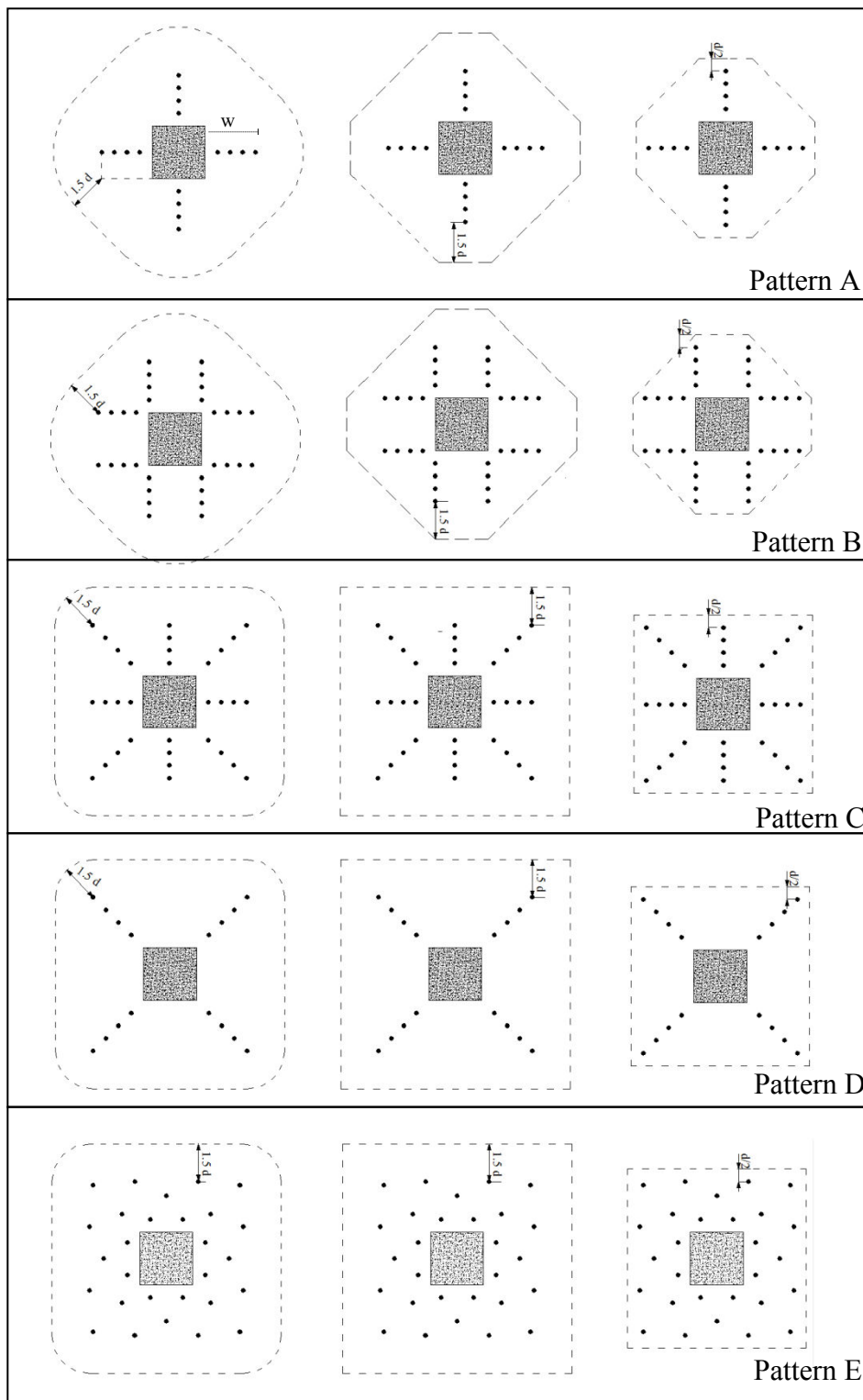


Figure 5.3 Strengthening patterns and punching perimeter definitions

Table 5.2 Amount of vertically applied CFRP laminates

	Specimen	# of rows	# of holes in each row	s/d	Amount of CFRP for each row (mm ²)							
					1	2	3	4	5	6	7	8
Sissakis	A4-149	4	4	0.5	724	724	724	724				
	A3-149	3	4	0.75	450	900	450					
	B3-149	3	8	0.75	666	666	666					
	B4-149	4	8	0.5	666	666	666	666				
	C3-149	3	8	0.75	822	822	822					
	C4-149	4	8	0.5	822	822	822	822				
	D3-149	3	4	0.75	822	822	822					
	D4-149	4	4	0.5	822	822	822	822				
	A3-223	3	4	0.5	411	822	411					
	A5-223	5	4	0.5	764	764	587	1175	587			
	B3-223	3	8	0.5	548	548	705					
	B5-223	5	8	0.5	705	705	705	705	705			
	C3-223	3	8	0.5	705	705	705					
	C5-223	5	8	0.5	1057	1057	1057	1057	1057			
	D3-223	3	4	0.5	705	705	705					
	D5-223	5	4	0.5	705	705	705	705	705			
	A4-223	4	4	0.5	568	568	568	568				
	A6-223	6	4	0.5	822	822	822	822	822	822		
	B4-223	4	8	0.5	587	587	587	587				
	B6-223	6	8	0.5	822	822	822	822	822	822		
	C4-223	4	8	0.5	822	822	822	822				
	C6-223	6	8	0.5	1136	1136	1136	1136	1136	1136		
	D4-223	4	4	0.5	764	764	764	764				
	D6-223	6	4	0.5	1116	1116	1116	1116	1116	1116		
Binici	B4-176-1	4	8	0.5	800	800	800	800				
	B4-176-2	4	8	0.5	400	400	400	600				
	B4-176-3	4	8	0.5	200	200	200	400				
	B4-176-4	4	8	0.5	400	400	400	400				
	B6-176	6	8	0.5	600	1000	600	1000	600	1000		
	B8-176	8	8	0.5	600	1000	600	1000	600	1000	600	1000
	C4-176	4	8	0.5	600	800	800	600				
	C6-176	6	8	0.5	1000	800	800	800	800	1000		
	C8-176	8	8	0.5	1000	800	800	800	800	800	800	1000
Erdoğan	B3-140	3	8	0.5	960	960	960					
	B4-140	4	8	0.5	960	960	960	960				
	B5-140-1	5	8	0.5	960	960	960	960	960			
	E4-140-1	4	8	0.75	960	960	960	480				
	E4-140-1	4	8	0.75	960	960	960	480				
	B5-140-2	5	8	0.5	960	960	960	960				
	B5-140-3	5	8	0.5	1440	1440	1440	1440	1440			
	B5-140-4	5	8	0.5	1440	1440	1440	1440	1440			

The amount of supplied CFRP laminates (in means of mm^2) for each perimeter of test specimens are presented in Table 5.2. It should be noted that the first perimeter of CFRP laminates were located $0.25d$ away from the loading plate face in both studies (Sissakis 2002 and Binici 2003). The consecutive perimeters were located $0.5d$ away for specimens tested by Binici and either 0.5 or $0.75d$ away for specimens tested by Sissakis (2002). ASTM test results (D-3039) of cured CFRP laminates reported by the manufacturers are presented in Table 5.3 and Figure 5.4. It is apparent from the results that the mechanical properties of the selected CFRP laminates for three studies are almost identical.

The generated database was used to classify the CFRP strengthened test specimens considering the main parameters affecting the punching failure such as concrete strength (f_c), column aspect ratio (c_1/c_2), number of CFRP perimeters (n), reinforcement ratio (ρ), strengthening pattern and CFRP spacing to effective depth ratio (s/d). The distribution of number of test specimens by means of aforementioned test parameters is presented in Figure 5.4.

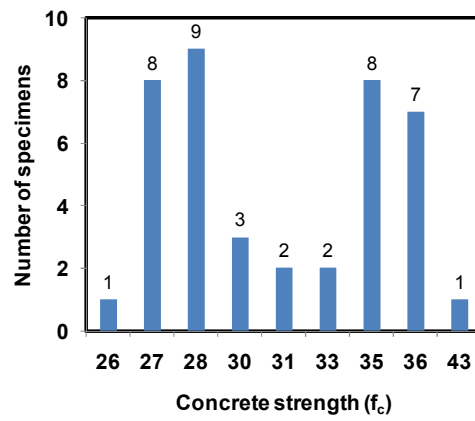
Table 5.3 FRP laminate material properties (manufacturer datasheet)

Researcher	Elasticity Modulus (MPa)	Thickness (mm)	Ultimate tensile stress (MPa)	Ultimate tensile strain
Sissakis	78600	0.89	991	0.0126
Binici	72400	1	876	0.0120
Erdoğan	79820	1	894	0.0112

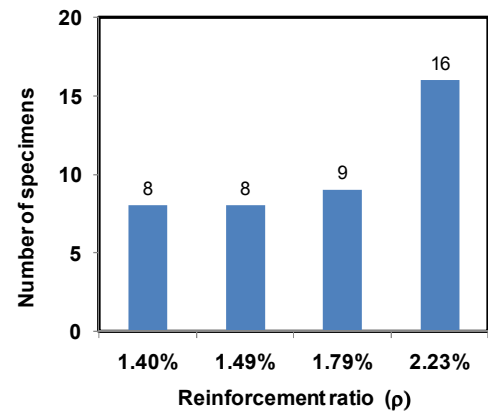
Figure 5.4a indicates that CFRP strengthening method was generally examined on normal concrete strength values ranging from 25 MPa to 45 MPa. Four different reinforcement ratios (1.4%, 1.49%, 1.79% and 2.23%) which is an influential parameter on attainable strength due to flexural capacity limitations chosen for the specimens in the database (Figure 5.4b). The number of CFRP strengthened test specimens with rectangular column is very rare as shown in Figure 5.4c. The majority of the specimens are strengthened with CFRP laminate spacing to effective depth ratio equal to 0.5 (Figure 5.4d).

The number of CFRP perimeters surrounding the slab-column connection region are ranged from 3 to 8 which approximately corresponds to distance of 1.5d to 4d away from column face (Figure 5.4e). Since the location and distribution of vertically applied CFRP laminates around the slab-column connection plays an important role on ultimate punching strength, five different CFRP patterns are discussed in three different studies. Most commonly preferred pattern is the traditional shear stud rail configuration (Pattern B, Figure 5.3) as indicated in Figure 5.4f.

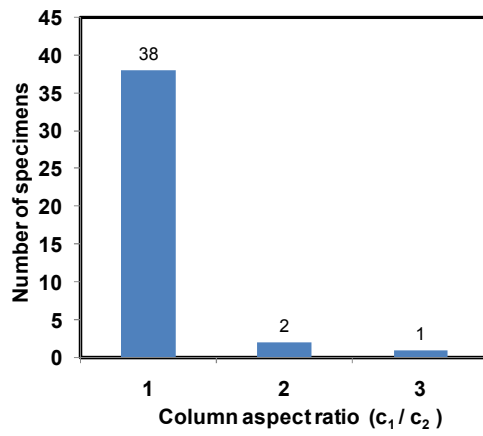
The amount of strength increase in CFRP strengthened specimens are illustrated in terms of ultimate load to reference specimen capacity ratio (V_u / V_{ref}) in Figure 5.4. The strength increase for strengthened specimens varied from 10% to 82% with respect to companion reference specimens. This wide range of difference can be attributed to influential parameters presented in Figure 5.5. The flexural capacity of flat-plate test specimens can be accepted as an upper limit for vertical load carrying capacity, therefore, it may be more reliable to compare test specimens in terms of experimental test result to flexural capacity ratio (V_u / V_{flex}) (Figure 5.6). The test specimens with V_u / V_{flex} values higher than unity solidifies the idea stated by Criswell that the theoretical flexural capacity can be exceed up to 20% for flat-plate specimens subjected to concentric loads.



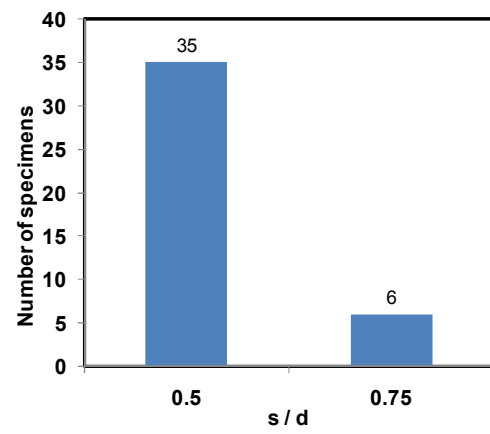
a)



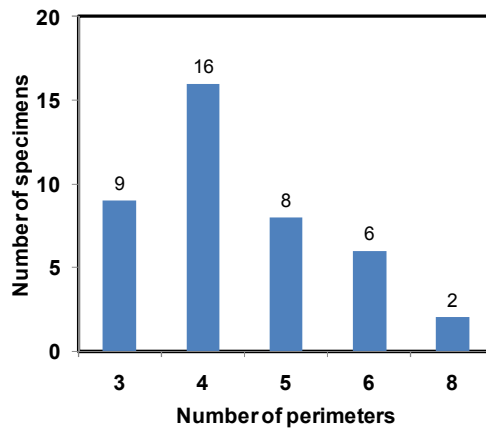
b)



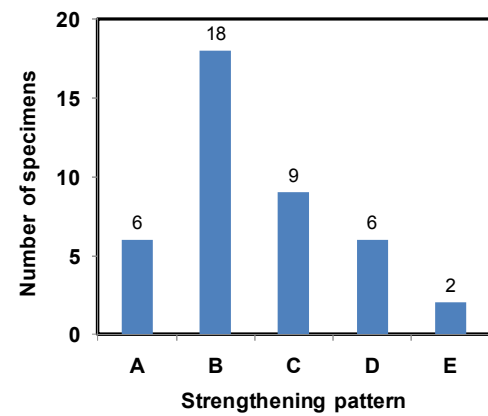
c)



d)



e)



f)

Figure 5.4 Distribution of number of specimens in terms of different variables

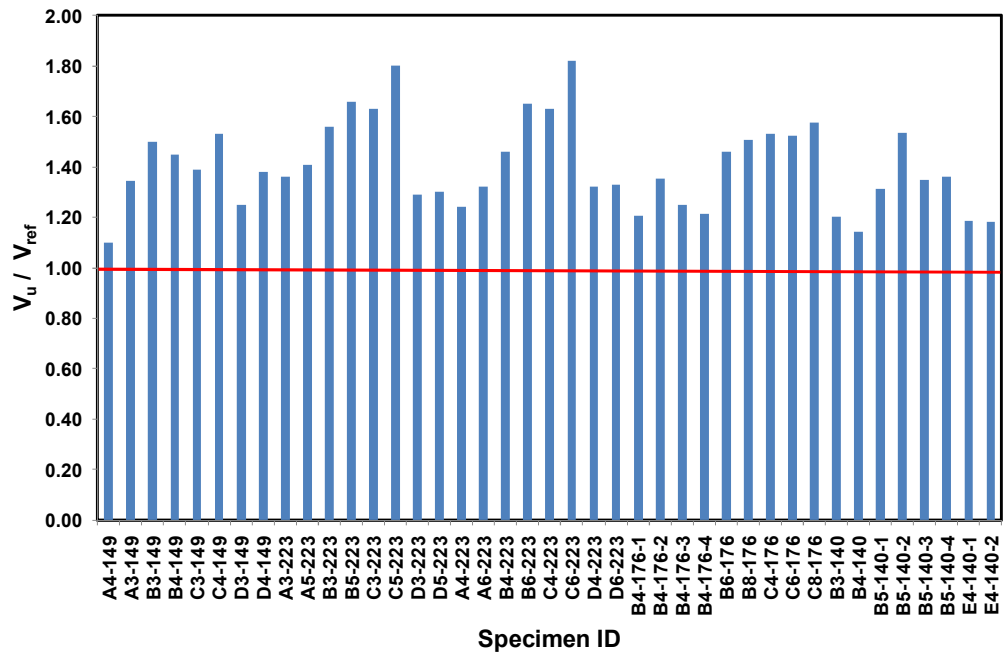


Figure 5.5 Amount of strength increase

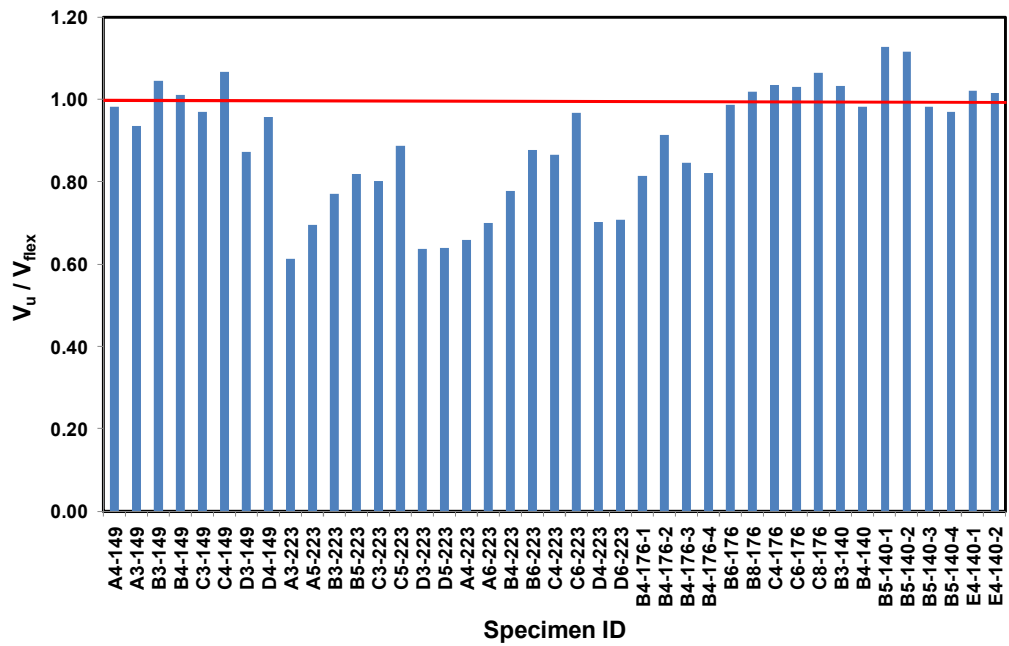


Figure 5.6 Flexural capacity to ultimate strength ratio

The experimental results indicated that the premature failure of strengthened specimens that occurs inside the strengthened region is directly affected by the type of strengthening pattern and perimeter spacing to effective depth ratio (s/d). Sissakis (2002) concluded that the specimens strengthened with patterns B and C are more likely to experience failure outside the strengthening region with higher strength and ductility enhancement compared to patterns A and D. The test results obtained from present study and the study conducted by Binici supports the reliability of patterns B and C. The test results also revealed that five of six specimens with CFRP perimeter spacing of $0.75d$ failed inside the strengthened zone. Figure 5.7 presents the comparison of CFRP perimeter spacing of specimens with outermost CFRP perimeter located $1.5d$ to $2d$ away from column face.

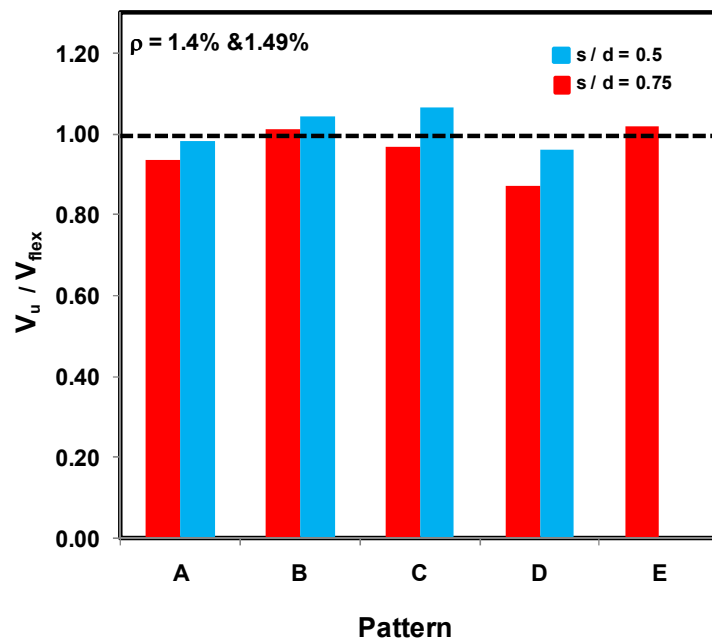


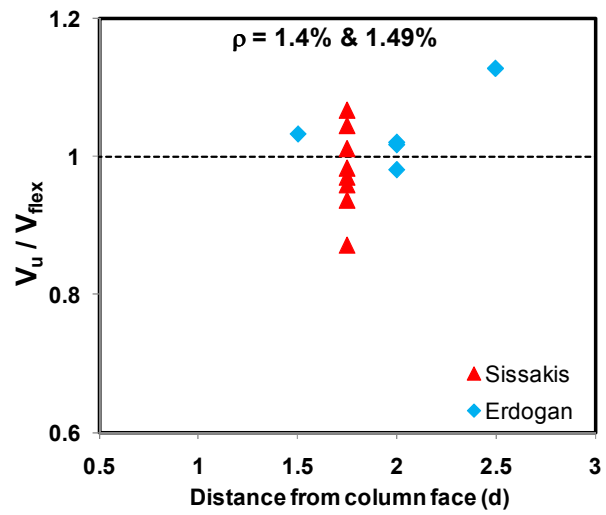
Figure 5.7 Effect of s/d ratio on ultimate capacity

The test results also pointed out that the increasing amount of reinforcement necessitate the increase of the distance (w) between the column face to outermost CFRP perimeter in order to enhance the punching strength at least up to flexural capacity level. In the light of this information, the relation between reinforcement ratio and the distance (w) from column face to outermost CFRP perimeter is presented in Figure 5.8.

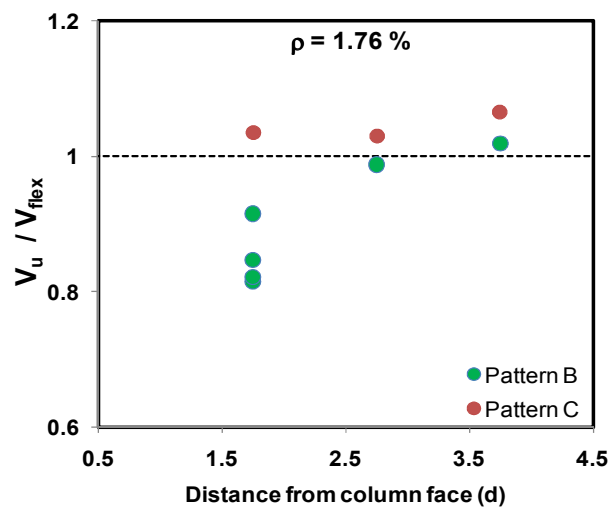
The outermost CFRP perimeter located between $1.5d$ to $2d$ away from the column face appears to be sufficient to provide flexural capacity of the strengthened specimens with reinforcement ratio of 1.4% and 1.49% as shown in Figure 5.7. However, extending the outermost perimeter up to $2.5d$ away from column face provides additional increase in ultimate load level over the flexural capacity.

For the specimens with 1.76% reinforcement ratio, the strengthening pattern plays an important role in addition to distance (w). Figure 5.8b implies that the distance (w) equal to $1.75d$ is sufficient for specimens strengthened with pattern C to obtain flexural capacity, on the other hand, outermost CFRP perimeter should be located at least $2.75d$ away from column face to ensure the theoretical flexural capacity for pattern B. Theoretical flexural capacity is exceeded for specimens with $w=3.75d$ for both patterns B and C.

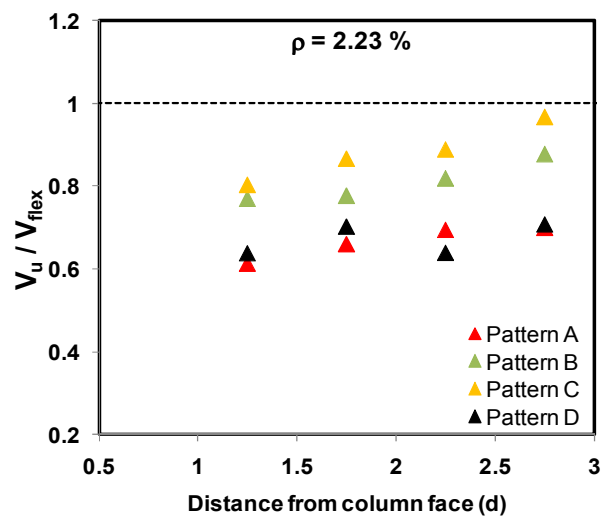
It is obvious that the outermost CFRP distance of $2.75d$ is not adequate for none of the specimens with 2.23% reinforcement ratio as shown in Figure 5.8c. In addition, the effectiveness of patterns B and C compared to patterns A and D can be easily observed from the Figure 5.8c.



a)



b)



c)

Figure 5.8 Relationship between reinforcement ratio (ρ) and w/d

5.2.1 Evaluation of Test Specimens Experiencing Outside Failure

The code provisions generally recommends two design equations considering the two failure modes (inside or outside the shear reinforced region), minimum of which governs the determination of punching load carrying capacity of shear reinforced (with studs or stirrups) slab-column connections. Since the failure inside the shear reinforced region is undesired mode of failure due to its influential effect on post-punching behavior explained in Chapter 2, the capacity outside the shear reinforced zone has prime importance for design of shear reinforcement. For this purpose, the punching load capacities of strengthened test specimens that failed outside the strengthened area are compared with different code estimations as shown in Figure 5.9 and tabulated in Table 5.4 together with the control specimen results. Hence, the codes have no specific punching perimeter definition for all the proposed strengthening patterns. The employed punching shear perimeter definitions considering the experimental failure modes are illustrated in Figure 5.3. Figure 5.9 indicates that the predictions of ACI 318-08 are always on the safe side due to negligence of reinforcement ratio effect and consideration of reduction in shear stress distribution along the distance from column face. On the other hand, Eurocode-2, BS8110-97 and TS500 are failed to predict all the test results safely (Figure 5.9). The main reason of this misprediction can be explained by negligence of shear stress variation with the distance from column face which is also stated previously by Sherif and Dilger (1996) and Voet et al (1982) that the triaxial state of stress at the column corner turns out to be uniaxial at a distance of $4d$ to $5d$ away from column face.

For a better understanding of the effect of shear stress distribution on punching capacity, a coefficient (ϕ) is defined for each building code by normalization of experimental load capacities as indicated in Equations 5.1 to 5.3. While calculating the ϕ values, specific u_o values are used for each code as shown in Figure 5.3. The relation between u_o / d ratio and ϕ_{ACI} is displayed in Figure 5.10 for ACI 318-08. The good conformity between the test results and

Table 5.4 Comparison of code provisions

	Specimen	V_{exp} (kN)	V_{ACI} (kN)	V_{BS8110} (kN)	V_{EC2} (kN)	V_{TS500} (kN)	$\frac{V_{ACI}}{V_u}$	$\frac{V_{BS8110}}{V_u}$	$\frac{V_{EC2}}{V_u}$	$\frac{V_{TS500}}{V_u}$
Sisakis	RS1-149	575	331	420	455	351	0.58	0.73	0.79	0.61
	RS2-149	439	305	398	431	323	0.69	0.91	0.98	0.74
	RS3-223	476	298	448	486	316	0.63	0.94	1.02	0.66
	RS4-223	479	261	411	445	277	0.55	0.86	0.93	0.58
	A3-149	591	554	534	543	587	0.94	0.90	1.01	0.99
	A4-149	632	601	564	633	638	0.95	0.89	1.00	1.01
	B4-149	638	554	534	599	587	0.87	0.84	0.94	0.92
	C4-149	673	642	696	675	747	0.95	1.03	1.00	1.11
	A4-223	595	475	551	619	504	0.80	0.93	1.04	0.85
	A5-223	671	593	669	746	658	0.88	1.00	1.11	0.98
	B3-223	744	462	533	612	490	0.62	0.72	0.82	0.66
	B4-223	701	475	551	619	504	0.68	0.79	0.88	0.72
	B5-223	791	593	669	746	658	0.75	0.85	0.94	0.83
	B6-223	791	555	676	750	651	0.70	0.85	0.95	0.82
	C3-223	775	571	688	659	612	0.74	0.89	0.85	0.79
	C4-223	781	551	719	697	641	0.71	0.92	0.89	0.82
	C6-223	872	649	895	882	849	0.74	1.03	1.01	0.97
Binici	RB-176	494	335	428	462	355	0.68	0.87	0.94	0.72
	B4-176-2	668	501	552	623	571	0.75	0.83	0.93	0.86
	B6-176	721	566	661	739	711	0.79	0.92	1.02	0.99
	B8-176	744	632	770	854	850	0.85	1.04	1.15	1.14
	C4-176	756	562	698	684	701	0.74	0.92	0.90	0.93
	C6-176	752	656	852	847	898	0.87	1.13	1.13	1.19
	C8-176	778	749	1007	1010	1095	0.96	1.29	1.30	1.41
Erdogan	RH1-140	500	310	381	412	329	0.62	0.76	0.82	0.66
	RH2-140	423	295	368	399	313	0.70	0.87	0.94	0.74
	RH3-140	414	252	372	403	318	0.61	0.90	0.97	0.77
	B3-140	601	502	485	548	537	0.84	0.81	0.91	0.89
	B4-140	571	479	499	560	545	0.84	0.87	0.98	0.95
	B5-140	656	558	583	651	671	0.85	0.89	0.99	1.02
	B5-140-2	564	522	576	643	660	0.92	1.02	1.14	1.17
mean							0.77	0.91	0.98	0.89
std.dv							0.12	0.12	0.11	0.19

ACI318-08 estimations implies the accuracy of ACI318-08 prediction and necessity of considering the shear stress distribution along the distance from column face for other design codes.

$$\phi_{BS8110} = \frac{V_u}{(100\rho f_c)^{1/3} (400/d)^{1/4} u_o d} \quad (5.1)$$

$$\phi_{EC2} = \frac{V_u}{(1 + (200/d)^{1/2}) (100\rho f_c)^{1/3} u_o d} \quad (5.2)$$

$$\phi_{TS500} \ \& \ \phi_{ACI} = \frac{V_u}{\sqrt{f_c} u_o d} \quad (5.3)$$

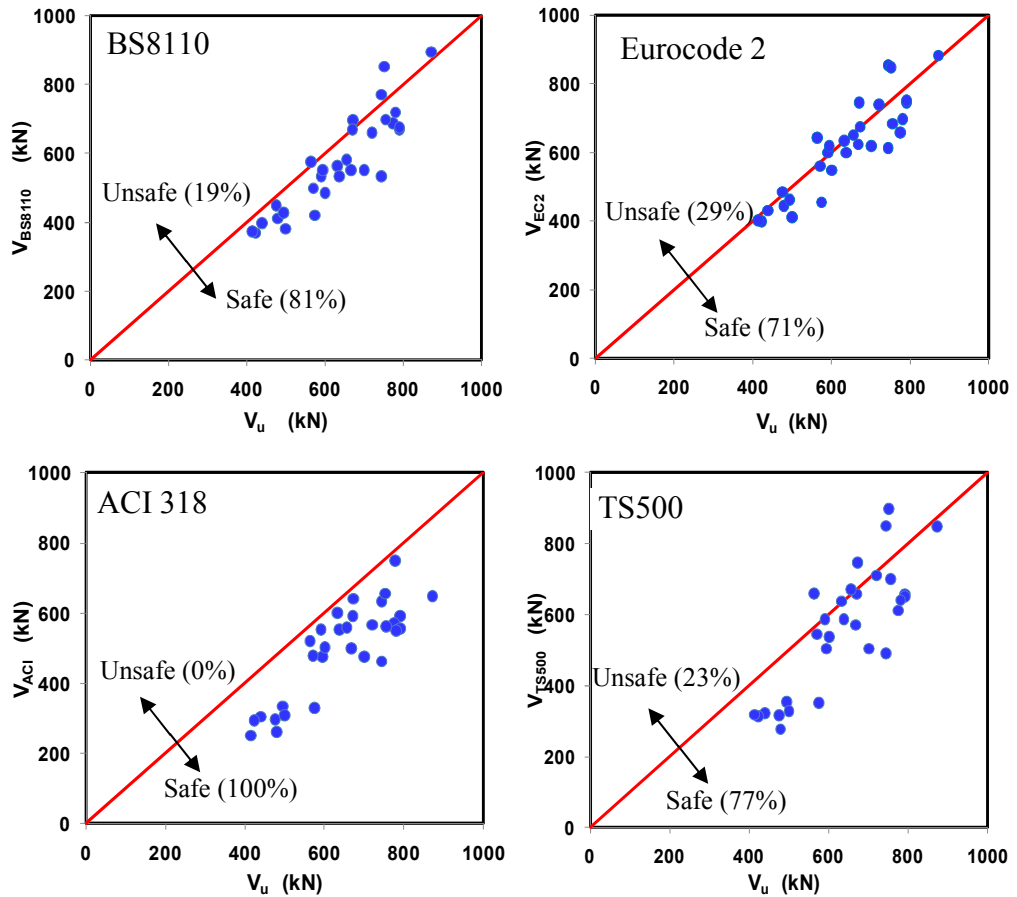


Figure 5.9 Comparison of code estimations and experimental results for the specimens failed outside the strengthened region

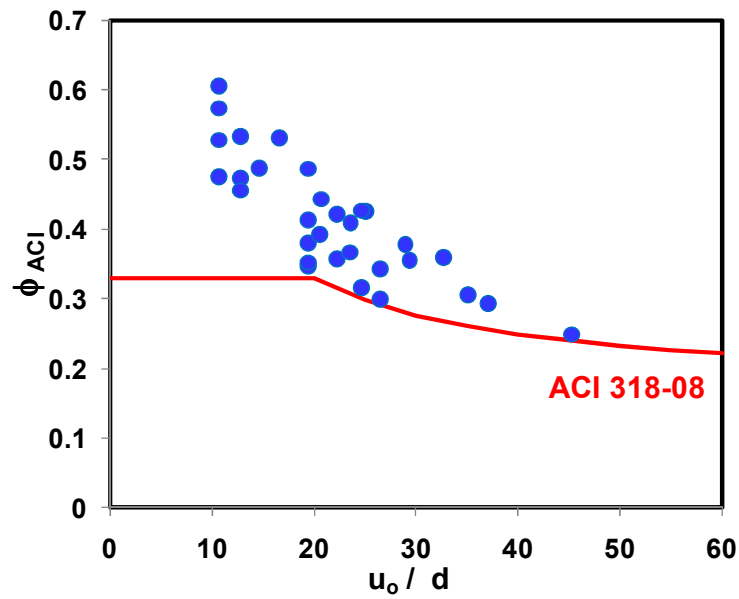


Figure 5.10 Relationship between ϕ_{ACI} and u_o / d ratio

In Figure 5.11, distribution of ϕ values are plotted against w/d ratio for three building codes (BS8110, TS500 and Eurocode-2). The code limitations are indicated with the red line shown in Figure 5.11. It is obvious from the Figure 5.11 that the code estimations become unsafe for greater values of w/d ratio. In the light of this information, a modification factor to punching shear formulation of those three codes is proposed in Equations 5.4 to 5.6. The dashed lines in Figure 5.11 which take into account the shear stress reduction represent the proposed modification for three building codes.

It is apparent from the Figure 5.12 that the code provisions become capable of predicting all the test results safely after application of the proposed modification. The obtained estimations of BS8110-97, Eurocode-2 and TS500 by using modified provisions are also tabulated in Table 5.5 with the predicted to experimental capacity ratio. The reduction in scatter of capacity comparison plots given in Figure 5.12 can also be confirmed with the reduction in terms of standard deviation of capacity ratios from range of 0.11-0.12 to 0.07- 0.09 for three building codes after the modification process.

The modified shear stress equations are given as follows;

$$v_{EC2} = 0.18(1 - 0.07(w/d))(1 + (200/d)^{1/2})(100\rho f_c)^{1/3} \quad (5.4)$$

$$v_{BS8110} = 0.29(1 - 0.07(w/d))(100\rho f_c)^{1/3}(400/d)^{1/4} \quad (5.5)$$

$$v_{TS500} = 0.35(1 - 0.09(w/d))\sqrt{f_c} \quad (5.6)$$

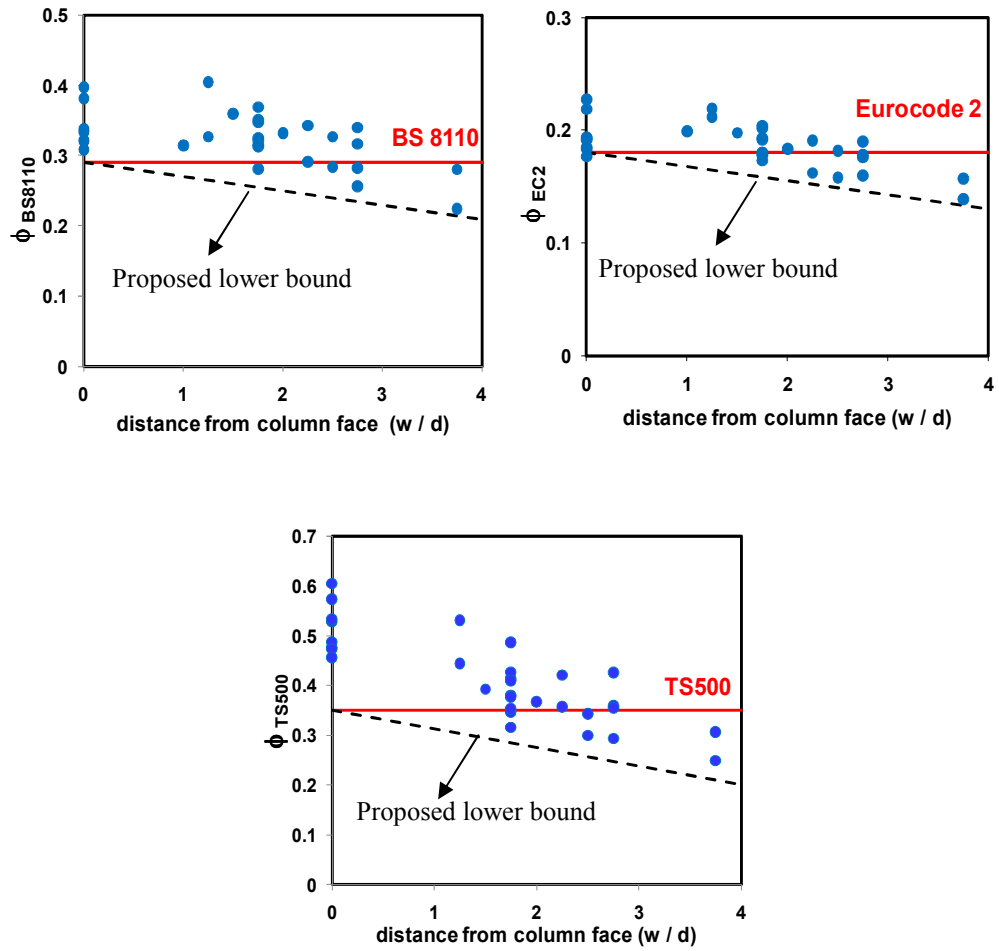


Figure 5.11 Relationship between ϕ and w / d ratios

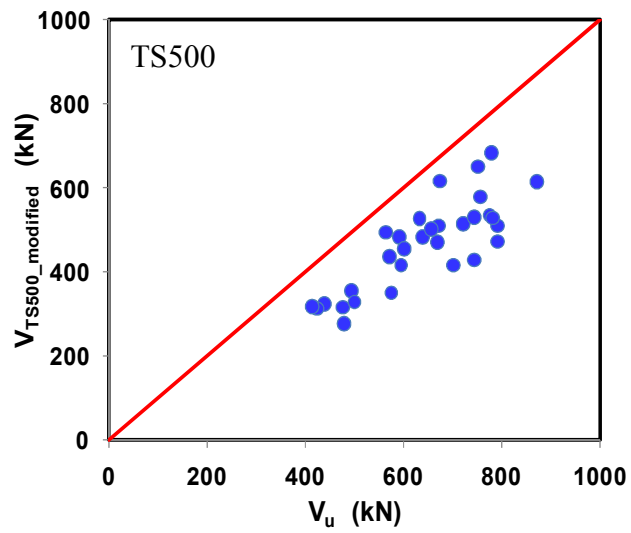
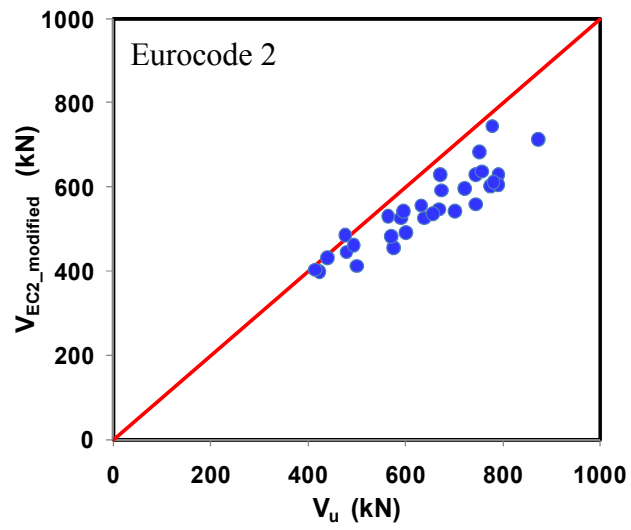
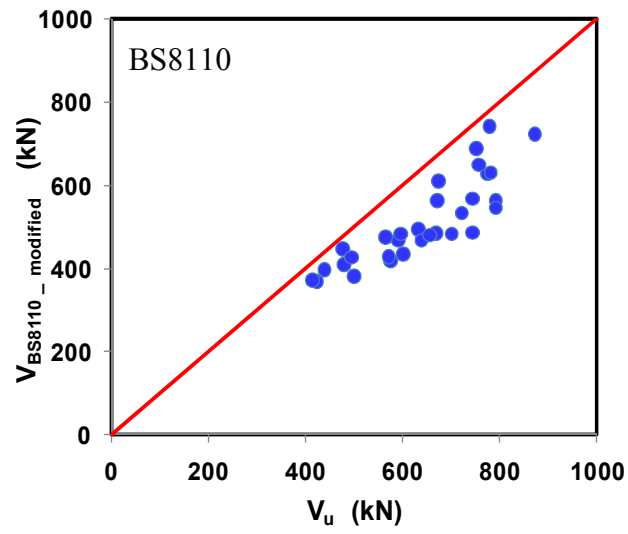


Figure 5.12 Comparison of modified code estimations and experimental results for the specimens failed outside the strengthened region

Table 5.5 Comparison of modified code provisions for outside failure

			Modified code predictions			Modified ratios		
	Specimen	V _{exp} (kN)	V _{BS8110} (kN)	V _{EC2} (kN)	V _{TS500} (kN)	$\frac{V_{BS8110}}{V_u}$	$\frac{V_{EC2}}{V_u}$	$\frac{V_{TS500}}{V_u}$
Sissakis	RS1-149	575	420	455	350	0.73	0.79	0.61
	RS2-149	439	398	431	323	0.91	0.98	0.74
	RS3-223	476	448	486	312	0.94	1.02	0.66
	RS4-223	479	411	445	277	0.86	0.93	0.58
	A3-149	591	415	526	484	0.70	0.81	0.82
	A4-149	632	495	556	526	0.78	0.88	0.83
	B4-149	638	468	526	484	0.73	0.82	0.76
	C4-149	673	611	592	616	0.91	0.88	0.92
	A4-223	595	484	543	416	0.81	0.91	0.70
	A5-223	671	564	628	510	0.84	0.94	0.76
	B3-223	744	487	558	429	0.65	0.75	0.58
	B4-223	701	484	543	416	0.69	0.78	0.59
	B5-223	791	564	628	510	0.71	0.79	0.64
	B6-223	791	546	606	472	0.69	0.77	0.6
	C3-223	775	518	601	535	0.67	0.78	0.69
	C4-223	781	631	612	529	0.81	0.78	0.68
	C6-223	872	723	712	616	0.83	0.82	0.71
Binici	RB-176	494	428	462	355	0.87	0.94	0.72
	B4-176-2	668	484	547	471	0.72	0.82	0.71
	B6-176	721	534	596	515	0.74	0.83	0.71
	B8-176	744	568	630	531	0.76	0.85	0.71
	C4-176	756	649	636	579	0.86	0.84	0.77
	C6-176	752	688	684	651	0.92	0.91	0.87
	C8-176	778	743	745	685	0.95	0.96	0.88
Erdogan	RH1-140	500	381	412	329	0.76	0.82	0.66
	RH2-140	423	368	399	313	0.87	0.94	0.74
	RH3-140	414	372	403	318	0.90	0.97	0.77
	B3-140	601	434	491	456	0.72	0.82	0.76
	B4-140	571	429	482	436	0.75	0.84	0.76
	B5-140-1	656	481	537	503	0.73	0.82	0.77
	B5-140-4	564	475	531	495	0.84	0.94	0.88
					mean	0.80	0.86	0.73
					std.dv	0.09	0.07	0.09

5.2.2 Evaluation of Test Specimens Experiencing Inside Failure

The experimental test results gathered from three different studies indicated that the capacity inside the CFRP strengthened region is not only dependent on the amount of vertical CFRP used for each perimeter but also directly affected by the strengthening pattern, the spacing of CFRP perimeters, detailing and proper anchorage.

The distribution of number of specimens with respect to failure modes and strengthening pattern are presented in Figure 5.13. It is apparent from the figure that patterns D and E are the worst method for punching shear strengthening. On the other hand, Pattern B and C come out to be comparatively reliable patterns for CFRP strengthening of slab-column connections. In addition, more experimental results are required for deciding the applicability of pattern A.

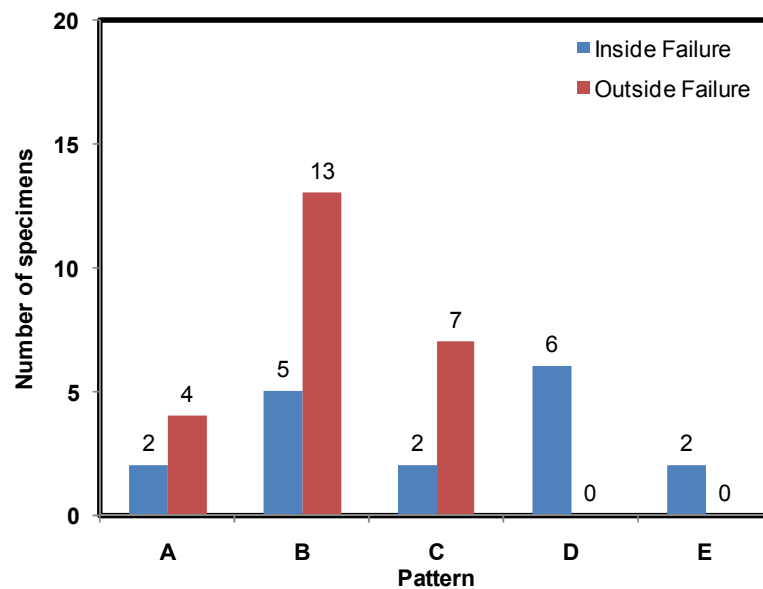


Figure 5.13 Effect of strengthening pattern on failure mode

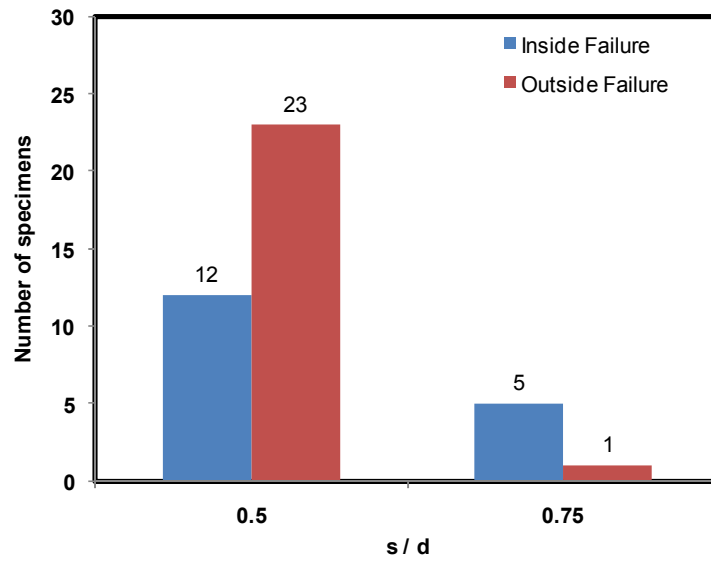


Figure 5.14 Effect of s/d ratio on failure mode

In Figure 5.14, the specimens are classified in terms of spacing of CFRP perimeters. Five of the six specimens that have CFRP perimeters spaced at $0.75d$ failed inside the strengthened region that point out the shear transfer deficiency for increasing values of s/d ratio greater than $0.5d$.

Besides the aforementioned factors, the punching shear capacity inside the strengthened area mainly depends on both contribution of concrete and CFRP reinforcement. According to code provisions, the amount of concrete contribution shows variety. For instance, in ACI 318-08 it is recommended to use 50% of unstrengthened punching capacity as concrete contribution, whereas this ratio is equal to 75% for Eurocode-2 and 100% for BS8110-97 as indicated in Chapter 1. On the other hand, the variables affecting the shear reinforcement contribution are vertical reinforcement area in a perimeter (A_{sv}), s/d ratio and strength of shear reinforcement as presented in Chapter 1.

Since being a brittle material, it is not easy to determine a specific stress limit for design of vertically installed CFRP laminates. The strain limit, 0.004, recommended by ACI 440 Committee is proposed considering the limitations of concrete deformations. The finite element analysis given in Chapter 5

supports this idea under the assumption of linear elastic behavior of CFRP and perfect bond between concrete and CFRP. However, experimental maximum strain values of CFRP indicated that excluding two specimens (B4-176-2 and B4-176-3), none of the specimens have reached strain value of 0.004. The maximum CFRP strain values are given in Table 5.6 and Table 5.7 for specimens failed inside and outside the shear reinforced area respectively. The specimens failed inside the strengthened region had an average maximum CFRP strain value of 2210 microstrain with a standard deviation of 378 excluding the minimum and maximum values. The average value is equal to 2013 microstrain with a standard deviation of 526 for the specimens failed outside the strengthened region.

Table 5.6 Maximum strain values of specimens with outside failure

Specimen	Pattern	s/d	ϵ_{FRP} (microstrain)
A3-149	A	0.75	1020
A4-149	A	0.5	1320
B4-149	B	0.5	1000
C4-149	C	0.5	1300
A4223	A	0.5	2310
A5-223	A	0.5	2000
B3-223	B	0.5	3020
B4-223	B	0.5	2100
B5-223	B	0.5	2000
B6-223	B	0.5	2200
C3-223	C	0.5	2700
C4-223	C	0.5	2450
C6-223	C	0.5	2200
B4-176-1	B	0.5	1939
B4-176-2	B	0.5	4008
B6-176	B	0.5	1677
B8-176	B	0.5	1803
C4-176	B	0.5	2779
C6-176	B	0.5	1366
C8-176	B	0.5	2052

Table 5.7 Maximum strain values of specimens with inside failure

Specimen	Pattern	s/d	ϵ_{FRP} (microstrain)
B3-149	B	0.75	2000
C3-149	C	0.75	2450
D3-149	D	0.75	2150
D4-149	D	0.5	2600
A3-223	A	0.5	1750
A6-223	A	0.5	1400
C5-223	C	0.5	2600
D3-223	D	0.5	2700
D4-223	D	0.5	1550
D5-223	D	0.5	1900
D6-223	D	0.5	2400
B4-176-3	B	0.5	9107

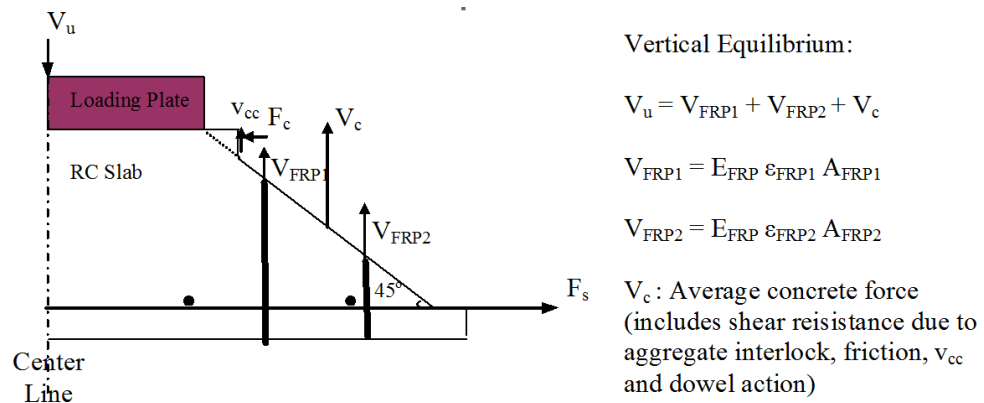


Figure 5.15 CFRP contribution model (adopted from Binici 2003)

Binici (2003) performed a series of calculations by the help of CFRP strain measurements in order to determine the contribution of concrete and CFRP for the strengthened specimens. Binici (2003) assumed 45° of shear crack inclination that intersects two perimeters of CFRP reinforcement as shown in Figure 5.15. The highest strain values are generally observed at first and second CFRP perimeter. This behavior is also supported by the finite element results presented in Chapter 4. The contribution of each perimeter was

calculated by multiplying the strain measurement with the area of CFRP at that perimeter and the elastic modulus of CFRP material reported in Table 5.3. The average ratio of estimated concrete contribution for strengthened specimens to experimental capacity of unstrengthened specimen (V_c/V_{ref}) is close to unity with a standard deviation of 0.15 (Table 5.8). According to those results, the amount of concrete contribution in the strengthened specimens may be assumed to be equal to that of unstrengthened capacity.

Table 5.8 Summary of FRP and concrete contribution
(adopted from Binici 2003)

Specimen	V _u (kN)	Perimeter	ε _{FRP} (microstrain)	V _{FRP} (kN)	V _{FRP1} + V _{FRP2} (kN)	V _c (kN)	V _c / V _{ref}
B4-176-1	595	1	1587	95	212	383	0.75
		2	1939	117			
B4-176-2	668	1	1770	53	174	494	0.97
		2	4000	121			
B4-176-3	618	1	2316	35	172	446	0.97
		2	9107	137			
B4-176-4	605	1	-	-	-	-	-
		2	-	-			
B6-176	600	1	1531	69	195	405	1.03
		2	1677	126			
B8-176	721	1	1271	57	193	528	1.08
		2	1803	136			
C4-176	744	1	1823	82	249	495	1.00
		2	2779	167			
C6-176	756	1	684	52	134	622	1.22
		2	1366	82			
C8-176	778	1	2052	155	234	544	1.09
		2	1313	79			
					Mean		1.02
					Std dev.		0.15

In the light of discussions owing to the variables affecting the inside punching capacity of strengthened flat-plates, it was decided to propose a reliable strain value for design of CFRP. For this purpose, the test results of properly detailed test specimens failed outside the strengthened region with strengthening patterns of B or C, CFRP perimeter spacing of 0.5 and w/d values greater than 2.25 were used (Table 5.9). The amount of CFRP contribution (V_{FRP}) and the strain capacity of test specimens, (ϵ_d), were calculated by using the Equation 5.7 and Equation 5.8 respectively. The evaluation of experimental data and calculated values for FRP strain indicated that 2000 microstrain would be a considerable safe limiting strain value for design of CFRP material provided that no reduction is applied to the calculated concrete contribution (V_c).

$$V_{FRP} = V_u - V_{ref} \quad (5.7)$$

$$\epsilon_d = \frac{V_{FRP} s}{A_{sv} E d} \quad (5.8)$$

Table 5.9 Comparison of experimental and design CFRP strains

Specimen	w/d	E (MPa)	A _{FRP} (mm ²)	V _u (kN)	V _{ref} (kN)	V _{FRP} (kN)	ϵ_{max} (microstrain)	ϵ_d (microstrain)
B6-176	2.75	72400	800	721	494	227	1677	1960
B8-176	3.75	72400	800	744	494	250	1803	2158
C6-176	2.75	72400	900	752	494	258	1366	1980
C8-176	3.75	72400	900	778	494	284	2052	2179
B5-223	2.25	78600	705	791	476	315	2000	2842
B6-223	2.75	78600	822	791	479	312	2200	2414
C6-223	2.75	78600	1136	872	479	393	2200	2201
Mean							1898	2247
Std dev:							283	280

5.2.3 Design Procedure

The code estimations based on the proposed modifications regarding the punching capacity inside and outside the strengthened region are compared with the experimental punching capacities (V_u) of the test specimens strengthened with patterns B and C are given in Figure 5.16. The database consisted of the specimens strengthened with either pattern B or pattern C as listed in Tables 5.10 to 5.13.

The concrete contribution (V_c) to inside punching failure capacity is proposed to be equal to unstrengthened specimen capacity (V_d) by using each individual code provisions given in Chapter 1. On the other hand, the FRP contribution to punching capacity inside the strengthened zone is assumed to be identical for all the codes with a limiting strain value of 0.002 based on the above analysis and computed with the Equation 5.9. The outside failure capacity of the specimens were computed by the help of modified equations given in Section 5.2.1 and critical perimeter definitions given in Figure 5.3.

$$V_{FRP} = 0.002 E_{FRP} \frac{d}{s} \quad (5.9)$$

The calculated values of V_c , V_{FRP} , V_i and V_o are given in Tables 5.10 to 5.13 for each code. In addition, the ratios of predicted to experimental capacities, the ratio of inside to outside capacities and the predicted and observed failure modes are also listed in mentioned tables. Figure 5.16 explicitly implies that all four codes provide conservative estimations for punching strength of test specimens. However, ACI 318-08 and TS500 estimations are relatively much more conservative compared to other two code estimations with an average predicted to observed capacity ratio of 0.74. The ratio of calculated inside capacity to calculated outside capacity is mostly above 0.90 for TS500 Eurocode-2 and BS8110-97. The lower limit for this ratio is equal to 0.74 for ACI 318-08 due to conservative nature of ACI provisions. This ratio directly affects the failure location predictions, since most of the estimated failure

locations obtained through the use of ACI 318-08 are inside failure. For this reason, ACI 318-08 has the worst predictions in terms of failure locations among the all four codes.

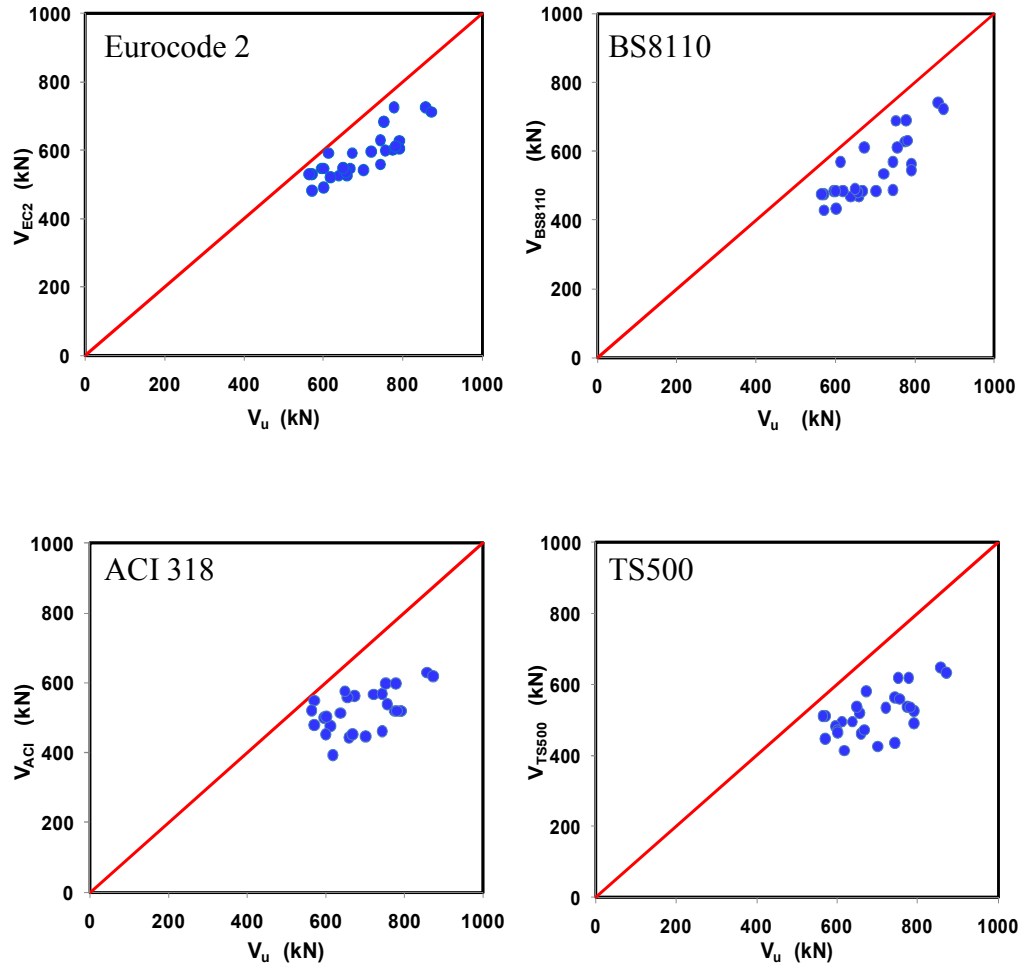


Figure 5.16 Comparison of modified code estimations and experimental results for the specimens strengthened with patterns B and C

Table 5.10 Calculated and experimental punching strength of test specimens (TS500)

	Specimen	V_{exp} (kN)	V_c (kN)	V_{FRP} (kN)	V_i (kN)	V_o (kN)	V_{TS500} (kN)	V_{TS500}	V_i	Failure mode		Failure mode Check
								V_u	V_o	Test	Code	
Sissakis	B3-149	659	323	139	462	495	462	0.70	0.93	inside	inside	√
	B4-149	638	323	209	532	495	495	0.78	1.08	outside	outside	√
	C3-149	612	323	172	495	629	495	0.81	0.79	inside	inside	√
	C4-149	673	323	258	581	629	581	0.86	0.92	outside	inside	X
	B3-223	744	316	172	488	435	435	0.58	1.12	outside	outside	√
	B4-223	701	277	184	461	425	425	0.61	1.09	outside	outside	√
	B5-223	791	316	221	537	525	525	0.66	1.02	outside	outside	√
	B6-223	791	277	258	535	490	490	0.62	1.09	outside	outside	√
	C3-223	775	316	221	537	543	537	0.69	0.99	outside	inside	X
	C4-223	781	277	258	535	540	535	0.69	0.99	outside	inside	X
	C5-223	858	316	332	648	677	648	0.75	0.96	inside	inside	√
	C6-223	872	277	357	634	639	634	0.73	0.99	outside	inside	X
Binici	B4-176-1	595	355	234	588	481	481	0.81	1.22	inside	outside	X
	B4-176-2	668	355	117	472	481	472	0.71	0.98	outside	inside	X
	B4-176-3	618	355	59	413	481	413	0.67	0.86	inside	inside	√
	B4-176-4	600	355	117	472	481	472	0.79	0.98	inside	inside	√
	B6-176	721	355	234	589	535	535	0.74	1.10	outside	outside	√
	B8-176	744	355	234	589	563	563	0.76	1.04	outside	outside	√
	C4-176	756	355	205	560	591	560	0.74	0.95	outside	inside	X
	C6-176	752	355	263	618	676	618	0.82	0.91	outside	inside	X
	C8-176	778	355	263	618	726	618	0.79	0.85	outside	inside	X
Erdoğan	B3-140	601	334	307	641	464	464	0.77	1.38	outside	outside	√
	B4-140	571	296	307	603	447	447	0.78	1.35	outside	outside	√
	B5-140-1	656	324	307	631	520	520	0.79	1.21	outside	outside	√
	B5-140-2	649	334	307	641	536	536	0.83	1.20	inside	outside	X
	B5-140-3	571	318	461	779	511	511	0.89	1.52	inside	outside	X
	B5-140-4	564	318	461	779	511	511	0.91	1.52	outside	outside	√
								mean	0.75	1.08		
								st.dev	0.08	0.19		

Table 5.11 Calculated and experimental punching strength of test specimens
(BS8110)

	Specimen	V_{exp} (kN)	V_c (kN)	V_{FRP} (kN)	V_i (kN)	V_o (kN)	V_{BSI} (kN)	V_{BSI}	V_i	Failure mode		Failure mode Check
								V_u	V_o	Test	Code	
Sissakis	B3-149	659	398	139	537	468	468	0.71	1.15	inside	outside	X
	B4-149	638	398	209	607	468	468	0.73	1.30	outside	outside	√
	C3-149	612	398	172	570	611	570	0.93	0.93	inside	inside	√
	C4-149	673	398	258	656	611	611	0.91	1.07	outside	outside	√
	B3-223	744	448	172	620	487	487	0.65	1.27	outside	outside	√
	B4-223	701	411	184	594	484	484	0.69	1.23	outside	outside	√
	B5-223	791	448	221	669	564	564	0.71	1.19	outside	outside	√
	B6-223	791	411	258	669	546	546	0.69	1.23	outside	outside	√
	C3-223	775	448	221	669	628	628	0.81	1.07	outside	outside	√
	C4-223	781	411	258	669	631	631	0.81	1.06	outside	outside	√
	C5-223	858	448	332	780	741	741	0.86	1.05	inside	outside	X
	C6-223	872	410	357	767	723	723	0.83	1.06	outside	outside	√
Binici	B4-176-1	595	427	234	661	484	484	0.81	1.37	inside	outside	X
	B4-176-2	668	427	117	544	484	484	0.72	1.12	outside	outside	√
	B4-176-3	618	427	59	486	484	484	0.78	1.00	inside	outside	X
	B4-176-4	600	427	117	544	484	484	0.81	1.12	inside	outside	X
	B6-176	721	427	234	661	534	534	0.74	1.24	outside	outside	√
	B8-176	744	427	234	661	568	568	0.76	1.16	outside	inside	X
	C4-176	756	427	205	632	612	612	0.81	1.03	outside	outside	√
	C6-176	752	427	263	690	688	688	0.92	1.00	outside	outside	√
	C8-176	778	427	263	690	743	690	0.89	0.93	outside	outside	√
Erdoğan	B3-141	601	385	307	692	434	434	0.72	1.59	outside	outside	√
	B4-141	571	355	307	662	429	429	0.75	1.54	outside	outside	√
	B5-141-1	656	377	307	684	481	481	0.73	1.42	outside	outside	√
	B5-140-2	649	384	307	692	491	491	0.76	1.41	inside	outside	X
	B5-140-3	571	372	461	833	475	475	0.83	1.81	inside	outside	X
	B5-140-4	564	372	461	833	475	475	0.84	1.81	outside	outside	√
								mean	0.79	1.23		
								st.dev	0.07	0.24		

Table 5.12 Calculated and experimental punching strength of test specimens
(ACI 318-08)

	Specimen	V_{exp} (kN)	V_c (kN)	V_{FRP} (kN)	V_i (kN)	V_o (kN)	V_{ACI} (kN)	V_{ACI}	V_i	Failure mode		Failure mode Check
								V_u	V_o	Test	Code	
Sissakis	B3-149	659	305	139	444	554	444	0.67	0.80	inside	inside	√
	B4-149	638	305	209	514	554	514	0.81	0.93	outside	inside	X
	C3-149	612	305	172	477	641	477	0.78	0.74	inside	inside	√
	C4-149	673	305	258	563	641	563	0.84	0.88	outside	inside	X
	B3-223	744	298	172	470	462	462	0.62	1.02	outside	outside	√
	B4-223	701	262	184	446	475	446	0.64	0.94	outside	inside	X
	B5-223	791	298	221	519	592	519	0.66	0.88	outside	inside	X
	B6-223	791	262	258	520	555	520	0.66	0.94	outside	inside	X
	C3-223	775	298	221	519	571	519	0.67	0.91	outside	inside	X
	C4-223	781	262	258	520	551	520	0.67	0.94	outside	inside	X
	C5-223	858	298	332	630	683	630	0.73	0.92	inside	inside	√
	C6-223	872	262	357	619	649	619	0.71	0.95	outside	inside	X
Binici	B4-176-1	595	334	234	568	501	501	0.84	1.14	inside	outside	X
	B4-176-2	668	334	117	451	501	451	0.68	0.90	outside	inside	X
	B4-176-3	618	334	59	393	501	393	0.64	0.79	inside	inside	√
	B4-176-4	600	334	117	451	501	451	0.75	0.90	inside	inside	√
	B6-176	721	334	234	568	567	567	0.79	1.00	outside	outside	√
	B8-176	744	334	234	568	633	568	0.76	0.90	outside	inside	X
	C4-176	756	334	205	539	562	539	0.71	0.96	outside	inside	X
	C6-176	752	334	263	597	656	597	0.79	0.91	outside	inside	X
	C8-176	778	334	263	597	749	597	0.77	0.80	outside	inside	X
Erdoğan	B3-141	601	315	307	622	502	502	0.84	1.24	outside	outside	√
	B4-141	571	379	307	586	479	479	0.84	1.23	outside	outside	√
	B5-141-1	656	305	307	612	558	558	0.85	1.10	outside	outside	√
	B5-140-2	649	315	307	622	576	576	0.89	1.08	outside	inside	X
	B5-140-3	571	300	461	761	549	549	0.96	1.39	outside	inside	X
	B5-140-4	564	300	461	761	522	522	0.93	1.46	outside	outside	√
								mean	0.76	0.95		
								st.dev	0.09	0.12		

Table 5.13 Calculated and experimental punching strength of test specimens
(Eurocode-2)

	Specimen	V_{exp} (kN)	V_c (kN)	V_{FRP} (kN)	V_i (kN)	V_o (kN)	V_{EC2} (kN)	V_{EC2}	V_i	Failure mode		Failure mode Check
								V_u	V_o	Test	Code	
Sissakis	B3-149	659	431	139	570	526	526	0.80	1.09	inside	outside	X
	B4-149	638	431	209	640	526	526	0.82	1.22	outside	outside	√
	C3-149	612	431	172	603	592	592	0.97	1.02	inside	outside	X
	C4-149	673	431	258	689	592	592	0.88	1.16	outside	outside	√
	B3-223	744	486	172	658	559	559	0.75	1.18	outside	outside	√
	B4-223	701	445	184	629	543	543	0.78	1.16	outside	outside	√
	B5-223	791	486	221	707	628	628	0.79	1.13	outside	outside	√
	B6-223	791	445	258	703	606	606	0.77	1.16	outside	outside	√
	C3-223	775	486	221	707	601	601	0.78	1.18	outside	outside	√
	C4-223	781	445	258	703	612	612	0.78	1.15	outside	outside	√
	C5-223	858	486	332	818	725	725	0.85	1.13	inside	outside	X
	C6-223	872	445	357	802	712	712	0.82	1.13	outside	outside	√
Binici	B4-176-1	595	462	234	696	547	547	0.92	1.27	inside	outside	X
	B4-176-2	668	462	117	579	547	547	0.82	1.06	outside	outside	√
	B4-176-3	618	462	59	521	547	520	0.84	0.95	inside	inside	√
	B4-176-4	600	462	117	579	547	547	0.91	1.06	inside	outside	X
	B6-176	721	462	234	696	596	596	0.83	1.17	outside	outside	√
	B8-176	744	462	234	696	630	630	0.85	1.10	outside	outside	√
	C4-176	756	462	205	667	600	600	0.79	1.11	outside	outside	√
	C6-176	752	462	263	725	684	684	0.91	1.06	outside	outside	√
	C8-176	778	462	263	725	745	725	0.93	0.97	outside	inside	X
Erdoğan	B3-141	601	416	307	723	491	491	0.82	1.47	outside	outside	√
	B4-141	571	385	307	692	482	482	0.84	1.44	outside	outside	√
	B5-141-1	656	408	307	715	537	537	0.82	1.33	outside	outside	√
	B5-140-2	649	416	307	548	723	548	0.84	1.32	outside	inside	X
	B5-140-3	571	403	461	531	864	531	0.93	1.63	outside	inside	X
	B5-140-4	564	403	461	531	864	531	0.94	1.63	outside	outside	√
								mean	0.84	1.20		
								st.dev	0.06	0.17		

Parametric studies were performed with proposed modifications for TS500 and Eurocode-2 in order to determine the suitability of proposed modifications for design purposes. The modified outside capacity equations regarding TS500 and Eurocode-2 were used to investigate the relationship between the capacity increase (V_o/V_d) and outermost shear reinforcement distance (w/d) for varying column side length to slab effective depth ratios (c/d). The allowable strength increase was limited with 50% in TS500. This ratio may also be assumed as a reliable allowable limit for Eurocode-2 provisions considering the experimental results given in Figure 5.5.

It is apparent from Figure 5.17 that the punching capacity has a tendency to decrease after reaching a maximum value for increasing values of w/d ratio. Figure 5.17 also indicated that the maximum capacity was generally reached at w/d ratio of 4 to 5.5 depending on c/d ratio for both codes. The degrading effect of c/d ratio on affordable punching capacity is obviously observed in Figure 5.17, since maximum punching capacity has a tendency to decrease for increasing values of c/d ratio. In addition, the modified equations are capable of considering the strengthening pattern, since it is possible to reach same amount of strength increase by using lower amount of FRP laminates by using pattern C compared to pattern B. Proposed modifications for TS500 design equation offers relatively economical design compared to Eurocode-2 by having smaller w/d ratio for achieving same amount of strength increase.

The maximum value of w/d ratio for obtaining ultimate load increase can be calculated by the help of Equation 5.9. The coefficients (A, B, X) values depending on the strengthening pattern and code provision are presented in Table 5.14. According to ACI 318-08 provisions punching shear capacity has a continuous increasing trend for increasing values of w/d ratio contrary to proposed modifications for TS500 and Eurocode-2 equations (Figure 5.17). Therefore, it is not required to compute maximum value of w/d ratio for ACI 318-08.

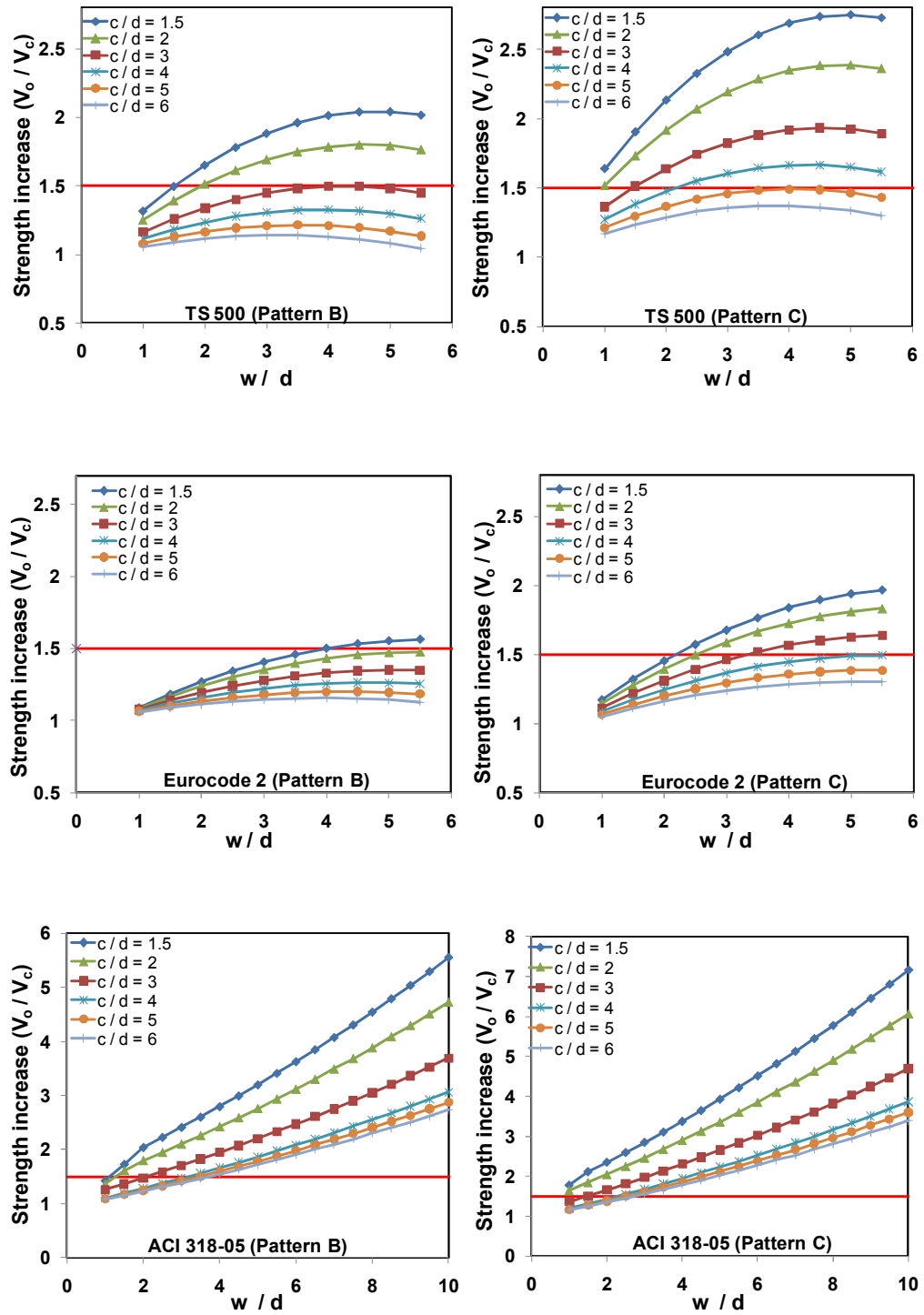


Figure 5.17 Parametric study results for design purposes

$$\frac{w_{\max}}{d} = A - B \left(\frac{c_1 + c_2}{d} \right) - X \quad (5.9)$$

Table 5.14 Coefficient values for calculation of (w_{\max} / d)

	TS500		Eurocode-2	
	Pattern B	Pattern C	Pattern B	Pattern C
A	5.56		7.14	
B	0.177	0.125	0.196	0.125
X	0.250	0.250	0.833	0.589

According to numerical evaluations, a flowchart chart is given in Figure 5.19 for proposed design procedure.

1. Determine the geometric and material properties of the slab-column connection
2. Compute the punching capacity of unstrengthened slab-column connection.
3. Select the strengthening pattern (B or C) with a spacing of 0.5 d
4. Assume the number of FRP perimeters around the slab-column connection
5. Compute the critical perimeter and punching shear capacity outside the shear reinforced region respectively. Calculate the maximum permissible punching shear strength by multiplying V_d by 1.5. Change the number of FRP perimeter till the equilibrium $V_d \leq V_o \leq 1.5V_c$ is satisfied.
6. Calculate the required amount of FRP per perimeter.

A design “employing this flowchart” example is presented in Appendix A.

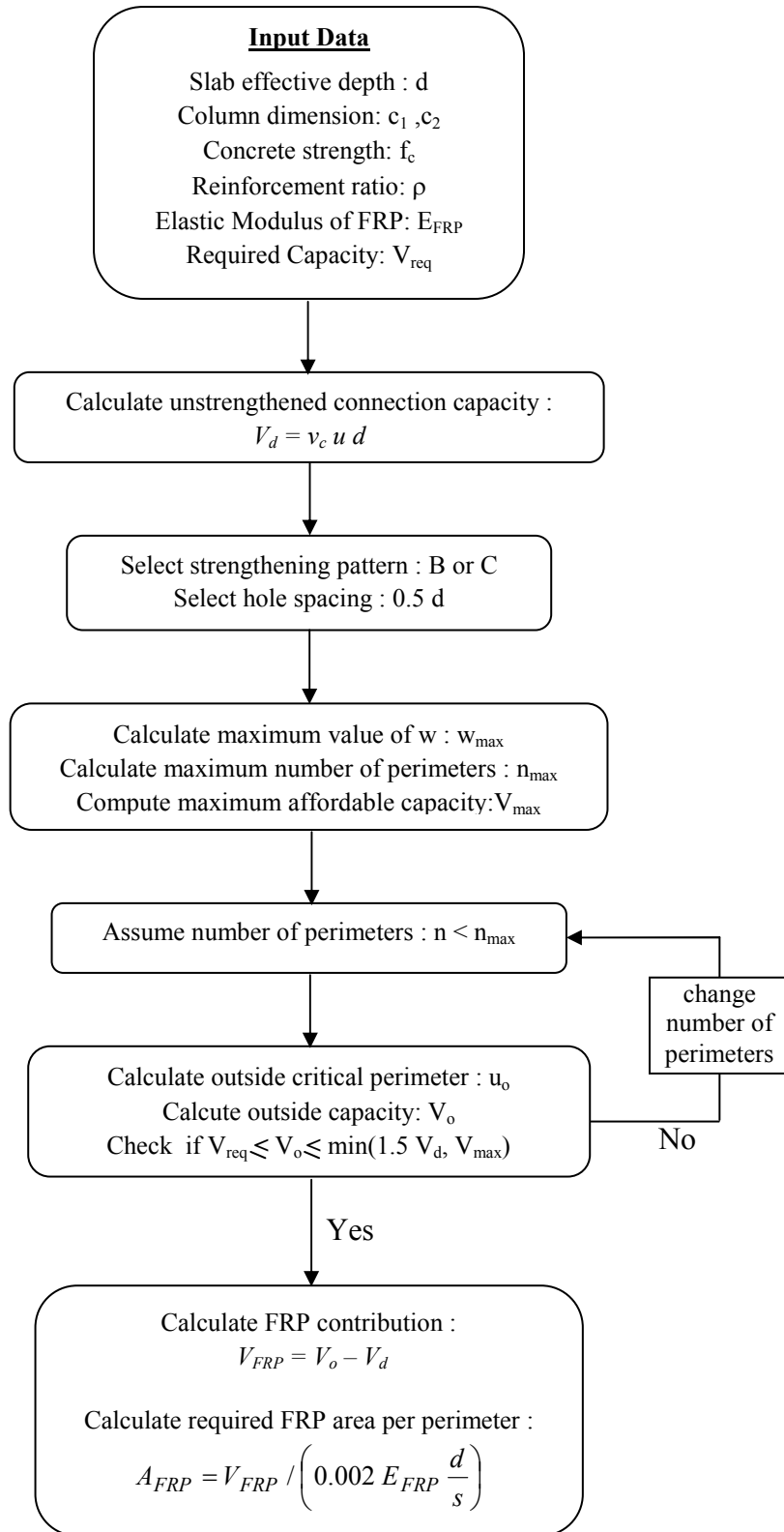


Figure 5.19 Strengthening design procedure

CHAPTER 6

SUMMARY AND CONCLUSIONS

6.1 SUMMARY

In this dissertation, an easy to install and economical strengthening technique for increasing the punching strength of interior slab-column connections by using vertically applied CFRP dowels was developed. Twelve $\frac{3}{4}$ scale specimens were tested under vertically applied monotonic loading. The effects of amount and arrangement of the CFRP dowels and column rectangularity on punching behavior of the specimens were investigated. The contributions of strengthening method to the punching load carrying, displacement and post punching capacities and failure mechanisms of the specimens were studied. The influence of detailing on the performance of strengthening method was examined.

Three dimensional nonlinear finite element analyses were performed to investigate the punching failure mechanism of test specimens. The validity of the proposed finite element models were examined with the experimental results of this study and also another study performed by Binici (2003). The discussions regarding the state of stress at failure, allowable strain limit for CFRP strengthening are presented.

A database of flat-plate test specimens strengthened with vertically applied CFRP laminates including the present study was constructed to investigate the safety of code provisions of ACI 318-08, Eurocode-2, BS 8110-97 and TS500 . According to evaluation of code provisions, some of the predictions of

Eurocode-2 (2003), BS 8110-97 (1997) and TS500 (2000) found to be unsafe. For this reason, some modifications on the mentioned code provisions were proposed to assure practical and safe design for CFRP strengthened flat-plate structures.

6.2 CONCLUSIONS

The conclusions drawn in the light of performed study are presented below:

1. Punching shear strength enhancement between 31% to 53% was obtained with the application of the proposed CFRP retrofit method. The displacement and the ultimate load capacities of strengthened specimens with rectangular column stub (OS25, OS25-b, and OS35-b) tended to decrease with respect to strengthened specimens having square column stub (OS15).
2. The arrangement and the spacing of the vertical CFRP dowels around the column stub were influential on the failure modes of the specimens considering the behavior of the strengthened specimens. The strengthened specimens OS13, OS14 and OS15 in which the CFRP dowels were arranged in double rail configurations in along four sides of the column stub, failed outside the shear reinforced zone whereas the strengthened specimens CSWOP and CSWP that are strengthened with CFRP dowel arranged in a circular pattern around the column stub, failed inside the shear reinforced zone for this particular study. However, further research is required to generalize the effect of strengthening pattern on the failure mode.
3. Post-punching capacity of the strengthened test specimens were about 2.4 times the post punching capacity of the unstrengthened test specimens. In other words, it was found that even after the punching failure, the strengthened slab-column connections were able to maintain 80 percent of their unstrengthened punching shear capacity. This ability of the CFRP

retrofit specimens is believed to provide a reserved capacity against progressive collapse.

4. In the light of performed tests, the effect of CFRP patches applied on the surface of the test specimens on the punching behavior of test specimens was negligible due to insufficient length of the CFRP patches. The identical test specimens with (CSWP) and without (CSWOP) CFRP patches exhibit almost identical behavior.
5. Column rectangularity had no significant effect on post-punching capacity of both strengthened and reference specimens. However, punching failure mode (inside or outside the shear reinforced region) is still crucial for strengthened specimens.
6. Finite element modeling approach was found to be reliable in estimating load-deformation, longitudinal reinforcement and CFRP strains. Furthermore, analytical results shed light on the initiation of punching failure when the triaxiality of the state of stress at the tip of punching crack is lost.
7. The parametric study performed by the nonlinear analysis revealed that the proposed limiting strain value (0.004) due to concrete deformation restrictions seems to be acceptable for designing CFRP dowels for punching shear enhancement. However, this value is reached for none of the specimens with only two exceptions as given in the database in Chapter 5. Based on this evidence, considering the modification in concrete contribution due to analysis performed by Binici (2003) is found necessary. Hence, it would be more realistic to adopt the limiting strain as 0.002.
8. ACI 318-08 provides safe estimations for the capacity of the strengthened test specimens in the database. Eurocode-2 and BS 8110-97 estimations, show less scatter with a better mean for estimated to observed capacity

ratios. Some of the unsafe predictions of Eurocode-2, BS 8110-97 and TS500 were eliminated, after applications of proposed modifications to Eurocode-2, BS 8110-97 and TS500 provisions.

6.3 RECOMMENDATIONS FOR FUTURE STUDIES

1. In order to examine the effect of redistribution and interaction among the neighborhood slab-column connections, full scale slab tests should be performed with multiple connections including interior, exterior and edge slab-column connections with combined vertical loads and moment transfer.
2. Since the number of experiments focused on CFRP strengthening of flat-plates supported on rectangular columns is very rare, additional experiments are required for better understanding the stress distribution around the rectangular columns.
3. The applicability of alternative fiber polymer based materials having lower costs should be examined for strengthening purposes.
4. The seismic performance of the proposed strengthening technique should be examined under the application of lateral cyclic loading.

REFERENCES

ACI Committee 318., 2002, “Building Code Requirements for Structural Concrete (ACI318-02) and Commentary (ACI 318R-02), American Concrete Institute, Farmington Hills, Michigan, 443 pp.

ACI Committee 318., 2005, “Building Code Requirements for Structural Concrete (ACI318-05) and Commentary (ACI 318R-05), American Concrete Institute, Farmington Hills, Michigan, 430 pp.

ACI Committee 318., 2008, “Building Code Requirements for Structural Concrete (ACI318-08) and Commentary (ACI 318R-08), American Concrete Institute, Farmington Hills, Michigan, 473 pp.

ACI Committee 440, 2002, “Guide for the Design and Construction of Externally Bonded FRP Systems for Strengthening Concrete Structures”, American Concrete Institute, Farmington Hills, Michigan, 45 pp.

Adetifa B. and Polak M.A., 2005, “Retrofit of Slab Column Interior Connections Using Shear Bolts”, ACI Structural Journal, 102(2), pp. 268-274.

Al-Yousif A.T. and Regan P.E., 2003, “Punching resistances of RC slabs supported by large and/or elongated columns”, The Structural Engineer, 81(3), pp. 30-34.

Anderson J.L., 1963, “Punching of Concrete Slabs with Shear Reinforcement”, Transactions of the Royal Institute of Technology, Stockholm, No. 212.

ASTM D3039, 2006, “Standard Test Method for Tensile Properties of Polymer Matrix Composite Materials” ASTM International, 13 pp.

Binici B., 2003, “Punching Shear Strengthening of Reinforced Concrete Slabs Using Fiber Reinforced Polymers”, Ph.D Thesis, Department of Civil Engineering, University of Texas, Austin.

Birkle G. and Dilger W.H., 2008, “Influence of Slab Thickness on Punching Shear Strength”, ACI Structural Journal, 105(2), pp. 180-188.

Bu W. and Polak M.A., 2009, “Seismic Retrofit of Reinforced Concrete Slab-Column Connections Using Shear Bolts”, ACI Structural Journal, 106(4), pp. 514-522.

Broms C.E., 1990, “Shear Reinforcement for Deflection Ductility of Flat Plates”, ACI Structural Journal, 87(6), pp. 696-705.

BS 8110, 1997, "Structural Use of Concrete, Part 1: Code of Practice for Design and Construction.", British Standards Institute, London.

Carpenter J.E., Karr P.H. and Hanson N.W., 1970, "Proposed Revision of ACI 318-63: Building Code Requirements for Reinforced Concrete", ACI Journal, 68(3), pp. 696-697.

Casadei P., Nanni A. and Ibell T., 2003, "Experiments on Two-way RC Slabs with Openings Strengthened with CFRP Laminates" CIES Report 03-39, Center for Infrastructure Engineering Studies, University of Missouri-Rolla, Rolla, Missouri, 8 pp.

CEB-FIP MC 90, 1993, "Design of Concrete Structures, CEB-FIP Model Code 1990." Thomas Telford, British Standard Institution, London.

Chen C.C. and Li C.Y., 2000, "An Experimental Study on the Punching Shear Behavior of RC Slabs", Proceedings, International Workshop on Punching Shear Capacity of RC Slabs, Stockholm, TRITA-BKN:Bulletin 57, pp. 415-422.

Chen C.C. and Li C.Y., 2005, "Punching Shear Strength of Reinforced Concrete Slabs Strengthened with Glass Fiber-Reinforced Polymer Laminates", ACI Structural Journal, 102(4), pp. 535-542.

Corley W.G. and Hawkins N.M., 1968, "Shearhead Reinforcement for Slabs", ACI Journal, 65(10), pp. 811-824.

Criswell M.E., 1974, "Static and Dynamic Response of Response Concrete Slab-Column Connections." ACI Publication SP-42, Shear in Reinforced Concrete", Farmington Hills, Mich., pp. 721-746.

Dilger W.H. and Ghali A., 1981, "Shear Reinforcement for Concrete Slabs", Journal of Structural Division, ASCE, 107(12), pp. 2403-2420.

DIANA, 2005, "Finite Element Analysis User's Manual Release 9.", TNO Building and Construction Research. Delft, Netherlands.

Ebead U. and Marzouk H., 2002, "Strengthening of two-way slabs using steel plates", ACI Structural Journal, 99(1), pp. 23-31.

Elgabry A. and Ghali A., 1987, "Test on Concrete Slab-Column Connections with Stud Shear Reinforcement Subjected to Shear-Moment Transfer", ACI Structural Journal, 84(5), pp. 433-442.

Elstner R.C. and Hognestad E., 1956, "Shearing Strength of Reinforced Concrete Slabs", Journal of the American Concrete Institute, 28(1), pp.29-58.

El-Salakawy E.F., Polak M.A. and Soudki K.A., 2003, "New Strengthening Technique for Concrete Slab-Column Connections", *ACI Structural Journal*, 100(3), pp.297-304.

El-Salakawy E., Soudki K.A. and Polak M.A., 2004, "Punching Shear Behavior of Flat Slabs Strengthened with Fiber Reinforced Polymer Laminates", *Journal of Composites for Construction*, 8(5), pp. 384-392.

Erki M.A. and Heffernan P.J., 1995, "Reinforced concrete slabs externally strengthened with fiber-reinforced plastic materials", 2nd International Symposium on Nonmetallic (FRP) Reinforcement for Concrete Structures, Belgium, pp. 509-516.

Ersoy U., Erdogan T. and Tankut T., 1981, "Investigation Report on the Failure of ASELSAN Building Submitted to Court", File N. Hz.981-5531, 17 pp., (in Turkish).

Eurocode 2-2003, 2003, "Eurocode 2: Design of Concrete Structures – Part 1-1: General Rules and Rules for Buildings.", European Committee for Standardization, Brussels.

Farhey D.N., Adin M.A., Yankelevsy D.Z., 1995, "Repaired RC Flat Slab-Column Connection Subassemblages under Lateral Loading", *Journal of Structural Engineering*, ASCE, 121(11), pp. 1710-1720.

Feenstra P.H., 1993, "Computational Aspects of Biaxial Stress in Plain and Reinforced Concrete.", Ph.D Thesis, Delft University of Technology, Netherlands.

Forsell C. and Holmberg Å., 1946, "Stämpellast på plattor av betong", *Betong*, 31(2), pp. 95-123.

Gardner N.J., Huh J., and Chung L., 2002, "Lessons from Sampoong Department Store Collapse", *Cement and Concrete Composites*, 24(2), pp.523-529.

Graf O., 1933, "Test of Reinforced Concrete Slabs under Concentrated Load Applied Near One Support (Versuche über die Widerstandsfähigkeit von Eisenbetonplatten unter konzentrierter Last nahe einem Auflager)", *Deutscher Ausschuss für Eisenbeton*, No. 73, Berlin, Germany.

Graf O., 1938, "Strength Test of Thick Reinforced Concrete Slabs Supported on all Sides under Concentrated Loads", *Deutscher Ausschuss für Eisenbeton*, Berlin, 88, pp. 22.

Harajli M.H. and Soudki K.A., 2003, "Shear strengthening of interior slab-column connections using carbon fiber-reinforced polymer sheets", *Journal of Composites for Construction*, ASCE, 7(2), pp. 145-153.

Harajli M.H., Soudki K.A. and Kudsi T., 2006, "Strengthening of Interior Slab-Column Connections Using a Combination of FRP Sheets and Steel Bolts", *Journal of Composites for Construction*, 10(5), pp. 399-409.

Hassanzadeh G. and Sundqvist H., 1988, "Strengthening of Bridge Slabs on Columns", *Nordic Concrete Research*, No. 21.

Hawkins N.M., Falssen H.B. and Hinojosa R.C., 1971, "Influence of column rectangularity on the behavior of flat plate structures", Publication SP-30, American Concrete Institute, Detroit, pp. 127-146.

Hordijk D.A., 1992, "Tensile and Tensile Fatigue Behavior of Concrete: Experiments, Modelling and Analyses. *Heron*, Delft, 37(1), pp. 1-77.

Hu H.T. and Schnobrich W.C., 1990, "Nonlinear analysis of cracked reinforced concrete", *ACI Structural Journal*, 87(2), pp.199-207.

Kaminetzky D., 1991, "Design and Construction Failures: Lessons from Forensic Investigations", McGraw-Hill, Inc., USA.

Kuang K.L. and Teng S., 2001, "Punching shear strength of slabs with openings and supported on rectangular columns", Final Report, A BCA-NTU Joint Research on Flat Plate Structures, Phase-1A , 298 pp.

Lovrovich J.S. and McLean D.I., 1990, "Punching Shear Behavior of Slabs with Varying Span-Depth Ratios", *ACI Structural Journal*, 87(5), pp. 507-511

Martinez-Cruzado J.A., Qaisrani A.N. and Moehle J.P., 1994, "Post-Tensioned Flat Plate Slab-Column Connections Subjected to Earthquake Loading", Proceedings, 5th U.S. National Conference on Earthquake Engineering, Chicago, Illinois, July 1994, pp. 139-148.

Megally S.H., 1998, "Punching Shear Resistance of Concrete Slabs to Gravity and Earthquake Forces." Ph.D Thesis, Department of Civil Engineering, The University of Calgary.

Megally S. and Ghali A., 2000, "Punching Shear Design of Earthquake Resistant Slab-Column Connections.", *ACI Structural Journal*, 97(5), pp. 720-730.

Menetrey P., 1996, "Analytical Computation of the Punching Strength of Reinforced Concrete", *ACI Structural Journal*, 93(5), pp. 503-511.

Michel L., Ferrier E., Bigaud D. and Agbossou A., 2007, "Criteria for Punching Failure Mode in RC Slabs Reinforced by Externally Bonded CFRP", *Composite Structures*, 81(3), pp 438-449.

Mitchell D., Tinawi R. And Redwood R.G., 1990, "Damage to Buildings Due to the 1989 Loma Prieta Earthquake – A Canadian Code Perspective", Canadian Journal of Civil Engineering, 17(5), pp. 813-834.

Mitchell D., De Vall R.H., Saatcioglu M., Simpson R., Tinawi R. And Tremblay R., 1995, "Damage to Concrete Structures due to the 1994 Northridge Earthquake.", Canadian Journal of Civil Engineering, 22(4), pp.361-377.

Moe J., 1961, "Shearing Strength of Reinforced Concrete Slabs and Footings under Concentrated Load", Bulletin D47, Portland Cement Association Research and Development Laboratories, Skokie, Illinois, USA.

Mokhtar A.S., Ghali A. and Dilger W., 1985, "Stud Shear Reinforcement for Flat Plates", ACI Structural Journal, 82(5), pp. 676-683.

Mowrer R.D. and Vanderbilt M.D., 1967, "Shear Strength of Lightweight aggregate reinforced concrete", ACI Structural Journal, 64(11), pp. 722-729.

Muttoni A., Fürst A., and Hunkeler F., 2005 "Deckeneinsturz der Tiefgarage am Staldenacker in Gretzenbach, Medieninformation vom 15.11.2005, Solothurn, Switzerland, 14 pp.

Muttoni A., 2008 "Punching Shear Strength of Reinforced Concrete Slabs without Transverse Reinforcement", ACI Structural Journal, 105(4), pp. 440-450.

Muttoni A., Fernandez R.M., Fürst A., Guandalini S., Hunkeler F., Moser K. and Seiler H., 2008, "Structural Safety of Parking Garages", Documentation D 0226 SIA, Swiss Society of Engineers and Architects, Zurich, Switzerland.

Fernandez R.M. and Muttoni A., 2009, "Applications of Critical Shear Crack Theory to Punching of Reinforced Concrete Slabs with Transverse Reinforcement", ACI Structural Journal, 106(4), pp. 485

Niksarlıoğlu B, 1998, "Punching Shear Reinforcement for Flat Plates", Ms.c Thesis, Department of Civil Engineering, Middle East Technical University.

Oliviera D.R., Melo S.R. and Regan P.E., 2000, "Punching Strengths of Flat Plates with Vertical or Inclined Stirrups", ACI Structural Journal, 97(3), pp. 485-491.

Oliviera D.R.C., Regan P.E. and Melo G.S.S.A., 2004, "Punching resistance of RC slabs with rectangular columns" Magazine of Concrete Research, 56(3), pp. 123-138.

Özden Ş., 1998 “Punching Shear Behavior of Normal and High-Strength Concrete Flat-Plates”, Ph.D Thesis, Department of Civil Engineering, Boğaziçi University, İstanbul, Turkey.

Paramasivam P. And Tan K.H., 2009, “Punching Shear Strength of Ferrocement Slabs” ACI Structural Journal, 90(3), pp. 294-301.

Richart F.E., 1948, “Reinforced Concrete Wall and Column Footings, Part 1”, Journal of the American Concrete Institute, 20(2), pp. 97-127.

Richart F.E., 1948, “Reinforced Concrete Wall and Column Footings, Part 2”, Journal of the American Concrete Institute, 20(3), pp. 237-260.

Ramos A.M.P., Lucio V.J.G and Regan P.E, 2000, “Repair and Strengthening Method of Flat Slabs for Punching”, Proceedings, International Workshop on Punching Shear Capacity of RC Slabs, Stockholm, Sweden, TRITA-BKN:Bulletin 57, pp. 125-133.

Robertson I.N.and Johnson G., 2001, “Repair of Slab-Column Connections using CFRP”, Earthquake Resistant Engineering Structures III, WIT Press, UK, pp. 505-514.

Robertson I.N.and Johnson G., 2004, “Repair of Slab-Column Connections using Epoxy and Carbon Fiber Reinforced Polymer”, Journal of Composites for Construction, 8(5), pp. 376-383.

Rochdi E.H., Bigaud D., Ferrier E. and Hamelin P., 2006, “Ultimate Behavior of CFRP Strengthened RC Flat Slabs Under a Centrally Applied Load”, Composite Structures, 72(1), pp. 69-78.

Selby R.G. and Vecchio F.J., 1993, “Three-Dimensional Constitutive Relations for Reinforced Concrete.”, Technical Report 93-02, University of Toronto, Department of Civil Engineering, Toronto, Canada.

Sharaf M.H., Soudki K.A. and Van Dusen M., 2006, “CFRP Strengthening for Punching Shear of Interior Slab-Column Connections”, Journal of Composites for Construction, 10(5), pp. 410-418.

Sherif A.G. and Dilger W.H., 1996, “Critical Review of the CSA A23.3-94 Punching Shear Strength Provisions for Interior Columns” Canadian Journal of Civil Engineering, 23, pp. 998-1101.

Sissakis K., 2002, “Strengthening Concrete Slabs for Punching Shear with CFRP Laminates”, Ms.c Thesis, Department of Civil Engineering, University of Toronto.

Stark A., Binici B. and Bayrak O., 2005, “Seismic Upgrade of Reinforced Concrete Slab-Concrete Connections Using Carbon Fiber-Reinforced Polymer”, *ACI Structural Journal*, 102(2), pp. 324-333.

Talbot, A.N., 1913, “Reinforced Concrete Wall and Column Footings”, Bulletin 67, University of Illinois Engineering Experiment Station, USA.

Tan K.H., 1996, “Punching Shear Strength of Reinforced Concrete Slabs Bonded with FRP Systems. 2nd International Conference on Advanced Composite Materials in Bridges and Structures, pp. 387-394.

Tankut A.T. (1969), “The Behavior of the Reinforced Concrete Flat-plate Structures Subjected to Various Combinations of Vertical and Horizontal Loads.” Ph.D Thesis, University of London.

Teng S., Cheong H.K., Kuang K.L. and Geng J.Z., 2004, “Punching shear strength of slabs with openings and supported on rectangular columns”, *ACI Structural Journal*, 101(5), pp. 678-687.

Thorenfeldt E., Tomaszewicz A. and Jensen J.J., 1987, “Mechanical Properties of High-Strength Concrete and Applications in Design. In Proc. Symp. Utilization of High Strength Concrete, Stavanger, Norway.

Turkish Standard Institute, 2000, “TS500 Requirements for Design and Construction of Reinforced Concrete Structures” Ankara, Turkey.

Van der Voet A.F., Dilger W.H. and Ghali A., 1982, “Concrete Flat Plates with Well Anchored Shear Reinforced Elements”, *Canadian Journal of Civil Engineering*, 9, pp. 107-114.

Vecchio F.J. and Collins M.P., 1993, “Compression Response of Cracked Reinforced Concrete.”, *Journal of Structural Engineering ASCE*, 119(19), pp. 3590–3610.

Wang J.W. and Tan K.L., 2001, “Punching Shear Behavior of Reinforced Concrete Flat Slabs Externally Strengthened with CFRP Systems. 5th International Conference on Fiber-Reinforced Plastic for Reinforced Concrete Structures,2, London, pp. 997-1005.

Whitney C.S., 1957, “Ultimate Shear Strength of Reinforced Concrete Flat Slabs, Footing Beams and Frame Members without Shear Reinforcement”, *Journal of the American Concrete Institute*, 29(4), pp. 265-298.

Widianto, 2006, “Rehabilitation of Reinforced Concrete Slab-Column Connections for Two-way Shear”, Ph.D Thesis, Department of Civil Engineering, University of Texas, Austin.

APPENDIX A

Design Example for Inner Slab-Column Connections Strengthened with Vertically Applied CFRP Laminates

Given: Column size, $c_1 = c_2 = 250$ mm; Slab thickness 150 mm, $f_c = 30$ MPa; reinforcement ratio, 1.4%; slab effective depth, $d = 114$ mm; $E_{FRP} = 70552$ MPa

Design: Determine the required amount of CFRP in order to obtain 50% increase in the punching capacity of given slab-column connection. (Design for TS-500 and Eurocode-2)

TS500 (Pattern B)

Unstrengthened specimen capacity :

$$V_d = 0.35\sqrt{f_c}ud = [0.35\sqrt{30}[4(250 + 114)](114)]/1000 = 318 \text{ kN}$$

Experiment: $V_u = 500$ kN

Number of CFRP perimeter $n=3$

Select CFRP spacing of 0.5 d

Critical perimeter outside the shear reinforced region

$$u_o = 4[250 + \sqrt{2}(2)(114)] = 2290 \text{ mm}$$

Punching shear capacity outside the shear reinforced region:

$$V_o = 0.35[1 - 0.09(w/d)]\sqrt{f_c} u d$$

$$V_o = [0.35(0.865)\sqrt{30}(2290)(114)]/1000 = 433 \text{ kN}$$

Experiment (OS13): $V_u = 601$ kN

Determine the CFRP contribution:

$$V_{FRP} = V_o - V_d = 433 - 318 = 115 \text{ kN}$$

Experiment (OS13): $V_{FRP} = 101 \text{ kN}$

Area of CFRP per perimeter:

$$A_{FRP} = \frac{V_{FRP}}{\left(0.002 E_{FRP} \frac{d}{s}\right)} = \frac{115000}{(0.002)(70552)(2)} = 408 \text{ mm}^2 \text{ per perimeter}$$

Number of CFRP perimeter n=4

Select CFRP spacing of 0.5 d

$$u_o = 2612 \text{ mm}, V_o = 468 \text{ kN}, V_{FRP} = 150 \text{ kN}, A_{FRP} = 532 \text{ mm}^2$$

Experiment (OS14): $V_u = 574 \text{ kN}$, $V_{FRP} = 101 \text{ kN}$, $A_{FRP} = 960 \text{ mm}^2$

Number of CFRP perimeter n=5

Select CFRP spacing of 0.5 d

$$u_o = 2935 \text{ mm}, V_o = 497 \text{ kN}, V_{FRP} = 179 \text{ kN}, A_{FRP} = 634 \text{ mm}^2$$

Experiment (OS15): $V_u = 656 \text{ kN}$, $V_{FRP} = 156 \text{ kN}$, $A_{FRP} = 960 \text{ mm}^2$

TS500 (Pattern C)

Number of CFRP perimeter n=3

Select CFRP spacing of 0.5 d

$$u_o = 2824 \text{ mm}, V_o = 534 \text{ kN}, V_{FRP} = 216 \text{ kN}, A_{FRP} = 765 \text{ mm}^2$$

Experiment (OS14): $V_u = 574 \text{ kN}$, $V_{FRP} = 101 \text{ kN}$, $A_{FRP} = 960 \text{ mm}^2$

Number of CFRP perimeter n=4

Select CFRP spacing of 0.5 d

$$u_o = 3280 \text{ mm}, V_o = 588 \text{ kN}, V_{FRP} = 270 \text{ kN}, A_{FRP} = 957 \text{ mm}^2$$

Experiment (OS14): $V_u = 574 \text{ kN}$, $V_{FRP} = 101 \text{ kN}$, $A_{FRP} = 960 \text{ mm}^2$

Number of CFRP perimeter n=5

Select CFRP spacing of 0.5 d

$$u_o = 3736 \text{ mm} , V_o = 633 \text{ kN} , V_{FRP} = 315 \text{ kN}, A_{FRP} = 1116 \text{ mm}^2$$

$$\text{Experiment (OS15): } V_u = 656 \text{ kN}, V_{FRP} = 156 \text{ kN}, A_{FRP} = 960 \text{ mm}^2$$

Eurocode-2 (Pattern B)

Unstrengthened specimen capacity :

$$V_d = 0.18 \left(1 + (200/d)^{1/2} \right) (100 \rho f_c)^{1/3} b d$$

$$V_d = 0.18 \left(1 + (200/114)^{1/2} \right) ((1.4)(30))^{1/3} (2433)(114) = 402 \text{ kN}$$

$$\text{Experiment: } V_u = 500 \text{ kN}$$

Number of CFRP perimeter n=3

Select CFRP spacing of 0.5 d

$$u_o = 3152 \text{ mm} , V_o = 466 \text{ kN} , V_{FRP} = 64 \text{ kN}, A_{FRP} = 227 \text{ mm}^2$$

$$\text{Experiment (OS14): } V_u = 601 \text{ kN}, V_{FRP} = 101 \text{ kN}, A_{FRP} = 960 \text{ mm}^2$$

Number of CFRP perimeter n=4

Select CFRP spacing of 0.5 d

$$u_o = 3474 \text{ mm} , V_o = 494 \text{ kN} , V_{FRP} = 92 \text{ kN}, A_{FRP} = 326 \text{ mm}^2$$

$$\text{Experiment (OS14): } V_u = 574 \text{ kN}, V_{FRP} = 74 \text{ kN}, A_{FRP} = 960 \text{ mm}^2$$

Number of CFRP perimeter n=5

Select CFRP spacing of 0.5 d

$$u_o = 3797 \text{ mm} , V_o = 518 \text{ kN} , V_{FRP} = 116 \text{ kN}, A_{FRP} = 411 \text{ mm}^2$$

$$\text{Experiment (OS15): } V_u = 656 \text{ kN}, V_{FRP} = 156 \text{ kN}, A_{FRP} = 960 \text{ mm}^2$$

Eurocode-2 (Pattern C)

Number of CFRP perimeter n=3

Select CFRP spacing of 0.5 d

$$u_o = 3442 \text{ mm} , V_o = 509 \text{ kN} , V_{FRP} = 107 \text{ kN}, A_{FRP} = 379 \text{ mm}^2$$

$$\text{Experiment (OS14): } V_u = 601 \text{ kN}, V_{FRP} = 101 \text{ kN}, A_{FRP} = 960 \text{ mm}^2$$

Number of CFRP perimeter n=4

Select CFRP spacing of 0.5 d

$$u_o = 3898 \text{ mm} , V_o = 554 \text{ kN} , V_{FRP} = 152 \text{ kN}, A_{FRP} = 539 \text{ mm}^2$$

$$\text{Experiment (OS14): } V_u = 574 \text{ kN}, V_{FRP} = 74 \text{ kN}, A_{FRP} = 960 \text{ mm}^2$$

Number of CFRP perimeter n=5

Select CFRP spacing of 0.5 d

$$u_o = 4354 \text{ mm} , V_o = 594 \text{ kN} , V_{FRP} = 192 \text{ kN}, A_{FRP} = 680 \text{ mm}^2$$

$$\text{Experiment (OS15): } V_u = 656 \text{ kN}, V_{FRP} = 156 \text{ kN}, A_{FRP} = 960 \text{ mm}^2$$

CURRICULUM VITAE

PERSONAL INFORMATION

Surname, Name: Erdoğan, Hakan
Nationality: Turkish (TC)
Date and Place of Birth: 10.10.1980, Kocaeli
Marital Status: Single
Phone: +90 (312) 210 54 75
Fax: +90 (312) 287 8951
Email: ehakan@metu.edu.tr

EDUCATION

2002-2010 Ph.D., Civil Engineering, METU
2008-2009 Research Fellowship at Florida International University
1998-2002 BS, Civil Engineering, Kocaeli University
1991-1998 Kocaeli Anatolian High School

WORK EXPERIENCE

2002-Present Research Assistant, Department of Civil Engineering, METU

PUBLICATIONS

1. **Erdogan H.**, Binici B. and Ozcebe G., “Punching Shear Strengthening of Flat-Slabs with CFRP Dowels”, Magazine of Concrete Research, 62(7), pp. 465-479.
2. **Erdogan H.**, Binici B. and Ozcebe G., “Punching Shear Strengthening of Flat-Slabs with CFRP Dowels”, Magazine of Concrete Research, in press

3. **Erdogan, H.**, Özcebe, G and Binici, B, “A New CFRP Strengthening Technique to Enhance Punching Shear Strength of RC Slab-column Connections.” Asia-Pacific Conference on FRP in Structures (APFIS 2007), Hong Kong.
4. **Erdogan H.** and Ozcebe G., 2008, “Punching Shear Strengthening of Rectangular Slab Column Connections.” 8th International Conference on Advances in Civil Engineering, 8 pp.
5. Mirmiran, A., **Erdogan, H.**, and Singhvi, A., 2009, “Design Implications of Creep and Long-Term Deflections in FRP-RC Beam-Columns.” ACI Special Publication SP264-10, Serviceability of Concrete Members Reinforced with Internal/External FRP Reinforcement, ACI, Vol. 264, 163-178.